TRIBOLOGY OF HIGH-PERFORMANCE POLYMERS AT EXTREME CONDITIONS FROM CRYOGENIC TO ELEVATED TEMPERATURES

A Dissertation

by

KIAN BASHANDEH KHODAEINAEINI

Submitted to the Graduate and Professional School of
Texas A&M University
in partial fulfillment of the requirements for the degree of

DOCTOR OF PHILOSOPHY

Chair of Committee,	Andreas A. Polycarpou
Committee Members,	Ali Erdemir
	Matt Pharr
	Mohammad Naraghi
Head of Department,	Guillermo Aguilar

August 2022

Major Subject: Mechanical Engineering

ABSTRACT

There is a strong need for long life bearings and tribological surfaces for expanding the ability of NASA and other space companies and agencies to explore the deep atmosphere and surface of different planets and comets using long-lived (days or weeks) balloons and landers. The missions would experience extreme temperatures - ranging from cryogenic temperatures of -220°C on Europa to upwards of 462°C on Venus, which impede the use of traditional oil lubricants and greases, resulting in dry sliding conditions that generally have significant detrimental effects on component performance; with the addition of abrasive dusty environment in Mars, the complexity is further compounded.

To address these challenges, high-performance polymers (HPPs) based on polyether ether ketone (PEEK), polytetrafluoroethylene (PTFE), polyimide (PI), and aromatic thermosetting co-polyester (ATSP) were selected for tribological experiments at extreme temperatures ranging from -196 to 300°C, simulating extreme operating conditions that bearing materials in space will encounter. The efficacy of adding solid lubricants such as PTFE, graphene nanoplatelets (GNPs), and graphite to ATSP polymer matrix was studied, and the best lubricant composition was selected. The addition of GNPs and PTFE was shown to significantly decrease the friction and improve the wear resistance of the polymer composite, compared to neat ATSP. The developed transfer film and its characteristics were found to substantially affect the tribological performance. Inspired by the beneficial effects of this "transfer layer," a novel method was proposed to deposit the

polymer coating on both pin and disks to simulate polymer coating sliding on pre-deposited “transfer layer.”

ATSP polymer composite was shown to outperform the other groups of HPPs with low coefficient of friction and unmeasurable “zero” wear from cryogenic to high temperatures (-196°C to 300°C) under dry sliding conditions, expanding the application of the polymer to 500°C temperature range. In addition, polymer-on-polymer sliding significantly mitigated the sand and dust accumulation at the interface, which is advantageous for Lunar/Mars explorations. The work contributes to the current and future research on the development of HPPs for space exploration devices and other engineering applications that require operation under extreme environments.

ACKNOWLEDGEMENTS

I would like to express my sincere and deepest gratitude to my research advisor Prof. Polycarou for being a remarkable mentor during my degree program and also in my personal life. I would like to thank my committee members Prof. Ali Erdemir, Prof. Mohammad Naraghi, Prof. Matt Pharr, and particularly my advisor Prof. Andreas A. Polycarpou, for their valuable guidance, support, and encouragement throughout this research.

I would like to thank my friends and colleagues, especially my research group members in the Microtribodynamics laboratory, for their help and friendship. I would also like to thank the department faculty and staff for making my time at Texas A&M University a great experience.

I would like to acknowledge the support from Small Business Innovation Research (SBIR) by NASA for providing the financial support for this research. In addition, I would like to thank Dr. Pixiang Lan, Dr. Malcolm Stanford, and Dr. Samuel Howard for their valuable suggestions during this research. I would like to also acknowledge the use of the Texas A&M Materials Characterization Facility (MCF), for the access to SEM, EDS, and XPS Instruments.

Last but not least, my warmest thanks to my wonderful wife and parents for their faith in me, unconditional love, constant support, and encouragement throughout my education journey.

CONTRIBUTORS AND FUNDING SOURCES

This work was supervised by a thesis committee consisting of the committee chair Prof. Andreas A. Polycarpou, and committee members, Prof. Ali Erdemir, and Prof. Matt Pharr of the J. Mike Walker ’66 Department of Mechanical Engineering and Prof. Mohammad Naraghi of the Department of Aerospace Engineering.

The studies in this thesis were conducted with the help of Dr. Pixiang Lan from ATSP Innovations, where the materials were supplied. Funding of the studies in Chapter 4 and Appendix A was provided by Small Business Innovation Research (SBIR) Phase I contract No. 80NSSC19C0517 from the NASA Glenn research center. Funding of the works in Chapters 5 and 6 was provided by Small Business Innovation Research (SBIR) Phase II contract No. # 80NSSC20C0180. All other work conducted in the thesis was completed by the student independently.

NOMENCLATURE

ATSP	Aromatic thermosetting co-polyester
PTFE	Polytetrafluoroethylene
PEEK	Polyether ether ketone
PI	Polyimide
FC	Fluorocarbons
FP	Fluoropolymer
PA	Polyamide
Al	Aluminum
Ti	Titanium
GNPs	Graphene nanoplatelets
HPPs	High performance polymers
HPPCs	High performance polymer coatings
COF	Coefficient of friction
μ	Friction coefficient
SEM	Scanning electron microscopy
EDS	Energy dispersive X-ray spectroscopy
XPS	X-ray photoelectron spectroscopy
DSC	Differential scanning calorimetry
DMA	Dynamic mechanical analysis
TGA	Thermogravimetric analysis

XRD	X-ray diffraction
ESP	Electrical submersible pumps
ESD	Electrostatic spray deposition
HVLP	High volume low pressure
Tg	Glass transition temperature
Tm	Melting temperature
ITR	Interchain transesterification
NMP	N-methylpyrrolidone
HTT	High temperature tribometer
HPT	High pressure tribometer
L	Total sliding distance
k	Wear rate
V	Wear volume
F_N	Normal load
Δm	Mass loss
ρ	Density
V	Wear volume
N_2	Nitrogen
LN_2	Liquid nitrogen
S_q	Root-mean-square roughness
S_{sk}	Skewness
RT	Room temperature

TABLE OF CONTENTS

Page

LIST OF FIGURES

Page

LIST OF TABLES

Page

CHAPTER 1

INTRODUCTION AND OBJECTIVES

1.1 Introduction

High performance polymers (HPPs) are materials at the top of the polymer pyramid: Among these materials, PEEK, PTFE, and Polyimide (PI), are recognized as the most attractive thermoplastics. Some of the properties that make them stand out in different technological applications are (a) high load-bearing capacity, (b) high operating temperature, (c) excellent dimensional stability due to small changes in volume by the influence of temperature and pressure, and (d) acceptable values of coefficient of friction (COF) and wear rates [1–10]. ATSP is another HPP that possesses good mechanical properties and chemical resistance, combined with low wear rates and low COF, when blended with PTFE [11–13]. It has been shown that high performance polymer coatings (HPPCs) based on PEEK, PTFE, and ATSP blended with solid lubricants can withstand high bearing loads and provide self-lubrication. This is due to their ability to form tribofilms by transferring material to the hard metal asperities of the counterpart, thus reducing friction and wear at the sliding interface [14,15]. HPPCs possess the advantage of deposition onto metallic substrates in the tenths of microns range (20-40 μm), where it has been shown that this thickness range is sufficient to form a well adhered and robust transfer film [16–18]. Inspired by the phenomenon of polymer transfer film, one can pre-deposit such transfer layer on the counterpart to form a polymer-on-polymer sliding from the beginning. In a study by the author (as will be discussed in chapter 2), the beneficial

effect of the pre-deposited film is indicated by performing pin-on-disk experiments. The results showed the beneficial effect of the pre-deposited transfer layer of ATSP in decreasing the friction and wear, stabilizing the contact, increasing the load-bearing, and protecting the metallic surface [19].

PEEK, PTFE, and ATSP in powder form can be blended with solid lubricants and be applied as coatings by electrostatic deposition on traditional engineering substrates, such as gray cast iron, sintered iron, bronze, and aluminum [16,20]. A literature review shows that in the last decade, a great effort has been made to study and understand the tribological behavior of HPPs and HPPCs under different conditions of normal load, sliding velocity, temperature, and pressure (using different atmospheres). Overall, these studies report that engineering substrates coated with HPPCs such as PEEK, PTFE, and ATSP are very promising in different technical and industrial applications. Specifically, under boundary/mixed lubrication regime, or in the absence of lubricant, metallic asperity interactions can be avoided by formation of transfer films from polymer to metal at the sliding interface [21]. In a study by the author (as will be discussed in chapter 3), it was shown that the formation of such transfer film is highly beneficial for improved tribological performance, especially at elevated temperatures.

To illustrate the importance of HPPs and HPPCs, for instance, in low earth orbit (LEO) space environments, when a spacecraft passes through the earth´s shade side, it suffers thermal cycling due to cryogenic changes in temperature, which can lower the self-lubricating capability of HPPs and their thermal and structural stability. Also, under LEO conditions, components made from HPPs are exposed to degradation caused by atomic

oxygen (AO), ultraviolet (UV) radiation, and high vacuum, which can negatively impact the tribological, thermomechanical and optical properties, and also erode the polymer surface, thus reducing their useful lifespan [22–25]. Moreover, advanced materials are used in the oil and gas industry for tilting pad bearings in electrical submersible pumps (ESP), where tribological problems are caused when the oil film breaks down, causing seizure of the hydrodynamic bearings by the action of rock debris in the pump seals [14]. In this regard, HPPs and HPPCs become an attractive solution in this industrial sector, where in the absence of lubricant they can provide self-lubricity and avoid scuffing or galling of the sliding components [20].

The given background on HPPs tribological properties indicates the effectiveness of self-lubricating polymer composites as bearing and tribological surfaces in applications where the liquid lubricant is infeasible. An example of this situation is in space-related exploration devices where significant variations in environmental temperature and atmosphere occur.

1.2 Background and challenges

According to NASA, there is an interest in expanding NASA's ability to explore the deep atmosphere and surface of the giant planets, rocky planet/moon surfaces, asteroids, and comets through the use of long-lived (days or weeks) balloons and landers. As planned, Dragonfly will launch in 2026 and arrive in 2034 on Titan; by drilling, collecting, and analyzing samples. The mission is looking for prebiotic chemical processes common on both Titan and Earth. Mars sample return is a proposed mission to return samples from the surface of Mars to Earth. Europa Lander is a concept for a potential

future mission that would look for signs of life in the icy surface material of Jupiter's moon Europa. Conceptual landing probes for Venus have been proposed and it will be equipped with a heat-resistant drilling, sampling system that can take Venusian soil samples for analysis. The Artemis program will land the first woman and next man on the Moon by 2024; then, NASA will take the next giant leap – sending astronauts to Mars [26]. However, the missions would experience extreme temperatures - ranging from cryogenic temperatures of -220 °C on Europa to upwards of 462 °C on Venus. In addition, the environmental pressures range from vacuum on the Moon to 9.3 MPa on Venus. Traditional oil lubricants and greases are infeasible at extreme temperatures, resulting in dry sliding conditions that generally have significant detrimental effects on component performance; in addition to different atmospheric pressure, composition, and abrasive dusty environments, the complexity is further compounded.

For example, “dust is the number one concern in returning to the Moon,” Apollo 16 Astronaut John Young, July 2004 [27]. The Moon is covered by large amounts of dust particles, called regolith, which could cause severe problems for tribological components on the Moon [28]. Because Mars and the Moon have large temperature spans during day and night, in addition to the abrasive study, the effect of temperature should be taken into account to better understand their tribological performance in combination with abrasive dust. The ATSP-based coating has shown good sand abrasive wear resistance due to its high elastic recovery rate observed in scratch tests [20]. That is, durable high bearing polymer coatings can be a good solution for aggressive dusty conditions.

The compositions of solid materials on Titan's surface are still essentially unknown [29]. The Dragonfly rotorcraft will be equipped with a rotary-percussive drill that can drill fast, acquire samples and feed the samples through a pneumatic tube to a mass spectrometer for composition analysis [29,30]. For the rotary-percussive drill, the percussion movement is achieved by a cam-follower structure. However, due to the high stress contact, the lubrication coatings on the cam (Magnaplate Nedox SF-2) and follower (Magnaplate Nedox FM-5) did wear out quickly or delaminated from the substrate in test runs targeted for sampling on Mars, as shown in **Figure 1** [31]. An updated design had the canted follower matching the cam's slope, thus decreasing the contact stress, but at the release location, the contact is still severe, and both coatings were worn out at the end of the test run [32]. In addition to the cryogenic temperature on Titan, this harsh contact condition could make cam-follower tribo-pair fail quickly. Polymers are good candidate materials because they become quite tough, and their wear resistance increases significantly under cryogenic conditions [33].

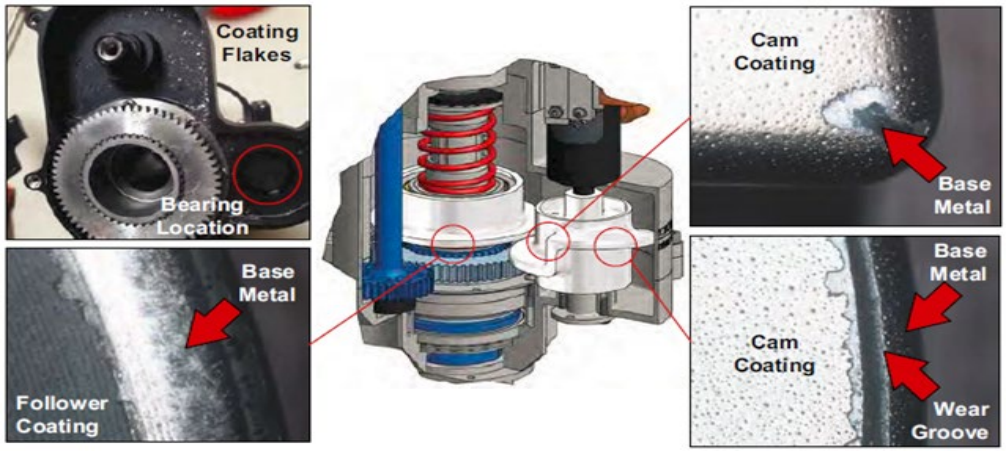

Figure 1. Coating failure issues for cam and follower in rotary-percussive drill [31].

As mentioned in **Figure 1**, the tribo-pair of Nedox FM-5 coating vs. Nedox SF-2 coating (both provided by General Magnaplate and coated on C300 alloy) showed delamination and wear for the testing run in the rotary-percussion drill. An updated design had the canted follower matching the cam's slope, thus decreasing the contact stress; but at the release location, the contact is still severe, and both coatings were worn out at the end of the test run [32]. In this research, as polymer becomes very tough and their wear resistance becomes much higher under cryogenic conditions [33], we propose to use two polymer coatings (ATSP-based and PEEK/PTFE coating) with polymer vs. polymer and polymer vs. metal sliding as a potential solution.

1.3 Objectives and outlines

The objective of this research is to investigate the tribological performance (friction and wear) of advanced bearing polymers in extreme temperature conditions, simulating the conditions that the bearings in remote sensing applications will encounter in the space for missions to Moon/Mars and Titan. The tribological study is largely dependent on experimental research that simulates the actual space-relevant environments. Therefore, to achieve this objective, this research will focus on a comprehensive experimental plan (as shown in **Figure 2**) to investigate and compare the tribological (i.e., friction and wear) response of selected tribo-pairs consisting of HPPs such as ATSP-based, PEEK-based, PTFE-based, and PI-based polymers. The lists of evaluated materials and their compositions are provided in **Table 1**.

Table 1. Description of blended polymer materials (e.g., coating and bulk) studied in this research.

Material	Composition
Coating	CB2AB2 + 5 wt% of Chemours Zonyl MP1300 PTFE
	C2A1 + 7.5 wt% of Chemours Zonyl® PTFE (5 wt% MP1300/2.5 wt% MP1100)
	C2A1 + 5 wt% GNPs (xGnP®, Grade M)
	Unreinforced C2A1
	PEEK (VICTREX® PEEK 150XF) + 20 wt% PTFE
	DuPont® 958G-303 (Fluoropolymer, Exact composition details are not known)
Bulk	Unreinforced polyamide 66 (Nylon 6,6)
	CBAB + 30% Graphite + 10% PTFE
	Vespel® (polyimide) + 25% PTFE/graphite
	PEEK + 30% Carbon fiber/graphite/PTFE

This research will contribute to introducing innovative polymeric products for bearing and sealing applications for extreme environmental conditions encountered in space environment. The particular emphasis here is to find the best performing polymer that yields a controlled and improved tribological performance over a wide range of temperatures from -196 to 300 °C spanning a range of almost 500 °C. In addition to extreme tribology experiments, the following characterizations were performed to obtain a fundamental knowledge of tribological performance and to find correlations with the tribological experiments: (1) (thermo)mechanical characterizations such as Nano/Micro-indentation, DMA, and TGA, and (2) morphological and chemical characterizations in and outside of the wear tracks such as optical microscopy, surface profiling, SEM/EDS, XPS, etc.

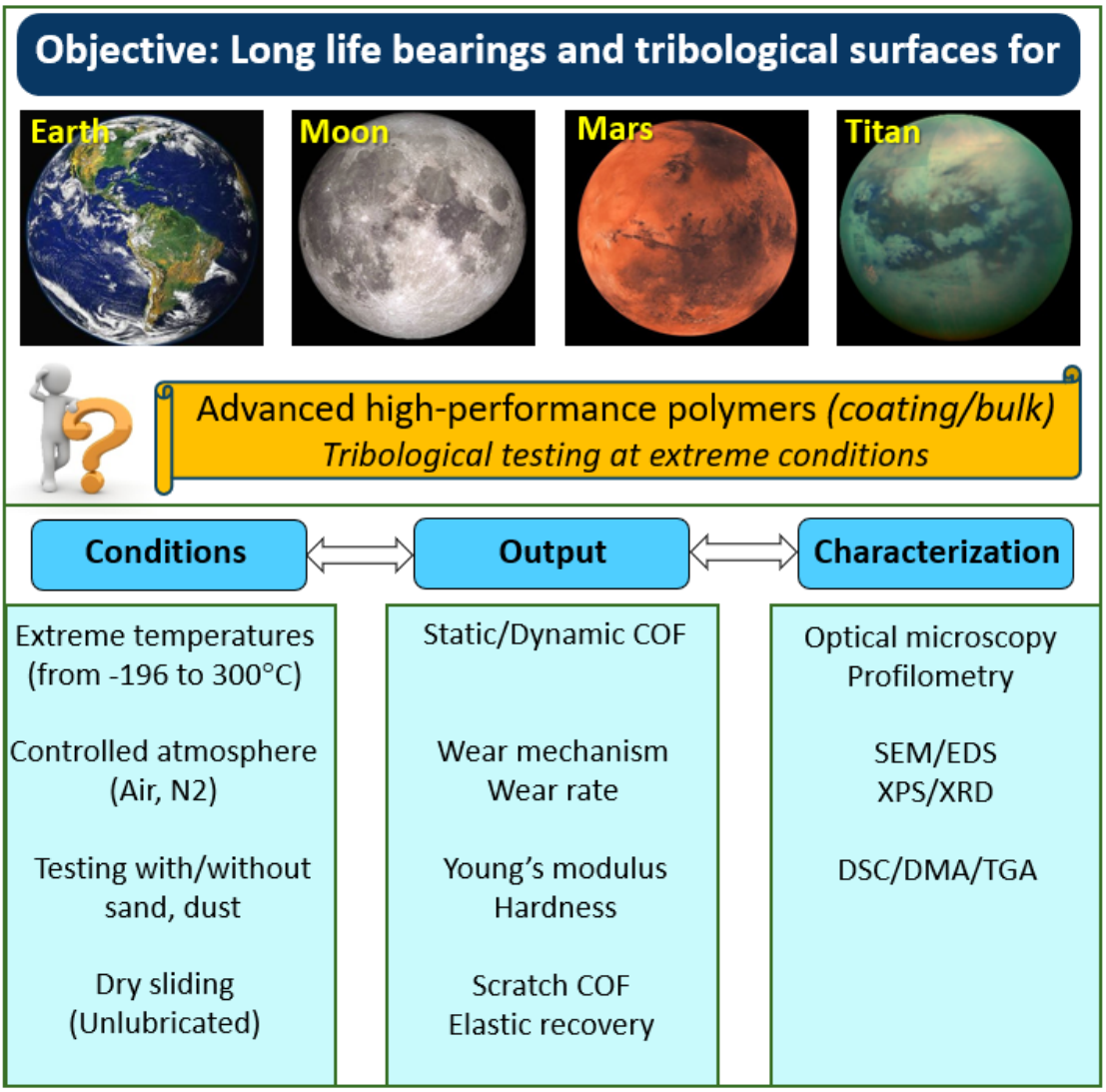

Figure 2. Research outline.

According to the outlined research flow chart shown in **Figure 3**, the current thesis can be divided into the following chapters:

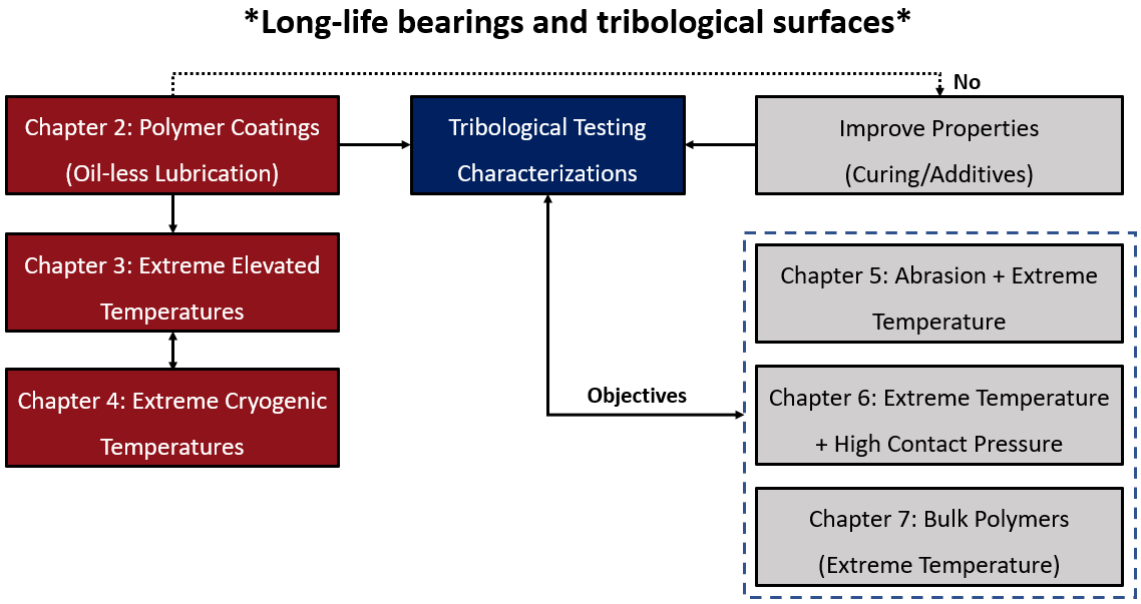

Figure 3. Flow chart of current research.

Chapter 2 explores the efficacy of the ATSP-based polymer coating to be applied as bearing material and to enhance the tribological performance for oil-less engineering applications. The Telescope base is chosen as a case study that composes of polyamide (PA) vs. stainless steel. The bare steel is coated with ATSP/PTFE polymer, and experiments are conducted using pin-on-disk configuration and dry sliding conditions.

Chapter 3 studies the effect of temperature on friction and wear of ATSP-based coating by performing pin-on-disk experiments from room temperature to 300 °C. The influence of adding solid lubricants such as graphene nanoplatelets (GNPs) and PTFE is studied, and the changes in friction, wear rate, wear mechanism, and transfer film formation are discussed as well.

The motivation behind the work in chapter 4 arises from the demonstrated performance of ATSP-based polymer coating in Chapter 2 and 3, namely low COF and

wear in a wide temperature application range from room temperature to 300 °C. In addition, the findings in Chapter 2 show that deposition of ATSP coating on bare steel can significantly improve the tribological performance of PA due to the beneficial effects of "transfer layer," which can efficiently reduce the friction. Therefore, in Chapter 4 the effectiveness of polymer-on-polymer sliding on friction and wear reduction is investigated over a wide range of temperature ranges from -196 to 300 °C for HPPs such as ATSP/PTFE, PEEK/PTFE, and Fluoropolymer coatings. Based on experimental findings in this Chapter, two best-performing tribopairs (i.e., ATSP/PTFE and PEEK/PTFE) are proposed for Lunar/Mars abrasive experiments and Titan simulated environment studies in Chapter 5 and 6, respectively.

The capability of ATSP and PEEK polymer coatings under dry sliding sand-dust abrasive environment is discussed in Chapter 5. Lunar regolith is used to simulate the dusty environment on Moon/Mars, and the temperature is varied from -150 °C up to 110 °C to account for the effect of temperature. Three configurations, namely metal-on-metal, metal-on-polymer, and polymer-on-polymer are employed to identify the best interface that leads to dust mitigation at the maximum level.

Since the dragonfly mission is to acquire samples on both Lunar/Mars and Titan, an experimental plan is developed in Chapter 6 to capture the properties of the suggested coatings in the temperature range of -180 °C to 110 °C to cover the environmental temperatures in all foregoing planets. Experiments are conducted using curved pin-on-disk configuration to simulate higher Hertzian contact pressure in the cam-follower.

Due to the high Hertzian contact pressure, the polymer coating on the pin might not be as durable as the coating on the disk, particularly under sand abrasive conditions. Therefore, it is necessary to evaluate the performance of similar polymers in the insert or bulk shapes and compare the performance with coatings. To this end, the bulk HPPs based on ATSP, PEEK, and PI are machined into pin shape, and their temperature tolerance is studied in Chapter 7 up to 300 °C and under dry sliding conditions.

CHAPTER 2

TRIBOLOGICAL PERFORMANCE IMPROVEMENT OF POLYAMIDE AGAINST STEEL USING POLYMER COATING[1]

2.1 Introduction

Owing to the specific and unique features of polymers such as low friction, self-lubrication, low cost, ease of manufacturing, good resistance to corrosion, and reduced level of vibration [34–40], an increasing tendency has been burgeoning to replace or coat metals with polymeric materials, especially for tribological applications where the use of lubricant is infeasible. Thereby, numerous studies have been conducted on polymer versus metal sliding to measure the friction and wear properties [15,41–46]. In some cases, such as for corrosive environments and weight reduction, there would be interest to replace the polymer on metal with a polymer on polymer sliding either in self-mating or in combination with another polymer. Nonetheless, there is insufficient information in the literature, especially for tribology of bulk polymers on polymer coatings.

Limitations on operating temperature, thermal conductivity, and pressure × speed (PV) values for polymers are amongst the main disadvantages that need to be considered for proper selection of tribo-pairs [47]. During sliding of tribo-pairs, the dissipated energy shows itself by the generation of heat (frictional heating) and deformation of the tribo-

[1]Reprinted with permissions from "Bashandeh K, Lan P, Polycarpou AA. Tribological performance improvement of polyamide against steel using polymer coating. Tribology Transactions. 2019;62(6):1051-62."

contacts [48–50]. Polymers are susceptible to this frictional heating in a way that a small change in the temperature can change their phase from glassy to rubbery, especially when they are operating near their glass transition temperature. Deposition of a thin layer of a polymer on a metal surface, i.e., polymer coating, rather than a complete bulk polymer could further reduce the generated heat by its transition through the steel body. This chapter focuses on the role of polymer coatings on steel substrates and the improvement of their tribological behavior, while in contact with another (bulk) polymer. An advanced bearing polymer, aromatic thermosetting co-polyester (ATSP) is selected as the coating material to serve as an oil-less solution to improve the tribological performance, and bulk polyamide 66 (PA66, or sometimes referred as nylon 6,6) as the second tribo-pair (due to its usage as a good frictional material).

Previous studies on ATSP coatings showed extremely low wear rate, especially under boundary lubrication conditions [51] and improved performance at temperatures from -160 °C to 260 °C under dry sliding conditions [33,52]. PA is a crystalline polymer being used in numerous industrial applications to reduce friction and wear in parts such as gears, bearings, and spacers in pipelines [53,54]. This widespread use is mainly due to PA's advantages such as high strength, good wear resistance, and low weight [55,56]. The literature is abundant with tribological experimental studies on using different composition and additives for PA sliding against steel or PA on another polymer with coefficient of friction (COF) values ranging from 0.2 - 1.2 [37,57–62]. However, no attention has been given to modify the surface of the steel with depositing a thin layer of

a polymer coating and the literature is absent as far as PA sliding against polymer coatings, especially at elevated temperature conditions.

The objective of this chapter is to investigate how the application of a polymer coating on a steel surface changes the friction and wear properties, compared to sliding of PA on bare steel, as is the case in applications today. An example is the base of telescope application, which has a PA versus bare metal contact with service temperatures up to 80 °C. To account for the effect of temperature, the experiments were carried out from room temperature to 80 °C. The wear and friction properties of PA, as well as the coating are discussed considering the changes in the environmental temperature.

2.2 Experimental

2.2.1 Materials and sample preparation

disks were machined out of 418 stainless steel with a diameter of 50.8 mm and thickness of 6.35 mm. The surface was machined to a root-mean-square surface roughness Rq = 0.135 µm using a grinder. Unreinforced PA66 was used as the pin material with a radius of 6.4 mm and length of 7 mm. The disks and pins were used as the rotating and stationary parts, respectively. The ATSP powder was prepared by mixing of two oligomer precursors of CB2 and AB2, with carboxylic and acetoxy end groups, respectively. The two precursors were ground and sieved with a 90 µm screen and mixed with a weight ratio of 1:1. Then, the powders were blended with 5 wt.% of DuPont Zonyl® MP1300 PTFE powder, with an average size of 12 µm (10 wt.% of the powder size is below 3 µm, and 90 wt.% below 25 µm). The PTFE additive is used to reduce friction. The blended powder was then coated on the surface of the sandblasted steel disk using an electrostatic spray

deposition (ESD) method. The disks were subsequently cured in an oven at a temperature of 270 °C for 30 min, and the final thickness of the coating was measured to be around 30 ± 5 µm. The thickness was measured by the vendor using a coating thickness gauge. The 30 µm thickness was selected because it was shown to be an optimum thickness for excellent performance in earlier studies for ATSP and other polymeric-based coatings [33,52,53,63]. Bearing-grade polymeric coatings with lower thickness values may not provide full and uniform coverage of the whole sandblasted surface. In addition, it could wear out too quickly. Thicker coatings could generate porous structures, which result from outgassing of the curing process. Typical photographs of a PA pin, a steel disk, and a coated steel disk, and a PA pin are shown in **Figure 4(a, b)**. The roughness of the steel disk and ATSP coating were measured using a Tencor P6 profilometer with 10 mm scan length. The steel disk and coating have Rq values of 0.135±0.01 µm and 4.32±0.24 µm, respectively.

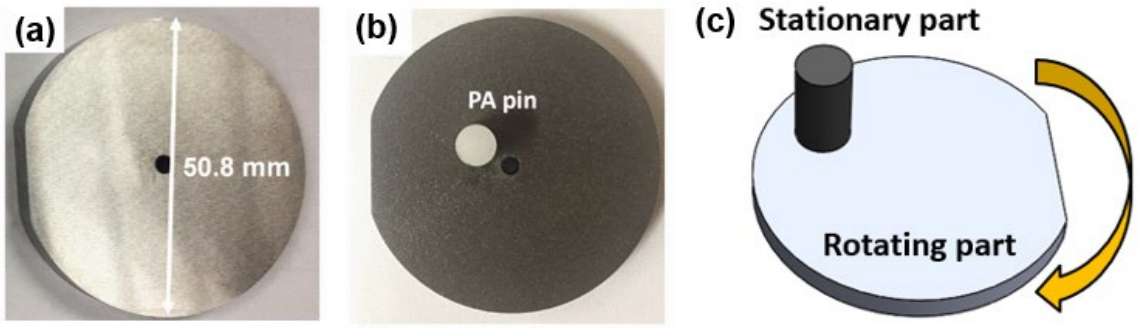

Figure 4. (a) uncoated disk, (b) ATSP coated disk with PA pin on top, and (c) Experimental configuration. Modified with permissions from "Bashandeh K, et al. Tribological performance improvement of polyamide against steel using polymer coating. Tribology Transactions. 2019;62(6):1051-62."

To clean the samples from any contaminants and debris, before each experiment, the samples were immersed in a glass jar full of acetone (for steel) and isopropyl alcohol (for ATSP coating and PA pin) and placed in an ultrasonic cleaner for 10 min at 50 °C. Then, they were rinsed and dried using warm air. Isopropyl alcohol instead of acetone is used for the polymers to prevent any discoloration or degradation. The same process was performed at the end of each experiment. The mass of each PA pin was measured (with a 0.01 mg precision scale) before and after each experiment to calculate the resulting wear rate.

2.2.2 Experimental procedure

The experimental conditions are summarized in **Table 2**. The experiments were performed using a nominally flat pin and disk configuration (**Figure 4(c)**), simulating a nominally flat contact between tribo-pairs. All experiments were performed under dry sliding conditions with ambient pressure. Specifically, two different types of experiments were performed: (a) constant load wear experiments to measure the friction and wear properties and (b) step-loading (scuffing) experiments to measure the load-bearing capacity of the tribo-pairs. To measure the influence of environmental temperature on the tribological behavior of PA, three temperatures, namely 25 °C, 50 °C, and 80 °C were selected for each tribo-pair for the wear experiments.

Table 2. Tribo experimental conditions. Reprinted with permissions from "Bashandeh K, et al. Tribological performance improvement of polyamide against steel using polymer coating. Tribology Transactions. 2019;62(6):1051-62."

Experiment type	Material (pin vs. disk)	Speed, rpm (linear speed, m/s)*	Temperature (°C)	Contact pressure, MPa (load, N)
Wear	PA on ATSP	13.5, 27, 54, 108 (0.025, 0.05, 0.1, 0.2)	25, 50, 80	15 (483)
	PA on Steel			3 (97)
Step-Loading (Scuffing)	PA on ATSP	54 (0.1)	25	4 MPa/min (129 N/min)

*The linear speeds are calculated based on 18 mm average radius for the wear tracks

For the wear experiments, the normal load was constant, and was substantially lower for the PA-steel tribo-pair. This is to minimize the frictional heating and deformation of the PA, while sliding on bear bare steel. Note that, when we conducted a PA-steel experiment under higher normal load at room temperature, the PA bulged and was unable to perform the experiment. A normal load of 483 N was selected for the PA on ATSP coating to simulate the extreme loading condition in the real application and 97 N for the PA on steel (corresponding to nominal contact pressures of 15 and 3 MPa, respectively). The sliding speed profile is shown in **Figure 5(a)**: four different sliding speeds (0.025, 0.05, 0.1, 0.2 m/s) were applied for 1 min before and after the one-hour duration wear experiments (with a speed of 0.1 m/s). The choice of experimental parameters were based on the conditions at the base of telescope application, which has a PA versus bare metal contact. Since the base of telescope moves at different speeds up to 0.1m/s, we needed to know the speed effect on the COF. The experiments were repeated at least Each experiment was performed two times to ensure repeatability. For the step-loading (or scuffing) experiments, the normal load was increased by 4 MPa/min at a

constant sliding speed of 0.1 m/s. The load function is shown in **Figure 5(b)**. The load started from 129 N and terminated at 1032 N. Since PA did not survive against steel with the same loading condition as ATSP, the scuffing step-loading experiments were performed only for PA-ATSP tribo-pair at room temperature to examine the maximum load in which the PA could survive by the deposition of the coating.

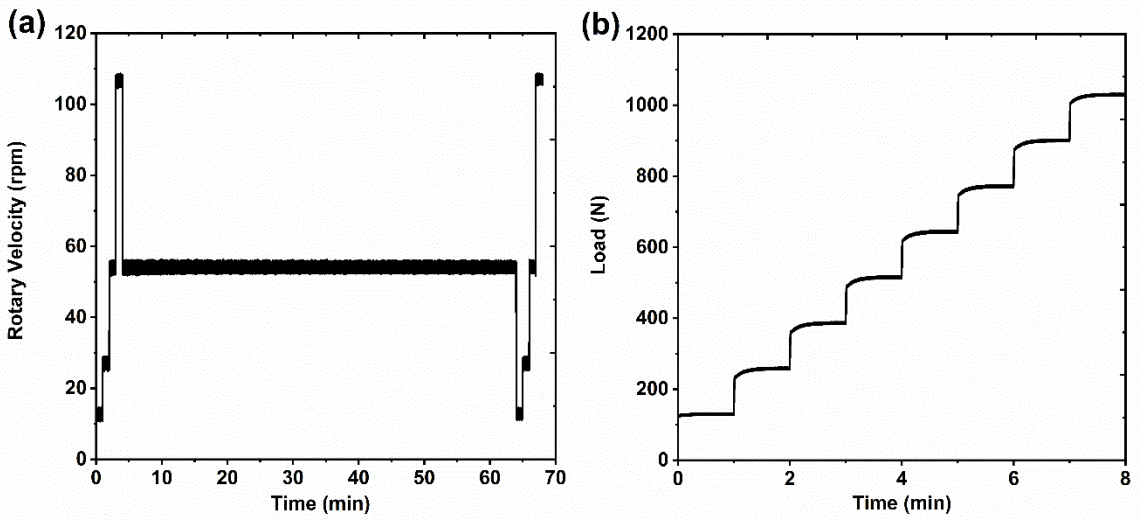

Figure 5. Applied (a) rotational speed for constant load wear experiments, and (b) normal load for step-loading experiments. Reprinted with permissions from "Bashandeh K, et al. Tribological performance improvement of polyamide against steel using polymer coating. Tribology Transactions. 2019;62(6):1051-62."

2.2.3 Surface characterization and wear measurements

To analyze the wear mechanisms, the worn and unworn surfaces of the samples, as well as the transfer layers, were examined using optical microscopy, scanning electron microscopy (SEM), and energy dispersive X-ray spectroscopy (EDS). SEM-EDS analyses were performed in a JEOL JSM-6060LV. A Tencor P-6 stylus profiler was used to measure the changes on the surface profiles on the steel disks and the ATSP coating. These

measurements were used to obtain the surface profiles after the transfer of PA film and to calculate the wear volume and the resulting wear rate for the ATSP coating. Profilometric line scans were performed across the wear scars at four different locations to obtain an average value. The total length of each scan was 13 mm including the 6.4 mm wear track. For a detailed description of the wear measurements, see Ref. [53].

The PA wear was measured based on the change in mass before and after the experiment. The wear rate based on the wear volume was then calculated using the following equation:

$$k = \frac{\Delta m}{L.F_N.\rho}$$

Where k is the wear rate (mm^3/Nm), Δm is the mass loss (mg), L is the total sliding distance (m), F_N is the applied normal load (N), and ρ is the density of PA (g/cm^3).

2.3 Results and Discussion

2.3.1 Constant load wear experiments: Friction

Figure 6(a) shows the in-situ COF with sliding time for the PA on ATSP coating and the PA on steel surface under the environmental temperatures of 25, 50, and 80 ºC and dry sliding conditions. From **Figure 6(a)**, the PA on ATSP is showing a very stable COF at all temperatures. No running-in period is observed for the temperatures of 25 and 50 ºC, as the experiments show steady-state behavior from the start. At 80 ºC, the COF shows 5min running-in period followed by a steady-state condition. The variation of the COF by change of speed is clearly observed while this is not evident for the PA on steel. In fact, the sliding of the PA on steel needs a longer time to reach a steady-state, and variation of the COF is also much higher compared to the ATSP coating even during steady-state period. These sharp peaks and instabilities in the COF lead to vibration and

squeaking noises during the sliding, which is entirely resolved by deposition of the ATSP coating on the steel surface. A significant improvement in friction is achieved by deposition of the ATSP coating. The friction remains stable during the whole sliding time for the PA sliding against ATSP coated steel disk with 80% reduction in the COF compared to the PA on steel.

Figure 6(b) shows the average COF for PA-ATSP and PA-steel combinations at different temperatures for the last 30 min in the one-hour duration experiments. The error bars designate the standard deviation of the averaged calculated COF in the experiments. An increasing trend in the COF with temperature is observed for PA-steel with a sharp increase at the highest temperature. For PA-ATSP, the dependency of the COF to temperature is negligible. The COF increases slightly from 0.113 at 25 ºC to 0.133 at 50 ºC and then decreases slightly to 0.122 at 80 ºC. This reduction could be attributed to the decrease of the shear strength of the PA at 80 ºC due to passing its glass transition temperature (Tg), and softening of the polymer. As the temperature increases, two phenomena occur: softening of the polymer as the temperature approaches the Tg, and reduction of the polymer elastic modulus. The first factor decreases the COF due to lower shear strength and as a result a lower tangential force, while the second factor increases the COF due to the increase in contact area. For PA-ATSP at 80 ºC, the first one is the dominant factor in determining the COF although the difference in the COF is minute with lower temperatures. In the case of PA-steel, the degradation of mechanical properties of PA and the reduction of its elastic modulus is the dominant factor for the sharp increase of the COF. As shown in [64], the storage modulus of PA66 drops significantly with the

increase of temperature from 50 ºC to 80 ºC, compared to 25 ºC to 50ºC. At higher temperatures, when the PA became softer, with same normal pressure, the real contact area increased, resulting in more area involved in bond/debond of the junctions. Thus, even with lower shear strength at higher temperatures, the resistance increases because the increase in the real contact area is larger than the decrease in shear, resulting in increasing the COF.

Overall, a significant reduction in the COF is achieved with the deposition of a very thin high bearing polymeric (ATSP) coating. All the COF values are below 0.14 for PA-ATSP, indicating a 70-80 % reduction in the COF, compared to PA-steel. It should be mentioned that for polymer on polymer sliding, the generation of frictional heating is a major concern [65]. Deposition of a thin layer of polymer coating (around 30 μm) on a steel substrate addresses the heat conductivity issue, as the coating is very thin and heat is easy to pass through, and reach the main steel substrate, which has high thermal conductivity.

Shown in **Figure 6(c, d)** are the average COF values for PA sliding against ATSP coated steel disks and steel surfaces at sliding speeds of 0.025, 0.05, 0.1, 0.2 m/s denoted by V1-V4, respectively for different temperatures. The two bars at each speed show the COF before and after the one-hour duration experiment, and the error bars designate the standard deviation of the averaged calculated COF. The 1 min duration for each speed is to obtain a quick result for the speed influence on the friction before and after the one-hour wear experiment, and therefore the friction is not in its steady-state condition, particularly for PA on steel. Referring to actual/industrial applications, the original sample

before the one-hour test denotes a new tribo-pair, while the sample after the one-hour test represents a tribo-pair after usage. Thus, the speed effect study before and after the one-hour experiments supply useful information regarding friction resistance at different speeds at fresh and after usage status.

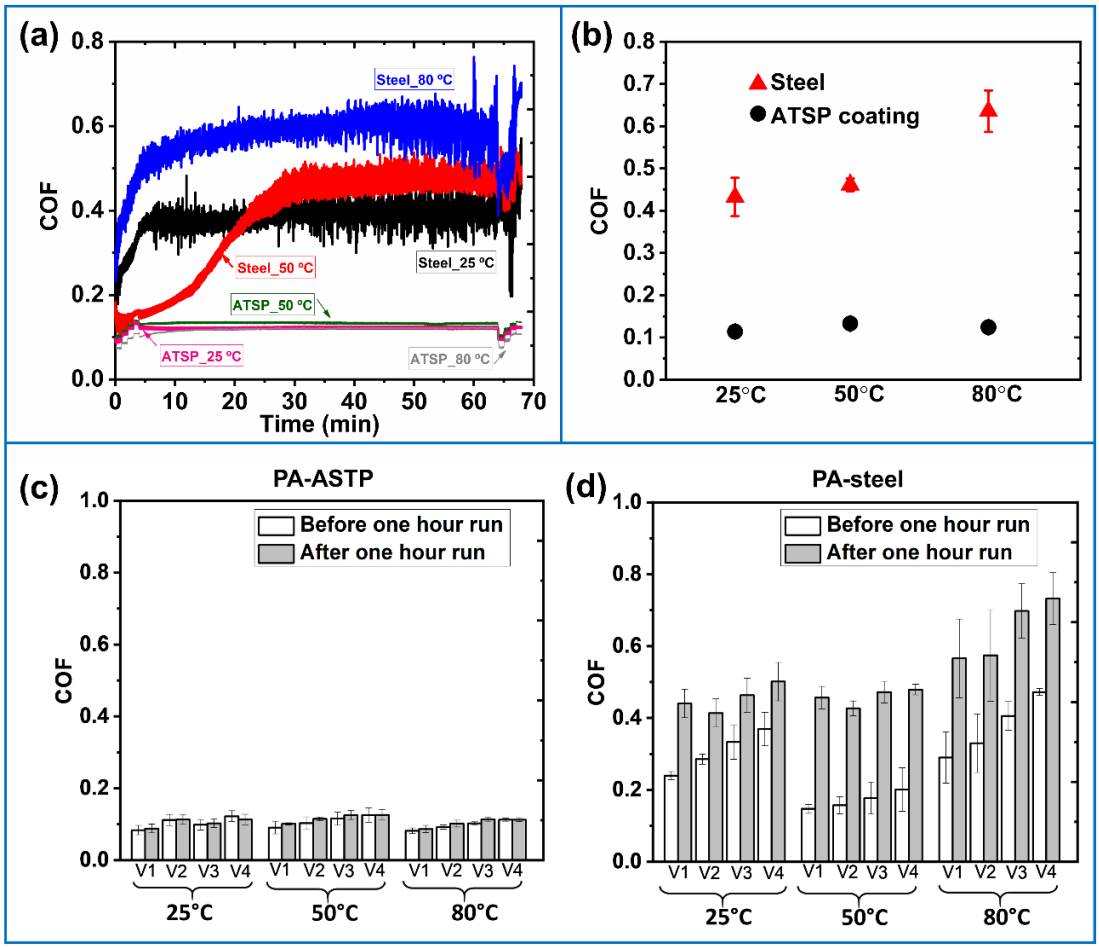

Figure 6. (a) In-situ COF at different environmental temperatures, (b) comparison of average COF for PA66 sliding on ATSP coating and steel disk, and (c, d) effect of sliding speed on the COF at different temperatures for PA66 pin vs. ATSP, and PA66 pin vs. steel disk, respectively. The error bars represent the ±1 standard deviation. Modified with permissions from "Bashandeh K, et al. Tribological performance improvement of polyamide against steel using polymer coating. Tribology Transactions. 2019;62(6):1051-62."

As shown in **Figure 6(c, d)**, for both ATSP coating and bare steel, in general, the COF increases with speed at all temperatures, in agreement with Ref. [37]. According to the friction model for viscoelastic polymers [66], higher speed increases the viscosity resistance of the polymer, thus increases friction. For the ATSP coating, the one-hour wear test does not affect the COF at different speeds, as shown in **Figure 6(c)**; however, as shown in **Figure 6(d)**, the COF at different speeds has a significant increase after the one-hour test; this increase is because of the transfer layer developed on the steel surface.

The dissipation of frictional energy for polymeric materials generally occurs in two different zones: the interface zone and the cohesive zone, which determine the friction caused by mainly adhesion and deformation, respectively [39]. The adhesion term results from formation and breakage of junctions between the polymer and its counterpart and is responsible for friction, whereas deformation arises from polymer ploughing and hysteresis loss and controls the mechanism of wear and transfer of the polymer. These factors are dependent on the temperature, and their influence vary with temperature. For the ATSP coating, the PTFE lubricant additive has very small surface energy and thus the adhesion force is small; additionally, the low surface energy will stop the formation of transfer layer on the ATSP coating due to the PA. For the steel surface, at the beginning of the experiments, the adhesion term is low and the COF is also relatively low. However, when the PA material transferred to the metal surface, the adhesive force became stronger and thus the COF increased after run-in period, as seen in **Figure 6(d)**.

2.3.2 Constant load wear experiments: Wear

Figure 7 shows the average specific wear rate of the PA sliding against ATSP coated steel disks and steel surfaces. The wear rates were calculated from the average mass losses shown in **Table 3**. The error bars designate the standard deviation of the averaged calculated wear in the experiments. An increasing trend in the PA wear rate is observed for both counterparts. However, the amount of wear for the PA on ATSP is one order of magnitude lower than the PA on steel (10^{-6} to 10^{-5} $mm^3/N.m$), indicating the improvement on the wear resistance through deposition of the coating. During the sliding of the PA on steel, hard asperities of the steel surface can easily remove the polymer from the base compared to the ATSP. This polymer removal would be much easier by increasing the temperature since the PA is getting softer and the mechanical properties degrade, especially at 80 ºC, where the wear rate is increasing by 133 % compared to 50 ºC.

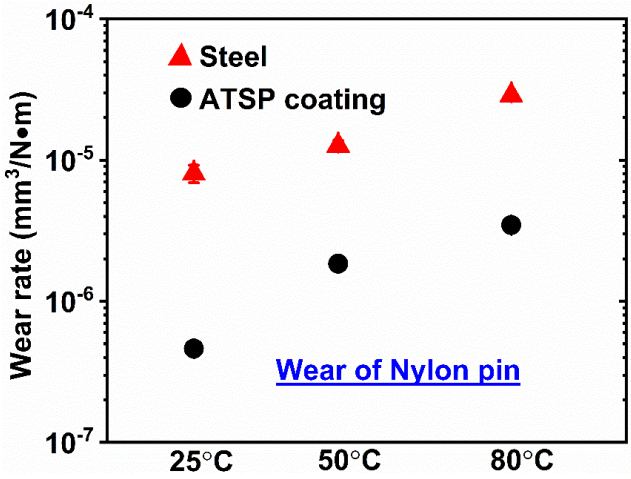

Figure 7. Comparison of wear rate of PA66 sliding on ATSP coating and steel disks. Note the scale is logarithmic for the wear rate axis. Reprinted with permissions from "Bashandeh K, et al. Tribological performance improvement of polyamide against steel using polymer coating. Tribology Transactions. 2019;62(6):1051-62."

Table 3. Measured values of mass loss for PA pins. Reprinted with permissions from "Bashandeh K, et al. Tribological performance improvement of polyamide against steel using polymer coating. Tribology Transactions. 2019;62(6):1051-62."

Material (pin vs. disk)	Temperature (°C)		
	25	50	80
	Mass loss (g)		
PA on ATSP	0.0001	0.0004	0.0006
PA on Steel	0.0004	0.0006	0.0012

Changes in the height inside the wear track can be observed from the wear scan measurements of the steel surface (shown in **Figure 8(a-b)**) at the temperatures of 25 ºC and 50 ºC, implying a discontinuous transfer of PA film to the subsurface. From **Figure 8(c)**, it is clear that smoothening of the surface is occurring with the increase of the temperature to 80 ºC, indicating filling up the valleys on the steel disk by the PA. This further supports the increase of the COF at 80 ºC. As the surface is getting smoother, the number of contact points and the resulting real contact area increases contributing to higher friction (due to higher adhesion force) [67]. SEM/EDS analysis provides further support on the effect of temperature on the COF and wear.

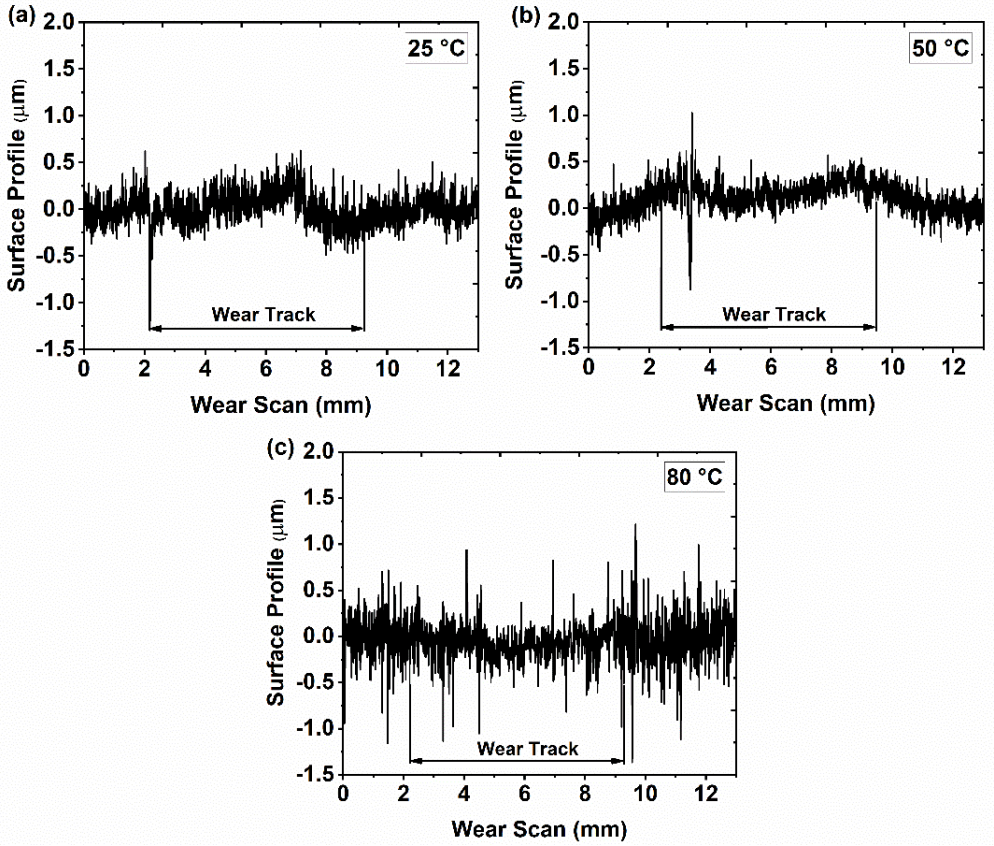

Figure 8. Representative profilometric wear scans of the steel disks after the experiments at temperatures of (a) 25 ºC, (b) 50 ºC, and (c) 80 ºC. Reprinted with permissions from "Bashandeh K, et al. Tribological performance improvement of polyamide against steel using polymer coating. Tribology Transactions. 2019;62(6):1051-62."

Figure 9(a-d) show typical wear scan profiles for the ATSP coating measured across the wear track at different temperatures after the experiments. The profiles show "zero wear" on the coating at all temperatures. Note the high initial roughness of the ATSP coating, which is a result of the specific deposition process. Since the profiles show unmeasurable wear after one-hour sliding, a longer duration (5-hour) experiment carried out at the temperature of 25 ºC with the same normal load and rotational speed as in **Table 2**. Nonetheless, no wear was still discernible from the profile (**Figure 9(d)),** indicating

high wear resistance of the coating. The COF during the 5-hour test is very stable with an average value of 0.1.

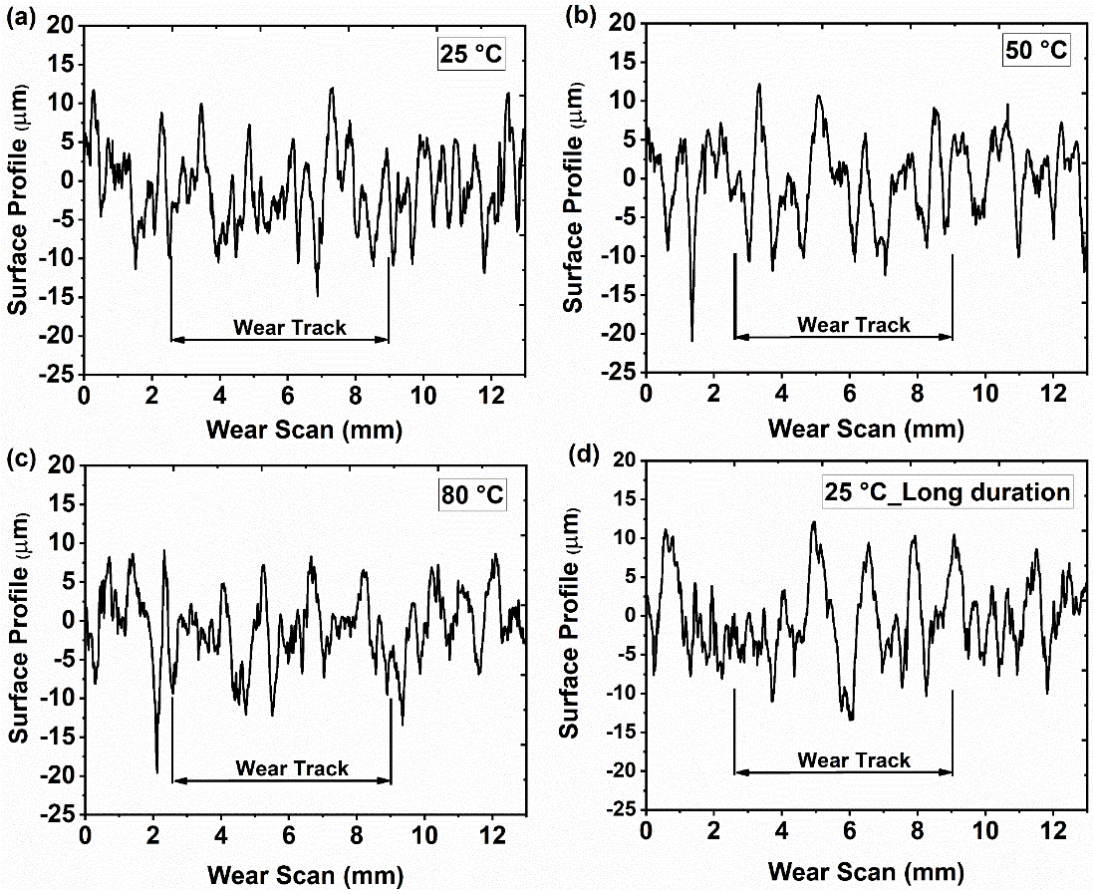

Figure 9. Profilometric wear scans of the ATSP coating after 1-hour long experiments at (a)25 ºC, (b) 50 ºC, (c) 80 ºC, and (d) 25 ºC for 5-hour of sliding. Reprinted with permissions from "Bashandeh K, et al. Tribological performance improvement of polyamide against steel using polymer coating. Tribology Transactions. 2019;62(6):1051-62."

Figure 10 shows optical microscopy images of the PA pin and ATSP coating for the temperatures of 25 ºC to 80 ºC. The only visible change is the formation of few mild abrasive marks on the surface of the coating as well as the pin, particularly at higher temperatures. The abrasive marks on the PA are because of two reasons; one is from the

stiffer ATSP coating's peaks scratching the PA, and the second is polymeric debris that was hardened by repeated plastic deformation during the sliding process, and then the hardened debris worked as third-body abrasive wear particles [8,68]. While for the scratches on the ATSP coating, the reason is mainly due to the hardened polymer wear debris since ATSP (tensile strength of 95 MPa) is stronger than PA (tensile strength of 69 MPa) and PA by itself is not easy to cause abrasive scratch on the ATSP coating.

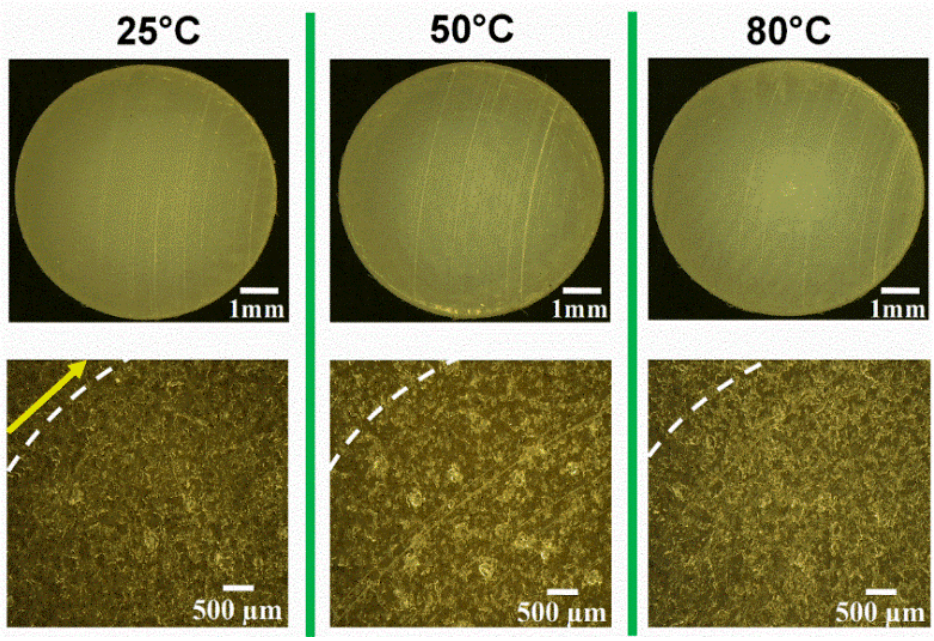

Figure 10. Optical microscopy images of PA66 pin and the ATSP coating (bottom images). The dash lines show the start of the wear track. The arrow shows the sliding direction. Reprinted with permissions from "Bashandeh K, et al. Tribological performance improvement of polyamide against steel using polymer coating. Tribology Transactions. 2019;62(6):1051-62."

2.3.3 Step-loading experiments

The constant load wear experiments showed nonmeasurable wear for the ATSP coatings. Hence, step-loading experiments were carried out under room temperature to

examine the maximum load-carrying capacity of the coating. The normal load was increased by 129 N every minute (4 MPa/min) until either the coating undergoes a wearing process or the PA deforms. The pin experienced a high deformation (1.3 mm increase in pin diameter) at the contact side by increasing the load to 1677 N. **Figure 11** shows the optical microscopy image of PA pin after the step-loading experiment. The pin plastically deformed at the contact with the increase of the load to 1677 N (52 MPa). However, when the load reduced to 1032 N (32 MPa) the pin stayed in good shape with only 0.2 mm increase in the diameter.

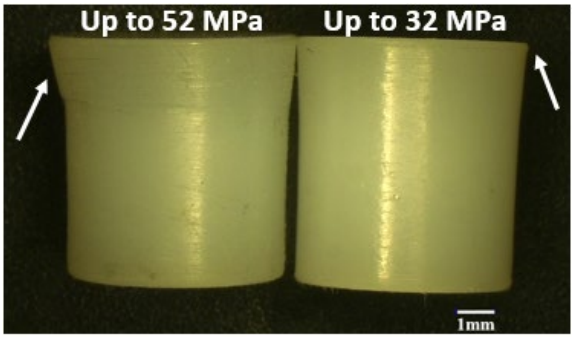

Figure 11. Optical microscopy images of the PA pin sliding against the ATSP-coated steel disc after the step-loading experiments. Reprinted with permissions from "Bashandeh K, et al. Tribological performance improvement of polyamide against steel using polymer coating. Tribology Transactions. 2019;62(6):1051-62."

Therefore, the final load was reduced to 1032 N (32 MPa). At this load, the pin diameter increased only by 0.2 mm. Still, under such loading conditions, no wear occured on the ATSP coating. **Figure 12(a)** shows the in-situ COF and wear scans of the coating after the experiments with the load function shown in **Figure 5(b).** The COF shows a decreasing trend with increasing normal load. For polymers with viscoelastic behavior, the COF varies with load according to the equation $\mu = K.N^{(n-1)}$ [69], where μ is the

COF, K is a constant, N is the normal load, and n is a constant within $2/3 < n < 1$. Based on this equation, the COF will decrease with the increase of normal load consistent with the results in this chapter. The comparison of the wear scans of the coatings for constant load wear experiments and step-loading experiments (**Figure 12(b)**) shows no change on the wear performance of the ATSP coating.

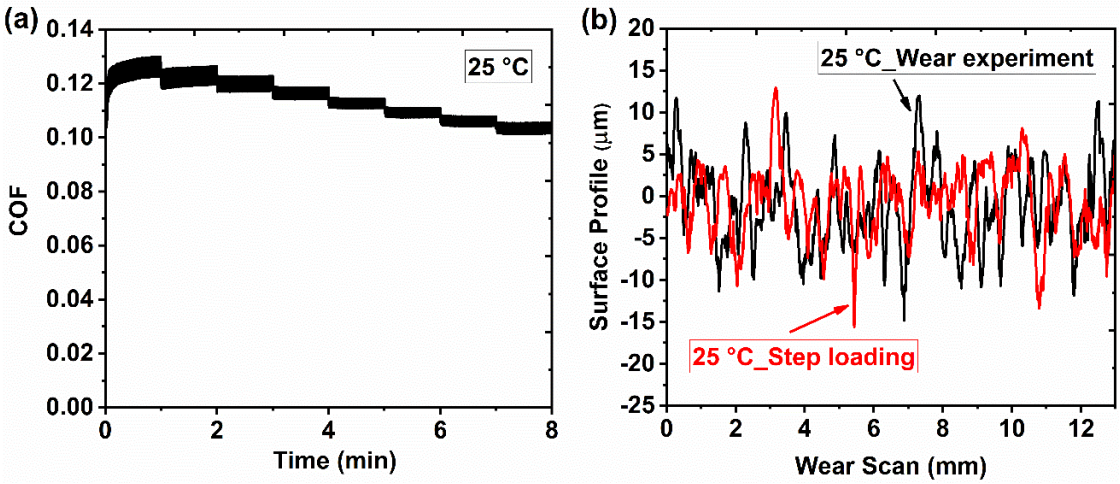

Figure 12. In-situ step-loading experimental results for ATSP coating (a) COF vs. sliding time, and (b) wear scan of the coating after testing. Reprinted with permissions from "Bashandeh K, et al. Tribological performance improvement of polyamide against steel using polymer coating. Tribology Transactions. 2019;62(6):1051-62."

2.4 SEM-EDS analysis

Figure 13(a-f) show the SEM images of the steel disks after the constant load wear experiments at temperatures of 25, 50, and 80 ºC. The transfer of material from the PA pin to the steel surface can be clearly distinguished with increasing temperature. This increase of transfer layer is another reason for the increase of wear with the increase of temperature. Owing to the softening of PA pin by the increase of the temperature from 25 ºC to 80 ºC,

the polymer will further fill up the crevices on the surfaces of the steel disks and also forms an additional layer on the surfaces, especially at the temperature of 80 ºC, leading to higher wear rate of the pin (**Figure 7**). Specifically, at 80 ºC, shown in **Figure 13(e)**, the darker areas on the steel surface are fully covered by the PA.

The EDS map in **Figure 13(g, h)** indicates that the darker areas are due to formation of carbon elements, which is the primary atom in the PA structure. From **Figure 13(h)**, it can be observed that the black spots in **Figure 13(g)** are indeed originated from transfer of PA (carbon elements) to the steel surface. The findings by [62] show that the tribological properties of PA have the worst performance in self-mated contacts. This is consistent with the result in this chapter since at 80 ºC, a larger portion of the steel surface is covered with the PA. The comparison of the SEM images at different temperatures shows smoothening of the surface at 80 ºC, consistent with the result shown in the wear scan measurements (**Figure 8(c)**), which resulted in a larger real contact area and increase of the COF.

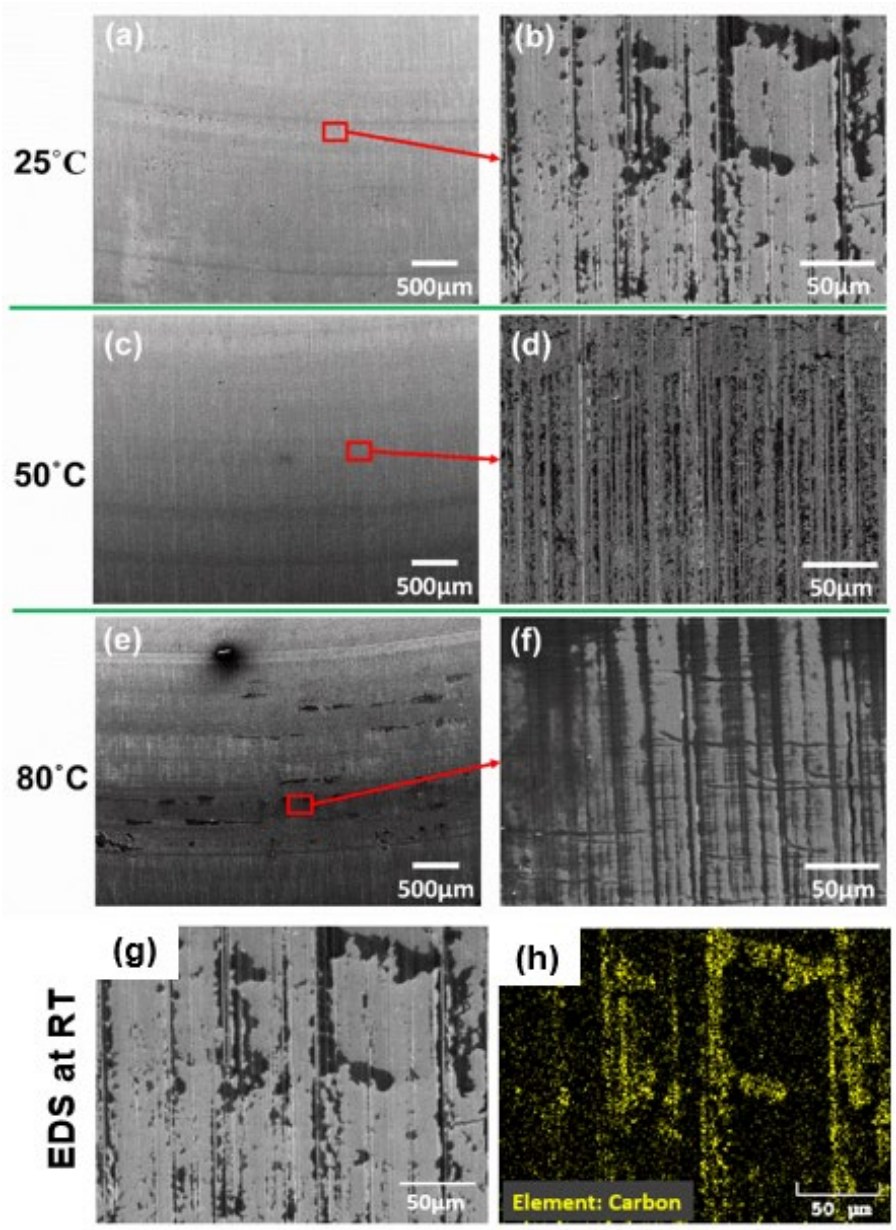

Figure 13. (a-f) SEM images of the steel surface showing the PA transfer film formation at different temperatures. (g) SEM image and (h) corresponding EDS analysis after testing at 25 ºC. Modified with permissions from "Bashandeh K, et al. Tribological performance improvement of polyamide against steel using polymer coating. Tribology Transactions. 2019;62(6):1051-62."

Because adhesive forces are one of the main reasons [66], we can also use the surface energy to explain the COF in the tribological experiments. PA 66 has higher

surface energy compared with PTFE [70]. Referring to **Figure 6(a)**, the COF of PA 66 pin vs. steel was increasing with time in the run-in period until it reached a stable contact, where the transfer layer was fully developed. In this case, a large portion of the contact was PA 66 pin vs. PA 66 transfer layer, and this same material contact had high adhesion, resulting in the high COF. For PA 66 pin vs. ATSP coating tribo-pair, ATSP coating works as a pre-deposited transfer layer, which has low surface energy due to the PTFE. Therefore, these different material contacts resulted in low adhesion and low COF.

Figure 14(a-d) show the SEM images of the ASTP coating before the experiments at different magnifications. From **Figure 14(a)**, the homogenous dispersion of the PTFE powder into the ATSP is observed. However, the depth of dispersion is not the same throughout. Higher magnification images (shown in **Figure 14(b-d)**) reveal that some particles are attached on top of the coating, **Figure 14(c)**, and some are semi-submerged, **Figure 14(d)**. It should be mentioned that the coating curing temperature is 270 ºC, which is lower than the PTFE melting temperature, therefore, it keeps the PTFE powder in the solid and rigid state in the coating. The EDS map of the coating, shown in **Figure 14(e)**, shows that the rigid particles are originated from the PTFE powder. The figure shows that carbon and fluorine are the main elements; the only atoms in the chemical structure of PTFE. (For repeated units in the molecular structure of ATSP and PTFE, 70 wt.% of the elements is carbon for ATSP, and 24 wt.% is for PTFE, thus the carbon on PTFE molecular structure is weaker and PTFE mainly shows fluorine in the EDS map).

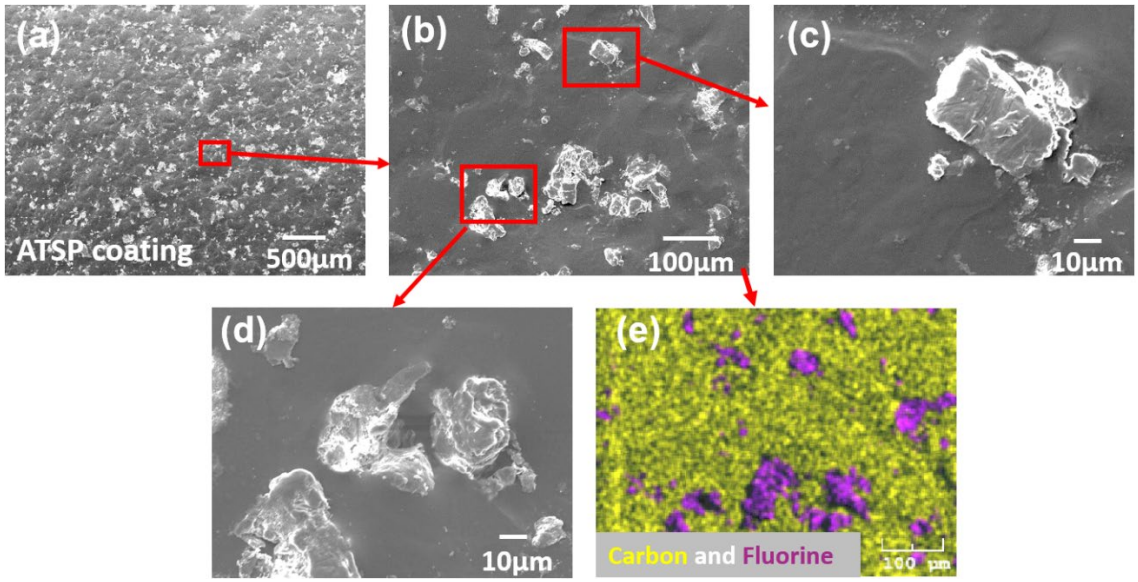

Figure 14. (a-d) SEM images of the virgin surface of the ATSP coating at different magnifications, and (e) corresponding EDS map of the coating. The squares in (b) represent the positions which have been magnified in (c) and (d). Reprinted with permissions from "Bashandeh K, et al. Tribological performance improvement of polyamide against steel using polymer coating. Tribology Transactions. 2019;62(6):1051-62."

Figure 15 shows SEM images of the ATSP coating after the constant load wear experiments at temperatures of 25, 50, and 80 ºC. The worn surfaces show no sign of wear and only contain very few scratches on the surface, parallel to the sliding direction. As the temperature increases to 50 ºC, higher number of visible scratches are created on the surface with finer shape. The comparison of the tested and virgin surfaces of the coating indicates no visible wear, consistent with the wear scan measurements shown in **Figure 9**. Compared with the original coating, the PTFE lubricant particles on the coating surface were smoothened, indicating that PTFE particles played an important role in reducing the COF, because of its low surface energy and low shear strength.

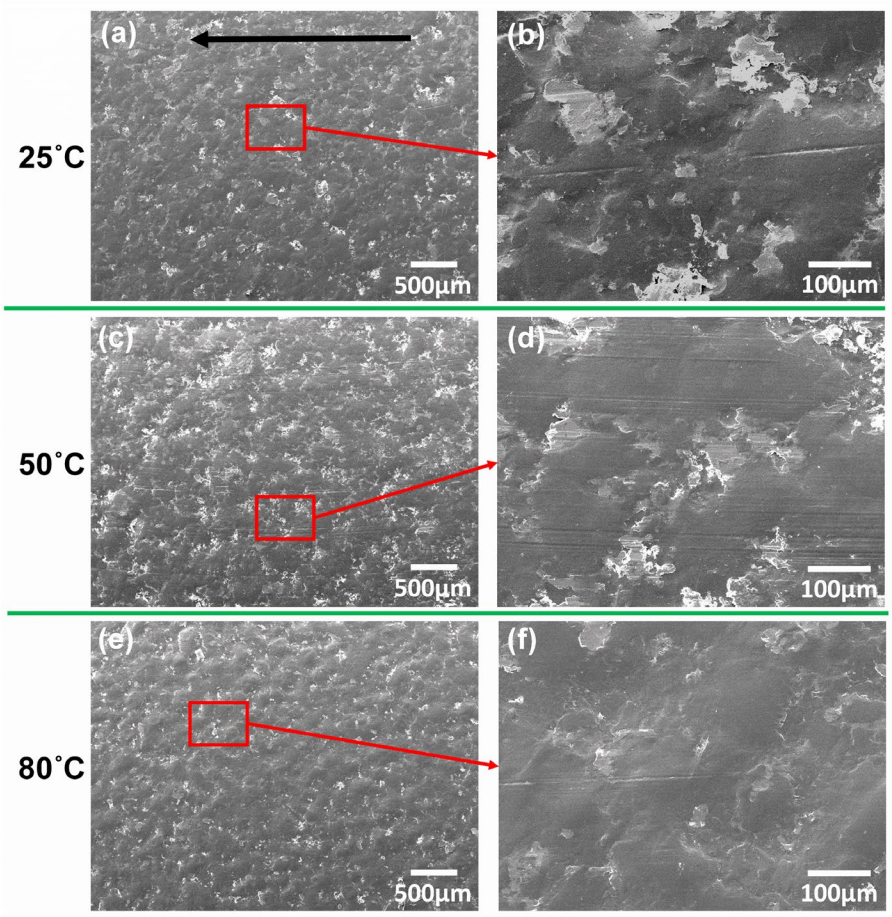

Figure 15. Different magnification SEM images of the worn surfaces of ATSP coating at different temperatures. The arrow in (a) shows the sliding direction. Reprinted with permissions from "Bashandeh K, et al. Tribological performance improvement of polyamide against steel using polymer coating. Tribology Transactions. 2019;62(6):1051-62."

Figure 16 shows a representative SEM micrograph of the PA pin sliding against the ATSP coated steel disk and steel surface at temperatures of 25, 50, and 80 ºC. The sliding of the PA on ATSP is causing mild scratches on both contact surfaces, but with much higher density in the PA pin. Deeper and wider scratches are created at higher temperatures, compared to 25 ºC, which is due to the lower mechanical strength of PA at higher temperatures. For the PA on steel shown in **Figure 16(d-f)**, because of the smooth surface of the steel and transfer layer, the worn surface on PA is smoother with no visible

scratch on the surface, compared to the PA on ATSP. Signs of plastic flow is evident at 50 ºC (**Figure 16(e)**) because the contact temperature of PA is approaching its Tg. However, when the temperature is 80 ºC, it has already passed the Tg and the contact is soft from the beginning of the sliding.

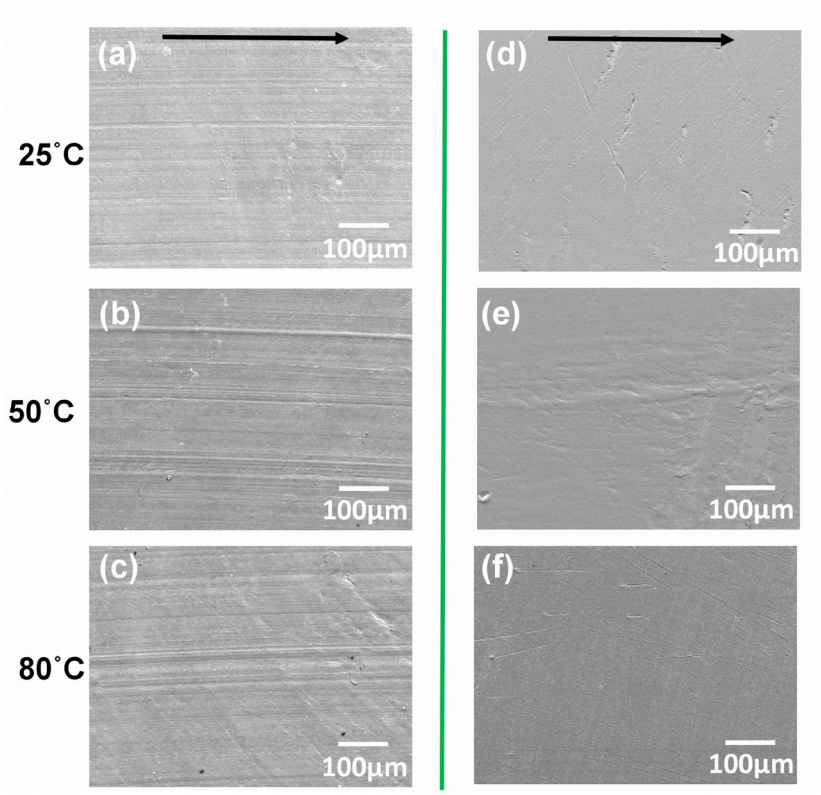

Figure 16. SEM images of the worn surfaces on PA66 pin at different temperatures for (a, b, c) PA66 pin vs. ATSP coated steel disk, and (d, e, f) PA66 pin vs. steel disk. The arrows show the sliding direction. Reprinted with permissions from "Bashandeh K, et al. Tribological performance improvement of polyamide against steel using polymer coating. Tribology Transactions. 2019;62(6):1051-62."

2.5. Summary

In this chapter, the tribological properties of PA66 were investigated under sliding against ATSP coated steel disks and steel surfaces under environmental temperatures of 25 °C, 50 °C, and 80 °C, under dry sliding conditions. Two sets of experiments, namely constant

load wear and step loading experiments were carried out to measure the wear/ friction, and load-bearing capacity of the PA and ATSP coating. The following conclusions were drawn:

- Significant reduction on friction and wear of PA were observed by depositing of ATSP coating on the bare steel surface at all temperatures. The COF and wear of the PA against ATSP coating were decreased by 70-80% and 85-95%, respectively compared to the PA sliding against steel surface.
- The variation of the COF with temperature was negligible for PA-ATSP, compared to PA-steel. For sliding of the PA against steel surface, due to the increase of contact area and shear force, the COF increased with temperature from 0.43 at 25ºC to 0.64 at 80ºC.
- The constant load wear experiments showed negligible wear of the ATSP coating for both one-hour and 5-hour duration at all temperatures.
- Step loading experiments showed the high load-bearing capacity of the coating even when PA was under high deformation. Still, the coating showed unmeasurable wear.
- From the SEM analysis, an increase of a transferred layer on the steel surface was observed with temperature. The high value of the COF at 80 ºC was attributed to smoothening of the surface and coverage of the surface by the transferred layer.

After demonstrating the efficacy of ATSP coating to be used as bearing material with thickness in the range of 30-40 μm, the performance of the coating under extreme elevated temperatures up to 300 °C needs to be evaluated at the next step. Next chapter discusses the materials and additives used to enhance the coatings performance at elevated temperatures and the results are analyzed in detail.

CHAPTER 3

TRIBOLOGICAL PERFORMANCE OF GRAPHENE AND PTFE SOLID LUBRICANTS FOR POLYMER COATINGS AT ELEVATED TEMPERATURES[2]

3.1 Introduction

Reducing friction and wear has always been a major challenge in tribological applications, especially those operating under extreme sliding conditions [71]. Such conditions are observed, for example, in cryogenic and high-temperature environments in space applications, where the use of conventional lubricants is not feasible [72,73], or with the high load/speed conditions on the bearing surfaces under starved lubrication condition, especially during start-up and shut-down periods [74]. To solve these problems, polymer coatings and their composites are increasingly being used as bearing and rubbing materials, especially in applications that require reliable operation over a wide range of temperatures [33,34]. The deposition of an appropriate polymer coating would not only maintain the advantages with bulk polymers but would also minimize their shortcomings by offering a higher load capability and higher dimensional precision and thermal stability [75]. A polymer coating would also help to mitigate the accumulation of frictional heating by its transfer through the metallic substrate. In addition, polymer coatings use cost-effective application methods, as they are easy to scale up for large surface areas, even

[2] Reprinted with permissions from "Bashandeh K, Lan P, Meyer JL, Polycarpou AA. Tribological performance of graphene and PTFE solid lubricants for polymer coatings at elevated temperatures. Tribology Letters. 2019 Sep;67(3):1-4."

with complicated shapes, and there is no need for expensive polishing/lapping process for the coating process. Many studies have pointed out the poor wear resistance and friction behavior of polymers when they are used in their pure or neat format. Researchers have tried to improve such behavior by adding different nano and micro fillers into the polymeric matrix [2,14,63,76,77].

PTFE, graphite, and molybdenum disulfide, as predominant solid lubricants, have been used to improve the friction and wear in polymers. At the nano-scale, the incorporation of carbon-based nanofillers such as carbon nanotube and graphene into the polymer can further enhance the wear resistance, friction, and mechanical properties. In the present research, the focus is to evaluate the tribological performance of graphene and PTFE as solid lubricants in Aromatic Thermosetting Polyester (ATSP) polymer coatings. ATSP is a high performance bearing polymer material that was developed by Frich and Economy [78]. Polycarpou et al. have been conducting tribological studies of ATSP and its composites and they reported that ATSP-based coatings have demonstrated excellent tribological performance: ‘zero wear’ over a wide range of temperature from -160 °C to 260 °C under dry sliding [33,53], extremely low wear coefficient under starved lubrication conditions [40,52], stable coefficient of friction (COF) and low wear rate under sand abrasive conditions [20], and extreme low COF for oil and gas drilling applications [79]. When the temperature is above its glass transition temperature, ATSP has a self-healing property which is enabled by a class of solid-state bond exchange reactions that are termed interchain transesterification (ITR) [80]. This self-healing property makes ATSP material suitable for high temperature tribological applications.

The use of PTFE as solid lubricant originates from its exceptionally low COF compared to other lubricants [81]. The high softening point, as well as the smooth molecular profile of PTFE chain, make it a well-suited lubricant [81]. Graphene is a 2D material comprised of a monolayer of carbon atoms arranged in a honeycomb structure [82,83]. Many researchers have studied the potential use of graphene (or its derivatives such as graphene oxide) in tribological applications owing to its excellent mechanical, thermal, and tribological properties [2,77,84–86]. Despite the large number of studies on the tribological behavior of graphene at the nano and micro scales, the literature lacks studies on polymer reinforced graphene at the macro scale, particularly at elevated temperatures [87,88]. Some studies have reported on the enhancement of the tribological performance for different polymer coatings and bulk polymers [89,90] with the addition of graphene. Nonetheless, the majority of the research works are associated with the tribological performance at environmental temperatures, whereas many tribological applications require a reliable operation of the polymer at elevated temperatures.

The objective of this chapter is to assess the tribological performance of ATSP/PTFE and ATSP/GNP polymer coatings at various temperatures from room temperature (RT) to 300 ºC. Dynamic mechanical analysis (DMA), Thermogravimetric Analysis (TGA), and nanoindentation tests were carried out to examine the thermal and mechanical properties of the coatings. We believe that this is the first report on the tribological behavior of graphene-reinforced polymer coatings under elevated temperatures up to 300 ºC.

3.2 Experimental details

3.2.1 Materials and sample preparation

Two oligomers C2 with carboxylic acid and A1 with acetoxy functional end groups were used as the precursors for ATSP coatings. A detailed synthesis and chemical structure of the oligomers can be found elsewhere [53]. Prior experience in lubricated conditions for air-conditioning compressor applications, as detailed in [40] indicated that the particular precursor configuration of ATSP/PTFE exhibited excellent wear resistance and synergistic decrease in COF in a PAG/r1234yf environment. The same precursor configuration (selected oligomers) is used in this study in the dry condition. These are referred to as the C2 and A1 oligomers. C2 is a liquid crystalline oligomer capped with an average of 4 carboxylic acid functional groups per molecule and A1 is an amorphous oligomer capped with an average of 3 acetoxy functional groups per molecule. Crosslinkable aromatic polyester oligomers are typically selected in terms of weight ratios such that the carboxylic acids and acetoxy functional units are in equimolar proportion, as was the case in this work. C2 and A1 were originally selected in the earlier study by virtue of their producing a mid-range crosslink density, mutual solubility in N-methylpyrrolidone (NMP) (as the study in [40] was conducted with the oligomer/PTFE blend solvated in NMP and deposited via high volume low pressure (HVLP) paint spray). In the ATSP resin system, a lower crosslink density is typically correlated with a higher plasticity, but a somewhat lower glass transition temperature.

To manufacture the ATSP oligomer powder, the solid bulk oligomers, after synthesis, were initially ground in a lab grinder and then sieved through a 90 μm screen.

The two oligomer powders were subsequently mixed by a cup-size small grinder with a weight ratio of 1.44:1 in respect of C2 to A1. Two compositions for the coatings were considered in this chapter, namely ATSP/PTFE and ATSP/GNP, which were also blended by the grinder. To prepare the ATSP/PTFE composite powders, the mixed oligomers were blended with 7.5 wt.% of Chemours Zonyl® PTFE powder (5 wt.% MP1300 and 2.5 wt.% MP1100, with an average size of 12 μm and 4 μm respectively). GNPs (xGnP®, Grade M) was purchased from XG Science Inc. with average particle diameters of 25 microns and a typical surface area of 120 to 150 m2/g. The ATSP/GNP nanocomposite powders were prepared by mixing 5 wt.% of GNPs with the mixed oligomers. Note that using the higher concentration of PTFE and GNP lubricants yielded a very rough surface, since the lubricants could not attach/embed well in the coatings. To form the ATSP coatings, the blended powders were sprayed on sandblasted 418 stainless steel disks (with a diameter of 50.8 mm and thickness of 6.35 mm) by using an electrostatic spray deposition (ESD) method. Thereafter, the deposited coatings were cured for 60 min in a convection oven at a temperature of 270 °C. Ultimately, coatings with 30 μm thickness were achieved. The pin was made out of E52100 bearing steel with diameter of 6.5 mm. Typical photographs of the coated disks and the steel pin are shown in **Figure 17(a, b)**.

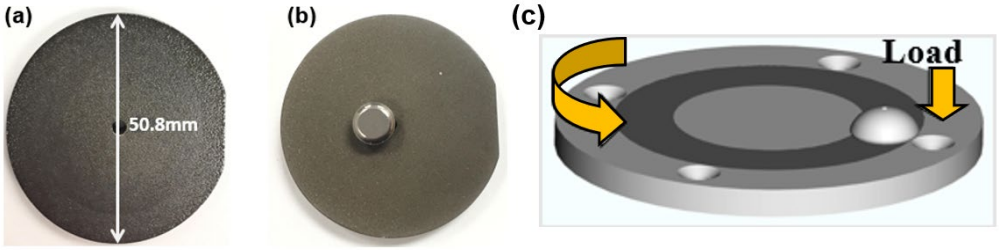

Figure 17. (a) ATSP/GNP, and (b) ATSP/PTFE coating and steel pin, and (c) experimental configuration. Modified with permissions from "Bashandeh K, et al. Tribological performance of graphene and PTFE solid lubricants for polymer coatings at elevated temperatures. Tribology Letters. 2019 Sep;67(3):1-4."

3.2.2 Experimental conditions

The tribological experiments were conducted using a commercial tribometer (Rtec-Instruments) with a flat pin-on-disk configuration (**Figure 17(c)**), simulating a nominal flat contact between the tribo-pairs. The pin holder is connected to a shaft perpendicular to the bottom rotating disk. The shaft is connected to a force transducer capable of measuring the in-situ friction and normal forces with measurement accuracy of 0.5% of full scale. The tribometer is capable of normal forces up to 5000 N, rotational speeds up to 5000 rpm, and environmental temperatures up to 1000 °C. The experiments were performed with a unidirectional motion under dry sliding conditions and ambient pressure. The experimental conditions are summarized in **Table 4**. The normal load was set to 135 N resulting in nominal contact pressure of 4 MPa. The nominal contact pressure was calculated by dividing the normal applied force by the flat area of the steel pin shown in **Figure 17(b)**. The ATSP coated disk was rotated against the steel pin (the stationary part) with a rotational speed of 530 rpm, corresponding to linear speed of 1 m/s. The linear speed is calculated based on 18 mm average radius for the wear tracks.

The experiments were stopped after 1 hour, equivalent to sliding distance of 3603 m. The air temperatures were set to 25, 100, 180, 260, and 300 °C (through a furnace with an accuracy of ±5 °C) to evaluate the performance of the coatings at elevated environmental temperatures. The purpose of the experiments with unreinforced (neat) ATSP coating was to check the effect of additives on the tribological performance. These experiments were performed only at RT since the neat coating failed at the end of the experiments. Each test was carried out at least three times to ensure repeatability. Before and after each experiment, the polymer coatings and steel pins were immersed in isopropyl alcohol and acetone, respectively and placed in an ultrasonic cleaner for 10 min at 50 °C. During the experiments, the in-situ friction and normal forces were measured to obtain the in-situ COF.

Table 4. Experimental conditions. Reprinted with permissions from "Bashandeh K, et al. Tribological performance of graphene and PTFE solid lubricants for polymer coatings at elevated temperatures. Tribology Letters. 2019 Sep;67(3):1-4."

Materials (disk)	Normal load [contact pressure]	Speed [linear speed]	Temperature (°C)
ATSP coating (95%C2A1+5%GNP)	135 N [4 MPa]	530 rpm [1 m/s]	25, 100, 180, 260, 300
ATSP coating (92.5%C2A1+7.5%PTFE)			
Neat ATSP			25 (RT)

3.2.3 Surface characterizations and wear analysis

To evaluate the worn surfaces on the coatings and the transfer film on the counterface, the surface morphology of the coatings and steel pins were characterized after the experiments using optical microscopy and scanning electron microscopy (SEM). The

SEM analyses were performed using a VEGA II LSU SEM. Each specimen was sputter-coated with 3 nm Pt/Pd alloy using a Cressington 208 HR Sputter coater.

The surface roughness of the coatings and the surface profiles across the wear tracks were measured using a Tencor P6 profilometer with 12 mm scan length. The surface profile was then used to calculate the wear rate ($\dot{W}$) from the volume of the worn off material (V) as:

$$V = \int_{r1}^{r2} 2\pi.r.h.dr = \sum 2\pi.r.h.\Delta r$$

$$\dot{W} = \frac{V}{F_N.d}$$

where r_1 and r_2 are the inner and outer radii of the wear track, h is the measured profilometric wear depth, F_N is the applied normal load, and d is the sliding distance [53]. The DMA experiments were carried out using a TA Instruments Q800 Dynamic Mechanical Analyzer in film tension mode on free-standing films of the deposited coatings. Thermogravimetric analysis of the coatings was performed by a TGA (TA-2950) from room temperature to 800 °C. The nanohardness of the coatings were measured using an instrumented nanoindenter (TI Premier, Bruker) equipped with a standard Berkovich probe.

3.3 Results and Discussion

3.3.1 DMA and TGA

DMA on related thermoset resins had previously shown that inclusion of graphene nanoplatelets and other carbonaceous nanofillers had strong effects on the observed glass

transition, including upshift of the peak position and broadening of the tan δ curve [91]. This was shown to be related to reactions producing covalent bonds between the acetoxy and carboxylic acid functional groups and oxygen-bearing functional groups (such as carboxylic acids and hydroxyls) typically found on the surface of GNPs. This produced a modification in the effective crosslink density with the GNPs acting as additional crosslinking sites. As in **Figure 18(a)** of the DMA results, the glass transition temperature as determined by peak in the tan δ curve of the neat C2A1-type ATSP resin was 238 ℃. In contrast to the upshift and broadening seen in earlier literature on related resins, the addition of GNPs to C2A1 produced separation of the tan δ curve, with an additional beta transition at 184 ℃ and a readily observable shoulder at 295 ℃, and a downshift in the glass transition to 233 ℃. Note that the particular resin precursor combination (termed CBAB in the earlier study [91]) had a higher crosslink density and a higher mesogenicity (more rod-like components in the form of biphenol diacetate substituted for hydroquinone diacetate). In the case of an even more closely related resin system (C1A1 – which has comparable mesogenicity to C2A1, and is composed of partly the same precursor oligomer, and differs mainly by virtue of a higher crosslink density), a marginal upshift in peak position of the tan δ was observed with no substantial changes to peak shape [92]. Herein, using the C2A1 set of precursor oligomers, instead, we observe a marginal drop in the peak Tg, a significant shoulder at 295 ℃ and a sub-Tg peak at 184 ℃. While observable and substantial changes to the tan δ curve were anticipated for the C2A1 system, this particular set of changes was not in line with prior observations in the related CBAB and C1A1 systems, and is likely due to the relatively lower crosslink density.

Addition of the Zonyl PTFE produced an upshift in measured Tg to 243℃, while maintaining approximately the same peak shape. This is surprising given PTFE's significantly lower tan δ peaks at -110 ℃ and 130 ℃ [93], which was not observed here due to the particulate format of the PTFE filler. One possible explanation is that the ATSP oligomers reacted with carboxylic acids present on the chain ends of lower molecular weight PTFE grades (such as Zonyl MP1100 and MP1300) produced by irradiation from higher molecular weight starting materials [94].

The thermal properties of the coatings were measured using TGA with a heating rate of 10 ℃/min under nitrogen environment. Before the TGA experiments, the free-standing coating samples were dried at 110 ℃ for half an hour and thus eliminated the effect of moisture. As shown in **Figure 18(b)**, the three coatings have almost identical leftover weight percentage vs. temperature. Specifically, at 300 °C, the weight loss for ATSP/GNP, ATSP/PTFE, and neat ATSP were 0.08%, 0.06%, and 0.11%. The temperature of thermal degradation at 5% of weight loss for ATSP/GNP, ATSP/PTFE, and neat ATSP were 445 °C, 454 °C, and 458 °C, respectively. This high thermal stability enables ATSP to be used as a high-temperature adhesive, applicable up to 380 °C in air environment [95].

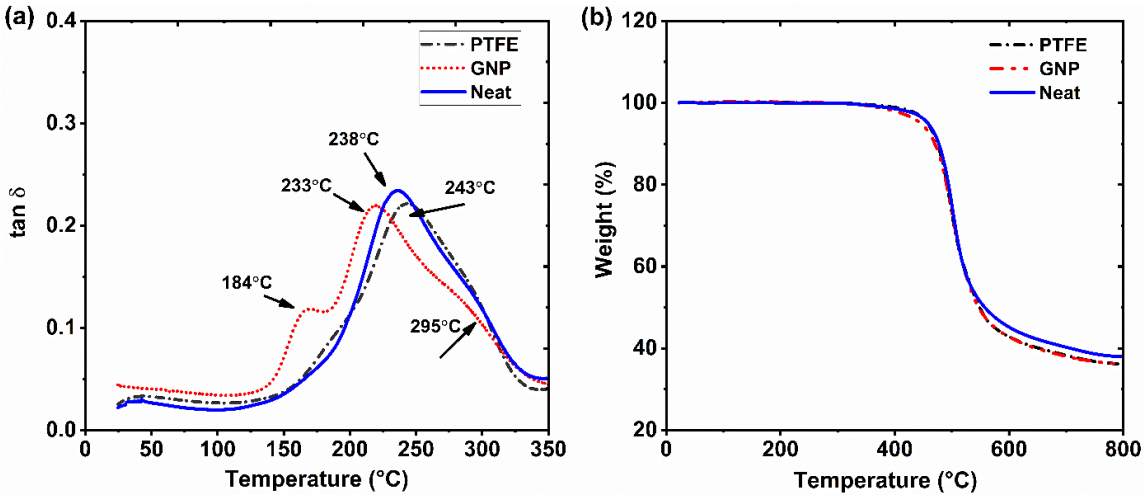

Figure 18. (a) Tan δ curves by DMA and (b) TGA results for ATSP/GNP, ATSP/PTFE, and neat ATSP coatings. Reprinted with permissions from "Bashandeh K, et al. Tribological performance of graphene and PTFE solid lubricants for polymer coatings at elevated temperatures. Tribology Letters. 2019 Sep;67(3):1-4."

3.3.2 Nanoindentation

Nanoindentation experiments were carried out to measure any changes in the hardness and elastic modulus of the composite coatings, compared to the neat coating. A high-load transducer (up to 10 N) equipped with a high-load Berkovich probe was used to obtain the in-situ load-displacement responses. A trapezoidal shape load function was used with 5 seconds of loading/ unloading and 2 seconds of holding to allow for viscous relaxation.

In order to obtain the mechanical properties of the coatings, it is necessary to minimize the substrate effect on the measurements by keeping the indentation depth below 10 percent of the coating thickness. Thus, to ensure minimal substrate effects, maximum normal loads of 10, 20, 30, 40, and 50 mN were selected to obtain different indentation depths (in all cases less than 3 μm). Five different measurements were performed for each

load. **Figure 19(a-c)** show the representative load-displacement curves obtained for ATSP/GNP, ATSP/PTFE, and neat ATSP coatings, respectively. The calculated mean values of hardness and reduced elastic modulus are shown in **Table 5**. The hardness was obtained by dividing the peak indentation load with the contact area, and the elastic modulus was calculated from the slope of the upper portion of the unloading curve based on the Oliver and Pharr method [96].

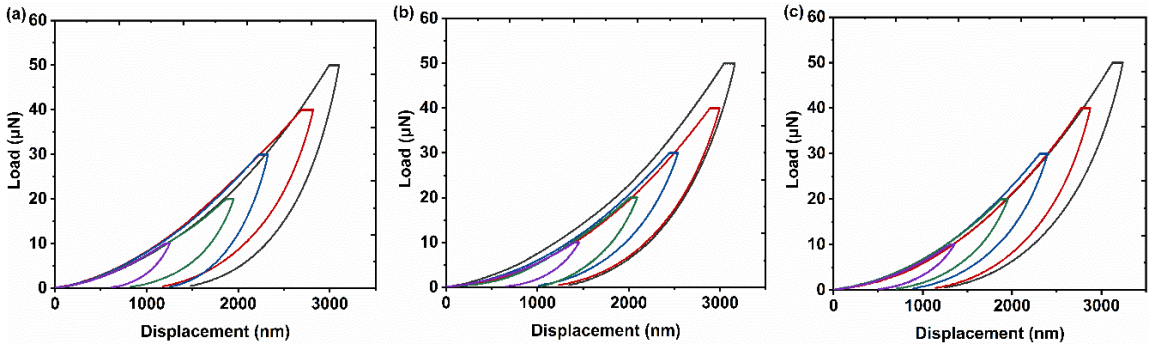

Figure 19. Indentation load vs. displacement curves (peak loads of 10-50 mN) for (a) ATSP/GNP, (b) ATSP/PTFE, and (c) neat ATSP coatings. Reprinted with permissions from "Bashandeh K, et al. Tribological performance of graphene and PTFE solid lubricants for polymer coatings at elevated temperatures. Tribology Letters. 2019 Sep;67(3):1-4."

Referring to **Table 5**, it can be seen that the ATSP composites exhibit higher elastic modulus than neat ATSP, whereas the hardness is weakly affected with addition of the fillers, similar to what was observed in [87]. Although graphene alone possesses an extraordinarily high elastic modulus, it does not necessarily improve the mechanical properties, when it is used as an additive. Several studies have reported on both enhancement and deterioration of the mechanical properties with the addition of graphene

to the polymeric matrix. These variations in mechanical properties have been attributed to filler/matrix interfacial interaction, and the amount and size of the filler [89,97–99].

Table 5. The properties of the coatings. Reprinted with permissions from "Bashandeh K, et al. Tribological performance of graphene and PTFE solid lubricants for polymer coatings at elevated temperatures. Tribology Letters. 2019 Sep;67(3):1-4."

ATSP coating composition	Roughness, *Rq* (μm)	Hardness, *H* (MPa)	Reduced elastic modulus, E_r (GPa)
95% C2A1+5% GNPs	9.1±0.69	254±16	4.54±0.17
92.5% C2A1+7.5% PTFE	2.55±0.25	229±11	3.6±0.24
Neat ATSP (100% C2A1)	2.51±0.24	256±17	3.68±0.07

3.3.3 Friction

To evaluate the tribological performance of the coatings at elevated temperatures, experiments were performed under temperatures of 25, 100, 180, 260, and 300 °C. **Figure 20(a, b)** show the evolution of in-situ COF as a function of sliding distance at different temperatures for ATSP/GNP and ATSP/PTFE coatings, respectively. The coatings showed a running-in behavior followed by a steady-state condition at all temperatures. From **Figure 20(a)**, the COF was lower at the beginning and started to increase during the running-in period and reached the steady-state after 10 min. It is generally believed that friction increases when the real contact area increases [67]. Referring to **Table 5**, the ATSP/GNP coating was rough, the surface asperities (where the actual contact takes place) transformed from a bumpy form to an even surface during the running-in period, thus the real contact area increased, leading to the increase of friction at the initial stages. This will be further supported by the SEM analysis. The ATSP/GNP showed a higher deviation from the mean compared to ATSP/PTFE. This is likely due to higher surface

roughness of the coating and local heterogeneities on the surface. The effect of temperature on friction is clearly observed from the figures. For both coatings, a reduction in friction was observed with the increase of temperature, except ATSP/PTFE at 260 and 300 °C, which was higher than 180 °C.

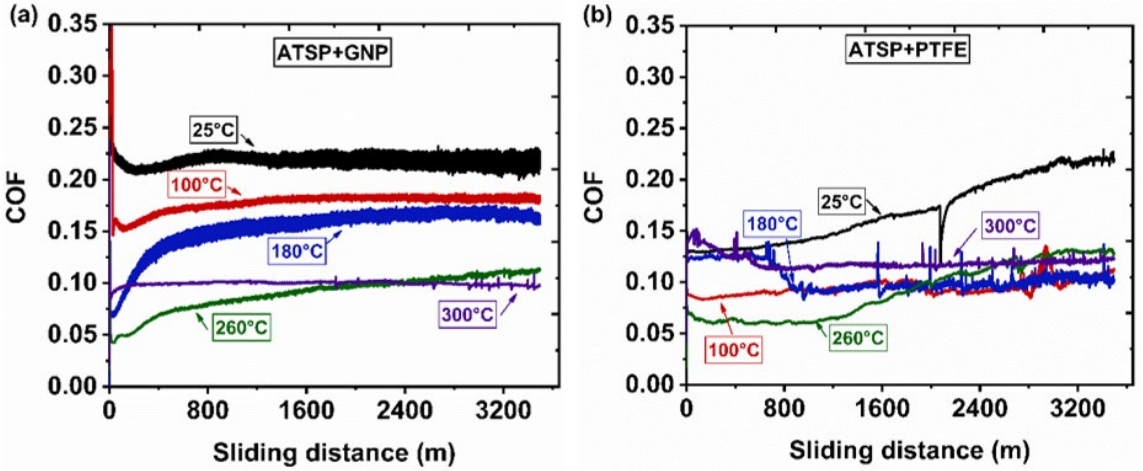

Figure 20. In-situ COF vs. sliding distance for steel pin sliding against (a) ATSP/GNP and (b) ATSP/PTFE coatings at different temperatures. Reprinted with permissions from "Bashandeh K, et al. Tribological performance of graphene and PTFE solid lubricants for polymer coatings at elevated temperatures. Tribology Letters. 2019 Sep;67(3):1-4."

Figure 21 presents the average values of the COF for the coatings at different temperatures. The increase of temperature caused a reduction in the COF for ATSP/GNP from 0.215 (±0.002) at 25 °C, 0.18 at 100 °C, 0.16 at 180 °C, 0.11 at 260 °C to 0.1 at 300 °C with the difference being 53% smaller compared with that of 25 °C. The same trend was observed for ATSP/PTFE except 260 °C with higher COF than 180 °C. The COF decreased from 0.22 at 25 °C to 0.098 at 180 °C resulting in a 54 % reduction and increased to 0.14 at 260 °C. When the temperature increased to 300 °C, the COF reduced again to 0.11. No difference was observed between 100 and 180 °C.

As depicted in **Figure 20,** the ATSP/PTFE coating was more susceptible to variation in temperature than ATSP/GNP, especially at the median temperature state. It should be noted that the neat coating failed after 50 min of sliding with an average COF of 0.45 (significantly higher than in the ATSP/PTFE and ATSP/GNP cases). This signifies the remarkable role of the additives in improving the friction and wear performance of the coating. The reduction in friction of the composite coatings compared to neat coating can be attributed to the self-lubrication characteristic and low surface energy of both graphene and PTFE, which results in stable friction and low adhesion between the mating surfaces [2,100]. The smooth linear structure of PTFE molecules with low bonding force between them results in easy sliding and low shear stress during the sliding [72]. Likewise, the atomically smooth surface and the weak van der Waals force between the graphene layers provide easy inter-layer sliding which enhances its easy shear capability and thus lowers the friction forces [101].

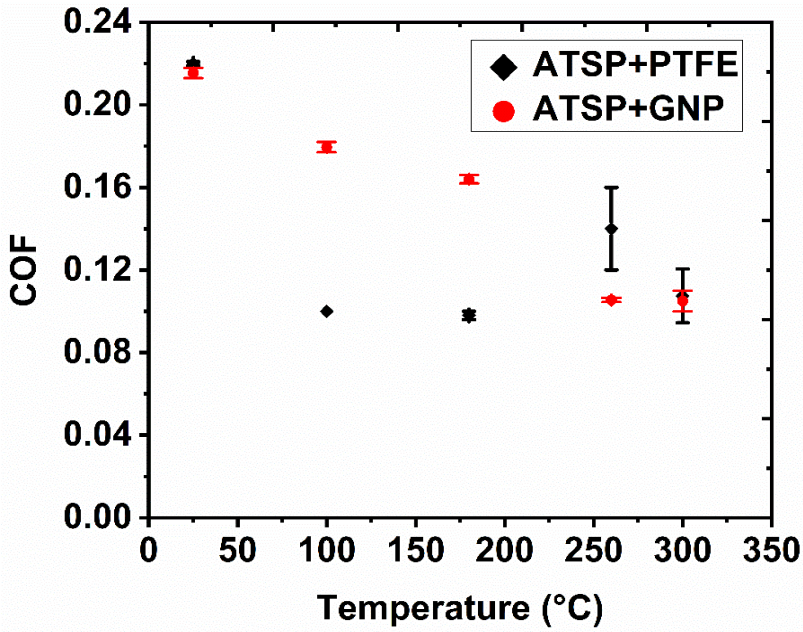

Figure 21. Comparison of average in-situ COF values of the coatings at different temperatures during steady-state. Note that the COF for neat ATSP coating is 0.45 at room temperature (and not shown). Reprinted with permissions from "Bashandeh K, et al. Tribological performance of graphene and PTFE solid lubricants for polymer coatings at elevated temperatures. Tribology Letters. 2019 Sep;67(3):1-4."

One of the main mechanisms for reduction of friction and wear by use of internal lubricants such as PTFE and GNP is attributed to their ability to form a protective transfer film on the counterface [14,77,83]. The presence of adhesive forces at the interface of the asperities of the tribo-pairs is the main mechanism involved in polymer transfer to the counterface. As the interfacial bond exceeds the cohesive bond of the polymer, the material would transfer from polymer to metal surface [102]. This is also revealed in this study using optical microscopic images of the steel pin counterfaces, depicted in **Figure 22(a, b)**. Both ATSP/GNP and ATSP/PTFE coatings formed a third body transfer film in the sliding direction on the steel pins at different temperatures. No accumulation of wear debris was discernible from the images. The microscopic analysis indicates that the

formation of transfer films is strongly affected by the increase of temperature. **Figure 22(a)** shows an increase in the amount of transfer film with temperature when the pin was sliding against ATSP/GNP, whereas less amount was observed for ATSP/PTFE, as seen in **Figure 22(b)**. The comparison of **Figure 22(a, b)** indicates that a more uniform and continuous transferred film was developed with increase of temperature by ATSP/GNP on the steel pin, whereas the ATSP/PTFE formed a non-uniform film. The uniform and stable transfer of polymer with addition of graphene was also observed in Ref [103] for polyimide nanocomposites. The improvement of tribological behavior at elevated temperature for ATSP/GNP can be attributed to the enhancement in formation of transfer film with temperature, as seen in **Figure 22(a)**.

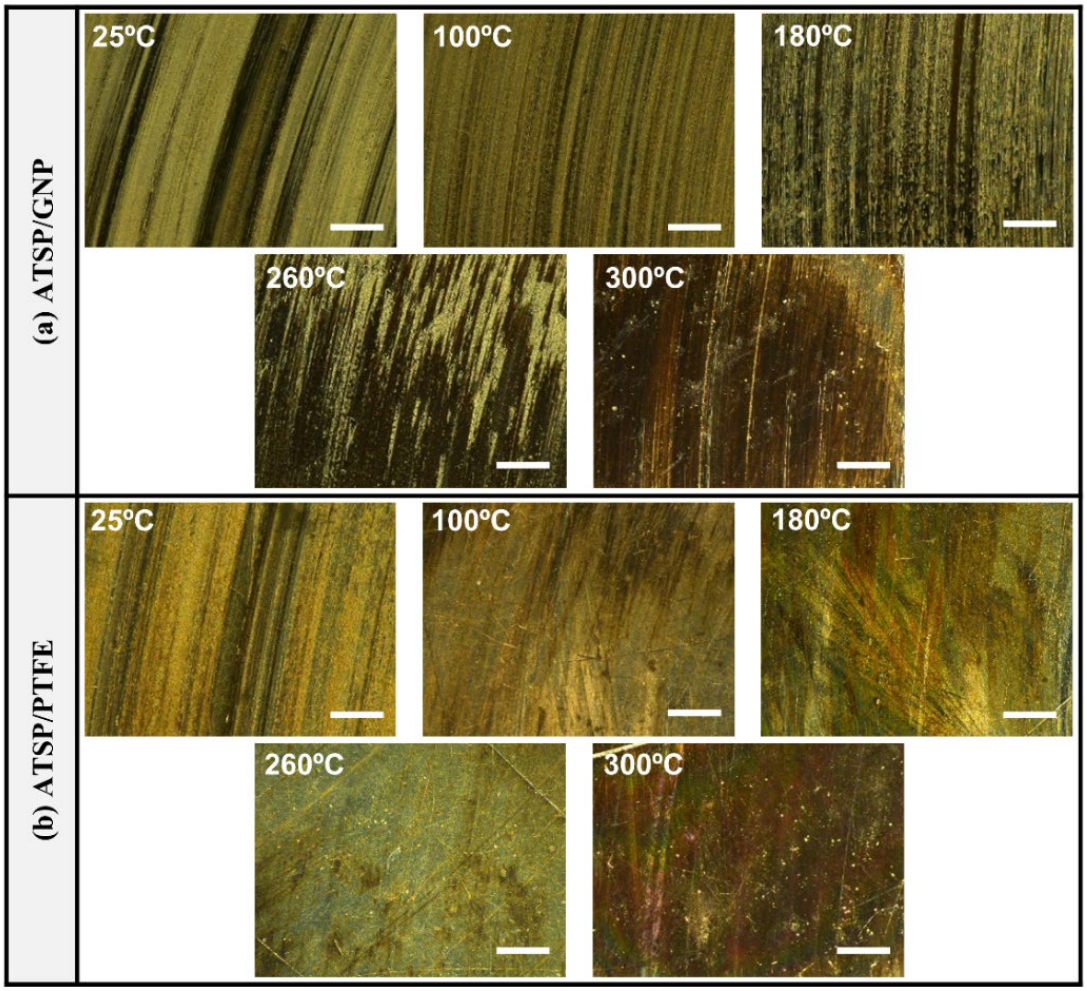

Figure 22. Optical microscopic images of the steel pins after the experiments at different temperatures against (a) ATSP/GNP, and (b) ATSP/PTFE coatings (scale bar is 500 μm for all images). Reprinted with permissions from "Bashandeh K, et al. Tribological performance of graphene and PTFE solid lubricants for polymer coatings at elevated temperatures. Tribology Letters. 2019 Sep;67(3):1-4."

The decreasing COF trend, shown in **Figure 21**, originates from the softening of the polymers with the increase of temperature. The transition of the polymer coatings from glassy to rubbery state with the increase of temperature facilitates the segmental motion of polymer chains, thus leading to easier sliding between the tribo-pairs. It should be noted that the softening of polymers with increasing temperature can have two contrary effects

on friction. Since the elastic modulus of the polymer reduces with softening, the real contact area will increase correspondingly, which increases friction. Here, for ATSP/PTFE at 260 °C (above its Tg, **Figure 18(a)**), the reduction of elastic modulus was the dominant factor, which increased the COF, compared to 180 °C. As the temperature was raised to 300 °C, cracks formed on the coating and the COF reduced again owing to thermal/mechanical fatigue of the ATSP/PTFE coating, in agreement with Ref [52].

For the ATSP/GNP coating, the COF dropped by 36% at 260 °C, compared to 180 °C and stayed at the same value at 300 °C. The findings by [91] showed that the incorporation of GNPs to ATSP improves the strength, toughness, and thermal stability of the coating. Here, as the temperature increased, the well-dispersed GNPs within the polymer matrix worked as a thermally conductive network, thus hindering heat accumulation on the ATSP. In addition, referring to **Table 5**, the elastic modulus of ATSP/GNP increased by 26% compared to ATSP/PTFE. Hence, the coating sustained the severe conditions at 260 and 300 °C with better performance, compared to the lower temperatures. Moreover, the GNPs improved the formation of transfer film with the increase of temperature as depicted in **Figure 22(a)**; more area was covered with the film on the steel surface, which could reduce the direct contact between the steel and the coating, leading to improved tribological performance at elevated temperatures.

3.3.4 Wear

Figure 23 shows the variation of the average wear rate after the experiments at different temperatures for ATSP/GNP and ATSP/PTFE coatings. The wear rates were calculated from the wear scan measurements across the wear track shown in **Figure 24(a)**.

As shown in **Table 5**, the roughness of the two coatings was not the same and ATSP/GNP was somewhat rougher; therefore, comparing the wear values of the two coatings directly should be done with care. Nevertheless, a trend for the two coatings can be deduced to find the best performing coating at elevated temperatures. Note that this high initial roughness is a result of the specific deposition process and also the type of GNP used in the coating. From **Figure 23**, two different trends can be observed for the coatings: higher wear rate with the increase of temperature for ATSP/PTFE, and a decreasing trend for ATSP/GNP coating. Therefore, the ATSP/GNP was more resistant to wear at elevated temperatures. When the temperature was raised to 100 and 300 °C, the wear rate dropped by 25 and 69 % respectively, compared to room temperature experiments, whereas for ATSP/PTFE the wear rate increased by 178% at 300 °C. A set of long-life experiments were carried out at RT with normal load and sliding speed shown in **Table 4**, to obtain the number of cycles to failure for both coatings. The ATSP/PTFE survived for 314,000 cycles (corresponding to 35.5 Km sliding distance, and a wear rate of $2x10^{-7}$), whereas the ATSP/GNP coating survived to 730,000 cycles (or 82.5 Km sliding distance, and a wear rate of $4x10^{-8}$), revealing a significant increase in durability of the coating with the addition of graphene.

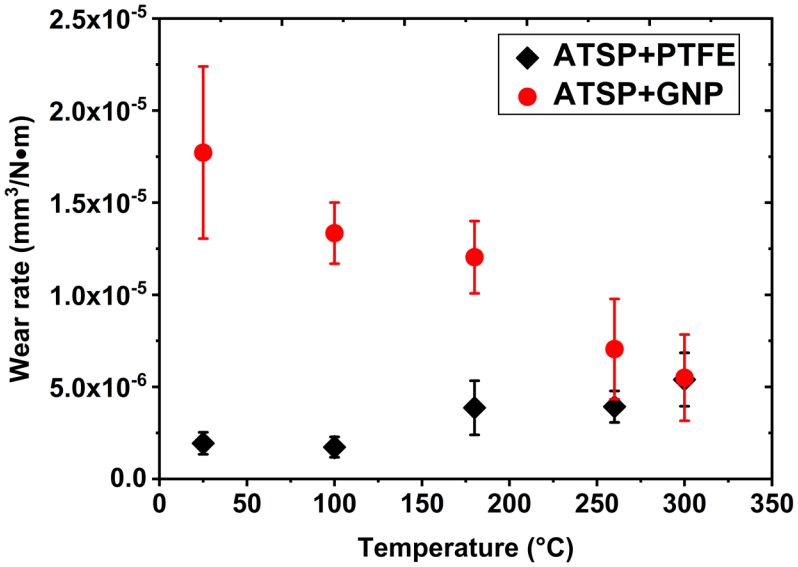

Figure 23. Calculated wear rates at different temperatures for ATSP/GNP and ATSP/PTFE coatings. Reprinted with permissions from "Bashandeh K, et al. Tribological performance of graphene and PTFE solid lubricants for polymer coatings at elevated temperatures. Tribology Letters. 2019 Sep;67(3):1-4."

The profilometric wear scans in **Figure 24(b, c)** provide qualitative insight into the changes on the wear performance. From the figures, it is clear that the wear depth is reducing with temperature for ATSP/GNP, while it is increasing for ATSP/PTFE. The inset image in **Figure 24(b)** indicates the burnishing of top asperities, implying the smoothening of the coating surface during sliding.

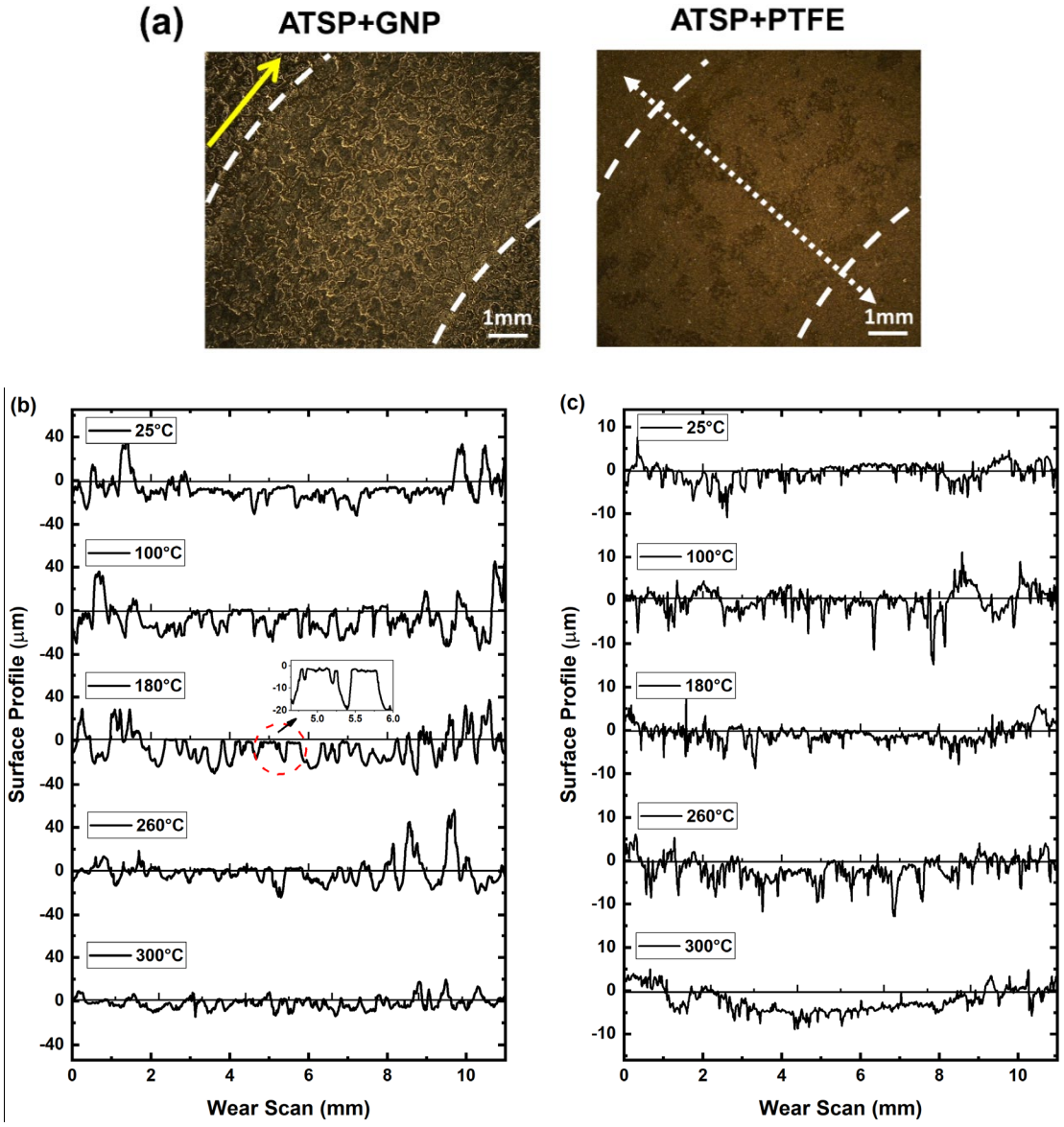

Figure 24. (a) optical microscopy images of the coatings after experiments at 25 °C (the arrow shows the sliding direction and the double arrow shows the scan direction), and (b, c) representative profilometric wear scans after the experiments at different temperatures for ATSP/GNP and ATSP/PTFE, respectively. Reprinted with permissions from "Bashandeh K, et al. Tribological performance of graphene and PTFE solid lubricants for polymer coatings at elevated temperatures. Tribology Letters. 2019 Sep;67(3):1-4."

Overall, the comparison of **Figure 21** and **Figure 23** shows that for ATSP/GNP, there is a transition between high friction high wear to low friction and low wear with the

increase of temperature, implying an improvement on the tribological performance at elevated temperatures. As discussed previously, the GNPs worked as a heat shield and created a thermal conductive network within the ATSP matrix. Hence, the heat flow to the matrix and contact region was restricted leading to higher thermal stability and more wear resistance at elevated temperatures compared to ATSP/PTFE. In addition, the presence of the GNPs with a large surface area within the matrix can efficiently transfer the applied load to the matrix, inhibit the initiation and propagation of cracks, and prevent the fracture of the polymer leading to low wear rate [97,99,104]. Meanwhile, as depicted in **Figure 22(a)**, the GNPs improved the ability of the ATSP coating to form the self-lubrication transfer film on its counterpart during the tribological experiments, resulting in better friction and wear at elevated temperatures up to 300 °C.

3.3.5 SEM

Figure 25(a, b) show typical SEM images of the untested surfaces of the ATSP/GNP and ATSP/PTFE coatings at different magnifications. From **Figure 25(a),** the ATSP/GNP coating features a rough surface (as mentioned earlier) with a bumpy structure and asperities having different shapes, heights, and surface areas. The initial contact will take place at the top of these asperities and depending on the loading conditions they might get smoother, larger, or fractured. For ATSP/PTFE coating, **Figure 25(b)**, the surface consists of multiple valleys with different depths throughout the coating. These valleys generally remain intact during sliding. From the SEM/EDS analysis shown in **Figure 25(c)**, where purple color denotes carbon element and green color denotes fluorine element, the PTFE powder is well distributed in the ATSP/PTFE coating. As both

graphene and ATSP consist of carbon, even in consideration of oxygen, EDS is not effective to identify graphene particles. However, from the uniform black color and morphology, we expect that graphene is also well dispersed on the ATSP/GNP coating.

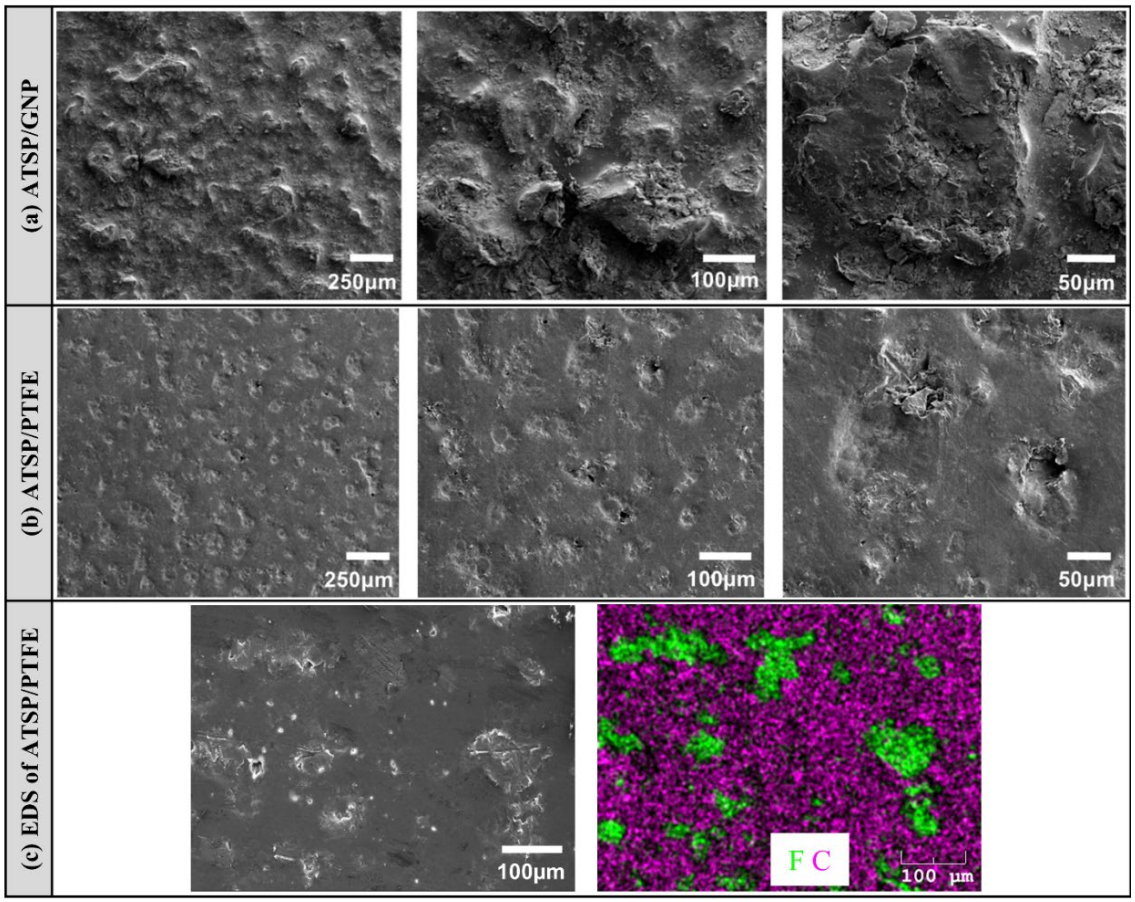

Figure 25. SEM/EDS images of the untested (as received) surface morphology of the coating: (a) SEM of ATSP/GNP coating, (b) SEM of ATSP/PTFE coating, (c) SEM/EDS of ATSP/PTFE coating. Reprinted with permissions from "Bashandeh K, et al. Tribological performance of graphene and PTFE solid lubricants for polymer coatings at elevated temperatures. Tribology Letters. 2019 Sep;67(3):1-4."

Figure 26(a-e) show the SEM images of the worn surfaces for ATSP/GNP coating after the experiments at different temperatures. All the figures indicate burnishing of the top asperities with different severities, similar to what was observed in profilometric wear

scans in **Figure 24(b)**. Many regions associated with the lower topographical areas remained intact during sliding, as depicted in **Figure 26(a)**. The comparison of the untested (**Figure 25(a)**) and worn surfaces (**Figure 26(a)**) of the coating indicates smoothening of the asperities and an increase in the real contact area accordingly due to plastic deformation of the asperity tips. The generated wear debris transferred to the steel counterface (as in **Figure 22(a)**) forming a protective layer on the surface, resulting in no further wear and a steady-state condition. **Figure 26(b)** shows a patch of the coating that is plucked from the surface and stuck at the edges. Some portion of these generated patches could transfer to the steel counterface and some redeposited on the coating, as shown in **Figure 26(d)**. The scattered holes and micro cracks observed in the worn surfaces of the coating are a feature that is also apparent on the untested coating, as in **Figure 25(a)** and are not created during the sliding process. From **Figure 26(e)**, one can see that when the temperature was raised to 300 °C, the top asperities were polished to a lesser extent, compared to lower temperatures, implying higher wear resistance, similar to what was observed by profilometric wear measurements, **Figure 24(b)**.

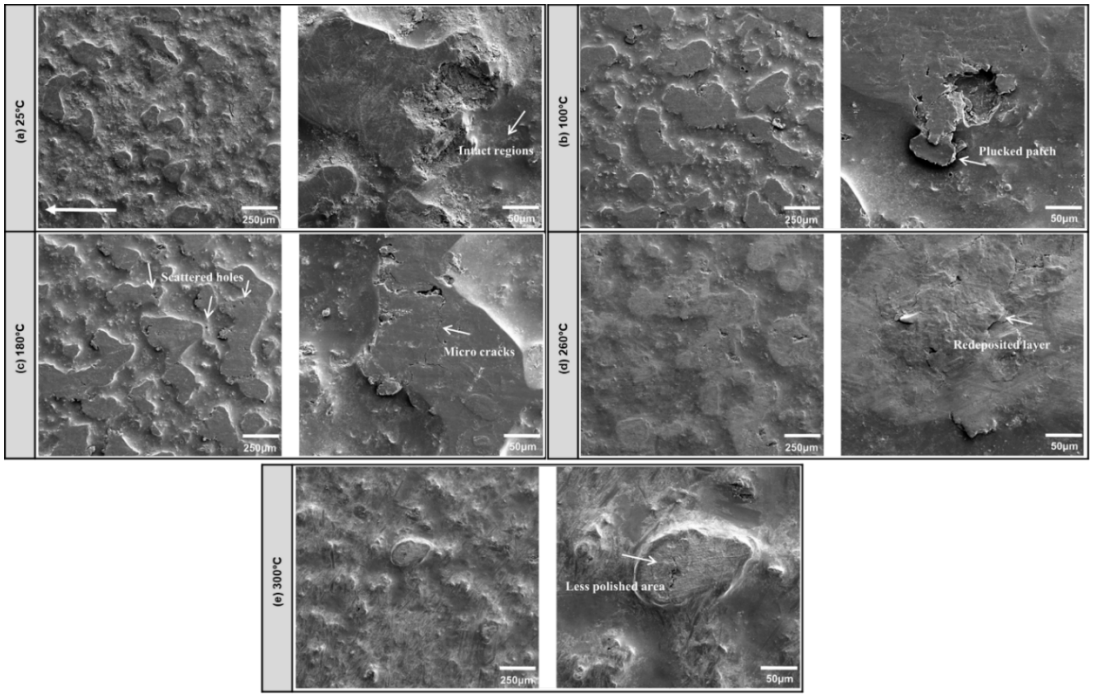

Figure 26. SEM images of the worn surfaces for ATSP/GNP coating at different temperatures: (a) 25 °C, (b) 100 °C, (c) 180 °C, (d) 260 °C, (e) 300 °C. Arrow in left image of (a) shows the sliding direction. Modified with permissions from "Bashandeh K, et al. Tribological performance of graphene and PTFE solid lubricants for polymer coatings at elevated temperatures. Tribology Letters. 2019 Sep;67(3):1-4."

Figure 27(a-e) depict the SEM images of the worn surfaces for the ATSP/PTFE coating after the experiments at different temperatures. Similar to ATSP/GNP, the lower topography (valleys) remained unaffected with sliding at all temperatures. The worn surfaces are clearly discernible in the areas with darker color compared to the fresh surfaces. Referring to **Figure 23**, the wear was quite low at temperatures of 25 and 100 °C, which is also confirmed by the SEM images in **Figure 27(a, b)** showing only mild polishing effect during sliding. The coating shows signs of mild abrasive marks as the temperature was increased to 180 °C and to a lesser extent at 260 °C. It is worth mentioning that the angled fine scratches and the scattered holes on the worn surfaces in the figures were not created during the sliding process as they were also visible on the

surface of the untested coating, shown in **Figure 25(b)**. The increase of temperature to 300 °C created pronounced marks of adhesion and cracks on the coating, corresponding to poor wear resistance of the coating at 300 °C. The formation of cracks could arise from the cyclic loading from the steel pin during the tribological experiments, which could create oscillatory stresses on the coating, providing the condition for fatigue wear[105].

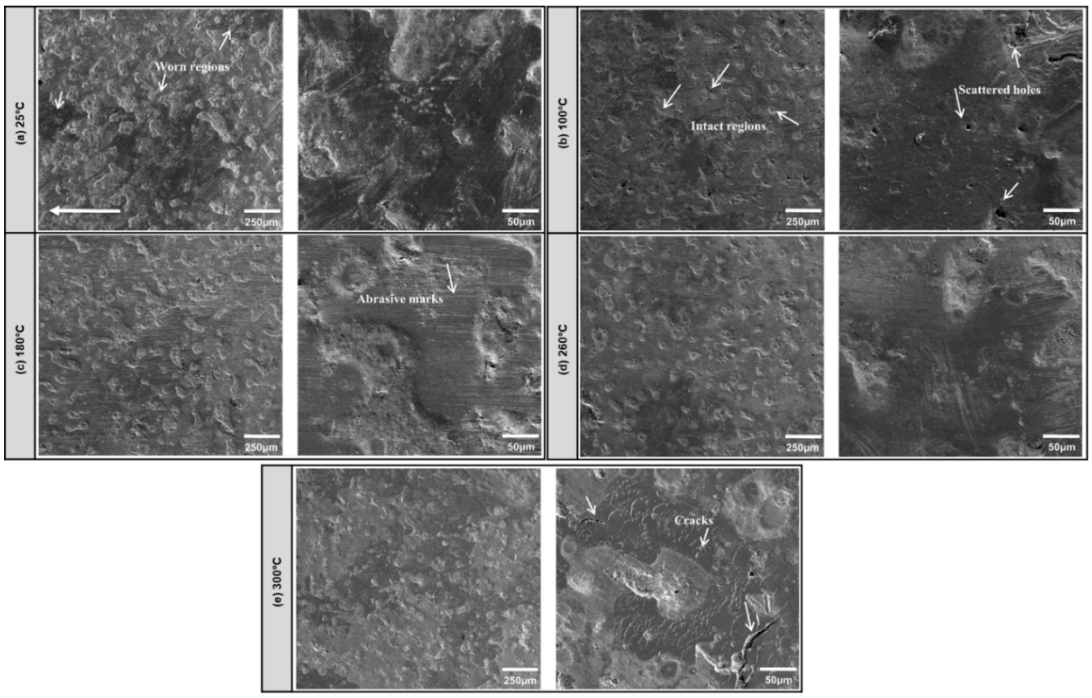

Figure 27. SEM images of the worn surfaces for ATSP/PTFE coating at different temperatures: (a) 25 °C, (b) 100 °C, (c) 180 °C, (d) 260 °C, (e) 300 °C. Arrow in left image of (a) shows the sliding direction. Modified with permissions from "Bashandeh K, et al. Tribological performance of graphene and PTFE solid lubricants for polymer coatings at elevated temperatures. Tribology Letters. 2019 Sep;67(3):1-4."

3.4 Summary

The tribological performance of two composite coatings, namely ATSP/GNP and ATSP/PTFE were experimentally investigated from 25 °C to 300 °C under dry sliding conditions. The main findings based on the results can be summarized as follows:

- The incorporation of 5 % GNP and 7.5 % PTFE dramatically improved the tribological performance of neat ATSP coating, although the hardness and glass transition temperature remained almost the same;
- The COF and wear rate continuously decreased with increasing temperature for ATSP/GNP coatings. The COF and wear rate reduced by 53 % and 69 %, respectively with the increase of temperature from 25 to 300 °C. SEM analysis showed burnishing of the asperities with sliding, which was reduced with the increase of temperature to 300 °C;
- For ATSP/PTFE coating, the COF reduced by 54% with the increase of temperature up to 180 °C, compared to 25 °C. However, compared to 180 °C, the COF increased by 43 % at 260 °C. Cracks formed on the coating when temperature was raised to 300 °C with 178 % increase in wear rate, compared to 25 °C;
- The ATSP/GNP coating developed a robust transfer film on the steel pin providing low wear rate and steady COF, particularly at elevated temperatures.

Both ATSP/PTFE and ATSP/GNP coatings demonstrated a great potential to be applied as a wear resistance coating on tribological parts operating over a wide range of temperatures. In addition, according to the results discussed in Chapter 2, the deposition of ATSP coating on bare steel was shown to significantly improve the tribological performance of PA due to the beneficial effect of "transfer layer." Therefore, in the next Chapter, inspired by this beneficial effect, the ATSP resin will be deposited on both pin and disk substrates to form a polymer-on-polymer sliding contact, and its effectiveness on friction and wear reduction will be investigated over a wide range of temperatures from -196 to 300 °C. For comparison purposes, other commercially available competitor materials such as PEEK/PTFE and Fluoropolymer coatings would be evaluated as well.

CHAPTER 4

EXTREME ENVIRONMENT TRIBOLOGICAL STUDY OF ADVANCED BEARING POLYMERS FOR SPACE APPLICATIONS [3]

4.1 Introduction

Reliable operation of moving parts and tribological components such as bearings, gears, and seals is essential for successful accomplishment of space exploration. The challenges with lubrication in space-related applications originate from extreme environmental conditions, which impedes the use of conventional liquid lubricants and greases [106]. Examples of extreme conditions include wide temperature ranges from cryogenic to elevated temperatures, electromagnetic and particulate radiation, and environmental pressures from vacuum to high pressure [107,108]. Tribological components require materials and lubricants with low friction and wear over a broad range of temperatures encountered in space. Therefore, the selection and design of new materials and protective surfaces are imperative for long-life bearing and tribological surfaces in space [109].

Polymers and polymer blends are promising tribological materials for space applications due to their unique advantages over metals, such as low friction, low to moderate wear resistance, low cost, lightweight, and self-lubricating properties [106,110].

---

[3] Reprinted with permissions from "Bashandeh K, Tsigkis V, Lan P, Polycarpou AA. Extreme environment tribological study of advanced bearing polymers for space applications. Tribology International. 2021;153:106634."

The main concern for polymers is their low thermal conductivity and relatively low load-bearing capability [37,109]. This can be addressed by using polymer coatings with 10's of micron thickness, and therefore the heat can effectively be transferred from the rubbing area through the thin coating to the metal substrate [111].

Polymers with self-lubricating properties have been used in different industrial applications as bearing and rubbing materials [22,112]. Polyether ether ketone (PEEK), polytetrafluoroethylene (PTFE), aromatic thermosetting co-polyesters (ATSP), and Fluorocarbons (FC) are the most widely used polymer-based coatings intended for applications that require high load-bearing capacity and improved tribological performance under unlubricated conditions [14]. Polymers in neat or pure format suffer from poor tribological performance and are typically used as composites mixed with different reinforcement and solid lubricants to improve the mechanical and tribological properties [49]. MoS2, graphite, and PTFE are commonly used solid lubricants with MoS2 and PTFE being the most preferred for space applications [113].

With the broad temperature range encounter in space, polymers are required to have improved and stable tribological performance from cryogenic to elevated temperatures. Polycarpou et al. have been studying the tribological performance of high bearing polymer coatings such as ATSP-based, PEEK-based, and Fluoropolymer-based (FP) coatings in various conditions simulating different working environments [14]. Among the three types of coatings, ATSP-based coatings showed the most desirable tribological performance: "unmeasurable wear" at temperatures ranging from -160 °C to 300 °C with dry sliding [33,53,114], extremely low coefficient of friction (COF) for oil

and gas drilling applications [52], and low wear rate and stable COF under sand abrasive conditions [20].

It is generally accepted that when polymer surfaces slide with metal counterparts under dry sliding conditions, a transfer layer would be typically formed on the surface of the metal counterpart. This transfer layer can have a beneficial effect on reducing the COF, making polymers an attractive solution for replacement or coating of metallic sliding components in oil-less engineering applications [36]. Therefore, numerous studies have been devoted to investigate the tribological performance of polymers sliding against metals [39]. However, the role of transfer layer could also be replicated by pre-depositing the polymer on the metal counter surface in the form of a thin coating. Therefore, a stable and uniform film will form on the metal surface before sliding, representing a polymer-on-polymer sliding condition. Polymer-on-polymer tribological studies have been mostly performed for polymers in bulk format in self-mated or other combinations [45,62,115], and few studies have reported bulk vs. coating [19,116].

Herein, we report on the tribological performance of polymer coating vs. polymer coating sliding contact for three high bearing polymers, namely ATSP-based, PEEK-based, and a commercially available FP-based coating known as DuPont® 958G-303. This concept of polymer coating sliding on polymer coating results in one of the coatings working as a pre-deposited “transfer layer.” The tribological performance of these coatings was investigated. The effect of proton exposure on morphological, mechanical, and tribological properties was also studied for the best performing tribo-pair with equivalent of 50-year low earth orbit proton exposure duration. The mechanical properties

of the coatings were examined at various temperatures using the nanoindentation technique and correlated with the tribological performance.

4.2 Experimental

4.2.1 Materials and sample preparation

Oligomers C2 and CB2 with carboxylic acid functional end group, and A1 and AB2 with acetoxy functional end groups were used as the precursors for the ATSP resins. Two different ATSP coatings were formulated by mixing two sets of oligomer powders, namely C2+A1 for C2A1 coating and CB2+AB2 for CB2AB2 coating. Upon curing, the crosslinks were formed by reaction between the end groups of the oligomers. **Figure 28** shows schematics of the polymerization reaction between the two oligomers and the generated crosslinked aromatic polyester backbone along with acetic acid as the reaction by-product.

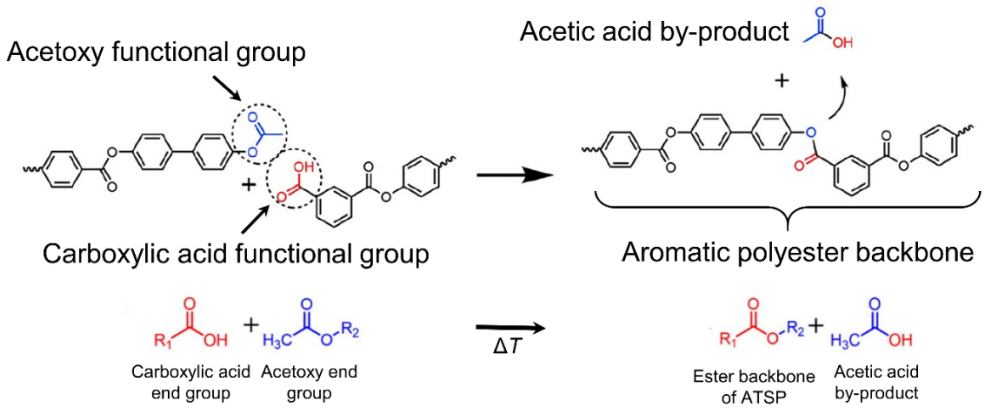

Figure 28. Schematic representation of polymerization reaction between oligomers and the generated aromatic polyester backbone, adapted from [117].

The oligomers were synthesized in a batch melt polymerization in a 2L reactor at 270 °C under Argon atmosphere and using the monomers biphenol diacetate (BPDA), 4-

acetoxybenzoic acid (ABA), isophthalic acid (IPA), trimesic acid (TMA), and hydroquinone diacetate (HQDA). Detailed synthesis method and purification procedures are described in [78,118]. After the reaction, the oligomers were then ground into powder with a lab grinder and sieved for a maximum particle size of 90 μm.

Thereafter, the oligomers were mixed by a cup-size grinder for C2A1 and CB2AB2, respectively. The ATSP powder was blended with different PTFE lubricant additives with the desired weight ratio as listed in **Table 6**. The blended powder was directly sprayed onto the sandblasted 7075 aluminum alloy plates and pins using electrostatic spray deposition (ESD). The aluminum substrates for ATSP-based coatings were fabricated with dimensions shown in **Figure 29(a)**. The coated samples were then cured at 270 °C for 60 minutes within a convection oven. Two polymeric coatings labeled as ATSP Coating 1 (C2A1) and Coating 2 (CB2AB2) were prepared, each having a thickness of 30±5 μm.

Table 6. Details of polymer coating materials. Reprinted with permissions from "Bashandeh K, et al. Extreme environment tribological study of advanced bearing polymers for space applications. Tribology International. 2021;153:106634."

Coating #	**Description**
ATSP Coating 1	**C2A1+7.5PTFE**: Powder coating on Al 7075 pins/plates Composition: 92.5 wt.% C2A1 + 7.5 wt.% PTFE
ATSP Coating 2	**CB2AB2+5PTFE**: Powder coating on Al 7075 pins/plates Composition: 95wt.% CB2AB2 + 5 wt.% PTFE
PEEK/PTFE	**PEEK+20PTFE**: Powder coating on Al 7075 pins/plates Composition: 80 wt.% VICTREX® PEEK 150XF + 20 wt.% PTFE
DuPont® 958G-303	**Fluoropolymer (FP)**: Solvent-based coating on Al 7075 pins/plates Commercially available coating system formulated with fluoroplastics to provide a tough, durable film for dry lubrication. The exact composition details are not known.

CB2AB2 was designed to have low crosslink density [95] and C2A1 with mid-range crosslink density [118]. The crosslink density was adjusted through the adjustment of the ratio of crosslinker (TMA) compared with other monomers. Lower crosslink agents resulted in longer chain length between the crosslinks and, therefore more degree of freedom for chain motion, which reduced the glass transition temperature (Tg). In fact, the lower crosslink density for ATSP resins is typically correlated with higher plasticity, but a somewhat lower Tg. For PEEK/PTFE coating, PEEK powder (VICTREX® PEEK 150XF) and PTFE powder mixture were deposited on the Al plates and pins by ESD and then the samples were placed in the convection oven at 360 °C for 30 min. Uncured DuPont® 958G-303 product is a liquid mixture and was deposited on the aluminum samples by high-volume low-pressure spray gun and then baked for 15 min at 343 °C. The final thicknesses of the coatings were obtained as 30±5 μm. The coated tribo-pairs (i.e., pin and disk) are shown in **Figure 29(c)**.

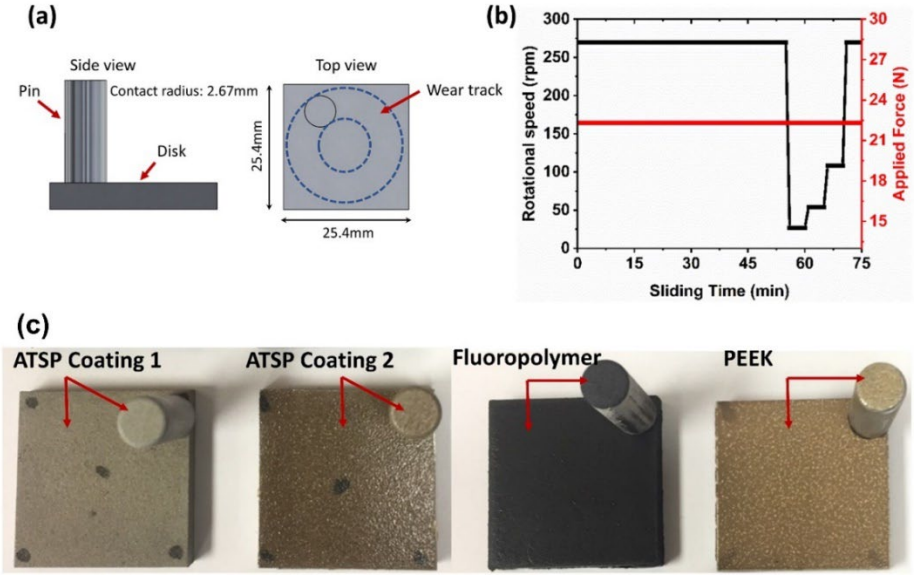

Figure 29. (a) Pin-on-disk experimental configuration, (b) speed and load functions used for the experiments, and (c) photographs of tribological samples showing the polymers coated on both pin and disk. Modified with permissions from "Bashandeh K, et al. Extreme environment tribological study of advanced bearing polymers for space applications. Tribology International. 2021;153:106634."

4.2.2 Specialized tribometer

Tribological experiments were carried out using a specialized tribometer, called High Temperature Tribometer (HTT). The HTT is designed for tribological experiments in a wide range of environmental temperatures from -196 °C to 1000 °C, rotational sliding speeds up to 1000 rpm, and normal loads up to 45 N. In-situ normal and friction forces are measured and used to calculate the in-situ COF. HTT has a glass/metal bell jar enclosure, which enables the control of the environmental atmosphere. Using a vacuum pump and ports, the bell jar could be evacuated, and the desired test gas can be introduced and maintained throughout the test. A detailed description of the tribometer, the working principle, and the heating mechanism can be found elsewhere [119]. In addition to the high-temperature range, a cryogenic testing stage was built inside the HTT chamber,

which enables experiments as low as -196 °C in liquid nitrogen (LN_2) or nitrogen (N_2) gas atmosphere with a temperature accuracy of ±3 °C. Further details of the cryogenic set-up can be found in [33].

4.2.3 Test procedure

A flat pin-on-disk configuration was used for tribological testing, as shown in **Figure 29(a)**. The disks and pins were used as the rotating and stationary parts, respectively. The tribo-pairs (i.e., pins and disks) were coated with ATSP, namely Coating 1 and Coating 2, PEEK/PTFE, and an FP (DuPont®) coatings, as described in **Table 6**. Two combinations of tribo-pairs were selected for the pin-on-disk experiments with ATSP-based material: Coating 2 vs. Coating 2 (C2/C2) and Coating 2 vs. Coating 1 (C2/C1). Self-mated contact was selected for PEEK/PTFE and FP coatings. To investigate the role of deposited polymers on the pin, two additional experiments were performed for the uncoated Al pins against ATSP coated disks.

Table 7 summarizes the experimental conditions. The experiments were performed at different environmental temperatures of -196 °C in LN_2, and -100, 25, 150, and 300 °C in N_2 gas under dry sliding conditions. A normal load of 22.3 N, equivalent to a nominal contact pressure of 1 MPa was applied during the experiments. The sliding speed was set according to the speed function shown in **Figure 29(b)**. Namely, four different sliding speeds (0.025, 0.05, 0.1, 0.25 m/s), equivalent to 17,145 cycles were applied each for 5 min after the 55 min long duration wear experiment (at 0.25 m/s). The varying speeds were intended to cover the potential operating speeds for different instruments in space applications and to capture the speed effect on the COF.

For all experiments at room and elevated temperatures, the bell jar of the HTT was vacuumed and flushed with N_2 gas trice to ensure minimal presence of air inside the chamber. During vacuum, the relative pressure reached -14.3 ± 0.1 psi, and by flushing of N_2 increased to 0.1 psi, which was maintained during the experiment. Two extra sets of experiments, namely durability and step-loading, were carried out on the best performing tribo-pair. The durability test was meant to evaluate the ability of the coating to withstand long duration sliding, and the step-loading was performed to determine the maximum load-bearing capacity before the coating fails catastrophically. Each sample was immersed in a glass beaker filled with isopropyl alcohol and placed in an ultrasonic cleaner for 10 min before and after each experiment for cleaning process. Subsequently, the samples were rinsed with isopropyl alcohol and dried using warm air.

Table 7. Tribological experimental conditions. Reprinted with permissions from "Bashandeh K, et al. Extreme environment tribological study of advanced bearing polymers for space applications. Tribology International. 2021;153:106634."

Experiment type	Materials	Temperature (˚C)	Contact pressure, MPa (load, N)	Linear speed, m/s* (Speed, rpm)	Ambient
Wear	ATSP Coating 1 ATSP Coating 2	-196, -100, 25, 150, 300	1 (22.3)	V1:0.025 (27), V2:0.05 (54), V3:0.1 (108), V4:0.25 (270)	N_2
	PEEK/PTFE DuPont	25, 150			
	Bare Al vs ATSP Coatings	25			
	Proton radiated ATSP Coating 2	25			
Durability	ATSP Coating 2	25	1 (22.3)	V4:0.25 (270)	Air
Step-Loading			22.3 N/min		

*The linear speeds were calculated based on 17.5 mm average diameter for the wear tracks

Micro/nanomechanical properties of the coatings, namely reduced elastic modulus and hardness were obtained at different temperatures using the indentation technique. 3D topographies of the surfaces of the coatings were obtained for fresh and tested samples using a contact surface profilometer. The surface profiles were used to evaluate the extent of wear and to extract the relevant surface roughness parameters such as root-mean-square roughness (S_q), and skewness (S_{sk}). Scanning Electron Microscopy (SEM) was performed to visually analyze the surface of the coatings and the corresponding wear mechanisms.

4.3 Results and discussion

4.3.1 Nanoindentation

Nanoindentation has been widely used for direct measurement of mechanical properties of different materials, including polymers in the form of bulk, thick and thin coating films [120–123]. In a typical indentation test, the probe tip is pressed into the surface of the sample at a constant loading rate and is withdrawn with similar rate. Since polymers show time-dependent properties due to viscoelastic behavior, a hold time is typically added at the peak load to remove the creep effect and to allow for viscous relaxation. Such loading profile is known as trapezoidal load function. During indentation, the in-situ load-displacement is recorded by the transducer. As shown by Oliver and Pharr [96], mechanical properties, such as reduced elastic modulus and hardness can be respectively obtained by the slope of the initial portion of the unloading curve, and dividing the indentation load at the peak load over the contact area.

Nanoindentation experiments were performed on each coating to evaluate their micro/ nanomechanical properties at room and elevated temperatures. A high temperature

nanomechanical instrument (TI Premier, Bruker) equipped with a Berkovich probe was used to perform the indentation tests. A trapezoidal shape load function was used with 5 seconds for each segment of load function. For indentations at elevated temperatures, the probe tip and samples were maintained at the experiment temperature for 15 min before the first indent, to minimize the thermal drift and allow for uniform dispersion of the heat over the sample. To obtain the properties of the coatings, the indentation depth was kept within 10% of the coating thickness, thus minimizing substrate effects.

Figure 30(a-d) show the load-displacement curves of the four coatings for indentations at temperatures of 25 °C, 150 °C, and 260 °C. Note the glass transition temperature for ATSP is within the range of 233-243 °C for C2A1 and 175 °C for CB2AB2, and therefore the indentation at 260 °C was performed above the Tg [114]. ATSP Coating 1 showed lower contact depth and shallower residual depth at 260 °C, which indicates its higher elastic recovery compared to ATSP Coating 2. This originates from the higher crosslink density of ATSP Coating 1, which confined the chain movements after Tg leading to more resistance against plastic deformation. The PEEK coating showed the highest residual and contact depth at 260 °C among all coatings tested.

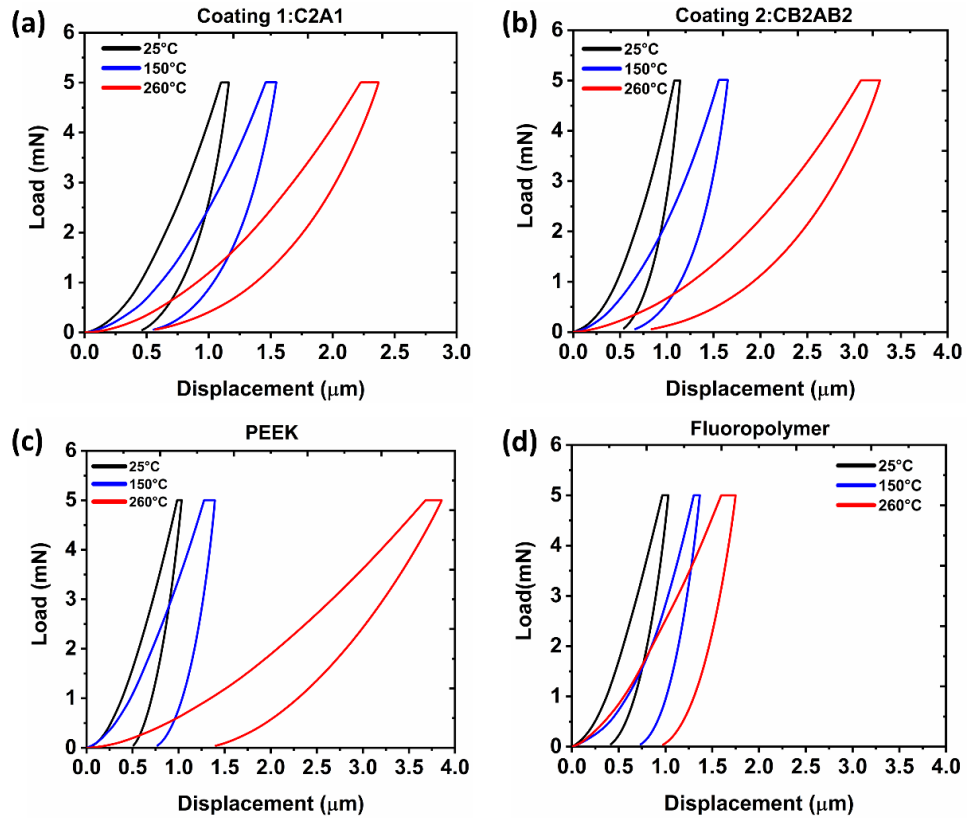

Figure 30. Representative indentation load-displacement curves of (a) ATSP Coating 1, (b) ATSP Coating 2, (c) PEEK/PTFE, and (d) FP coatings at different temperatures. Reprinted with permissions from "Bashandeh K, et al. Extreme environment tribological study of advanced bearing polymers for space applications. Tribology International. 2021;153:106634."

Figure 31(a, b) show the values of hardness and reduced elastic modulus of the four coatings extracted from the load-displacement curves. The reported values are the average of 4 indentations on different areas of the coatings, and the standard deviations are represented by the error bars in the figures. From the figures, the hardness and elastic modulus of all coatings decreased as the temperature increased, and significant softening was observed for all coatings at 260°C. The exception was with the FP coating (DuPont®), where the reduced modulus did not change to the extent of the other coatings. **Table 8**

summarizes the calculated averaged values of hardness and reduced elastic modulus for all coatings. PEEK/PTFE and FP indicated the highest reduced modulus and hardness values at temperatures of 25 and 150 °C. However, at 260°C, although the FP retained its superior mechanical properties, the PEEK/PTFE showed minimal hardness and reduced modulus, as the temperature of the test was much higher than the reported Tg value of PEEK (~143°C) [124]. Both ATSP-based coatings exhibited similar hardness and elastic modulus at temperatures of 25 and 150 °C. However, at 260 °C, the hardness and elastic modulus of ATSP Coating 2 dropped by 47%, compared to ATSP Coating 1, which could be justified by its lower crosslink density and lower Tg, compared to ATSP Coating 1.

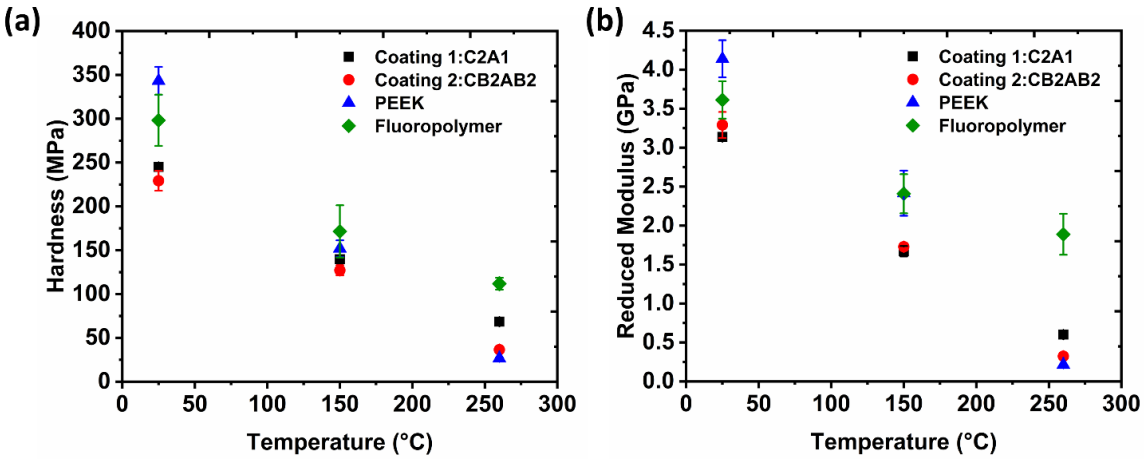

Figure 31. Nanoindentation results: (a) hardness and (b) reduced elastic modulus at different temperatures for ATSP Coatings 1 and 2, PEEK/PTFE, and Fluoropolymer (FP) coatings. Reprinted with permissions from "Bashandeh K, et al. Extreme environment tribological study of advanced bearing polymers for space applications. Tribology International. 2021;153:106634."

Table 8. Micromechanical properties of polymeric coatings tested. Reprinted with permissions from "Bashandeh K, et al. Extreme environment tribological study of advanced bearing polymers for space applications. Tribology International. 2021;153:106634."

Material	25°C		150°C		260°C	
	H (MPa)	Er (GPa)	H (MPa)	Er (GPa)	H (MPa)	Er (GPa)
Coating 1	245±3.81	3.14±0.05	140±4.77	1.67±0.07	68±2.12	0.60±0.01
Coating 2	229±11.35	3.29±0.17	127±5.78	1.73±0.05	37±0.33	0.32±0.03
PEEK/PTFE	343±15.90	4.14±0.24	151±9.47	2.42±0.29	27±1.15	0.21±0.01
DuPont	298±29.28	3.61±0.24	171±29.81	2.41±0.25	112±6.76	1.89±0.26

4.3.2 Friction

Figure 32(a, b) show the evolution of the in-situ COF vs. sliding time for the pin-on-disk experiments of Coating 2 vs. Coating 2 (C2/C2) and Coating 2 vs. Coating 1 (C2/C1). The last 20 min of the plots in **Figure 32(a, b)** correspond to the step speed function shown in **Figure 29(b)**. Additional experiments were carried out at RT for uncoated Al vs. C1 and uncoated Al vs. C2 to understand the role of pre-deposited transfer layer in the friction performance. For both tribo-pairs of C2/C2 and C2/C1, the variation of the COF with speed was clearly evident at cryogenic conditions, whereas the speed effect could hardly be identified at temperatures equal or greater than 25 °C. The running-in behavior was more pronounced at -196 °C, while other temperatures were at steady-state condition from the start. Compared to C2/C2, the experiments with C2/C1 required a longer time to reach steady-state condition. The change of COF with sliding for C2/C1 at -196 °C could be attributed to the changes in the surface roughness of the coatings during the experiments, as will be discussed later. For experiments with uncoated Al pins, both coatings showed similar higher COF, compared to experiments with coated pin. In

addition, the speed effect was more pronounced for uncoated Al and followed an increasing trend with sliding speed. It is noteworthy that the experiments for uncoated Al vs. C1 and uncoated Al vs. C2 were carried out to compare the results with C2/C2 and C2/C1 at RT to demonstrate the beneficial effect of pre-deposited transfer layer. Thereafter, the role of environmental temperature on the tribological performance was investigated only for tribo-pairs with better tribological performance (i.e., C2/C2 and C2/C1).

Figure 32(c, d) show the effect of sliding speed on the averaged COF of the two ATSP-based tribo-pairs sliding at different temperatures. The error bars designate the ± one standard deviation of the averaged calculated COF. Two distinct trends could be observed from the figures for both tribo-pairs: I) at temperatures of 25 °C and above, the higher sliding speed resulted in higher COF, and II) at cryogenic temperatures of -100 °C and -196 °C, higher sliding speed resulted in lower COF. From **Figure 32(c)**, when the temperature was ≥ 25 ˚C, the COF slightly increased with the increase of speed due to higher viscosity resistance [66]. However, at cryogenic temperatures, friction decreased when the speed increased due to the beneficial effect of generated frictional heat and its dissipation at the contact. At cryogenic conditions, the increase of contact temperature (due to increased speed) softened the surface, reduced the scratch resistance, and therefore reduced the COF at higher sliding speeds.

Figure 32(e) summarizes the COF vs. temperature for the long duration experiments at 0.25 m/s, which were calculated from 35 min to 55 min. Both tribo-pairs showed lower COF at higher temperature. C2/C2 exhibited higher COF in cryogenic but

lower COF at high temperatures. For C2/C2, the COF decreased by 47% from 0.163 at RT to 0.087 at 300 °C. For C2/C1, the COF decreased by 26% from 0.155 at RT to 0.114 at 300 °C. At -196 °C, the COF experienced a large increase from -100°C.

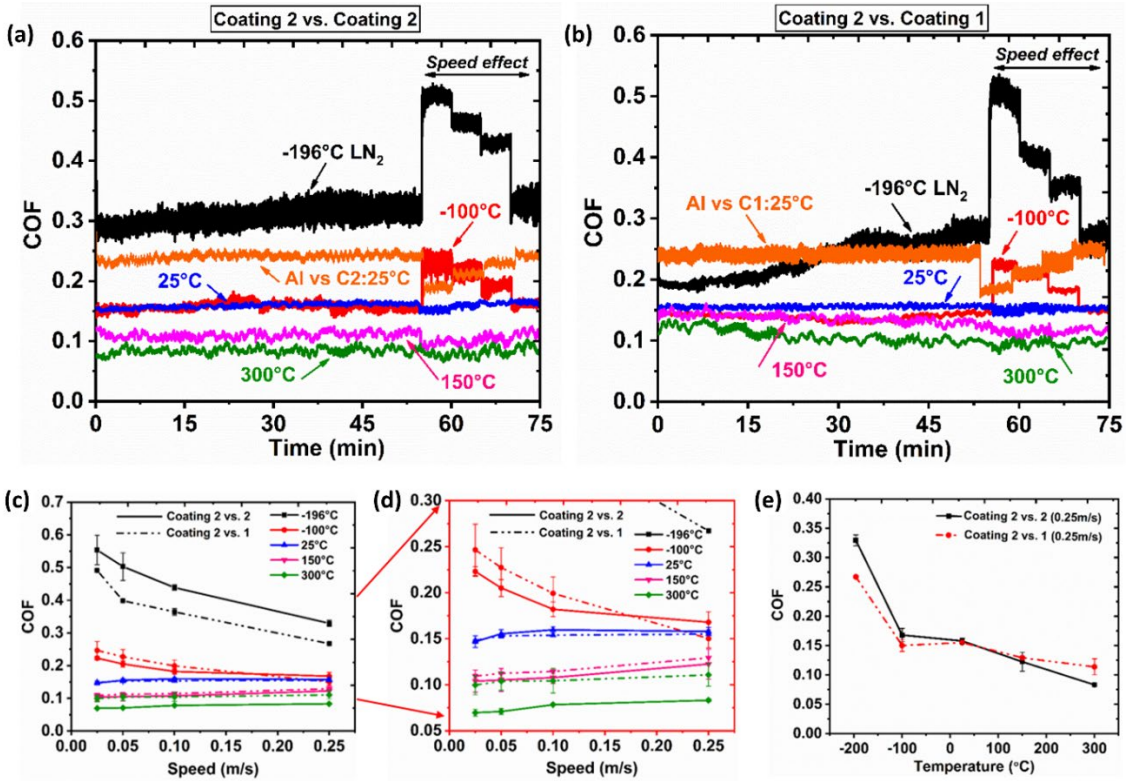

Figure 32. In-situ COF vs. time for ATSP coatings: (a) Coating 2 vs. Coating 2, and (b) Coating 2 vs. Coating 1, (c) Variation of COF with sliding speed at different temperatures, (d) zoom in of COF from 0 to 0.3, and (e) COF vs. temperature for long-duration experiments at 0.25m/s. Reprinted with permissions from "Bashandeh K, et al. Extreme environment tribological study of advanced bearing polymers for space applications. Tribology International. 2021;153:106634."

Changes in temperature may create two opposing effects at the interface between sliding bodies: change in real contact area due to changes in elastic modulus, and changes in the interfacial shear strength. Depending on which is more dominant, different trends for friction could be obtained. Here, it is postulated that when the temperature increased

from RT, the decrease of interfacial shear strength due to softening of the polymers (as shown in hardness measurements in **Figure 31**) was dominant, and therefore the friction reduced with the increase of temperature. It is noteworthy that according to hardness measurements in **Figure 31**, the softening effect was more pronounced for Coating 2, compared to Coating 1, particularly at maximum temperature of 260 °C. Therefore, lower friction was obtained for C2/C2 at 300 °C. When the temperature decreased to -100°C, the elastic modulus increased significantly, as revealed by DMA measurements [33]. Hence, the real contact area decreased, leading to a decrease in the COF. At -196 °C, the polymer chains became frozen, which impeded smooth sliding between the tribo-pairs, which generated abrasion, as will be shown in the SEM images. Besides, the frictional heat could dissipate into LN_2 faster compared with dry sliding, which caused higher friction compared to -100 °C.

Figure 33(a) shows the in-situ COF for experiments at 25 and 150 °C for the tribo-pairs PEEK/PTFE vs. PEEK/PTFE and FP vs. FP coatings. Except for the experiments with FP at RT, all the other tests showed steady-state behavior from the start. The increase of temperature to 150 °C markedly reduced the COF of FP coating due to lower adhesion and pitting at 150 °C, which ultimately caused a smoother shear layer in the tribo-contact. This mechanism will be shown in the SEM analysis of the coating in section 3.4. As shown in **Figure 33(b)**, increasing the sliding speed slightly increased the COF for both coatings, similar to the results obtained for the ATSP coatings and consistent with the results in [124]. **Figure 33(c)** shows the summary of the averaged COF values for long-duration experiments (55 min) at room and elevated temperatures. All coatings exhibited a

decreasing trend with increase of temperature due to softening of the coatings at elevated temperatures, as shown in **Figure 31**. For the experiments at RT, the FP coating showed the highest friction with 52% higher COF among the other coatings, whereas the rest of the coatings exhibited similar COF.

The deposition of the ATSP coatings on the Al pins resulted in 35-40% reduction in COF, implying the beneficial effect of pre-deposited "transfer layer" on the pin. At 150 °C, all coatings showed a negligible difference in the COF with maximum of 0.129 for ATSP C2/C1. For the experiments at 300 °C, the PEEK/PTFE coating failed after 10 min sliding, and the coating was worn out entirely from both pin and disk. Since FP coating did not show promising behavior at RT, no additional experiment was performed at 300 °C. For ATSP coatings, the tribo-pair C2/C2 indicated the best performance with averaged COF of 0.083, which was 27% less than C2/C1. The difference in the friction behavior could be attributed to a more pronounced softening effect in C2 compared with C1, as shown in hardness measurements in **Figure 31(a)**. Regarding space applications, the ultimate goal is to find a tribo-pair with coverage of potential operating temperatures in the space environment from cryogenic to elevated temperatures. In this chapter, we investigated the temperature range from -196 to 300 °C. Hence, tribo-pair C2/C2 was selected as the best performing pair for this wide range of operating temperatures and was further studied.

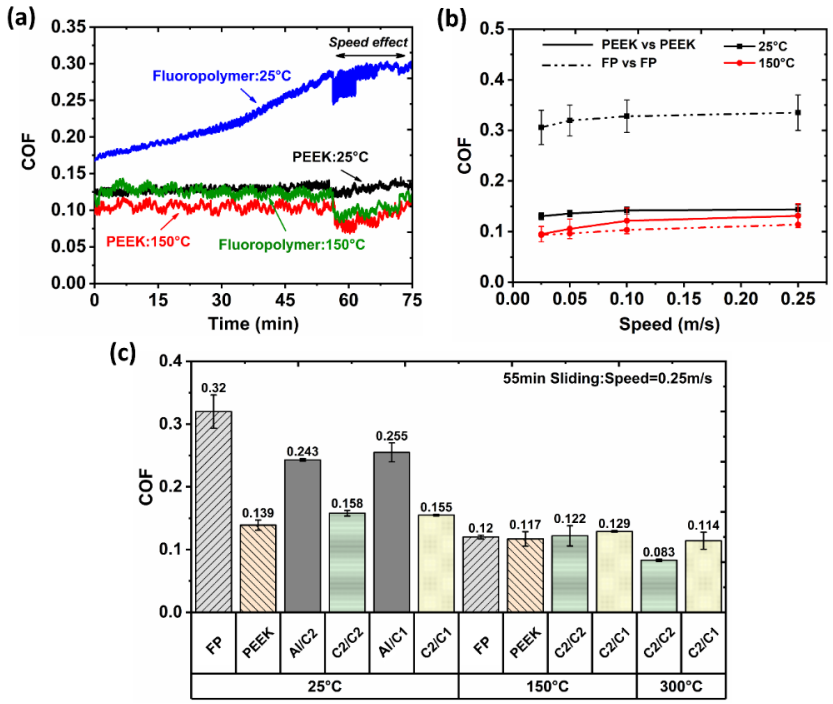

Figure 33. (a) Evolution of COF vs. time for PEEK/PTFE and FP (DuPont®) coatings, (b) variation of COF with sliding speeds at temperatures of 25 and 150 °C, and (c) comparison of averaged COF for all coatings at different temperatures for long-duration experiments. Reprinted with permissions from "Bashandeh K, et al. Extreme environment tribological study of advanced bearing polymers for space applications. Tribology International. 2021;153:106634."

4.3.3 Wear analysis

To investigate the surface changes due to sliding, Sq and Ssk values were calculated from the measured 3D topographies of the untested and tested ATSP coatings (after the experiments at different temperatures). **Figure 34** shows the comparison of Sq and Ssk values for Coating 1 and Coating 2. The corresponding values are also listed in **Table 9**. While Coating 2 showed slightly higher Sq in as-received condition, a significant difference was found in the skewness values being positive for Coating 1 and negative for Coating 2. The skewness represents the degree of asymmetry of the surface profile and distribution of peaks and valleys about the mean plane. Positive Ssk indicates a surface

with high peaks and shallow valleys, whereas a negative Ssk represents a surface with deep valleys and more flattened peaks.

Table 9. Measured roughness and skewness values for ATSP coatings before and after tribological testing. Reprinted with permissions from "Bashandeh K, et al. Extreme environment tribological study of advanced bearing polymers for space applications. Tribology International. 2021;153:106634."

Condition	Coating 1		Coating 2	
	rms roughness (*Sq*)	**Skewness (*Ssk*)**	**RMS roughness (*Sq*)**	**Skewness (*Ssk*)**
Untested	4.53±0.19	0.85±0.42	4.88±0.87	-0.40±0.20
-196°C	5.83±0.02	-0.21±0.13	4.91±0.21	-0.52±0.13
-100°C	4.50±0.09	0.17±0.03	4.70±0.08	-0.25±0.05
25°C	4.01±0.18	0.21±0.01	3.44±0.21	-0.17±0.02
150°C	3.96±0.12	0.32±0.01	4.50±0.14	-0.41±0.003
300°C	2.09±0.06	-0.10±0.08	4.02±0.39	-0.16±0.05

For C2/C1 experiments at -100, 25, and 150 °C, the roughness of Coating 1 remained nearly unchanged as the variations were in the range of the standard deviation, which implies slight burnishing of the top asperities. However, the roughness value increased for experiments in LN_2 at -196 °C, compared to as-received condition. Since Coating 2 had a slightly higher roughness, the hardened asperities of the coating 2 (due to cryogenic temperature) abraded the smoother surface of Coating 1 (as shown in the SEM images later) and increased roughness with sliding. The formation of grooves and abrasive wear could also be inferred from the transition of skewness to negative values. Thus, the increase of COF with sliding time in **Figure 32(b)** could be attributed to changes in surface roughness. For experiments at 300 °C, the surface roughness reduced by 54%, which indicates a marked polishing effect for the coating. Moreover, the skewness changed to

negative value due to removal of the asperities and flattening of the top peaks. For C2/C2 experiments, no specific trend could be obtained as the variations were insignificant.

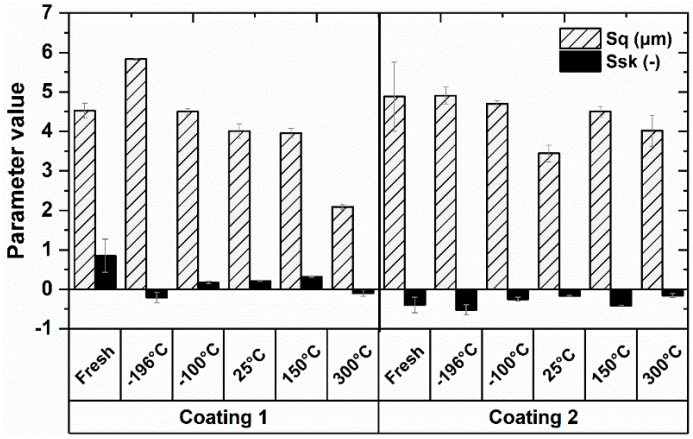

Figure 34. Variation of rms roughness Sq and skewness Ssk of the ATSP coatings on the disk, after experiments at different temperatures. Reprinted with permissions from "Bashandeh K, et al. Extreme environment tribological study of advanced bearing polymers for space applications. Tribology International. 2021;153:106634."

Figure 35(a, b) show the profilometric wear scans of the ATSP tribo-pairs after experiments at different temperatures. The wear could hardly be distinguished from scans for both coatings, and therefore the wear was unmeasurable at all temperatures, which will also be confirmed by the SEM images. This is a remarkable finding for the coatings to exhibit "zero" wear under dry sliding conditions in the full range of 500 ^{o}C. Coating 2 maintained its original topography and showed mild burnishing of the top asperities at elevated temperatures. Similar behavior was observed for Coating 1, except two distinct behaviors at the extreme temperatures of -196 °C and 300 °C. For the experiments at -196 °C in LN_2, a wide groove could be identified in the Coating 1 profile indicating abrasive wear mechanism. Compared to Coating 2, the polishing effect was more severe at 300 °C,

which caused the smoothening of the surface of the coating. The SEM analysis will further support these surface changes.

Figure 35(c, d) show the profilometric wear scans of PEEK/PTFE and Fluoropolymer coatings, respectively. As seen in the scans, the surface of PEEK/PTFE was rougher than FP, which originated from the difference in the deposition process of the two coatings. For PEEK/PTFE, the wear was not discernible from the scans at both temperatures of 25 and 150 °C. However, the FP coating experienced relatively high wear at 25 °C and, to a lesser extent at 150 °C.

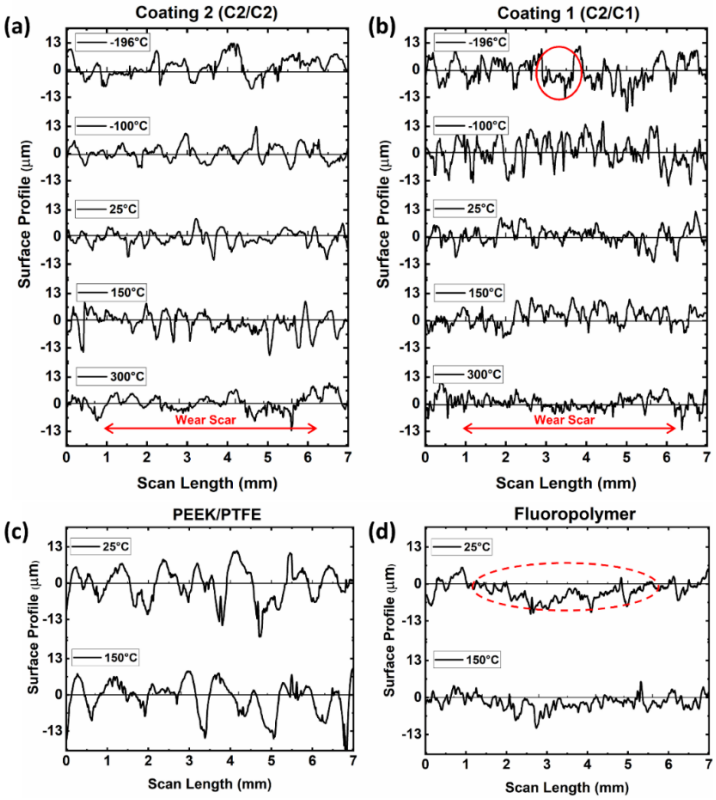

Figure 35. Typical profilometric wear scans measured across the wear scars on the disks: (a) ATSP Coating 2, (b) ATSP Coating 1, (c) PEEK/PTFE coating, and (d) FP coating. Reprinted with permissions from "Bashandeh K, et al. Extreme environment tribological study of advanced bearing polymers for space applications. Tribology International. 2021;153:106634."

Since the ATSP coatings experience unmeasurable wear at different temperatures, two additional experiments, namely long duration wear and step loading experiments were carried out to examine the durability and load-bearing capability of the coating, respectively. The experimental conditions for each test are shown in **Table 7**. **Figure 36(a, c)** show the in-situ COF for tribo-pair C2/C2, which was sliding for 18 hrs, corresponding to 16.2 Km sliding distance, and a typical wear scan of the coating after the experiment. The average COF was 0.17±0.007 with "zero" wear. For the step loading experiment, the normal load was increased by 22.3 N/min until the coating was removed from pin or disk. **Figure 36(b)** shows the in-situ COF, which indicates a sudden increase of the COF after 7 min sliding. This increase in the COF was due to removal of the coating from the pin. Therefore, the tribo-contacts changed from polymer-on-polymer to metal-on-polymer. Yet, the surface of the coating on the disk remained in good condition, as revealed from the wear scan of the coating, shown in **Figure 36(d)**. It is noteworthy that the delamination on the pin could be avoided by improved substrate preparation before the coating process. For example, surface laser texturing method could be employed to significantly increase the bonding strength of the coating and substrate [125].

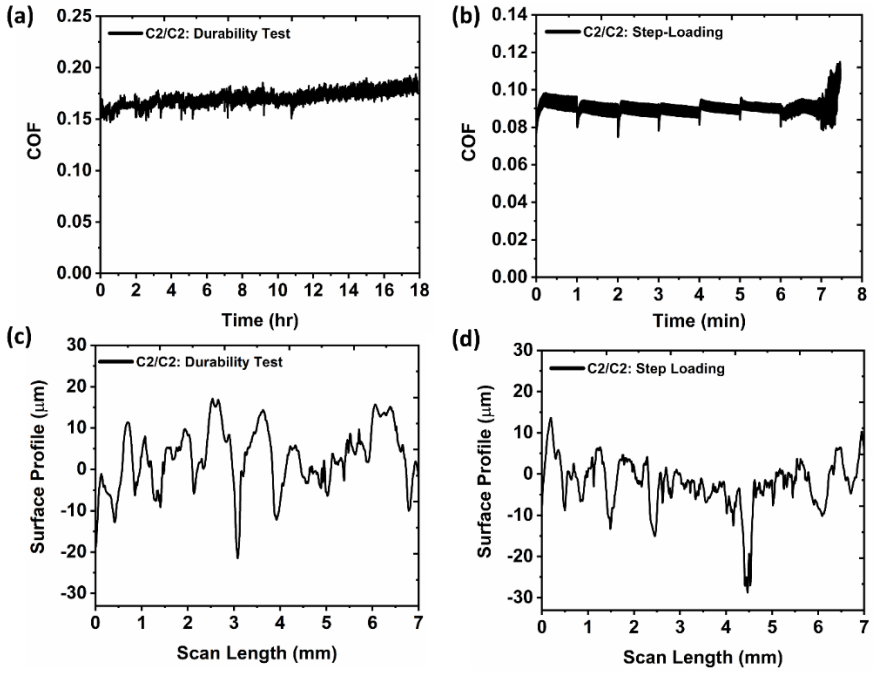

Figure 36. In-situ COF vs. sliding time and profilometric wear scans of ATSP Coating 2 for (a, c) durability experiments, and (b, d) step loading experiments. Reprinted with permissions from "Bashandeh K, et al. Extreme environment tribological study of advanced bearing polymers for space applications. Tribology International. 2021;153:106634."

4.3.4 SEM analysis

Due to strong dependency of mechanical properties of polymers with temperature, properties such as hardness and modulus could markedly change with transition of temperature from cryogenic (-196 °C) to elevated (300 °C) temperatures. Therefore, changes in wear mechanism are expected with temperatures, from abrasive wear at cryogenic to adhesive wear or polishing wear at elevated temperatures. SEM was used to examine the worn surfaces after tribological experiments at different temperatures. To obtain the SEM images of the coatings after the experiments, each coating was sputter coated with a thin (3 nm thickness) layer of Pt/Pd.

Figure 37(a-d) depict the SEM images of all the coatings in their as-received (untested) condition. The overall morphologies of the ATSP Coatings 1 and 2 are the same and show a uniform distribution of hills and valleys throughout the surface. The PEEK/PTFE coating features a rough bumpy structure with different distribution and surface areas. The FP coating contains blends of fluoroplastics, and the exact composition is not known. Nonetheless, the multi-phase characteristic of the coating is clearly identified from the SEM image in **Figure 37(d)**.

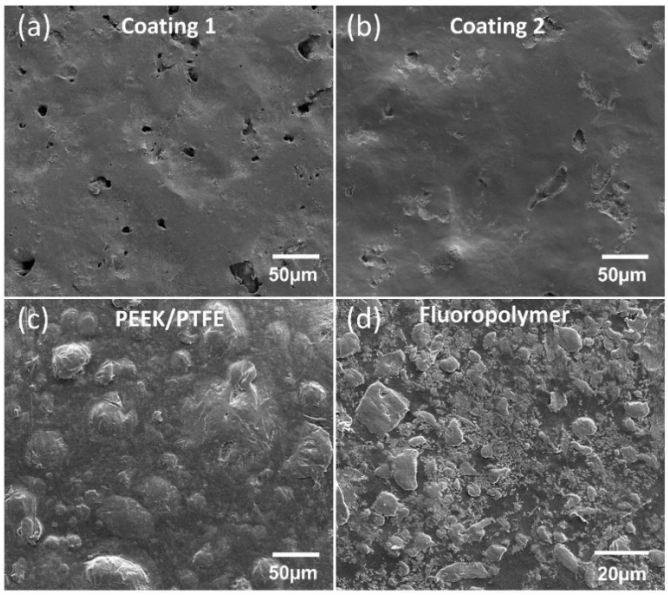

Figure 37. SEM images of untested surfaces of polymer coatings: (a) ATSP Coating 1, (b) ATSP Coating 2, (c) PEEK/PTFE, and (d) FP. Reprinted with permissions from "Bashandeh K, et al. Extreme environment tribological study of advanced bearing polymers for space applications. Tribology International. 2021;153:106634."

Figure 38 shows the SEM images of ATSP Coating 1 after the experiments with C2/C1 at -196, 25, and 300 °C. The figures for each temperature reveal a distinct wear mechanism. At -196 °C, the wear was dominated by abrasion due to formation of wide

grooves and scratch marks on the wear scar on the disk. These grooves were caused by either the hardened asperities of Coating 2 on the pin when sliding against Coating 1, or the agglomerated hardened wear debris. Such wear mechanism could be attributed to drastic increase of stiffness at cryogenic temperatures, which were reported by the DMA studies of the ATSP coatings, where a remarkable increase of storage modulus by 90% occurred when the temperature decreased from RT to -140 °C [33]. At 25°C, the wear could hardly be identified from the worn surface compared to the unworn surface shown in **Figure 37(a)**, which substantiates the unmeasurable "zero" wear of the coating at this temperature. A combination of microcracks and notable burnishing effect could be observed on the wear scar after experiments at 300 °C, which justifies the reduction in roughness shown in **Figure 35**. Microcracks were formed on the worn surface due to fatigue wear, which could arise from the generated repeated stresses by the cyclic loading from the pin. Similar microcracks were found for sliding of steel against ATSP at 300 °C [114]. The magnified image in the right column of **Figure 38(c)** shows the reattachment of wear debris on the coating due to the interchain transesterification reactions (ITR) of the ATSP [80], which is a unique property of the ATSP material. The solid-state ITR bond exchange reaction occurs by formation of a contiguous network between two fully thermoset layers through two proposed reaction mechanisms, namely esterolysis and acidolysis-type transesterifications. It should be mentioned that the observed difference in the wear mechanisms is arising from the difference in the experimental temperatures. At -196 ℃, the asperities were hard enough to cause abrasive wear, while at 300 ℃ the polymer was softened significantly compared to -196 ℃ and 25 ℃ and therefore fatigue

wear occurred, which caused the generation of microcracks on the coating. This fatigue crack is mainly the crack at the boundary between ATSP resin and PTFE additive, based on two reasons. First, the orientation of cracks is random and not on a preferred direction such as perpendicular to sliding direction; second, the PTFE powders were not melted during curing or experiments and therefore the boundary between the two polymers could be sharp. In addition to the repeated sliding friction, the mechanical properties of the two the polymers were different as well and internal stress could be generated at the boundary, and thus the boundary broke and formed the micro-cracks at 300 ℃.

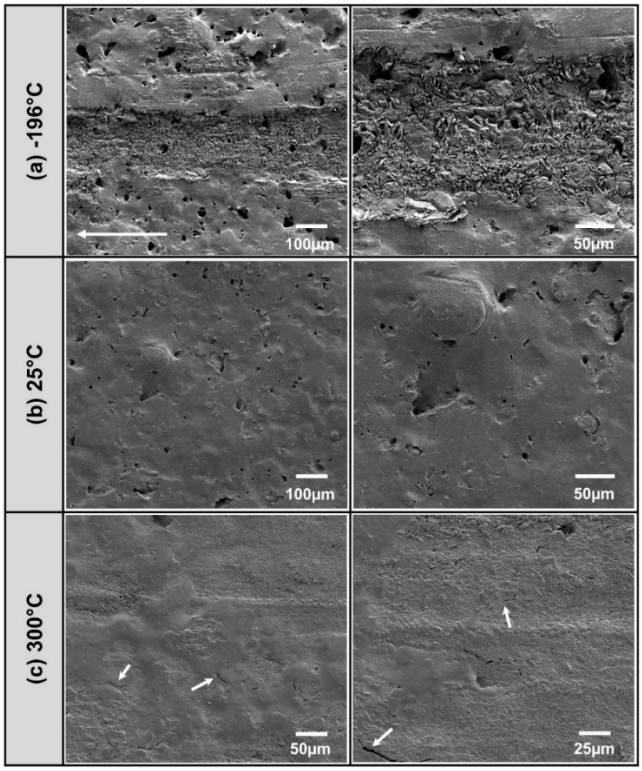

Figure 38. SEM images of worn surfaces of ATSP Coating 1 after experiments C2/C1 at (a) -196 °C, (b) 25 °C, and (c) 300 °C. The arrow in (a) shows the sliding direction, and arrows in (c) show microcracks. Reprinted with permissions from "Bashandeh K, et al. Extreme environment tribological study of advanced bearing polymers for space applications. Tribology International. 2021;153:106634."

Figure 39 shows the SEM images of ATSP Coating 2 on the disk after experiments with C2/C2 at -196, 25, and 300 °C. The wear could be characterized by low abrasion microgrooves parallel to sliding direction at -196 °C, with less severity compared to Coating 1. Similar to Coating 1, the wear was not discernible at 25 °C. Unlike Coating 1, Coating 2 retained its original topography at 300 °C and showed minor burnishing effect. The microcracks that were visible on Coating 1 could not be observed on Coating 2. This could be attributed to lower crosslink density of Coating 2, which allowed higher flexibility of inter-crosslink chains upon deformation. Coating 2 showed lower hardness at temperatures above Tg, as shown in **Figure 31(a)**. Therefore, the combined effect of higher flexibility and lower hardness resulted in more resistance to fatigue wear, which is appealing for applications experiencing fatigue wear.

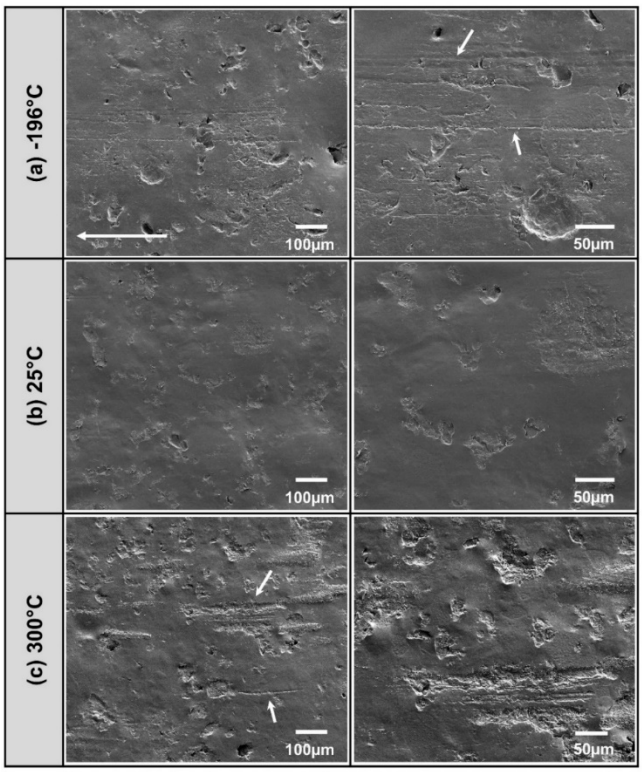

Figure 39. SEM images of worn surfaces of ATSP Coating 2 after experiments C2/C2 at (a) -196 °C, (b) 25 °C, and (c) 300 °C. The arrow in (a) shows the sliding direction, and arrows in (c) show scratches. Reprinted with permissions from "Bashandeh K, et al. Extreme environment tribological study of advanced bearing polymers for space applications. Tribology International. 2021;153:106634."

Figure 40 depicts the SEM images of PEEK/PTFE coating on the disk after the experiments. As shown in **Figure 37(c)**, the as-received surface of the coating featured a rough bumpy structure, where the initial contact occurred. The burnishing and smoothening of these asperities were therefore the expected outcome of sliding [18], which is depicted in **Figure 40(a)** for the experiment at RT. In addition to burnishing, parallel microgrooves and plastic plowing were formed in the sliding direction when the temperature was raised to 150 °C. The EDS analysis of the coating after RT experiment is show in **Figure 40(c)**. The fluorine and carbon elements are denoted with green and red

colors, respectively. Comparing the worn and unworn surfaces indicates the burnishing of the embedded PTFE particles in the coating, which are uniformly distributed throughout.

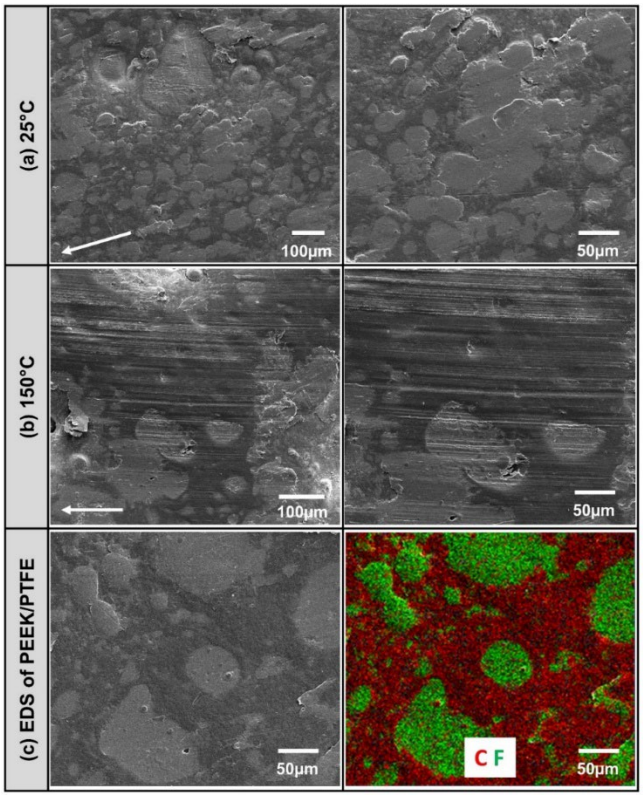

Figure 40. SEM images of the worn surfaces of PEEK/PTFE coated disk after the experiments at (a) 25 °C, and (b) 150 °C, and (c) SEM/EDS of the coating after RT experiment. The arrows show the sliding direction. Reprinted with permissions from "Bashandeh K, et al. Extreme environment tribological study of advanced bearing polymers for space applications. Tribology International. 2021;153:106634."

As seen in **Figure 41(a)**, the FP coating was uniformly worn out and polished across the wear track at both temperatures. Adhesive wear was the wear mechanism at both temperatures but with higher intensity at RT. A clear distinction between the two temperatures is the formation of microgrooves at 150 °C and pitting areas at RT. Similar pitted areas were observed for sliding of steel against FP coating [63]. Lower adhesion

and absence of pitting marks at 150 °C caused a smoother shear layer in the tribo-contact, which ultimately led to lower friction and wear at elevated temperature.

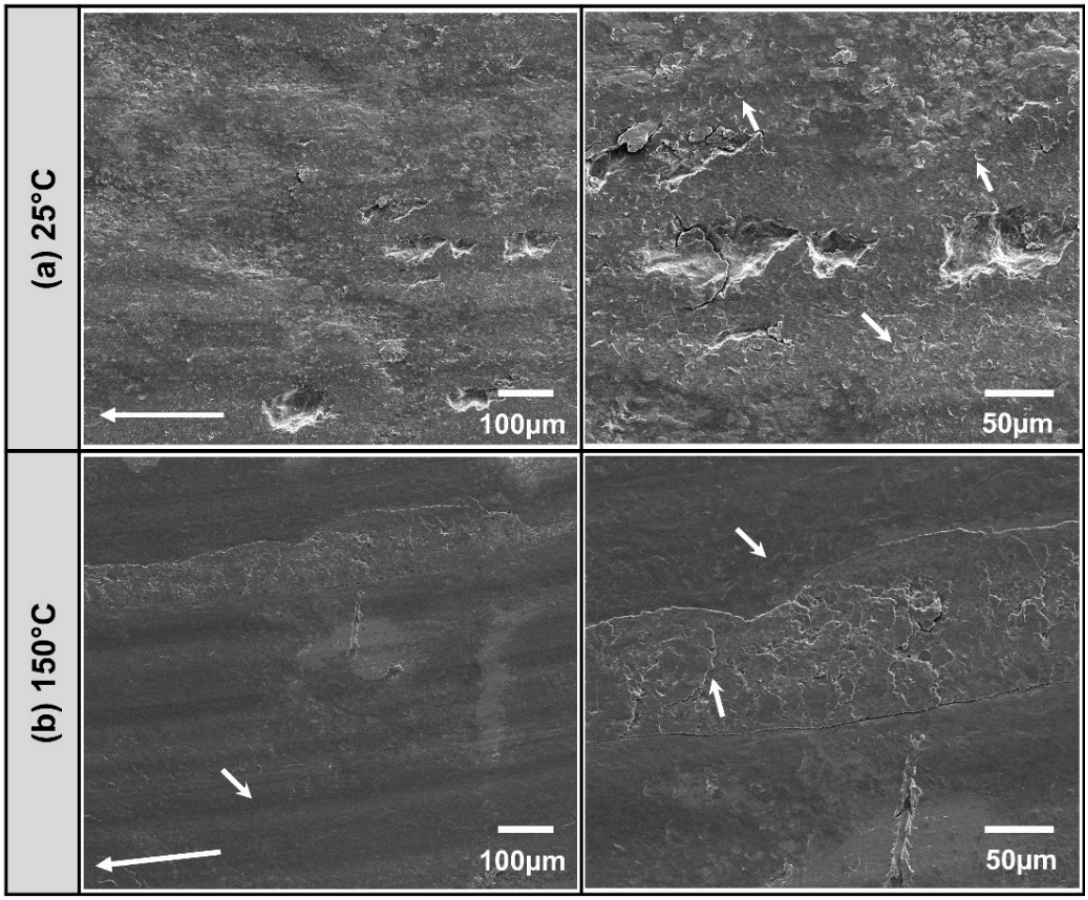

Figure 41. SEM images of the worn surfaces of FP coated disk after experiments at (a) 25 °C, and (b) 150 °C. Longer arrows show the sliding direction, and shorter arrows show adhesive wear. Reprinted with permissions from "Bashandeh K, et al. Extreme environment tribological study of advanced bearing polymers for space applications. Tribology International. 2021;153:106634."

4.3.5 Radiation exposure

Solar cosmic rays generate space radiation in the form of predominantly proton radiation. The protons can create internal defects in structures due to atomic displacement, which can lead to damage of the devices, including bearing materials. The damage of

space radiation is cumulative, although the dose of radiation is low. Therefore, the cumulative damage to the device and its susceptibility from proton exposure should be investigated before starting space missions [126,127]. The assessment of the problems caused by radiation requires first determining radiation type, energy, and dose as a function of time of the mission. Second, the performance of the representative material needs to be assessed through exposure to radiation environment. Lastly, the best material should be selected for a complete design [128]. To this end, the selected coating, namely ATSP Coating 2 was exposed to proton radiation exposure with the equivalent of 50-year duration. The proton beam had fixed energy of 2 MeV. The radio frequency quadrupole (RFQ) was utilized to generate this beam runs, pulsed at a duty factor of up to 1%.

To investigate the effect of radiation exposure on the morphology of the coatings, 3D mapping was carried out for the coating before and after 50-year exposure. **Figure 42** shows the 3D surface topographies of ATSP Coating 2 before and after exposure. Comparing the 3D topographies, the overall morphology remained mostly unchanged. However, the surface roughness (Sq) decreased by 20%. This surface roughness change could be due to surface attack by protons, and therefore the high peaks or loose structures were broken off the surfaces. A similar decrease in surface roughness upon proton radiation was seen for PEEK samples [129].

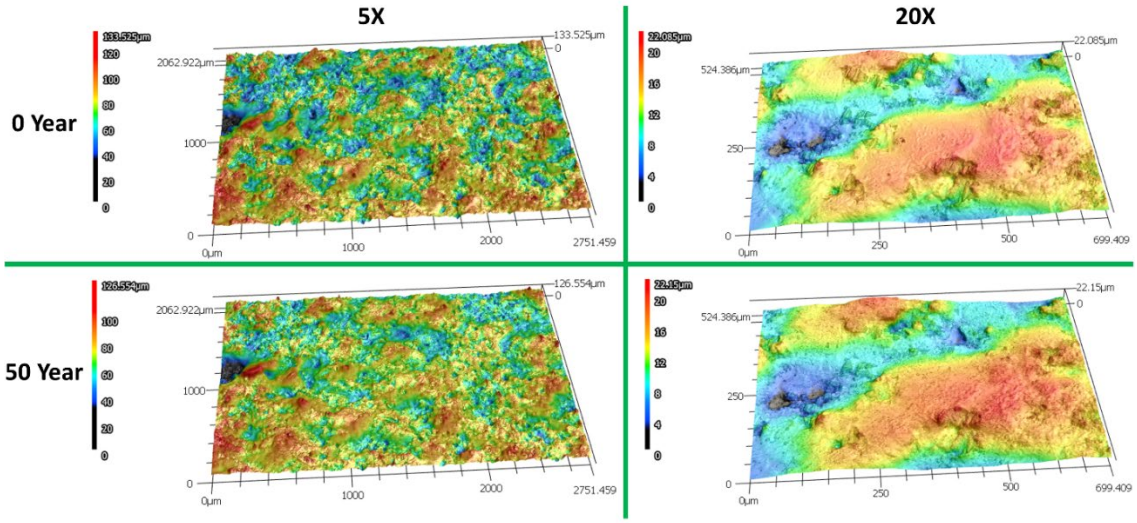

Figure 42. Typical 3D contact profilometry surface topographies of ATSP coating 2 with 0-year and 50-year radiation exposure, showing no significant changes. Reprinted with permissions from "Bashandeh K, et al. Extreme environment tribological study of advanced bearing polymers for space applications. Tribology International. 2021;153:106634."

Nanoindentation experiments were performed to examine the effect of radiation on the micromechanical properties of the top surface layers. The effect of temperature was studied through indentations at different temperatures of 25, 150, and 260 °C. **Figure 43(a, b)** show the obtained hardness and reduced elastic modulus values of ATSP Coating 2 before and after radiation, respectively. The coating retained its mechanical integrity upon proton exposure, as the hardness and elastic modulus values remained relatively unchanged before and after radiation.

To compare and investigate the changes in the tribological behavior upon exposure of the coatings to radiation, two additional experiments for C2/C2 were carried out at RT under the same conditions as before (**Table 7**). As shown in **Figure 43(c, d)**, there was no performance (COF and wear) change between the unirradiated and radiated coatings.

Earlier studies demonstrated dependency of the tribological behavior on proton radiation dose. Besides, various increasing or decreasing trends for COF and wear were found for different materials such as PEEK and polyimides [129,130]. Nonetheless, no such dependency is seen with the ATSP coating.

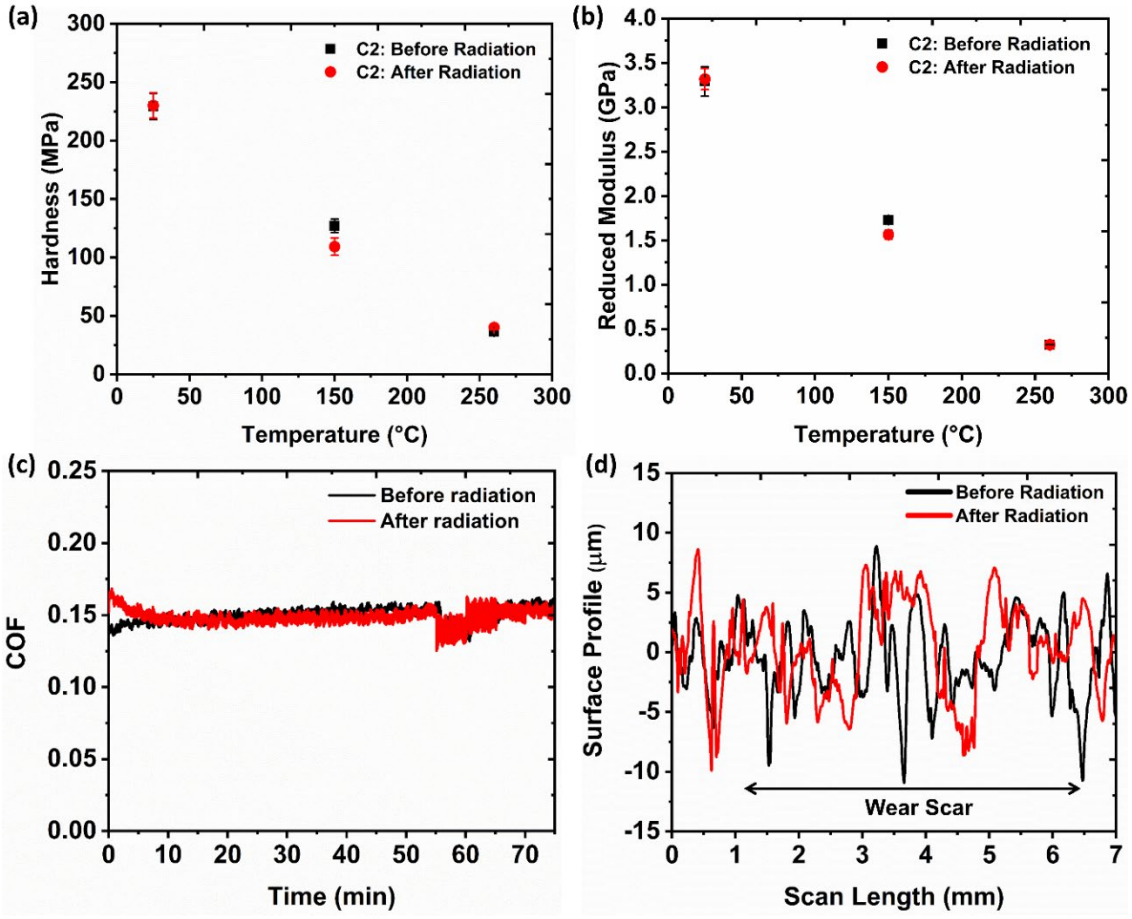

Figure 43. Comparison of micro-mechanical and tribological behavior of C2/C2 before and after proton radiation: (a) hardness, (b) reduced elastic modulus, (c) COF vs. time, and (d) profilometric scans across the wear scars, showing "zero" wear. Reprinted with permissions from "Bashandeh K, et al. Extreme environment tribological study of advanced bearing polymers for space applications. Tribology International. 2021;153:106634."

4.4 Summary

The tribological performance of different high bearing polymeric-based coatings, namely ATSP, PEEK, and a FP-based, were investigated using pin-on-disk experiments at different environmental temperatures spanning a range of almost 500 °C. Both pins and disk were coated with the polymeric materials to simulate a polymer on pre-deposited "transfer layer" sliding. The variations of COF with temperature, evolution of surface topography, and wear mechanism were studied and the following conclusions could be drawn:

1. For the two ATSP-based tribo-pairsthe COF monotonically reduced with increase of temperature from 25 °C to 150 °C, and 300 °C due to softening of the polymer with temperature. For C2/C2, the lowest COF of 0.087 was obtained at 300 °C, which was 27% lower than C2/C1; At cryogenic temperatures, the COF reduced with decreasing temperature to -100 °C and showed a large increase from -100 °C to -196 °C;

2. Compared to experiments with uncoated Aluminum at RT, the COF reduced by 35-40% for ATSP coating on ATSP coating, indicating the beneficial effect of a pre-deposited transfer layer on the counter-surface (pin);

3. PEEK/PTFE coating performed similar to ATSP coating and better compared to FP coating in terms of friction and wear within a lower temperature range (25 and 150 °C). However, PEEK/PTFE could not survive at 300 °C. Both PEEK and ATSP coatings showed unmeasurable "zero wear." On the other hand, the FP coating exhibited higher wear at RT and, to a lesser extent at 150°C;

The best performing ATSP Coating 2 is recommended due to superior performance from RT to 300 °C, as summarized in **Figure 44**. The morphological, mechanical, and tribological properties of the coating remained unchanged upon proton radiation exposure. This suggests that this coating performs well with "zero wear" and controlled COF at a range of almost 500 °C and does not suffer deterioration due to proton exposure.

Polymer	Wear & COF at 25 °C	Wear & COF at 150 °C	Wear & COF at 300 °C	Wear & COF at cryogenic
ATSP				
PEEK/PTFE				NA
Fluoropolymer			NA	NA

Figure 44. Comparison of tribological performance of ATSP, PEEK/PTFE, and Fluoroplastic coatings under different testing conditions simulating space applications. Reprinted with permissions from "Bashandeh K, et al. Extreme environment tribological study of advanced bearing polymers for space applications. Tribology International. 2021;153:106634."

Based on experimental findings in this Chapter, ATSP coating 2 and PEEK/PTFE coating showed the best performance in terms of maintaining low COF and "zero wear" over a wide temperature range. Therefore, these two polymer composite coatings are proposed for Lunar/Mars abrasive experiments and Titan simulated environment studies, as will be discussed in Chapter 5 and 6, respectively.

CHAPTER 5[4]

ABRASIVE WEAR OF PEEK AND ATSP-BASED POLYMER COMPOSITE COATINGS UNDER LUNAR REGOLITH CONDITIONS

5.1 Introduction

Two-body and three-body abrasion are widely used terms for the classification of abrasive wear and are defined as the material removal or displacement by either embedded hard particles and perturbances on the surface, or the wear by trapped particles at the interface, respectively [131]. The reported cost associated with the operation of replacing machinery components and parts due to abrasive wear is shown to be as high as 63% among different wear types, and abrasive wear loss is accounted for 50% of wear problems in industry [132,133], which is concerning for applications where abrasive wear mitigation is desired. An example of destructive abrasion was seen during Apollo 11 mission caused by Lunar regolith, which is claimed to be the number one concern for returning to the moon surface [27]. Therefore, the development of technologies for dust mitigation on the tribological components and equipment is imperative for successful explorations on the Moon, Mars, and other planetary surfaces [134]. Surface pre-treatment is shown to be an effective method for dust mitigation and is performed by modifying the surface through physical or chemical treatments [134]. This chapter reports a sand-dust mitigation approach to achieve long-life bearing and tribological surfaces by treating the original

---

[4] Bashandeh K, Lan P, Polycarpou AA, Abrasive wear of PEEK and ATSP-based polymer composite coatings under lunar regolith conditions, under revision in Wear journal, 2022.

metal-on-metal tribo-interface to metal-on-polymer and subsequently polymer-on-polymer interface. The samples were deposited with polymer coatings with micrometer thickness range and tribologically tested under Lunar regolith simulant abrasive conditions.

Polymers with self-lubricating properties are promising materials for design purposes, particularly in applications where the use of external conventional lubrication is not feasible such as in space-related applications [107]. Polytetrafluoroethylene (PTFE), molybdenum disulfide, and graphite are commonly used solid lubricants that could be incorporated into the polymer matrix to provide a lubricious film on the counterface and reduce the coefficient of friction (COF) and wear [113]. The load-bearing capability and specific wear rate are important design considerations under abrasive conditions [135]. Some studies have reported the beneficial effect of adding fiber reinforcements and nanoparticles to improve polymers' abrasive wear resistance [135–138]. The deposition of appropriate polymer coating on a harder metallic substrate is shown to further enhance the load-bearing, dimensional, and thermal stability, compared with bulk polymers [19,75].

The literature is relatively abundant with tribological studies for two- and three-body abrasive wear behavior of bulk polymer-based composites such as PEEK-based, PTFE-based, polyimide (PI)-based, and polyamide-based under dry or lubricated sliding [135,137,139–142]. Metal-on-polymer configuration is the primary experimental configuration in the literature and the foregoing studies. The objectives are on the comparative studies of different polymers and the enhancement on the tribological

performance by adding various quantities and types of fillers. Nonetheless, little attention is given to polymer coatings, and in particular polymer-on-polymer tribo-contacts, as an alternative approach for enhancing the tribological performance and sand-dust mitigation, and specifically Lunar regolith.

The objective of this chapter is to investigate the tribological performance of two high-performance polymer composite coatings, namely PEEK and ATSP-based polymers mixed with desired amount of PTFE lubricant additive under two sizes of Lunar regolith simulant, referred to as sand (38-125 μm) and dust (<38 um) abrasive conditions. ATSP is a high-performance polymer, also known as a Vitrimer, which is defined as a thermoset that processes like a thermoplastic [78]. Its tribological performance, particularly in thin coating form, has been under investigation, demonstrating its excellent tribological performance compared with PEEK- and PTFE-based coatings. For example, reported "unmeasurable zero wear" from cryogenic to high temperatures (-196 to 300 °C) under dry sliding [114,143], low wear and stable COF under sand contaminated oil abrasive conditions [20] and in the presence of HFO-1234yf refrigerant under starved lubrication [40].

Herein, ATSP and PEEK tribological performance was evaluated under dry sliding lunar regolith simulant abrasive conditions to identify tribopairs for future explorations to the Moon, Mars, and other planetary surfaces with abrasive environments. The efficacy of polymer coating-on-polymer coating in sand-dust mitigation was demonstrated through comparison with metal-on-polymer and metal-on-metal sliding. In addition, the wear mechanism was thoroughly examined through scanning electron microscopy (SEM) and

energy-dispersive X-ray spectroscopy (EDS) characterizations, and correlations were made with the tribological performance.

5.2 Experimental

5.2.1 Materials and sample preparation

The ATSP powders were prepared by mixing two sets of cross-linkable aromatic oligomer powders, namely CB2 and AB2 with carboxylic and acetoxy functional groups, respectively. The oligomers were synthesized in a batch melt polymerization at temperature of 270 °C in a 2L reactor and under argon gas environment. During this process, the acetic acid by-product of the reaction was distilled out through a gas outlet until no condensed gas remained. After the reaction, the hot liquid oligomer was poured out into a PTFE fabric-covered container for the cooling process and turned into solid state at room temperature (RT). The dried solidified oligomers were then ground into powders using a lab grinder and sieved to obtain particles with maximum size of 90 μm. The detailed description of oligomer synthesis is available elsewhere [118].

After the synthesis of the oligomers, the CB2 and AB2 powders were mixed in a small size grinder with weight ratio of 1:1 to form the ATSP polymer powder. Thereafter, the ATSP powder was blended with 5wt.% PTFE lubricant additive and deposited on the sandblasted Aluminum (Al) plates and Grade 5 Titanium (referred as Ti) curved pin substrates using electrostatic spray deposition (ESD) method. The sandblasting was used to improve the coating adhesion to the substrate [144]. Thereafter, the coated samples were placed in a convective oven and cured for 60 minutes at 270 °C to obtain a coating with thickness of approximately 40±5 μm. Upon curing, the oligomers were crosslinked at their

end groups, which generated a thermally stable ATSP/PTFE polymer with crosslinked aromatic polyester backbone. The PEEK/PTFE (1704 PEEK/PTFE®, 20wt% PTFE) coating was deposited on similar substrates by an authorized applicator (Southwest Impreglon Inc.) using the ESD method. Note that PEEK/PTFE is a dispersion coating, where it is dried after spraying the dispersion, followed by a melting process under temperature range of 371-399 °C.

The Lunar dust simulant was acquired from CLASS Exolith Lab and sieved into two particle sizes, namely between 38-125 μm referred to as sand and less than 38 μm referred to as dust. **Figure 45(a-d)** show SEM images of sieved lunar sand/dust simulants showing the random shape of the particles. The geometry of the particles varies between blocky, acicular, and angular shapes with different sizes and aspect ratios. The surface, features a relatively smooth texture with randomly distributed debris on the surface. The debris are more pronounced on the dust particles compared with sand. The edges are relatively sharp with minimal roundness.

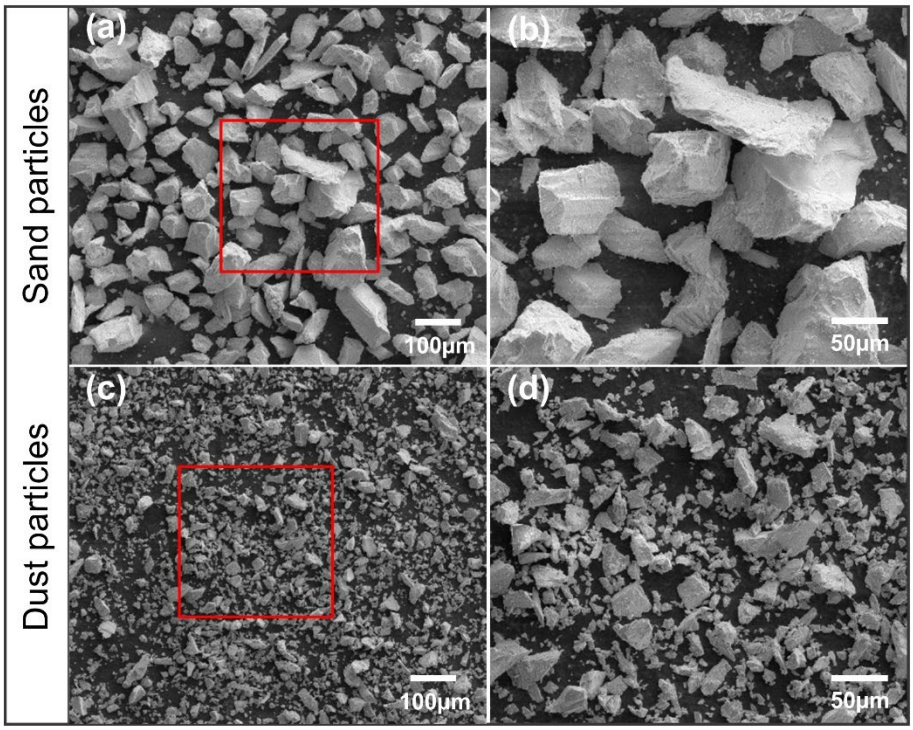

Figure 45. Two different magnification SEM images of sieved Lunar regolith simulant (a, b) sand and (c, d) dust particles. The square boxes are the areas where the higher magnification images were taken

5.2.2 Experimental procedure

A custom-built tribometer referred to as High Temperature Tribometer (HTT) was used to conduct the tribological pin-on-disk experiments, as shown in **Figure 46(a)**. The unique feature with the tribometer is its capability to control the test atmosphere using a glass/metal bell jar enclosure (**Figure 46(b)**). Once the bell jar is closed, the interior environment could be evacuated using a vacuum pump and ports, and the desired gas could then be flushed and maintained at a certain flow rate throughout the test. The force transducer is attached to the pin holder that is capable of applying normal forces up to 45 N and measurement of the in-situ friction and normal forces to obtain the in-situ COF. The disk is the rotary part that is placed on a disk holder mounted on a servo motor. The motor

can rotate at speeds up to 1000 rpm and oscillation frequencies up to 5 Hz. An installed transparent furnace enables the increase of environmental temperature up to 1000°C through a heat radiation mechanism.

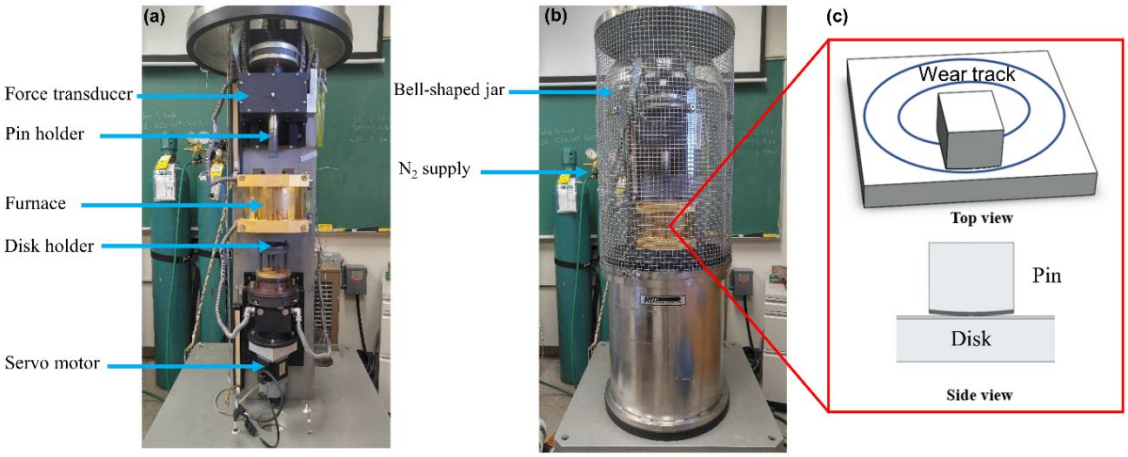

Figure 46. Experimental setup: photograph of HTT for (a) open and (b) controlled environment tribological experiments, and (c) curved pin-on-disk configuration.

A curved pin-on-disk configuration (**Figure 46(c)**) with a mean wear track diameter of 17.5 mm was used to simulate the bushing-shaft line contact. This curved pin helps to trap the abrasive particles between the interfaces rather than push/ swipe the particles away. NASA is in search of reliable tribopairs to be used in future missions without specifying the exact tribopairs, which could be an articulating arm, or a bushing or rolling element type of locomotion. Thus, the study is somewhat of generic conditions. The pins were machined using wire EDM (Electric Discharge Machining) technique out of a bulk Ti cylinder (Grade 5) with a radius of 25.4 mm and thickness of 6 mm. The disks were machined from a 6061 Al plate with a 25.4 mm×25.4 mm square shape. The list of tribopairs and the experimental conditions are summarized in **Table 10**.

Table 10. List of tribopairs and experimental conditions.

Tribopairs	Temperature (˚C)	Contact pressure, MPa (load, N)	Linear speed, m/s* (Speed, rpm)
Bare Ti vs. Bare Aluminum (Ti-on-Al)	23 (RT)	19.5 (5)	0.25 (270)
Bare Ti vs. ATSP/PTFE (Ti-on-AP)			
Bare Ti vs. PEEK/PTFE (Ti-on-PK)			
ATSP/PTFE vs. ATSP/PTFE (AP-on-AP)	-150, -60, 23, 110		
PEEK/PTFE vs. PEEK/PTFE (PK-on-PK)			

*The linear speeds were calculated based on 17.5 mm average diameter for the wear tracks.

To assess the performance of each candidate polymer coating (namely ATSP/PTFE and PEEK/PTFE) on friction and wear reduction, three sets of tribopairs were evaluated: I) metal-on-metal contact serving as the baseline, II) metal-on-polymer contact, and III) self-mating polymer-on-polymer contact. The experiments were performed under N_2 gas environment at RT, constant normal load of 5 N corresponding to an initial nominal Hertzian contact pressure of 19.5 MPa, and sliding speed of 270 rpm (0.25 m/s). A speed effect study (ranging from 0.025 m/s to 0.25 m/s) was conducted in our earlier study [143] under non-abrasive conditions, which showed the unmeasurable zero wear of ATSP coatings. This wide speed range was to capture different speeds of potential moving parts [145,146] in Lunar exploration. In the current study, the maximum speed of 0.25 m/s was selected under abrasive wear conditions to obtain the sufficient wear for comparison of different tribopairs. In order to identify the best tribopair and interface for sand/dust mitigation, the metal-on-metal and metal-on-polymer experiments were conducted only at RT. However, besides lunar dust effect, it is also imperative to consider the variation of

environmental temperature. Therefore, the polymer-on-polymer experiments were conducted at all temperatures from -150 °C to 110 °C to cover the environmental temperature variation influence. Note that these experiments were performed only under dusty condition.

To ensure repeatability, each experiment was repeated at least three times and a duration of 30 min. Different bearing systems will exhibit different contamination from the dusty Lunar and Martian surfaces. Some instruments can be at a higher elevation, thus having smaller dust particle contamination, compared with the instruments that are in direct contact, or near the dusty ground. Therefore, it is necessary to study the effect of particle size on the performance. Hence, before each experiment, the surface of each sample was covered with two ranges of particle sizes that were referred to as sand and dust with surface coverage density of 5 g/m^2. Hereinafter, this coverage state would be referred to as sand (S) and dust (D) conditions. Before and after each test, the samples were ultrasonically cleaned with isopropyl alcohol for 10 min to remove contamination and subsequently dried using warm air and stored in a desiccator.

SEM/EDS analyses were employed to study the surface morphology of the samples, wear mechanisms, and sand distribution or embedment on the samples after tribological experiments. To acquire higher quality SEM images and reduce the charging effect, the surface of the polymers was sputter-coated with 4 nm thick Pt/Pd. The profilometric measurements were performed across the wear tracks to capture the change in surface profile and obtain the amount of wear [147]. The crystalline structure of the polymers was examined before and after each test using X-ray diffraction (XRD).

5.3 Results and discussion

5.3.1 Room temperature experiments: Friction

Figure 47(a, b) show the evolution of in-situ COF vs. sliding time for different tribopairs listed in **Table 10** under dust and sand conditions, respectively. For both coverages, the in-situ COF shows a running-in behavior followed by a steady-state condition. The in-situ COF shows a similar trend for all the tribopairs except for the tribopairs with metal-on-metal configuration (i.e., Ti-on-Al). Due to the occurrence of micro scuffing at the metal-on-metal interfaces, the in-situ COF showed sharp increases and high variations, particularly under dust environment. As shown in **Figure 47(a, b)**, the deposition of PEEK and ATSP polymer composite coatings on the Al surface of the disk samples resolved the harsh conditions at the Ti-on-Al interface and a smoother sliding was achieved. Once the polymer coatings were deposited on both Al disk and Ti pin (i.e., polymer-on-polymer sliding), the most steady-state condition was obtained, accompanied by a further reduction in the COF.

Figure 47(c, d) show the summary of average COF values calculated from the last 20 min of the in-situ COF curves during the steady-state period. The COF was reduced continuously by depositing the polymer coating on the metallic surfaces for both dust and sand experiments. Therefore, the minimum COF was obtained for polymer-on-polymer sliding configuration, while the maximum COF was obtained for the samples in their as-received state (i.e., bare Ti pin against bare Al disk), as was expected. As seen in **Figure 47(a)** under dust environment, once the uncoated Ti-on-Al interface was treated to metal-on-polymer and polymer-on-polymer, the COF reduced by 25 and 69% for ATSP and 40

and 65% for PEEK coatings, respectively. Under sand, both ATSP and PEEK coatings behaved similarly and reduced the COF by 35 and 64%, respectively. The comparison of the COF between dust and sand experiments indicated slightly higher COF for experiments under dust conditions, and therefore, lower size particles referred to as dust were more detrimental and caused higher friction. As seen in **Figure 47(c)**, the ATSP coating showed relatively higher COF compared with PEEK coating, whereas under sand condition (**Figure 47(d)**), the COF values were the same between the two tribopairs.

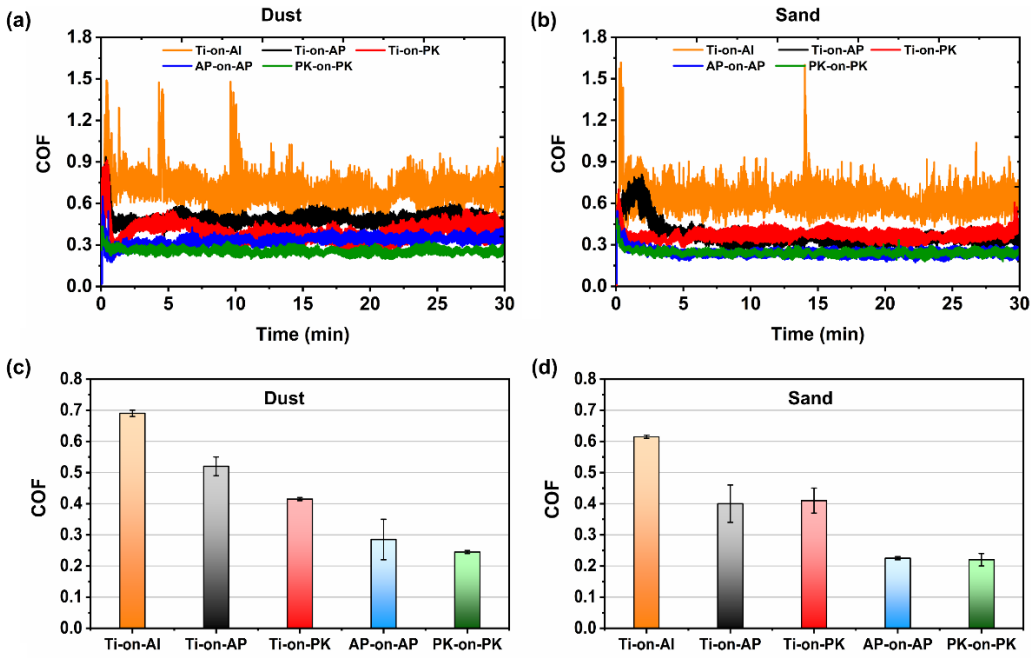

Figure 47. Experimental results for different tribopairs for dust and sand conditions showing (a, b) in-situ COF vs. sliding time, and (c, d) average COF at the steady-state period. Error bars designate ±1 standard deviation.

5.3.2 Room temperature experiments: Wear

I) Metal-on-metal: **Figure 48(a, b)** shows the profilometric wear scans measured across the wear track on the disk samples after the experiments with dust and sand,

respectively. Sliding of uncoated Ti-on-Al tribopairs (i.e., metal-on-metal) under sand and dust conditions resulted in moderate micro scuffing wear behavior, revealed by roughening and grooves that were formed on the wear tracks, compared with the smooth surface outside the wear track. The experiment under dust was under more severe sliding, revealed by the higher intensity of grooves and spikes on the wear track as well as higher COF, as shown in **Figure 47(c)**. Deposition of the ATSP and PEEK coatings on the Al disk surface (i.e., metal-on-polymer) significantly improved the wear resistance for both sand and dust experiments.

II) Polymer-on-metal: as shown in **Figure 48(a, b)** of the metal-on-polymer tribopairs (i.e., Ti-on-AP and Ti-on-PK), the accumulation of sand and dust particles on the coating surfaces was major, as indicated by the formation of hills with different step height and width on the surface. However, the extent of such accumulation was significantly lower for Ti-on-AP tribopair compared with Ti-on-PK. In addition, the tribopair Ti on PK-S showed a large wear groove as well as spikes (due to embedded particles) with depth and height of 35 and 30 μm on the coating, respectively. Therefore, the resistance of PEEK coating to sand abrasion was lower compared with ATSP. Similarly, more material was worn out from PEEK coating under dust condition, whereas the ATSP coating showed only dust accumulation on certain spots on the coating surface that resulted in slightly higher COF.

III) Polymer-on-polymer: deposition of the polymer coatings on both Ti pins and Al disks resolved the dust/sand accumulation seen in Ti-on-AP and Ti-on-PK (S, D) tribopairs, as shown in **Figure 48(a, b)**. However, a higher number and deeper grooves

were formed on the coatings, particularly under dust conditions. Such behavior could be explained by the difference between uncoated and polymer coated Ti pins. When the uncoated Ti pin slid against ATSP or PEEK coating, the sand/dust particles could act as third body particles that were entrapped at the interface. Moreover, the accumulation of sand/dust particles on the coating surfaces was easier in case of uncoated Ti pins due to higher Hertzian contact pressure as well as inability of the particles to embed in the pin surface. However, when the polymer coated Ti pin slid against ATSP or PEEK coating, the sand/dust particles could embed in the coating on the pin side as well, creating the condition for two-body abrasive wear. This hypothesis will be substantiated in the SEM section.

Figure 48(c) shows the variation of the average wear rate after the experiments with different tribopairs. The wear rates were calculated from the wear scan measurements across the wear tracks shown in **Figure 48(a, b)**. For the sliding of Ti on polymeric samples, only the PEEK coating showed measurable wear under dust condition. As it was shown in the profilometric wear scans, the majority of coating surfaces were covered with embedded sand/dust particles for sliding of uncoated Ti on polymer coated samples, and therefore the actual polymer wear rate could not be calculated. For AP-on-AP and PK-on-PK, the maximum wear rate occurred for PK-on-PK under dust condition, while the ATSP coating showed immeasurable “zero” wear. For testing with sand, both ATSP and PEEK coatings demonstrated similar wear rate. Overall, the ATSP coating was more resistant to abrasive wear under both sand and dust conditions.

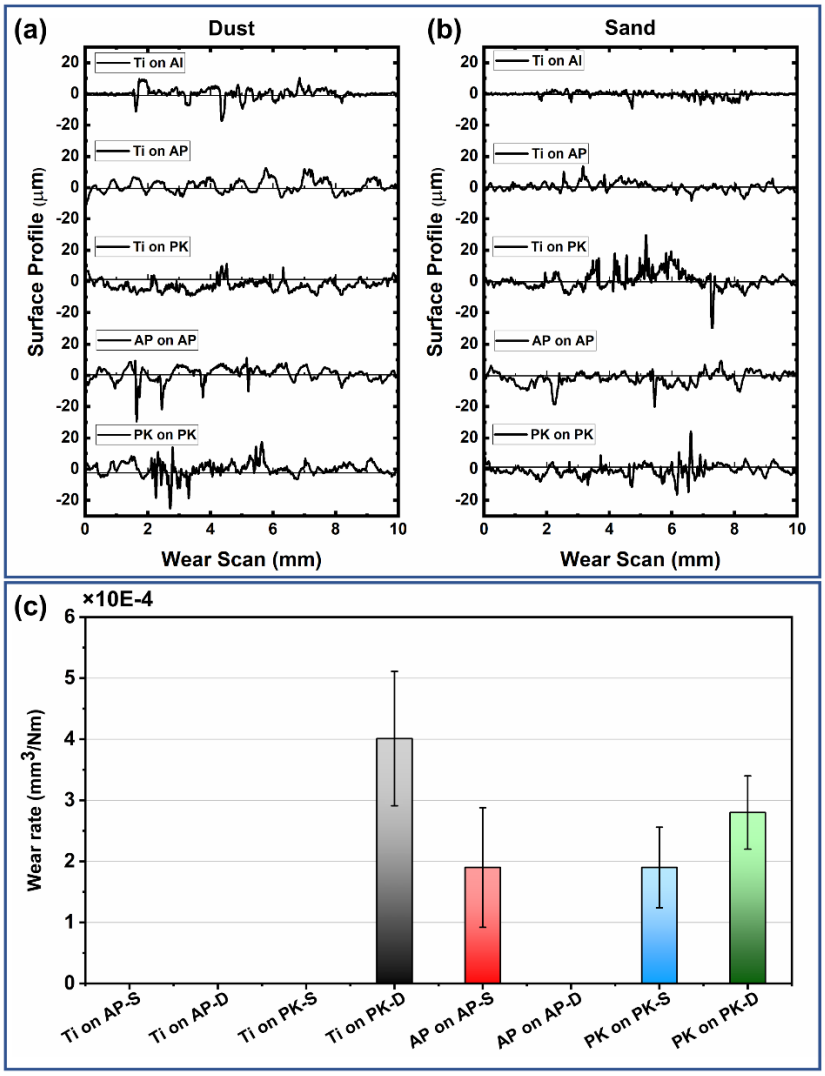

Figure 48. Profilometric wear scans measured across the wear tracks after experiments with different tribopairs under (a) dust (D), and (b) sand (S) conditions. (c) The coatings wear rates were measured from profilometric scans.

5.3.3 Room temperature experiments: SEM/EDS analysis

Figure 49(a-c) depicts SEM images of the top surfaces of Al, ATSP/PTFE coating, and PEEK/PTFE coating in their as-received (untested) condition. The Al surface shows directionality resulting from the polishing process. The homogeneous dispersion of PTFE additives can be distinguished on the ATSP coating, revealed by the shinier grey color.

Since the PTFE melting temperature is higher than the coating curing temperature (270 °C), the additives maintained their solid and rigid state in the coating. On the other hand, the PTFE powders were entirely embedded inside the PEEK coating due to the melting process of the PEEK polymer composite under temperature of 371-399 °C.

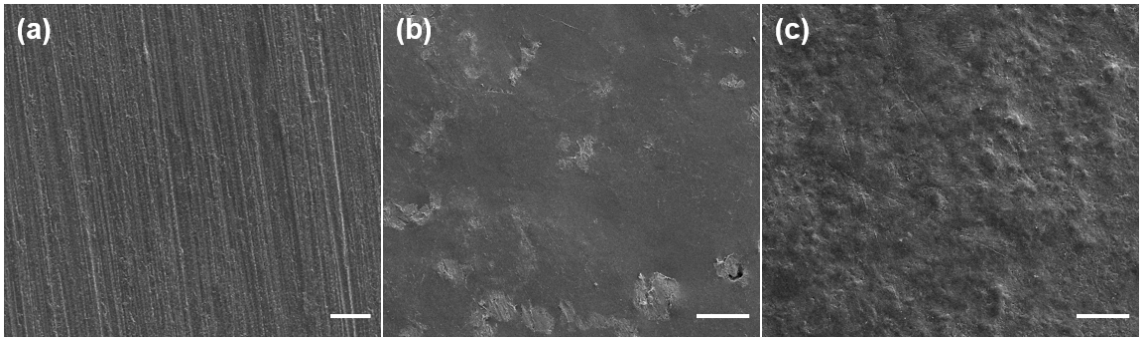

Figure 49. Top surface SEM images of the as-received surfaces of (a) Aluminum, (b) ATSP/PTFE coating, and (c) PEEK/PTFE coating (scale bar is 50 μm).

Figure 50(a-i) show the SEM images of the worn surfaces of the disk samples after the experiments under sand environment with tribopairs Ti-on-Al, Ti-on-AP, and Ti-on-PK, respectively. As shown in **Figure 50(a, b)**, the uncoated Al surface shows signs of micro scuffing and abrasive wear due to the entrapped sand particles and metal-on-metal sliding. According to the SEM image shown in **Figure 50(c)**, the majority of the embedded and distributed sand particles on the Al surface were due to the smaller size sand particles. The larger particles acted as either third body abrasive particles or washed away from the interface. As shown in **Figure 50(d-i)**, the deposition of ATSP and PEEK coatings on the Al substrate entirely resolved the micro scuffing wear observed on the uncoated Al surface. Nonetheless, the majority of the two polymer coating surfaces were still covered with sand particles with different sizes, as shown in the SEM images in

Figure 50(f, i) and profilometric wear scans in **Figure 48**. In addition, micro grooves were formed on the coatings surfaces, and with larger intensities (e.g., size and number) on the PEEK coating (**Figure 50(h)**), compared with ATSP coating (**Figure 50(e)**). Therefore, PEEK was less resistant to abrasive wear, and grooves as deep as 20 μm were formed on the coating, as was also measured in the wear scans in **Figure 48(b)**. In addition to two-body abrasive wear by Ti asperities, the embedded and entrapped sand particles resulted in respectively two-body and three-body abrasive wear as the major wear mechanism.

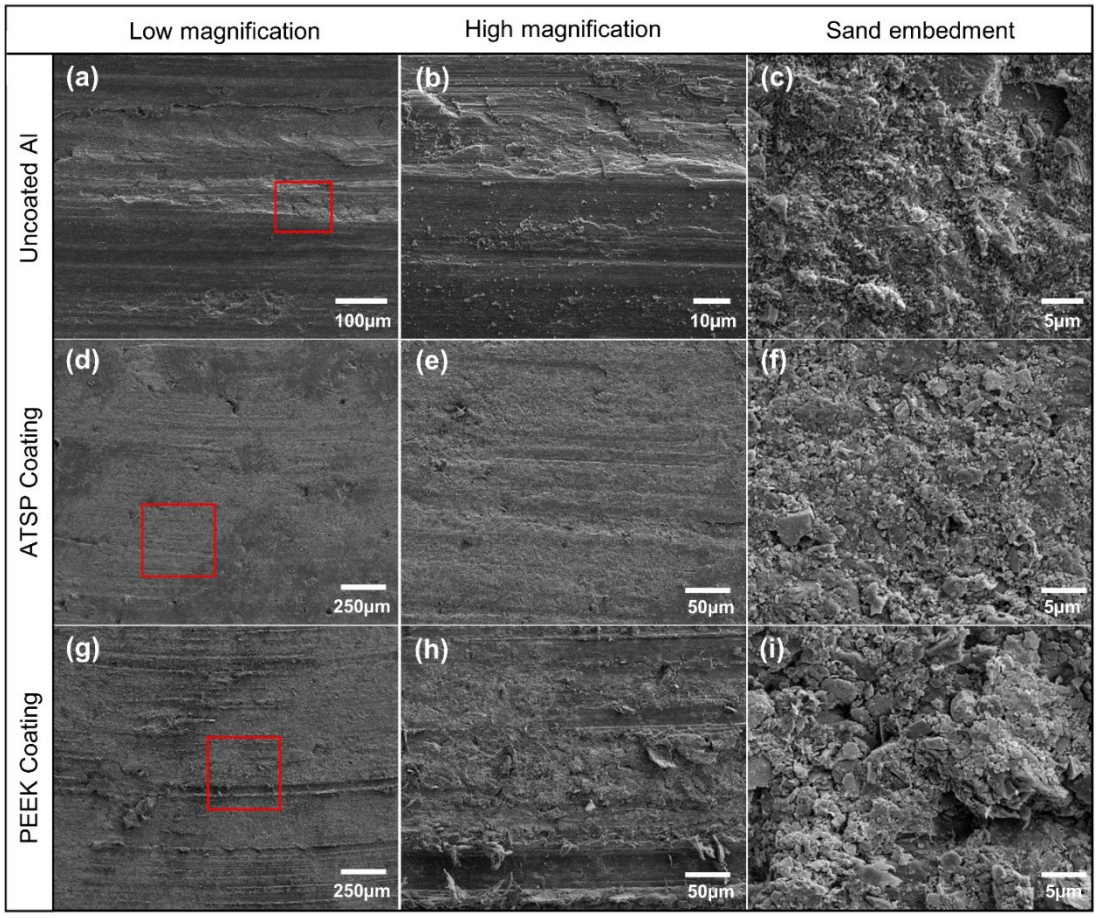

Figure 50. SEM images of the disk worn surfaces after pin-on-disk experiments with (a-c) Ti-on-Al (d-f) Ti-on-AP, and (g-h) Ti-on-PK coatings under sand conditions. The square boxes are the areas where the higher magnification images were taken.

As depicted in **Figure 50(f, i)**, the ATSP and PEEK coating surfaces were mainly covered with sand particles. The EDS mapping on the ATSP coating surface was taken to verify the sand embedment. As shown in **Figure 51(a-c)**, most of the coating surface is covered by sand particles depicted by the green color that represents the Si element, and in agreement with profilometric and SEM measurements. Another observation is the formation of deep indent marks by the loosely embedded sand particles as well as colliding of the moving sand particles with the embedded ones that stopped the formation of a continuous groove on the coating.

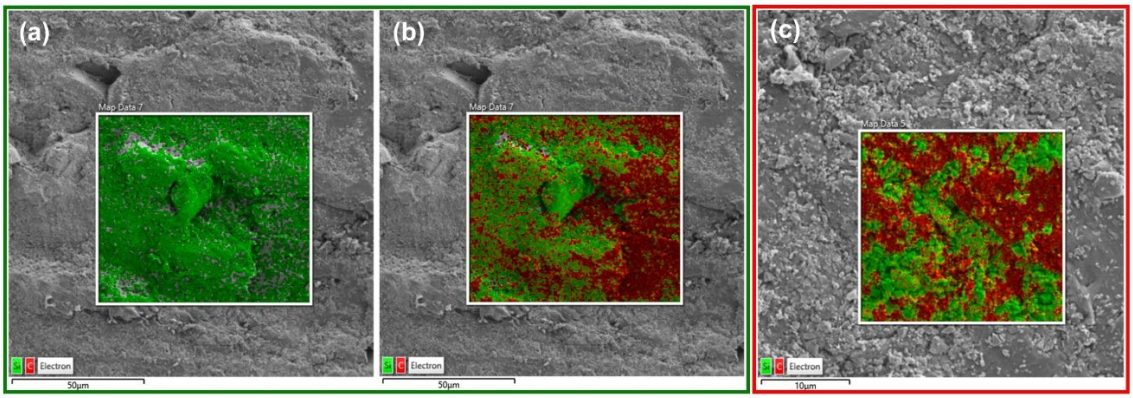

Figure 51. EDS mapping showing (a) embedded sand, (b) sand and the polymer, and (c) sand distribution on the ATSP coating for Ti-on-AP tribopair under sand condition.

Figure 52(a-f) show the SEM images of the worn surfaces of the coatings on the disk samples after the experiments under sand condition with tribopairs AP-on-AP, and PK-on-PK, respectively. A clear difference between metal-on-polymer (**Figure 50**) and polymer-on-polymer is the inhibition of sand accumulation and embedment (sand mitigation) on the ATSP and PEEK coatings once the Ti pins were coated. Therefore, three-body abrasive wear was the dominant wear mechanism due to rolling/sliding of

entrapped sand particles at the interface, as is indicated by the grooves on the surface of both ATSP and PEEK coatings.

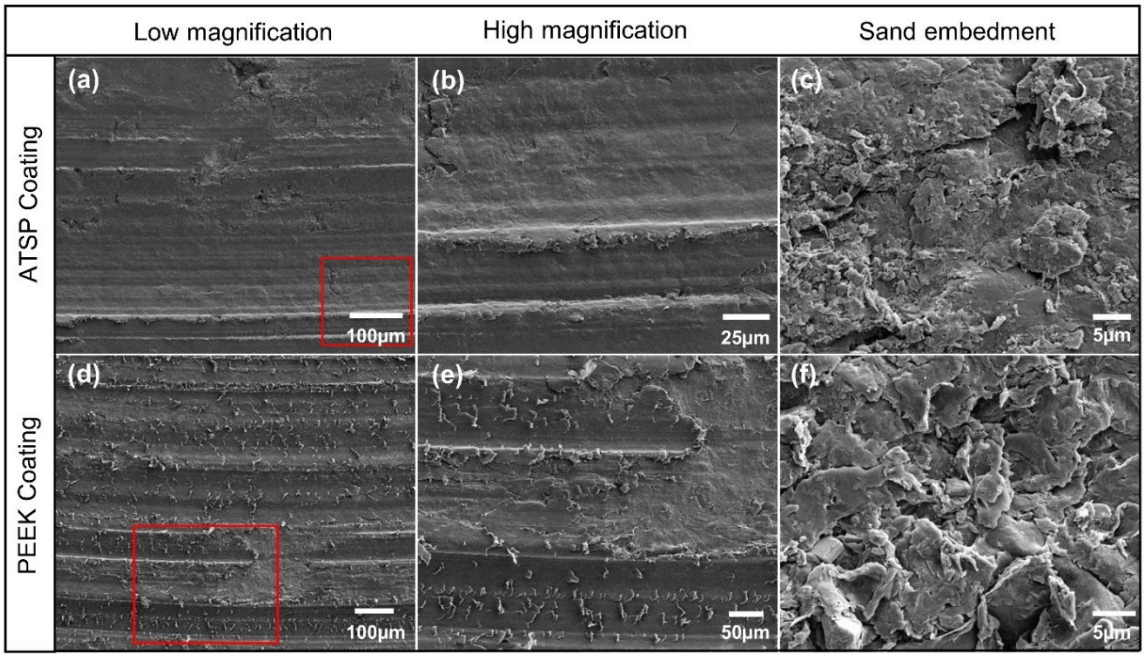

Figure 52. SEM images of the coatings worn surfaces after pin-on-disk experiments with (a-c) AP-on-AP and (d-f) PK-on-PK coatings under sand condition. The square boxes are the areas where the higher magnification images were taken

Figure 53(a-c) show the SEM images of the worn surfaces of the disk samples after the experiments under dust condition with the tribopairs Ti-on-Al, Ti-on-AP, and Ti-on-PK coatings, respectively. As shown in **Figure 53(a)** for the Al surface, micro scuffing and abrasive wear were still the main wear mechanisms caused by metal-on-metal contact, as well as entrapped dust particles, similar to what was observed under sand environment. However, as shown in **Figure 53(c)**, more of the surface is covered with small-sized dust particles with higher intensities, compared with the test under sand, **Figure 50(c)**, which resulted in higher COF and wear. From **Figure 53(d-i)**, the ATSP and PEEK coatings

showed only dust accumulation and sporadic dust embedment on the coatings caused by larger dust particles. Compared with sand, the abrasive marks on PEEK coating were finer and less continuous due to smaller size particles, while ATSP coating did not show noticeable abrasion. A distinct difference between dust and sand experiments is the embedment of particles with sizes greater than 20 µm on both ATSP and PEEK coatings that could impede a direct metal-on-polymer contact, resulting in higher COF under dust.

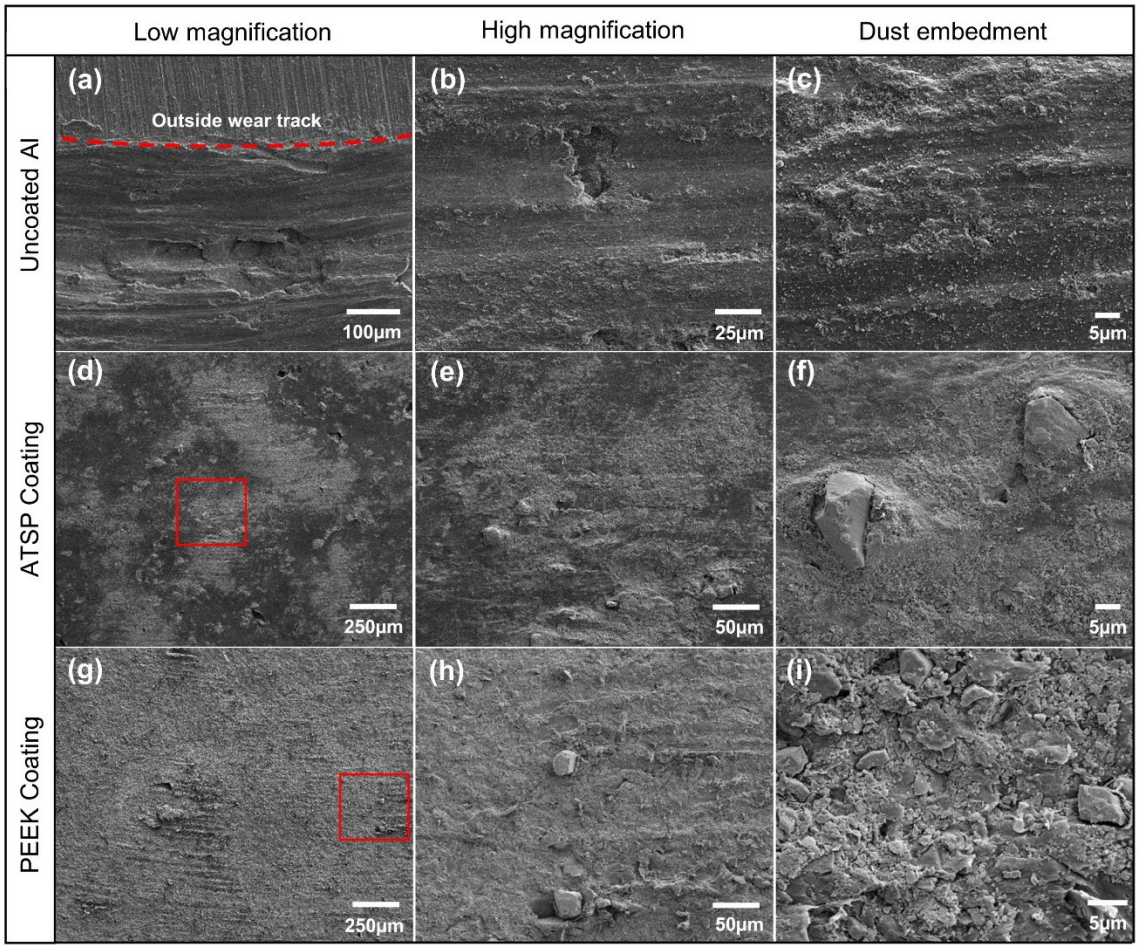

Figure 53. SEM images of the worn surfaces of the disks after pin-on-disk experiments with (a-c) Ti-on-Al (d-f) Ti-on-AP, and (g-h) Ti-on-PK coatings under dust condition. The square boxes are the areas where the higher magnification images were taken

Figure 54(a-f) show the SEM images of the worn disk surfaces after the experiments under dust condition with the tribopairs AP-on-AP, and PK-on-PK, respectively. Similar to sand, once the Ti pins were coated, the dust accumulation and embedment were mitigated but the coatings experienced higher intensity of abrasive wear. Compared with the experiment with sand, dust caused more abrasion on the polymers, and particularly for the PEEK coating, wide and deep wear grooves as high as 30 μm were generated, **Figure 54(e)**. This is in agreement with the profilometric measurements and the corresponding higher wear rate of PEEK coating compared with ATSP, as shown in **Figure 48(a, c)**.

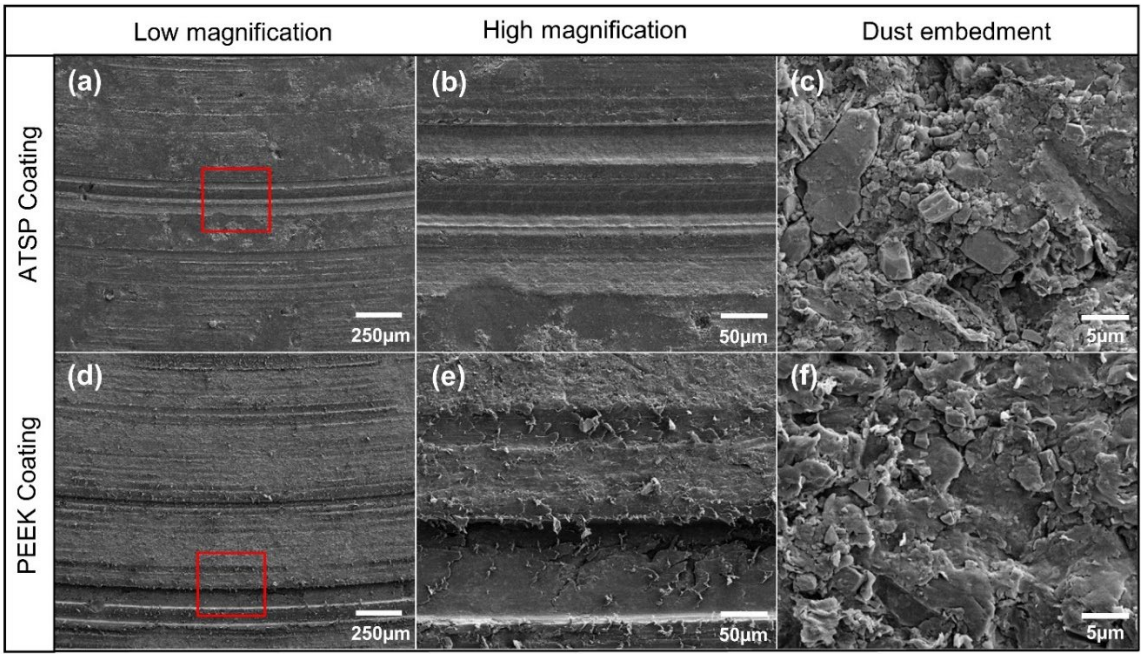

Figure 54. SEM images of the coatings worn surfaces after pin-on-disk experiments with (a-c) AP-on-AP, and (d-f) PK-on-PK coatings under dust condition. The square boxes are the areas where the higher magnification images were taken.

Abrasive wear is defined as material displacement or removal from the surfaces in relative motion either by (I) abrasion due to hard particles entrapped at the interface, (II) abrasion by the embedded particles in one of the surfaces, or (III) abrasion by the sliding of hard protuberances present on the surface of any of the counterparts [148]. According to this definition and based on the SEM images, the wear could be classified into two groups for this study: three-body abrasive wear caused by sliding/rolling of entrapped sand/dust particles (I), and two-body abrasive wear caused by embedded sand/dust particles or hard asperities of the Ti counterpart (II& III). As demonstrated in **Figure 55(a)** of the metal-on-polymer contact, the sand/dust particles could easily embed inside the polymer coating due to the high Hertzian pressure from the harder metallic (Ti) pin. Upon sliding, the embedded particles could therefore generate two-body abrasive wear as the predominant wear mechanism. In addition, the harder asperities from the Ti pin generated fine to medium level scratches as was depicted in the SEM images, leading to secondary two-body abrasive wear. As depicted in **Figure 55(b)** and the foregoing SEM images, the deposition of the ATSP and PEEK polymer coatings on the bare Ti pins significantly improved the interface resistance to sand/dust embedment and accumulation, resulting in three-body abrasive wear as the dominant wear mechanism that was caused by rolling/sliding of the entrapped particles. Hence, polymer-on-polymer tribo-contact is an efficient sand and dust mitigation method at the interface.

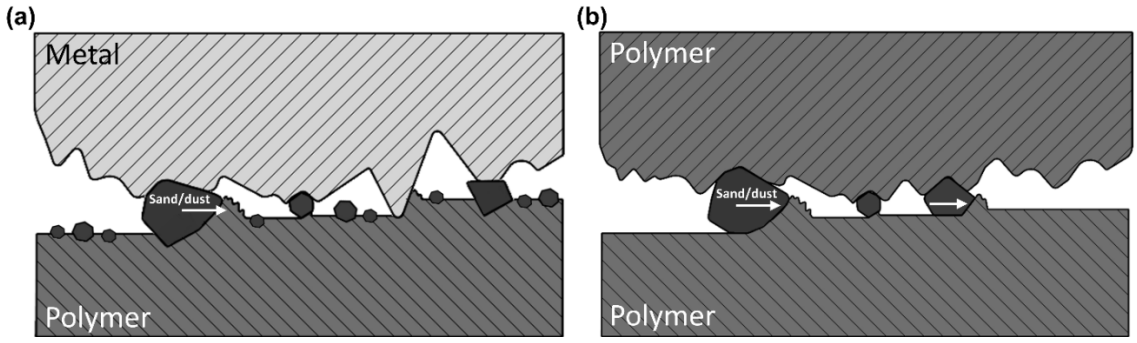

Figure 55. Schematic representation of two and three-body abrasive wear for (a) metal-on-polymer and (b) polymer-on-polymer sliding.

5.3.4 Room temperature experiments: XRD analysis

XRD analysis was performed inside and outside the wear tracks on each polymer coating after the metal (Ti) on polymer experiments under sand environment to examine the changes in crystalline structure of the coatings upon wear testing. A BRUKER D8 X-ray was used with a Cu sealed tube as the X-ray Source. **Figure 56(a, b)** depict the XRD pattern of ATSP and PEEK coatings for the characteristic diffraction angle (2θ) ranging from 15 to 35°. The ATSP coating demonstrated an amorphous structure with characteristic peak at 2θ=20°. On the other hand, the PEEK coating showed a semi-crystalline structure, and its predominant orthorhombic crystals are shown in the spectrum. The crystallization peaks of PTFE appeared on both spectrums and with larger intensity for PEEK coating, compared with ATSP, due to higher amount of PTFE additive in PEEK. A reduction in the intensity could be identified after the wear test for both coatings, which could be attributed to the decrease in crystallization of the PEEK coating and wear of the materials upon sliding. Abrasion and plastic deformation by embedded sand particles on the PEEK coating could disrupt the chain reorientation into a crystalline form and

therefore caused a reduction in peak intensities. The appearance of an extra peak could be identified from the spectrums on the wear tracks, which could be attributed to the embedded sand particles on both ATSP and PEEK coatings.

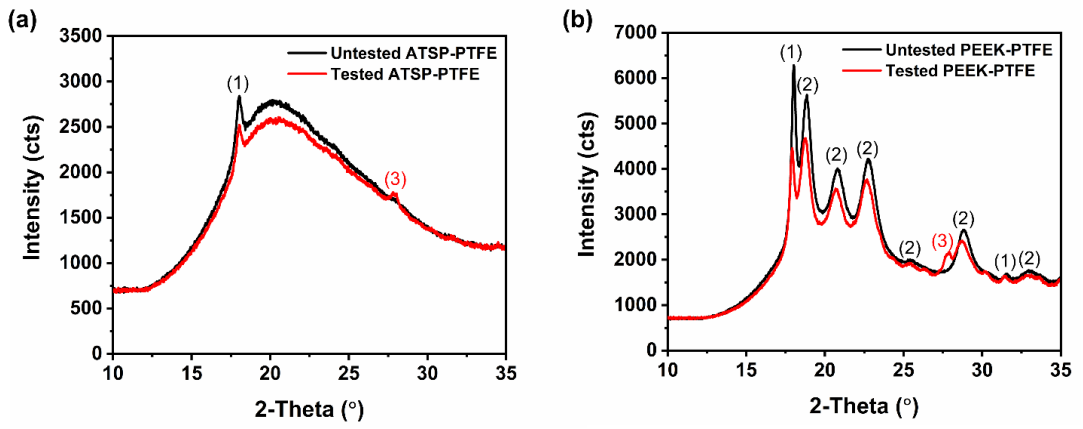

Figure 56. XRD profile of (a) ATSP/PTFE, and (b) PEEK/PTFE coatings before and after wear testing under sand condition. (1), (2), and (3) represent the peaks corresponding to PTFE, PEEK, and embedded sand particles, respectively

The RT experiments indicated higher resistance of ATSP coating to abrasive wear compared with PEEK, and dust was more detrimental to tribological performance (i.e., friction and wear), particularly for PEEK coating. The coating-on-coating was shown as an effective method to improve the tribological performance and mitigate the sand and dust at the interface. Therefore, the temperature effect experiments were conducted only under dust environment and for tribo-pairs Ti-on-AP, Ti-on-PK, AP-on-AP, and PK-on-PK coatings.

5.3.5 Temperature effect study: Friction

Figure 57(a-d) shows the evolution of in-situ COF vs. sliding time for different tribo-pairs listed in **Table 10** at different temperatures. The in-situ COF curves show a

running-in behavior followed by a steady-state condition for all conditions. The running-in time took much longer metal-on-polymer configurations compared with polymer-on-polymer with initial COF as high as 0.8-1. This behavior could be attributed to the presence of dust particles at the interface which inhibited the lubrication effect of the polymer on the counterpart. Thereafter, a transient stage in COF occurred where the dust particles were rolling, sliding, and embedding on the coating until a stable interface was reached.

On the other hand, for the polymer-on-polymer sliding, the transient behavior was minimal and the COF was roughly stable from the start. For the metal-on-polymer tribo-pairs, the lowest fluctuation in COF occurred at cryogenic condition and particularly at -150 ℃ (**Figure 57(a)**), while the largest variation and fluctuation in the COF was observed at elevated temperature of 110°C, as shown in **Figure 57(d)**, which was noticeable for Ti-on-AP. At -60 ℃ (**Figure 57(b)**), the in-situ COF took the longest time to reach the steady-state period for both Ti-on-PK and Ti-on-AP, whereas at RT (**Figure 57(c)**), the time to reach the steady-state was minimal. Such instability and fluctuations on the in-situ COF was entirely resolved at all temperatures by the depositing the ATSP and PEEK polymers on the metal pin.

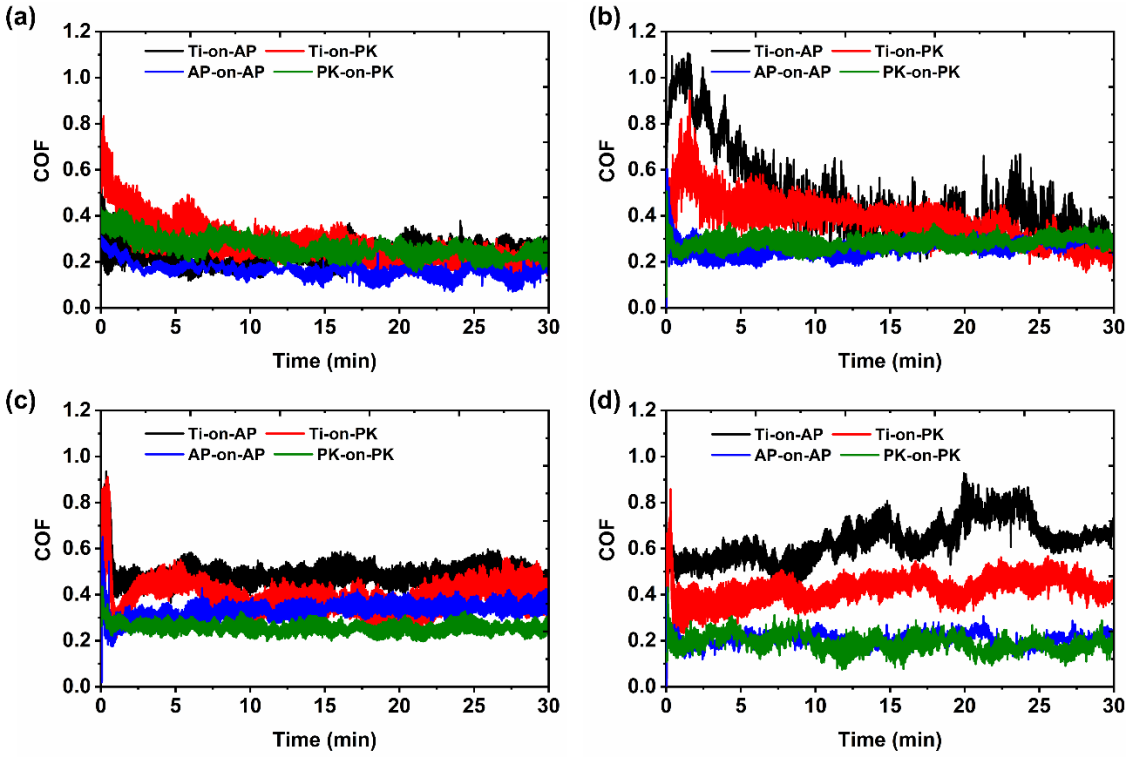

Figure 57. In-situ COF vs. sliding time for experiments under dust environment and different temperatures of (a) -150 °C, (b) -60 °C, (c) 25 °C, and (d) 110 °C.

Figure 58(a-d) show the summary of average COF values at all temperatures which were calculated from the last 20 min of the in-situ COF curves shown in **Figure 57**. A common observation at all temperatures is the reduction of COF by changing the tribo-pairs from metal-on-polymer to polymer-on-polymer sliding. However, the ratio of the reduction was significantly affected by the temperature. The largest reduction in COF happened at 110 ℃, followed by RT, -60 ℃, and -150 ℃. The decrease of the temperature to -150 and -60 ℃ reduced the COF for all tribo-pairs as seen in **Figure 58(a, b)**, respectively. The least difference on the COF between metal-on-polymer and polymer-on-polymer was seen at temperature of -150℃ among all temperatures where the COF was nearly the same for PEEK samples and reduced by 22% for ATSP samples. As seen

in **Figure 58(c)** of the RT experiment, a continuous decrease in COF happened by depositing the polymer coating on the Ti pins. The ATSP coating showed slightly higher COF compared with PEEK coating for both interfaces. **Figure 58(d)** shows the comparison of COF after experiments at a temperature of 110℃. The COF reduced by 65% once the coating was used on both pins and disks. The increase of temperature increased the COF for Ti-on-AP and Ti-on-PP samples compared with RT, while lower friction obtained for AP-on-AP and PK-on-PK.

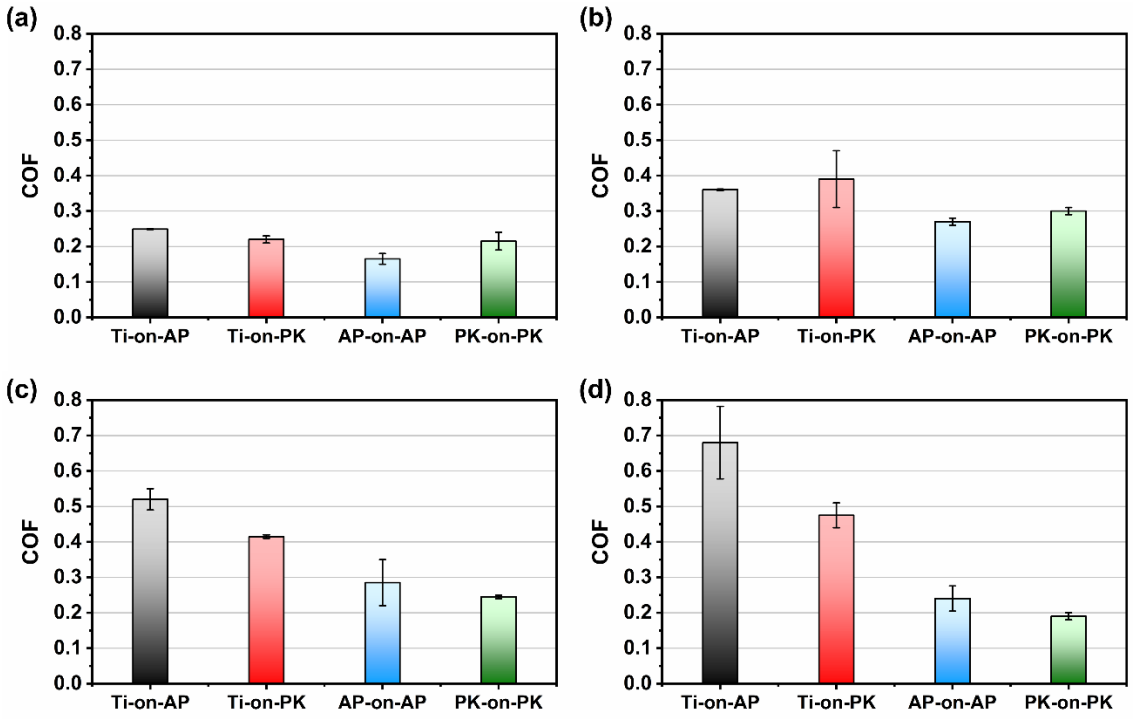

Figure 58. Variation of average COF for experiments under dust environment and different temperatures of (a) -150 °C, (b) -60 °C, (c) 25 °C, and (d) 110 °C.

Overall, for the metal-on-polymer interface, COF increased with an increase in temperature from -150 ℃ to 110 ℃. The maximum COF was obtained at 110 °C for Ti-on-AP, and the minimum COF was for Ti-on-PK at -150 ℃. The increase of COF with

temperature could be attributed to the softening of the coatings, which facilitated the dust embedment on the polymers and resulted in a harsher interface compared to lower temperatures.

Deposition of the ATSP and PEEK coatings on the Ti pins significantly reduced the COF at all temperatures, with maximum difference seen under elevated temperatures. The AP-on-AP tribo-pair showed superior performance compared with PK-on-PK at cryogenic temperatures, while at elevated temperatures, the COF was slightly higher. Contrary to the metal-on-polymer, the tribo-pairs with polymer-on-polymer configuration did not show any specific trend with temperature, and the COF difference between each tribo-pair was minimal. Therefore, the polymer-on-polymer configuration was identified as the least affected tribological surface in a wide range of temperatures from -150 ℃ to 110 ℃.

5.3.6 Temperature effect study: Wear

Figure 59(a-d) show the profilometric wear scans measured across the wear track on the disk samples after the experiments for Ti-on-AP, Ti-on-PK, AP-on-AP, and PK-on-PK, respectively. As shown in the figures, the accumulation of dust particles increases with the temperature increase from -150 to 110 ℃. Therefore, the increase in temperature showed adverse effects on dust mitigation. This is consistent with the higher COF seen at the elevated temperatures. As shown in **Figure 59(a)**, the sliding of Ti on the ATSP coating did not cause noticeable wear, and the wear trace was not detectable on the profiles at all temperatures except for -60 ℃, where the coating was under burnishing effect. For Ti-on-PK tribo-pairs (**Figure 59(b)**), the coating showed the highest degree of dust

accumulation at 110 ℃ followed by RT. At RT, the coating experienced about 5μm wear depth as well as dust embedment. At cryogenic temperatures, the coating surface showed a smoother profile indicating the more polishing of the coating and higher resistance to dust accumulation. However, the coating was worn out to higher extent up to 3-4μm wear depth.

Figure 59(c) show the wear scans of ATSP coating on the disk surface for AP-on-AP tribo-pair. The coating showed unmeasurable zero wear at all temperatures except for -150 ℃, where the coating showed polishing effect. At RT and 110 ℃, a deep wear groove formed on the coating while there was no groove identified at cryogenic temperatures. This can be attributed to the hardening of the polymer at cryogenic temperatures, which increased the coating resistance to abrasive wear. Similar grooves were identified on PEEK coating (For PK-on-PK tribo-pair as in **Figure 59(d)**) at RT, whereas at cryogenic temperatures, the coating was more resistant to abrasion. Nonetheless, the coating showed a noticeable burnishing effect at RT, -60, and -150 ℃, and therefore, PEEK coating was less resistant to wear compared with ATSP.

Overall, the deposition of coatings on the Ti pin was shown to be an effective approach to mitigate the dust accumulation on the coating surfaces, particularly at RT and 110 ℃. The coatings were shown to be more tolerant to dust accumulation at cryogenic temperatures due to the increased elastic modulus, which impeded the dust embedment on the coatings. The PEEK coating showed higher extent of wear depth caused by sliding of uncoated Ti pin.

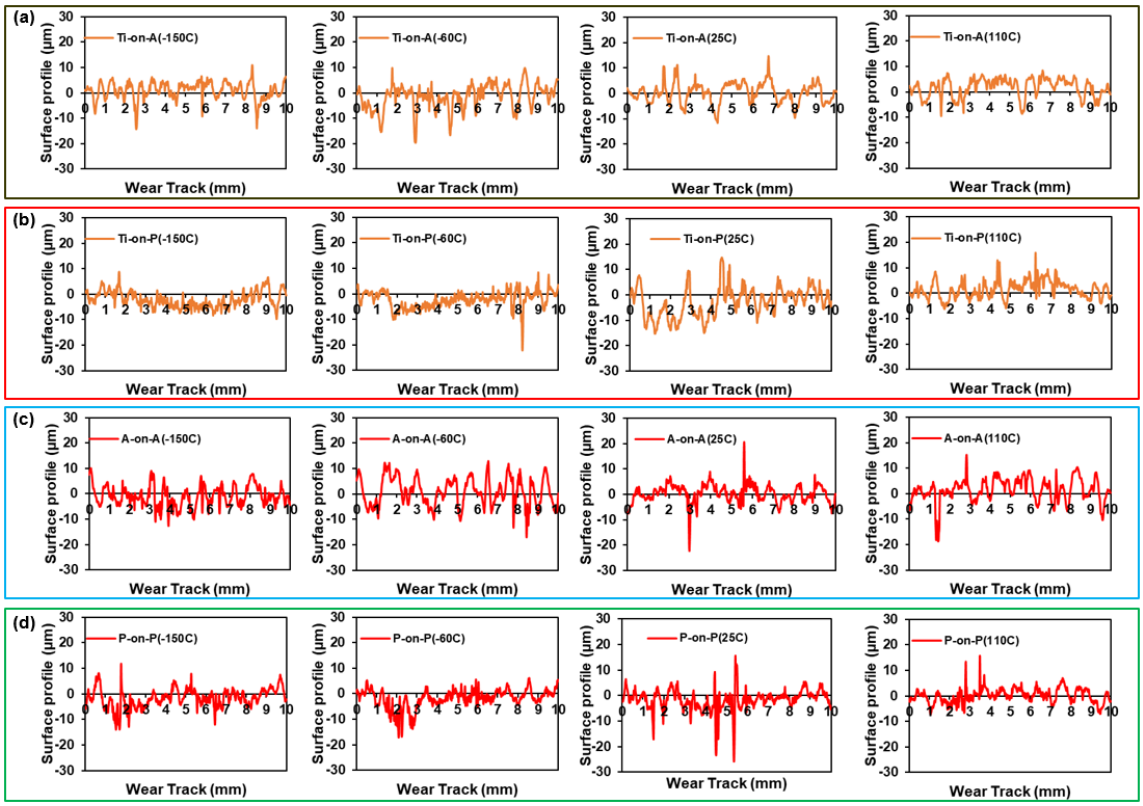

Figure 59. The profilometric wear scans measured across the wear tracks after experiments at different temperatures with different tribo-pairs of (a) Ti-on-AP, (b) Ti-on-PK, (c) AP-on-AP, and (d) PK-on-PK coatings.

Figure 60 shows the average calculated wear rate from the profilometer wear scans shown in **Figure 59(a-d)**. All the tribo-pairs show immeasurable zero wear at 110 °C. Due to the extent of dust accumulation on ATSP and PEEK coatings at this temperature, the wear could not be realistically measured for Ti-on-AP and Ti-on-PK. However, since dust accumulation for AP-on-AP and PK-on-PK was minimal, the measured zero wear shows the realistic wear resistance of both coatings. At RT, the ATSP coating shows unmeasurable zero wear for both Ti-on-AP and AP-on-AP, whereas the wear for PEEK coating was high enough to be measured. The sliding of Ti-on-PK caused 30% higher wear than PK-on-PK. At -60 °C, the Ti-on-PK shows double wear than Ti-on-AP, and the

wear was significantly reduced by using polymer-on-polymer configuration by 100 and 50% for ATSP and PEEK coatings, respectively. Similar wear and trend was observed for PEEK coating at -150 ℃ where the coating showed higher wear compared with ATSP, and the wear of PEEK was reduced by 50% once the coating was used on both counterparts.

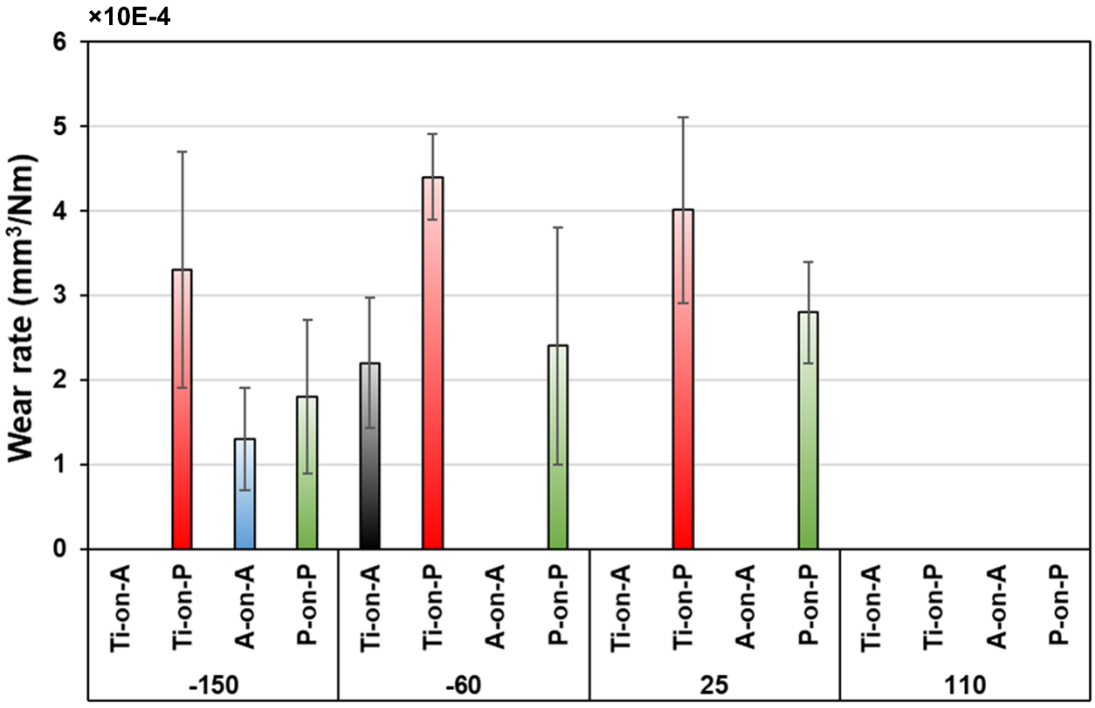

Figure 60. The summary of the calculated averaged wear rate for different combination of tribo-pairs at different temperatures.

5.4 Summary

PEEK and ATSP-based polymer composite coatings were tribologically tested under dry sand and dust environments, simulating Lunar regolith conditions. To understand the role of the polymers on friction/wear and sand-dust mitigation, the original surface of the metal curved pins and disks were coated with the polymers to modify the

tribopair surfaces from metal-on-metal to metal-on-polymer and polymer-on-polymer (self-mated) configurations. Based on the experimental results and analyses, the following conclusions could be drawn:

- Depositing the ATSP and PEEK polymer coatings was shown as an effective method to improve the tribological performance and mitigate the sand and dust at the interface. The ATSP-on-ATSP and PEEK-on-PEEK sliding contact showed the lowest COF and sand-dust accumulation compared with the other tribopairs;
- *Dust environment (RT):* compared with Ti-on-Al interface, the COF for metal-on-polymer and polymer-on-polymer reduced by 25 and 69% for ATSP and 40 and 65% for PEEK coating, respectively;
- *Sand environment (RT):* both ATSP and PEEK coatings behaved similarly and compared with Ti-on-Al interface, the COF reduced by 35 and 64% for metal-on-polymer and polymer-on-polymer, respectively. The COF was found to be slightly higher for dust compared with sand. The smaller size particles were more detrimental to friction;
- *Wear mechanism (RT):* the uncoated Ti-on-Al showed micro scuffing, which was entirely resolved by deposition of polymers on the Al disk surface. However, a mixed mode of two and three-body abrasive wear were identified due to sand and dust accumulation on the coatings' surfaces. Once the Ti pin surfaces were coated, the wear was changed to three-body abrasive wear as the dominant mechanism; and

- ATSP coating showed higher resistance to abrasive wear than PEEK, and dust was more detrimental to tribological performance (i.e., friction and wear), particularly for PEEK coating.
- The environmental temperature was shown to significantly affect the dust accumulation, COF, and wear rate. In general, higher temperatures increased the COF and the extent of dust deposition, particularly for metal-on-polymer configurations. The ATSP coating showed relatively similar behavior to PEEK in terms of friction and significantly better performance in terms of wear.

In addition to the Lunar/Mars simulated environment experiments, it is essential to investigate the tribological performance of the two polymer composite coatings under simulated environment of Titan to assess the efficacy of the selected coatings as a replacement material for the failed Nedox coating on the cam-follower surfaces of the dragonfly shown in **Figure 1**. An experimental procedure is designed in the next chapter to conduct the tests under higher Hertzian contact pressure as well as extreme temperatures ranging from -180 to 110°C.

CHAPTER 6

TRIBOLOGICAL STUDY OF PEEK- AND ATSP-BASED POLYMER COMPOSITE COATINGS FROM -180°C TO 110 °C

6.1 Introduction

Lubrication of bearing components and tribological surfaces in space exploration devices presents challenges due to extreme environmental conditions encountered in space [106]. An example is the wide variations in temperature ranging from cryogenic temperatures of -220 °C on Europa to upwards of 462 °C on Venus [26]. Under such conditions, the use of conventional liquid lubricants or grease is not feasible, and solid lubricants are suggested instead by applying them either as a separate lubricating film or as an additive inside a binding matrix to produce a self-lubricating composite [149,150].

Polymers are shown to be among the top candidate materials as binding matrices for solid lubricants such as polytetrafluoroethylene (PTFE) and MoS_2 due to advantages over metals such as low weight, low friction and wear, and low cost [2,72,151]. However, the large temperature variation in the space environment, as well as low thermal conductivity of polymers, may limit their use in bulk shape. On the other hand, deposition of polymer coatings with 10's of micron thickness on a metallic substrate has been shown to improve the foregoing deficiencies with bulk polymers by increasing the load-bearing capability, dimensional precision, and heat transfer through the metal substrate [19].

Due to large temperature variations in the space environment, it is imperative to develop and implement polymers with enhanced tribological properties across a wide

range of temperatures. The studies conducted by Polycarpou et al. [14,19,114,143] have demonstrated the efficacy of polymer coatings based on Aromatic Thermosetting Co-Polyester (ATSP) and polyether ether ketone (PEEK) for extreme environments ranging from -196 to 300 °C, once the polymers were mixed with the desired weight ratio of solid lubricants such as PTFE to provide the polymer with the self-lubricity.

The self-lubrication is achieved in the form of a protective polymer transfer layer once the sliding components rub against each other at a certain duration. The characteristics of the developed film, such as thickness and homogeneity play an important role in the friction and wear reduction. Therefore, many studies have investigated the transfer film formation by varying the parameters such as filler type, load, sliding speed, counterpart surface roughness, etc. [14,15,152,153]. Nonetheless, the effect of temperature change on transfer film formation is not well understood, particularly under cryogenic conditions.

Cui et al . [154] studied the transfer film formation of PEEK/PTFE hybrid composite on a steel ball at temperatures from 20 to -100 °C using optical microscopy and FTIR spectroscopy. The formation of transfer film occurred at temperatures below -30 °C and increased by further decrease in temperature. While the presence of the PEEK/PTFE was verified using FTIR analysis, the quantitative changes in the elements and transfer film were not demonstrated. Wang et al. [155] claimed that the transfer film is not able to form on the steel ball at low temperatures, and the friction is mainly determined by the real contact area, whereas in a study by Lan et al. [33], the increase of the normal load was shown to generate the polymer film at temperatures as low as -160 °C. Gtheiler et al. [156]

studied the tribological properties of PTFE composite against steel disk. While a homogeneous film with a thickness of 200nm was formed at RT, the film thickness increased up to 1.2 to 1.5 μm by decreasing the temperature down to T=77 K in He-gas and 4.2K in liquid He. On the other hand, liquid N_2 produced much thinner film of scattered polymer particles with thickness of 100nm. The presence of fluorides was detected using XPS analysis, but no quantitative comparison was made between different temperatures. Bashandeh et al. [114] tested ATSP/PTFE and graphene-enhanced ATSP polymer coatings from RT up to 300 °C. The graphene was shown to enhance the film formation with increased homogeneity by temperature, while the ATSP/PTFE developed a non-uniform film with the rise in temperature.

As the literature shows, the tribological studies of a particular polymer from cryogenic to high temperatures are scarce, while it is necessary to evaluate the properties in wide temperature ranges encountered in space. In addition, the studies relevant to cryogenic environments are mainly under liquid phase cryogen. The effect of temperature change on the transfer film formation is not well understood and quantified, and some studies have reported contradictory results.

Therefore, the aim of this chapter is to assess the tribological properties of two polymer-based composite coatings, namely ATSP/PTFE and PEEK/PTFE at temperatures from -180 to 110 °C, covering the environmental temperatures on Titan to Lunar/Mars planets. Specific attention was given to the role of temperature on developed transfer film on the steel counterparts, and the film was examined using SEM and XPS analysis. Furthermore, the thermomechanical properties of the coatings and wear mechanism were

characterized using dynamic mechanical analysis (DMA) and SEM, respectively, and correlations were made with the experimental findings.

6.2 Experimental

6.2.1 Materials and sample preparation

The oligomers CB2 with carboxylic functional group and AB2 with acetoxy functional group were synthesized in a batch melt polymerization and mixed with the weight ratio of 1:1 to produce the ATSP powder according to the description shown in Ref. [118]. 5wt.% PTFE was blended with ATSP powders as the lubricant additive. The mixture was then deposited on the sandblasted disks using the electrostatic spray deposition (ESD) technique. To cure the coatings, the samples were placed inside a convective oven at a temperature of 270 °C for 60 min to obtain the coating with an approximate thickness of 40±5 μm.

The PEEK/PTFE coatings were fabricated by an authorized applicator (Southwest Impreglon Inc.). Briefly, the PEEK powders were mixed with 20wt% PTFE (1704 PEEK/PTFE®), and the dispersion was sprayed on similar substrates using the ESD method, followed by melting under a temperature range of 371-399 °C. The pins and disks were machined out of a C300 alloy steel with radius of 12.7 mm and thickness of 6 mm (curve pin) and 25.4 mm×25.4 mm×3 mm (square disk), respectively.

Figure 61(a, b) depicts the SEM images of the ATSP/PTFE and PEEK/PTFE composite coatings, respectively. The shinier gray colors in **Figure 61(a)** indicate the dispersion of PTFE additives inside the ATSP coating [19], which reveals various penetration depths throughout the thickness. The degree of penetration could be grouped

into three categories of fully submerged, semi-submerged, and some particles that are protruded on the coating. Since the melting temperature of PTFE powder is higher than ATSP curing temperature, the particles maintained their solid and rigid state and formed a two-phased composite coating. On the other hand, the PTFE powders were fully submerged inside the PEEK/PTFE (**Figure 61(b)**) coating due to higher curing temperature than PTFE melting temperature and therefore, the coating appears as a one-phase composite coating.

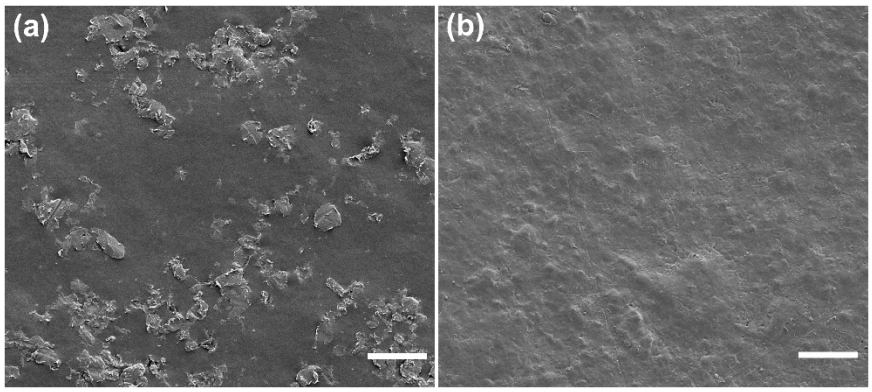

Figure 61. SEM images of the untested surface of (a) ATSP/PTFE and (b) PEEK/PTFE coatings (the scale bar is 500 μm).

6.2.2 Specialized cryogenic to high temperature tribometer

The tribological experiments were carried out using a custom-made tribometer known as High Temperature Tribometer (HTT). The HTT is equipped with a heating furnace and a glass/metal bell jar enclosure (**Figure 62(a)**) that enables running of experiments at temperatures up to 1000 °C and under controlled atmosphere. The environment is controlled by closing the bell jar, vacuuming the inside, and flushing the desired gas throughout the test at a certain rate. The in-situ normal and friction forces are

measured using a force transducer at the top side to calculate the in-situ coefficient of friction (COF). The sliding movement is achieved using a servo motor at the bottom side with capability of rotational speeds up to 1000 rpm.

To conduct the experiments under cryogenic temperatures, a cooling testing equipment was designed and fabricated as shown in **Figure 62(b)** with the capability of running the experiments under dry sliding conditions as low as -196 °C. Using the gas feedthrough, the inside environment close to the samples was first flushed for a certain duration with N_2 gas to evacuate the interior air atmosphere and moisture. The LN_2 was then passed through a series of vacuum insulated and non-vacuum insulated tubing with a controlled valve to fill the cryogen medium of the chamber through the cryogen feedthrough, as shown in the zoom-out image of **Figure 62(b)**. The chamber temperature could be controlled by balancing the two flows, namely N_2 gas and LN_2. It is noteworthy that during the early stages of LN_2 feeding, a substantial positive N_2 gas pressure was created due to partial expansion and evaporation in the tubing, which helped to maintain the environment free from ambient air and moisture.

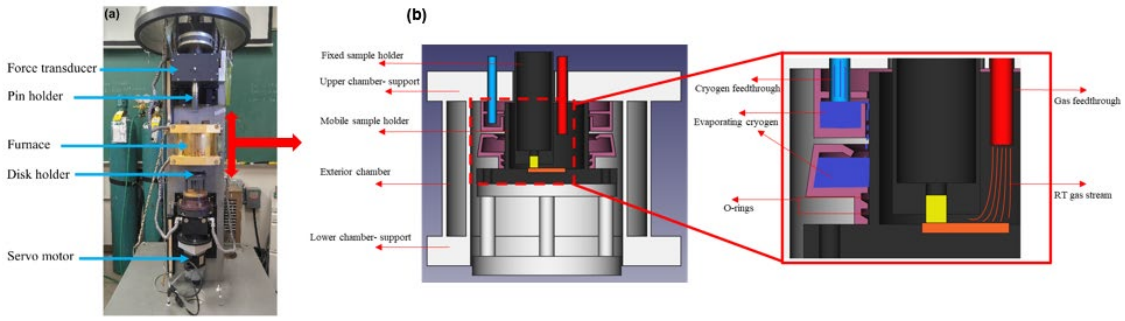

Figure 62. Experimental setup: (a) photograph of HTT, and (b) schematic of specialized cryogenic set-up.

6.2.3 Test procedure and characterizations

A curved pin-on-disk configuration was used to conduct the experiments according to the experimental conditions shown in **Table 11**. The experiments were performed under N_2 gas environment, constant normal load of 20 N equivalent to nominal Hertzian contact pressure of 32.5 MPa, constant sliding speed of 0.5 m/s for 1 hour duration, and different environmental temperatures, namely -180 °C, -100 °C, 25 °C (RT), and 110 °C. The temperatures were to capture the changes on environmental temperatures in the planets such as Titan and Lunar/Mars, and its subsequent effect on the tribological performance. Each sample was cleaned from contamination with isopropyl alcohol before and after each test by placing them inside an ultrasonic cleaner for 10min and drying using warm air.

Table 11. Experimental conditions

Tribopairs	Temperature (˚C)	Contact pressure, MPa (load, N)	Linear speed, m/s* (Speed, rpm)
Steel vs. ATSP/PTFE (St-on-AP)	-180 -100 25 (RT) 110	32.5 (20)	0.5 (540)
Steel vs. PEEK/PTFE (St-on-PK)			

*The linear speeds were calculated based on 17.5 mm average diameter for the wear tracks.

SEM/EDS analyses were used to characterize the surface morphology of the coatings and associated wear mechanism after tribological experiments as well as transfer film formation on the steel pin counterparts at different temperatures. The polymer coatings were sputter-coated with 4 nm Pt/Pd alloy to enhance the SEM image quality and decrease the charging effect. The profilometric wear scans were measured across the wear

tracks to calculate the wear rate on the coatings according to the method described in [147].

6.3 Results and discussion

6.3.1 Friction and wear

Figure 63(a, b) show the evolution of in-situ COF vs. sliding time at different temperatures for ATSP/PTFE and PEEK-PTFE coatings, respectively. For both coatings, the in-situ COF reached the steady-state condition at all temperatures after the running-in period. The PEEK coating demonstrated higher fluctuations on the COF and the time to reach the steady-state was temperature dependent and lower for ATSP coating compared with PEEK. As the temperature reduced from 110 °C to -180 °C, the interface took longer time to reach the steady-state. The differences on the fluctuations in the COF as well as running-in time could be explained by the differences in the transfer film formation on the steel counterparts as will be discussed later.

Figure 63(c, d) shows the summary of average COF values at all temperatures, calculated from the last 30 min of the in-situ COF curves shown in **Figure 63(a, b)**. The COF was maximum at -180 °C and reduced by 40% at 110 °C for both coatings. The COF did not follow a linear trend with temperatures from -180 to 110 °C. The COF increased at RT compared with -100 °C, and reduced at 110 °C again. Lower COF was obtained for ATSP coating at all temperatures compared with PEEK except for -100 °C where PEEK coating indicated 8% lower friction.

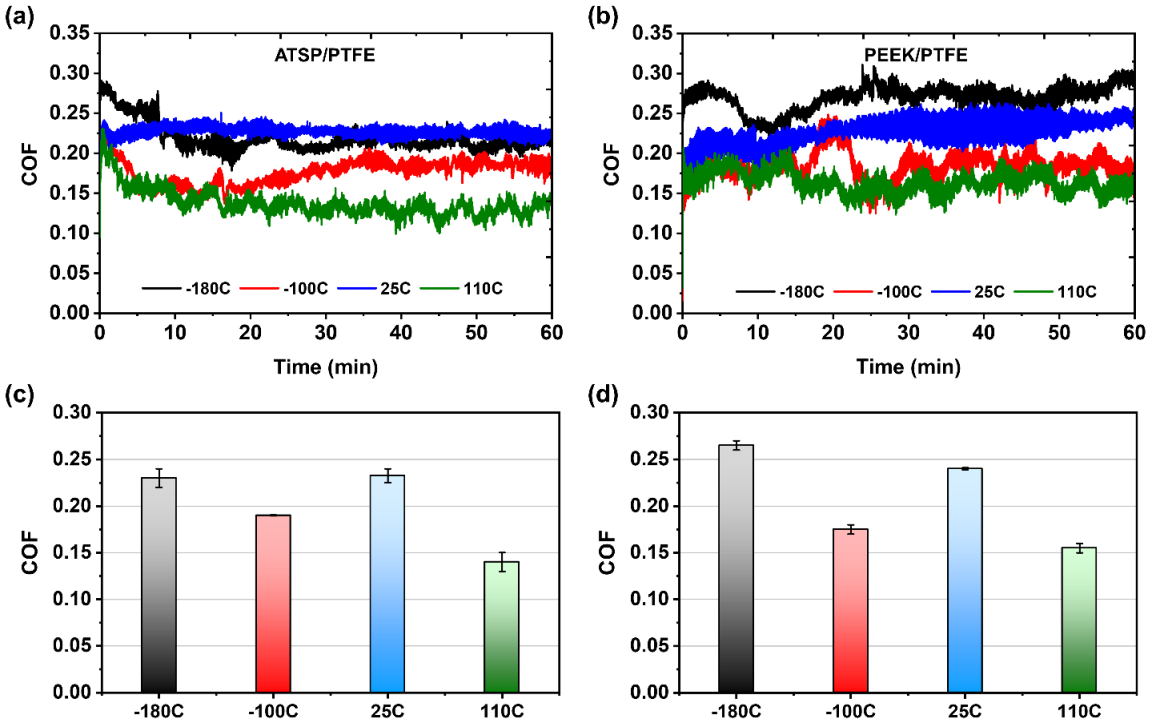

Figure 63. Tribological experimental results at different temperatures showing (a, b) the in-situ and (c, d) average COF for ATSP/PTFE and PEEK/PTFE coatings. (The error bars represent the ± one standard deviation).

It is generally accepted that the softening of the polymers by increase of temperature could generate two contrary effects in polymers friction, and depending on the dominant factor, different trends could be obtained: I) the reduction in COF due to lower interfacial shear strength caused by easier segmental motion of the chains, and II) increase in COF due to increased real contact area caused by lower elastic modulus. Besides, the characteristics of the developed transfer film also play a key role in the ultimate friction and wear behavior, which will be discussed later. Based on the DMA measurements shown in Ref [33,114], the storage modulus of ATSP was significantly increased from HT to -160 °C. The increase in the modulus as well as transfer film containing PTFE elements (as will be shown later) were dominant factors at cryogenic

temperatures and resulted in the decrease of COF at -100 °C and similar COF to RT at -180 °C, although an increase in interfacial shear strength occurred as well. At 110 °C, the decrease in interfacial shear strength was dominant and reduced the COF.

The profilometric wear scans were measured across the wear tracks after the experiments with ATSP/PTFE and PEEK/PTFE coatings, and the results are shown in **Figure 64(a, b)**. The wear scans on the ATSP coating do not indicate any discernible wear since the profile inside and outside of the wear track looks the same. The only evident difference is the polishing of top asperities revealed by partial flattening of the peaks inside the wear track particularly at 110 ℃, indicating a burnishing type wear mechanism. On the other hand, according to **Figure 64(b)**, the PEEK/PTFE coating showed different extent of wear depth at different temperatures. Except for -100 ℃ where the coating is under significant burnishing effect, at the remaining temperatures, the coating showed appreciable wear up to 10 μm wear depth.

Figure 64(c) shows the calculated average wear rate from the profilometer wear scans shown in **Figure 64(a, b)**. The ATSP coating showed unmeasurable zero wear at all temperatures since the wear was extremely low to be identified and measured from the profilometric wear scans. Similarly, the PEEK coating showed unmeasurable zero wear at -100 ℃, whereas at the remaining temperatures, the wear was high enough to be identified from the wear scans. Similar results were obtained for PEEK/PTFE composite, where the wear rate dropped significantly from RT down to -100 ℃ [154]. Herein, the maximum wear occurred at RT followed by -180 and 110 ℃.

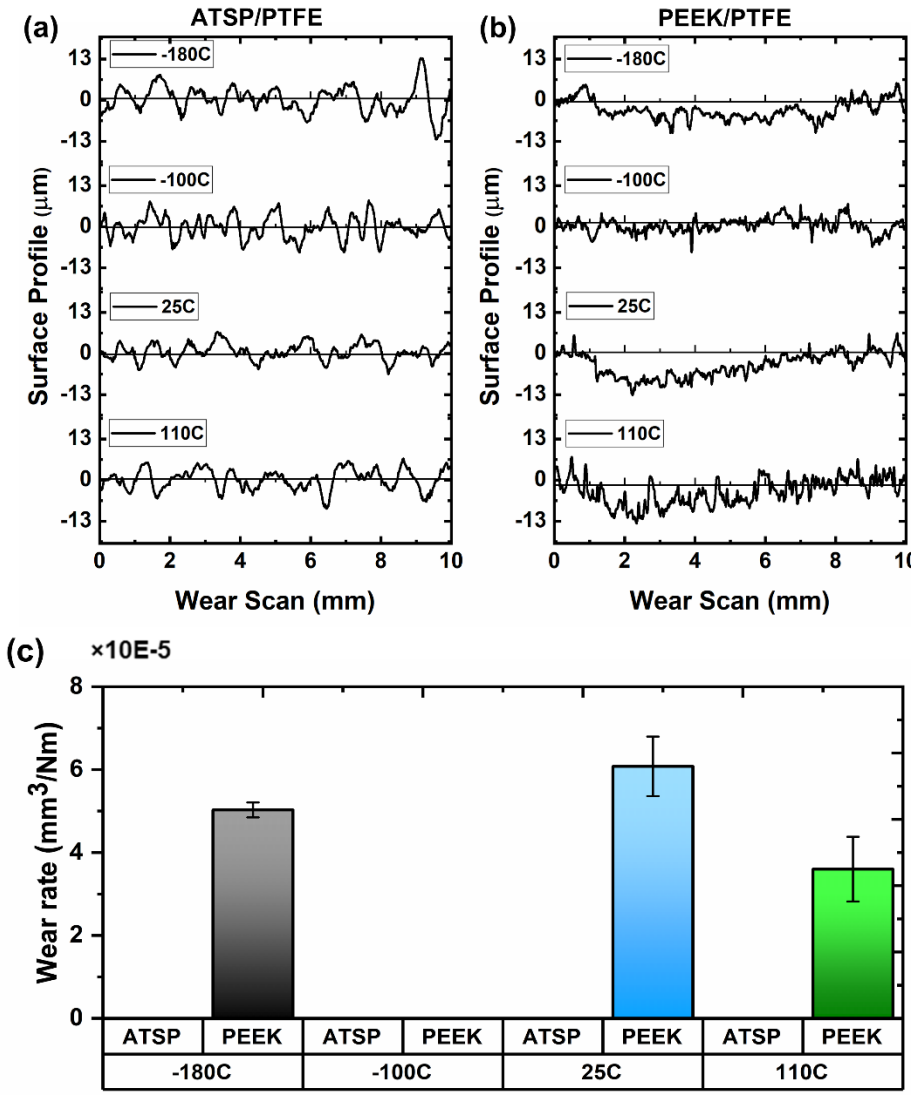

Figure 64. (a, b) Profilometric wear scans measured across the wear tracks on ATSP/PTFE and PEEK/PTFE coatings, respectively, and (c) calculated average wear rate at different temperatures.

6.3.2 Transfer film analysis

The characteristics of the developed transfer film play a critical role in the ultimate friction and wear performance. Therefore, the film should be evaluated in terms of properties such as homogeneity/uniformity, thickness, and developed elements to get a better understanding of tribological performance. Herein, SEM, EDS, and XPS were

employed to analyze the topography and chemical nature of the transferred film from the polymers and to find the correlation with tribological performance.

Figure 65(a-h) shows the SEM images of the transferred film to the steel pin counterpart at different temperatures. A common trend between the two coatings is the increase in the thickness and extent of the transferred film with decreasing the temperature from 110 ℃ to -180 ℃. In addition, an extra layer with lighter color was formed with decrease in temperature that could be attributed to the transfer of fluorine elements in the PTFE composition. This shinier grey color was identified in the PTFE additive inside as-received state of ATSP coating [157] as well. The complementary XPS analysis will further substantiate this observation. The comparison of the transfer film from the two coatings at -180 ℃ shows that a more uniform film was created by ATSP compared with PEEK, which developed a patchy shape film. This resulted in higher COF and wear at this temperature for PEEK coating, while the transfer film from ATSP was beneficial in friction and wear reduction. On the other hand, at -100 ℃, the film from PEEK was substantially more uniform (**Figure 65(f)**) compared with -180 ℃, and therefore a lower COF and minimal wear were obtained. ATSP coating could yet maintain its good film with similar characteristics seen at -180 ℃. At RT and 110 ℃, both ATSP and PEEK coating demonstrated similar film characteristics with lower surface coverage and thickness compared to cryogenic conditions. In addition to the temperature effect on the mechanical properties and associated wear rate, this lower surface coverage of film on the pin could also be identified as one of the reasons for higher wear of PEEK at RT and 110

℃ compared with -100 ℃. Overall, the ATSP coating could form a more homogenous film at all temperatures compared with PEEK.

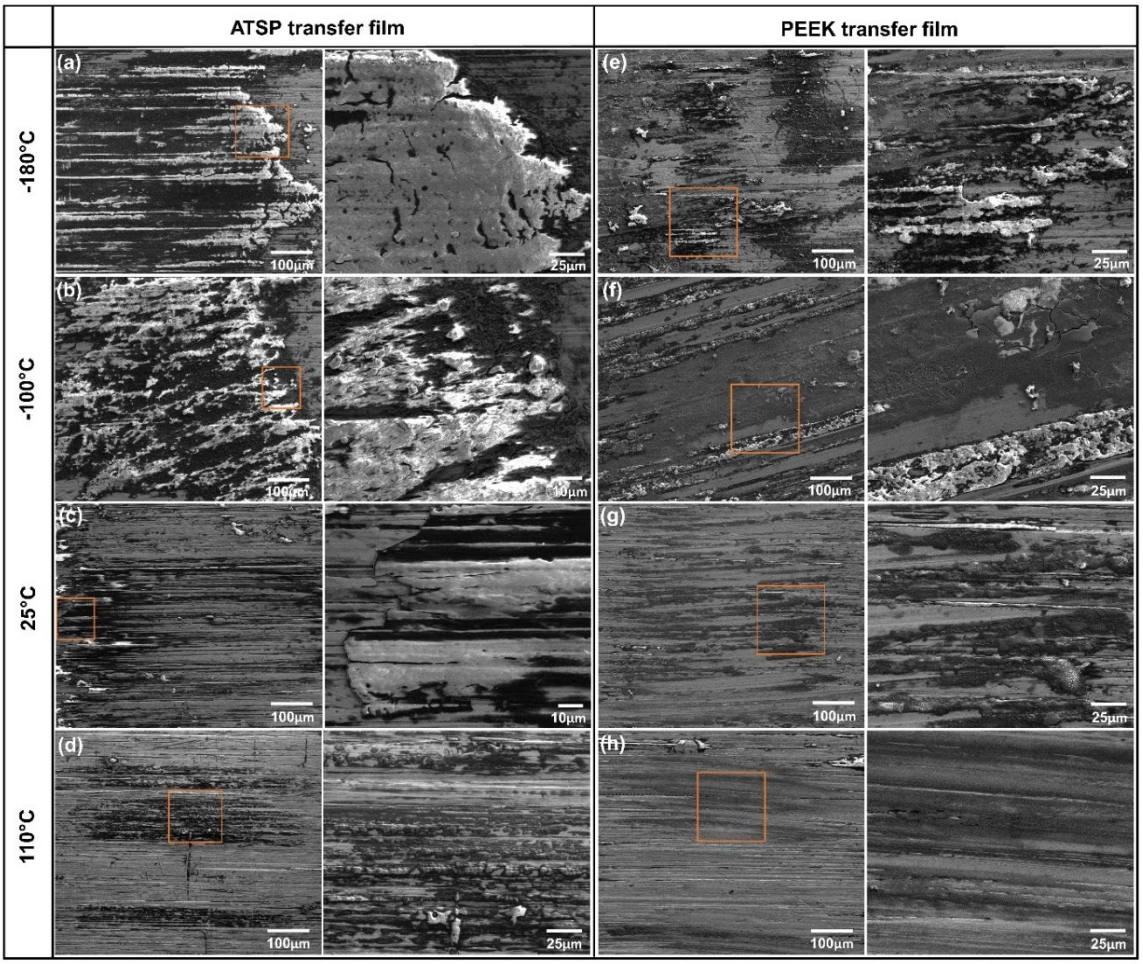

Figure 65. SEM images of the steel pins after the experiments at different temperatures depicting the transfer film formation from (a-d) ATSP/PTFE and (e-h) PEEK/PTFE coatings.

EDS analysis was conducted on the transferred film from ATSP and PEEK coatings at RT, and the results are shown in **Figure 66(a, b)**. The red and green color indicates the presence of the iron and carbon elements on the surface, which are attributed to the main elements found in the chemical structure of steel pin and the ATSP and PEEK

polymers, respectively. Therefore, the extra layer with black/grey colors seen in the SEM images of **Figure 65(a-h)** could be attributed to the transferred film from ATSP and PEEK coatings.

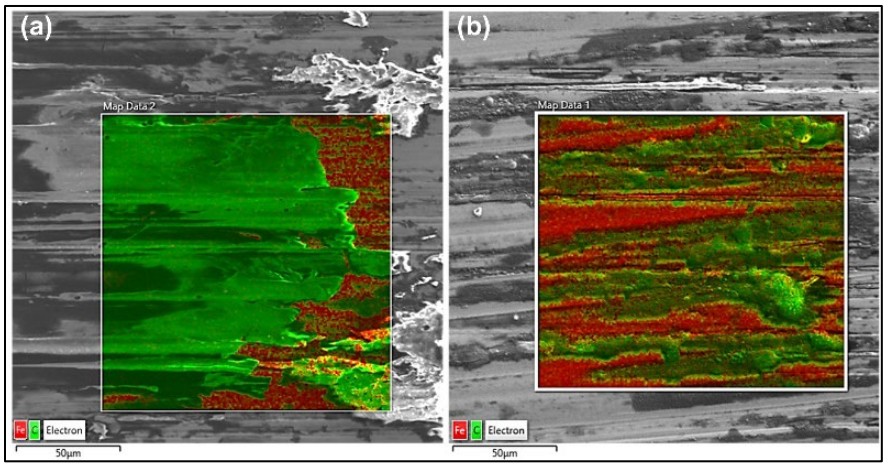

Figure 66. EDS analysis of the steel pin surface after RT experiments with (a) ATSP/PTFE and (b) PEEK/PTFE coatings.

Since the EDS detector could not identify the presence of fluorine elements on the spots with shinier grey color, likely due to a very low thickness, the XPS was performed which has a higher resolution compared with EDS and can detect the elements at the nanometer penetration depth. The transferred film on pins was chemically and elementally analyzed at different temperatures from -180 °C to 110 °C, as shown in **Figure 67(a-d)**, respectively. The high-resolution C 1*s*, O 1*s*, and F 1*s* spectra for all the transferred films at different temperatures were entirely similar with minor changes in the intensity of the peaks. **Figure 67(a-d)** shows the high-resolution F 1*s* spectra of the transferred film on pins at different temperatures. As shown in **Figure 67**, all the F 1*s* spectra are deconvoluted to a lone peak at ~689.0 eV, corresponding to the CF2 group in PTFE. It

can be concluded that the topmost layers shown in the SEM images in **Figure 65** were composed of PTFE. According to the XPS analysis, the PTFE was not undergone any side reactions at different temperatures. However, the only change is associated with the drop in the peak intensity with temperature, indicating that the fluorine content is reduced as the temperature increases.

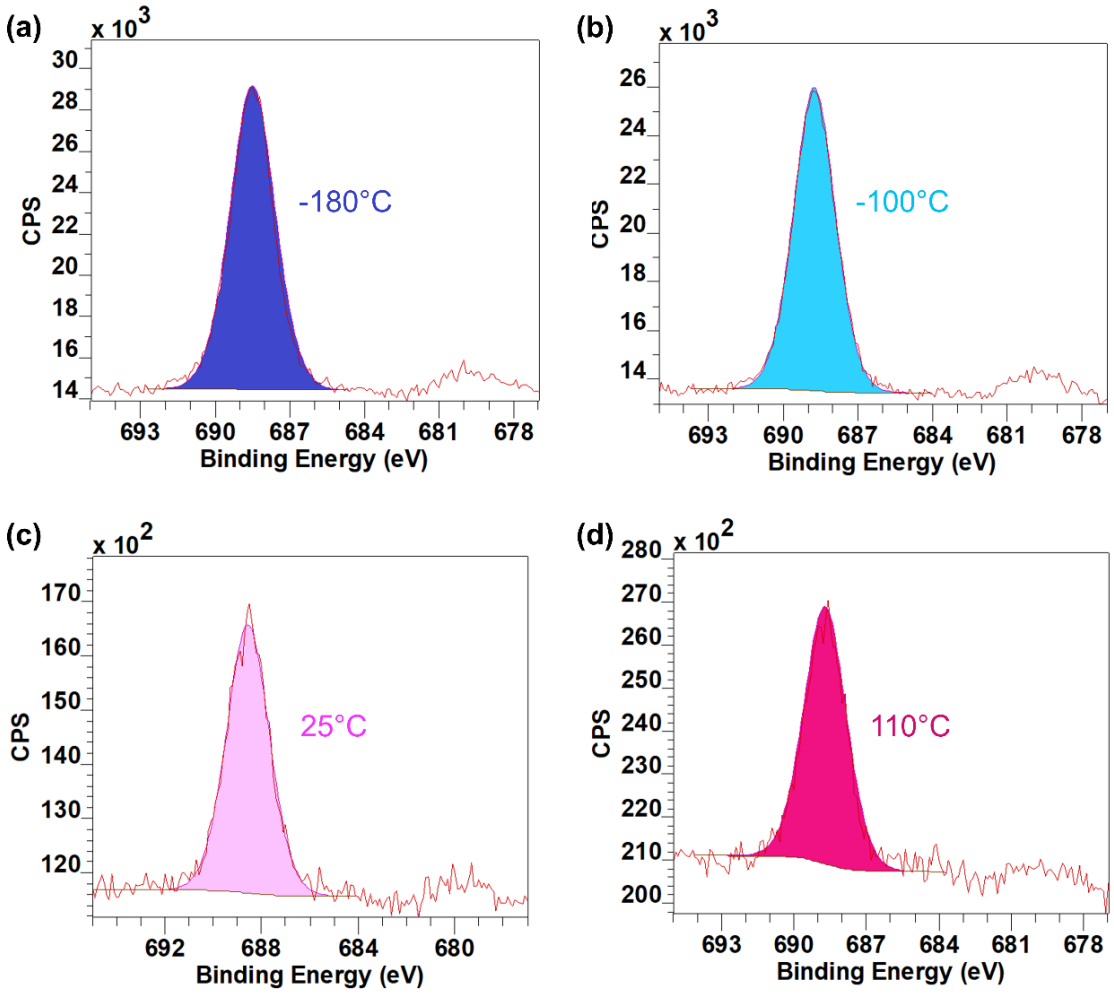

Figure 67. High-resolution F 1s peak of transferred film on the steel disks from ATSP-based coating at temperatures of (a) -180 °C, (b) -100 °C, (c)25 °C, and (d) 110 °C.

As shown in **Table 12**, the percentage of PTFE in the transferred film was greater at lower temperatures. These results make two assumptions possible: 1) compared to ATSP, PTFE becomes more brittle at lower temperatures, consequently separating more quickly; and 2) The thermal expansion coefficient of PTFE is higher than ATSP. Lowering temperature caused a higher shrinkage in the PTFE phase, leading to stress concentration at the interface of PTFE and ATSP and, consequently, final debonding and transferring on the metal pin counterpart.

Table 12. Elemental analysis of the XPS spectra of ATSP transferred film at different temperatures.

Test Temperature (°C)	C (At%)	N (At%)	O (At%)	F (At%)
-180	73.5	1.6	13.8	11.1
-100	74	1.9	14.1	10
25	71.4	1.8	20.9	5.9
110	68.7	1.5	24.2	5.6

6.3.3 Wear mechanism (SEM)

SEM was performed to visually analyze the wear mechanism on the coatings surfaces and to find the correlations with testing temperature. The low and high magnification (LM&HM) images are depicted in **Figure 68(a-h)** for ATSP and PEEK coatings. The wear could hardly be identified on ATSP coating from LM images, and a few shallow scratches were evident, particularly under cryogenic conditions. The scratches could be attributed to the hardened wear debris from the polymer as well as top asperities of the steel pin. The ATSP coating showed a burnishing wear mechanism from the HM images, particularly at the spots where the PTFE additives protruded, as indicated

by double-sided dashed arrows in the figures. This is in agreement with the wear measurements shown in **Figure 64(a, c)**.

On the other hand, the PEEK coating showed a distinct difference in the wear mechanism compared with the ATSP coating. A combination of adhesive and abrasive wear could be identified at all temperatures but with different intensities. An example of adhesive marks is shown with a solid arrow in **Figure 68(e)**, which indicates an adhesive wear mechanism. The extent of the adhesive wear was reduced by increasing the temperature, particularly at 110 ℃, where minimal COF was obtained. A distinctive difference between cryogenic and elevated temperatures was the formation of some back transferred polymer film or piled-up wear debris on the surface, indicated with double-sided solid arrows in **Figure 68(e,f)**. This layer was more pronounced under -100 ℃ at different spots on the coatings, which helped to reduce the wear of the coating to the same extent as ATSP, which was not measurable.

Overall, the ATSP coating showed a burnishing type wear mechanism at all temperatures resulting in superior wear resistance compared with PEEK coating. Adhesive wear was the dominant wear mechanism observed for PEEK coating and with maximum intensity at -180 ℃.

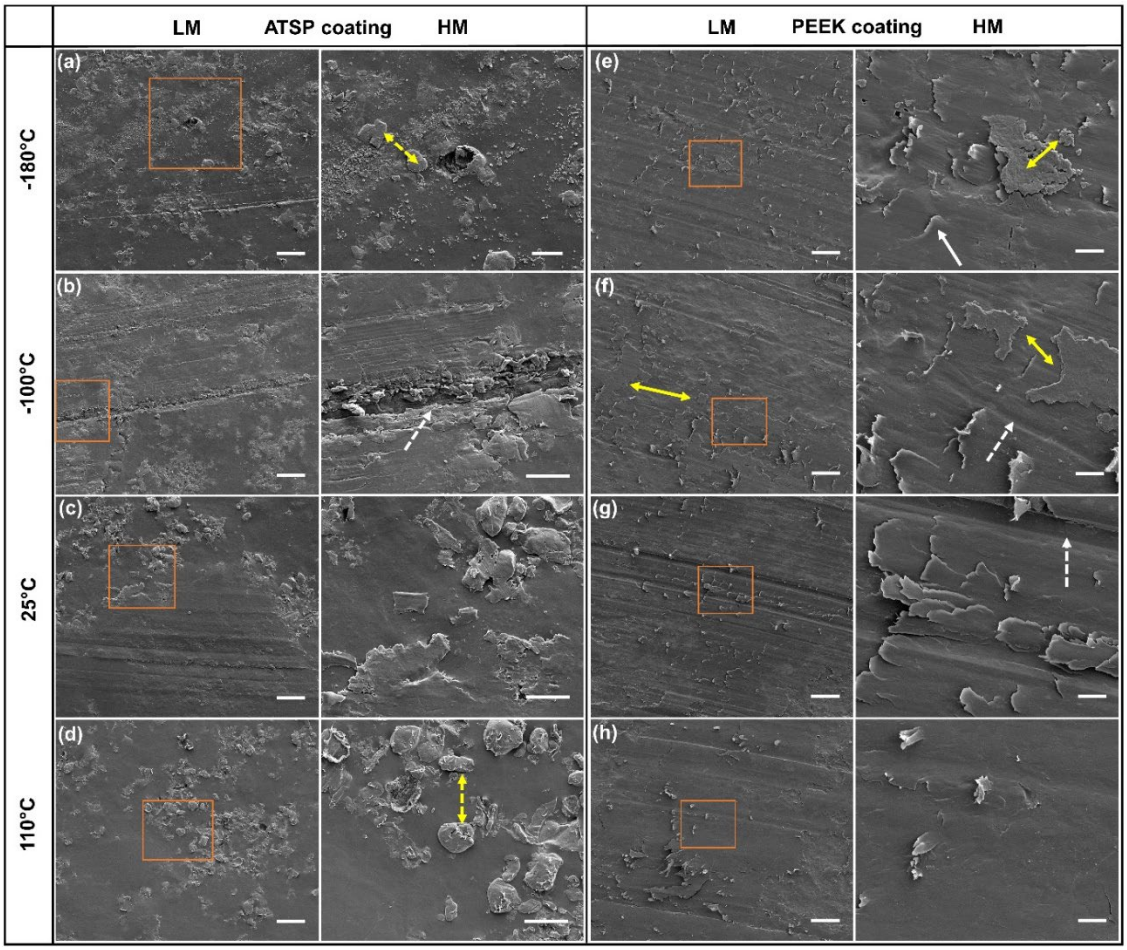

Figure 68. SEM images of the (a-d) ATSP/PTFE coating and (e-h) PEEK/PTFE coating at low and high magnifications (LM and HM) after the experiments at different temperatures. (The scale bar for LM images are 50µm and for HM images of ATSP and PEEK coatings is 20 and 10µm, respectively).

6.3.4 Transfer film replication

As seen in section 6.3.2, the transfer film was beneficial for friction and wear reduction once a homogeneous film was developed on the steel counterpart. Inspired by this beneficial effect of transfer film, the ATSP and PEEK polymers were deposited on the steel pins to form a polymer-on-polymer sliding from the beginning of the experiments. To evaluate the efficacy of this interface, tribological experiments were

conducted similar to the procedure discussed in Section 6.2.3 and following the experimental conditions shown in **Table 11**. These experiments were conducted only at RT.

Figure 69(a) shows the comparison of average COF values between metal-on-polymers and polymer-on-polymer experiments at RT for both ATSP and PEEK coatings. The predisposition of transfer film on the metal pins reduced the COF for both ATSP and PEEK coatings and the COF reduced by 22 and 30%, respectively. Furthermore, according to **Figure 69(b)**, the ATSP coating maintained its zero wear rate by changing the interface, and the wear rate for PEEK coating was significantly reduced by 59%. Therefore, the coating-on-coating configuration effectively improved the tribological performance by lowering the COF and wear rate.

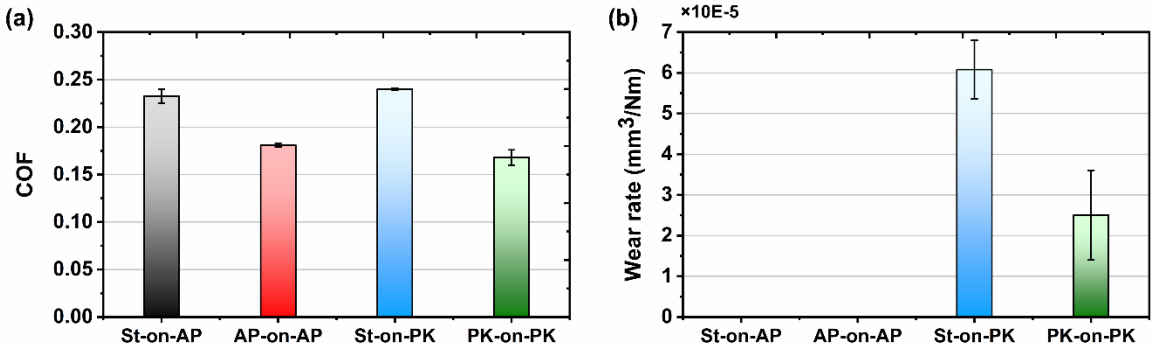

Figure 69. Comparison of average (a) COF and (b) wear rate between metal-on-polymer and polymer-on-polymer experiments at RT (St, AP, and PK denotes steel, ATSP, and PEEK, respectively).

6.4 Summary

PEEK and ATSP-based polymer composite coatings were tribologically tested under different environmental temperatures from -180 °C up to 110 °C, simulating the

Titan and Lunar/Mars environmental temperatures. Specific emphasis was given to the role of temperature on the transfer film formation to find the correlations with tribological performance. The following conclusions could be drawn:

- The maximum COF occurred at -180 °C followed by RT, -100 °C, and 110 °C for both ATSP and PEEK composite coatings. ATSP coating showed lower COF at all temperatures except for -100 °C where PEEK coating indicated 8% lower friction.
- ATSP coating indicated unmeasurable zero wear at all temperatures, whereas PEEK coating showed the maximum wear at RT followed by -180 and 110 °C. The wear was unmeasurable at -100 °C.
- The decrease of temperature to cryogenic conditions increased the extent and thickness of transfer film from ATSP and PEEK coatings. Transfer film was shown to be uniform and homogeneous for ATSP coating at all temperatures, while PEEK coating formed a patchy and non-uniform film at -180 °C that resulted in higher COF and wear.
- The presence of PTFE elements was greater at cryogenic temperatures based on XPS analysis, and no side reactions were detected.
- ATSP coating showed a burnishing type wear mechanism at all temperatures, whereas the PEEK coating indicated adhesive and abrasive wear mechanisms. The adhesive wear was maximum at -180 °C and reduced by the increase of temperature to 110 °C resulting in lower COF.

- ATSP was shown to have superior tribological performance compared with PEEK coatings and could be identified as a candidate material for use in bearing components and tribological surfaces for applications such as space exploration devices to planets such as Titan, Moon, and Mars that require long-life bearings over a wide range of temperatures from -180 to 110 °C.

The high Hertzian contact pressure as well as sand abrasive environment in Lunar/Mars surfaces might ultimately cause the failure of the coating on the pin side in a long duration of sliding. Therefore, it is imperative to develop and assess similar polymers in bulk or insert format to increase the life expectancy. To this end, the bulk HPPs based on ATSP, PEEK, and PI were machined into pin shape, and their tribological performance is studied in the next chapter at temperatures up to 300 °C and under dry sliding conditions.

CHAPTER 7[5]

TRIBOLOGY OF SELF-LUBRICATING HIGH PERFORMANCE ATSP, POLYIMIDE, AND PEEK-BASED POLYMER COMPOSITES UP TO 300 °C

7.1 Introduction

High-performance polymers (HPPs) have been used as promising candidate materials for bearing and tribological components that demand operation with low friction and wear under extreme conditions such as cryogenic and elevated temperature environment, where the use of external lubrication is not feasible. The broad use of HPPs stems from their satisfactory properties such as ahigh load bearing capacity, lightweight, low cost, self-lubricity, and good friction and wear properties [2,158,159]. Since unfilled polymers suffer from poor tribological performance (high friction and/or wear), they are typically blended with solid lubricants such as polytetrafluoroethylene (PTFE) and graphite flakes, and reinforcements such as carbon/glass fibers to improve their tribological and mechanical performance, respectively [160].

HPPs based on polyether ether ketone (PEEK), Polyimide (PI), and aromatic thermosetting co-polyester (ATSP) have been shown to provide self-lubrication and enhanced tribological performance by blending them with solid lubricants [14]. As solid lubricant, PTFE and graphite are shown to enhance the self-lubricity due to their capability to form transfer film on the surface of harder metallic counterpart [18]. The development

[5] Reprinted with permissions from "Bashandeh K, Lan P, Polycarpou AA. Tribology of self-lubricating high performance ATSP, PI, and PEEK-based polymer composites up to 300° C. Friction. 2022 Apr 28:1-3."

of transfer film is shown to play an important role in the reduction of friction and wear at the sliding interface, which makes polymers an attractive selection for dry sliding components [14]. The transfer film formation depends on parameters such as sliding speed, normal load, temperature, surface roughness, polymer structure, and the type of filler in the polymer matrix [15,161].

PEEK is a thermoplastic polymer with measured glass transition temperature (Tg) of 143 °C whose composites are widely used in many tribological applications [14]. For elevated service temperatures, a maximum operating temperature of 250 °C was reported [162]. PI-based composites are categorized among high operating temperature polymers with excellent friction and wear resistance under unlubricated conditions, particularly at elevated temperatures [163,164]. ATSP is part of a newer family of HPPs (called Vitrimers; which is a thermoset that processes like a thermoplastic) that was invented in the mid-1990s [78]. Several studies conducted by Polycarpou et al. demonstrated the superior tribological performance of ATSP, compared to PTFE and PEEK polymer coatings for a wide range of temperatures from -196 to 300 °C [19,33,52,53,114,143]. However, tribological studies in bulk form are scarce, and some studies investigated the performance of ATSP/PTFE composites under R-134A refrigerant environment and temperature of 60 °C for air-conditioning compressor applications [15,165,166].

The focus of the present chapter is to investigate the role of environmental temperature (room temperature (RT) up to 300 °C) on the tribological performance of commercially available high-performance polymer-based composites, namely PEEK bearing grade (HPV), a polyimide (PI)-based composite known as Vespel SP-211, and an

ATSP-based polymer composite, which are shown to stand in the top of the polymer pyramid among the HPPs [2,14]. The effect of temperature on the development of transfer film from polymer to steel counterpart was studied to examine its correlation with tribological performance.

7.2 Experimental

7.2.1 Materials and sample preparation

Three different polymer composite pins namely ATSP-based, PI-based (Vespel SP-211), and PEEK bearing grade were used for tribological testing. ATSP resins were synthesized using crosslinkable aromatic copolyester oligomeric systems, namely CB and AB (forming CBAB oligomer system) with carboxylic acid and acetoxy functional end group, respectively. The oligomers synthesis were performed in a 2 L reactor through batch melt polymerization at temperature of 270 °C and under Argon gas atmosphere. Thereafter, the oligomers were ground and sieved using a 90 μm sieve size. Detailed description of synthesis procedure can be found elsewhere [118]. To produce the ATSP-based bulk composites, the oligomers (CB and AB) were mixed with the desired graphite (Microfyne, Asbury Graphite Mills, Inc.) and PTFE (7A X, The Chemours Company FC, LLC) additives, with the weight ratios listed in **Table 13**. The mixture was then cured at 360 °C for 2 hours and ground into smaller size particles that pass through 125 μm sieve. The ground compound was then compressed in compression molding at a temperature of 360 °C under 5000 psi pressure for 2 hours, and then naturally cooled down to RT to obtain the final condensed ATSP bulk composite plate.

Table 13. Description of blended polymer materials. Reprinted with permissions from "Bashandeh K, et al. Tribology of self-lubricating high performance ATSP, PI, and PEEK-based polymer composites up to 300° C. Friction. 2022 Apr 28:1-3."

Materials	Composition	Vendor
ATSP-based	CBAB + 30%Graphite + 10% PTFE	ATSP Innovations
Vespel SP-211 (PI)	Vespel® (polyimide) + 25% PTFE/Graphite	DuPont
PEEK bearing grade (HPV)	PEEK + 30% Carbon fiber/graphite/PTFE	Boedeker plastics

Thereafter, the sample was machined into cylindrical pins with a diameter of 6.35 mm for tribological testing. The Vespel and PEEK polymer composites were commercially available and were purchased from the vendors in stock shapes and machined into 6.35 mm diameter pins. Vespel SP-211 is a PI-based polymer that is blended with graphite and PTFE to improve its friction and wear properties. PEEK bearing grade is blended with graphite and PTFE to improve the tribological properties, and carbon fiber to enhance the dimensional stability [1]. Note that the exact weight percentage of the PEEK and PI additives were not provided by the vendor. 416 stainless steel (416SS) disks were machined with dimension of 50.8 mm in diameter and 6.35 mm in thickness to use as the counterpart. The root-mean square surface roughness (Rq) of 0.215 μm was obtained through surface grinding.

7.2.2 Experimental procedure

The tribological experiments were performed under dry sliding conditions and using a flat-pin-on-disk configuration. The experiments were conducted at environmental temperatures ranging from RT to 300 °C, as shown in **Table 14**. The PEEK composite was tested only at 25 and 150 °C as the maximum operating temperature is below 300 °C.

For each test, a constant normal load of 130 N equivalent to a nominal contact pressure of 4 MPa was applied from the pin side. The disk was unidirectionally rotating against the pin at 1 m/s (530 rpm) sliding speed of for 1-hour duration equivalent to sliding distance of 3600 m. The in-situ friction and normal forces were recorded by a two-axis transducer to calculate the in-situ coefficient of friction (COF) during the experiment. The experiments with each material were repeated at least three times to assess the reproducibility. The samples were ultrasonically cleaned by immersing them in isopropyl alcohol for 10 minutes before the experiments. Thereafter, the samples were rinsed with isopropyl alcohol and dried by blowing warm air. The same procedure was followed after each test and the tested coupons were used for characterization.

Table 14. Details of blended polymers and experimental conditions. Reprinted with permissions from "Bashandeh K, et al. Tribology of self-lubricating high performance ATSP, PI, and PEEK-based polymer composites up to 300° C. Friction. 2022 Apr 28:1-3."

Polymer composites	Temperature (˚C)	Contact pressure, MPa (load, N)	Speed, m/s* (rpm)
ATSP	25 150, 300	4 (130)	1 (530)
PI			
PEEK	25, 150		

*The linear speed was calculated considering the average wear tracks diameter as 18 mm

The mass of each polymer pins was measured before and after each experiment using a scale with a precision of 0.01 mg to calculate the wear rate according to the following equation:

$$k = \frac{\Delta m}{F_N L} \quad (1)$$

Where k is the wear rate (mg/Nm), Δm is the polymer mass loss (mg), F_N is the applied normal load (N), and L is the total sliding distance (m). The worn and unworn surfaces of the polymers were examined using scanning electron microscopy (SEM) to depict the surface changes and associated wear mechanisms by the tribological testing. Energy-dispersive X-ray spectroscopy (EDS), X-ray photoelectron spectroscopy (XPS), optical microscopy, and profilometric scans were performed on the tested surfaces of the steel disks to evaluate formation and variation of polymer transfer films with temperature. Differential scanning calorimetry (DSC) measurements were performed to determine the Tg of each polymer using a TA Instrument 2910 MDSC V4.4 E.

7.3 Results and discussion

7.3.1 DSC analysis

To measure the Tg of each polymer, the prepared specimens were heated at a heating rate of 10 °C/min under nitrogen gas flow from 25 to 400 °C. **Figure 70** shows the DSC heating curves of each polymer composite. The DSC curve of PI shows no Tg or melting temperature (Tm) due to the thermosetting nature of the polymer. For ATSP polymer composite, there exists an endothermic peak at 332 °C corresponding to Tm, and a shoulder at 307 °C corresponding to the Tg. The PEEK DSC curve shows a double melting behavior with lower endothermic peak at 212 °C and a higher endothermic peak at 341 °C. Such behavior could be ascribed to annealing effect and partial recrystallization and melting at heating between Tg and Tm [167]. For PEEK, the Tg was measured as 155 °C.

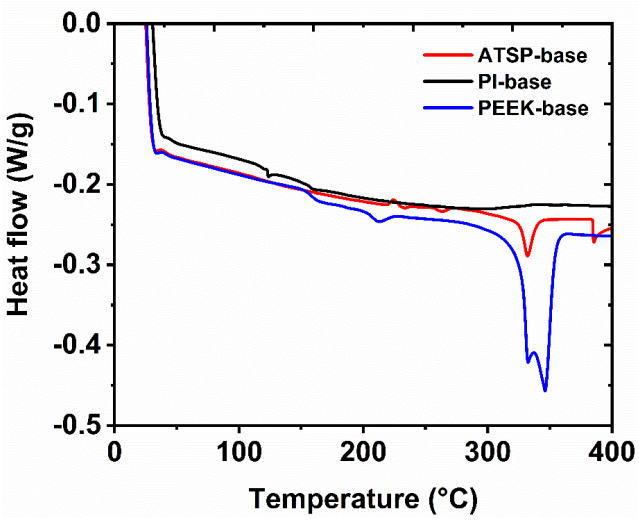

Figure 70. DSC scans of ATSP-, PI-, and PEEK-based polymer composites. Reprinted with permissions from "Bashandeh K, et al. Tribology of self-lubricating high performance ATSP, PI, and PEEK-based polymer composites up to 300° C. Friction. 2022 Apr 28:1-3."

7.3.2 Friction and wear

Figure 71(a) shows the evolution of unfiltered in-situ COF as a function of sliding distance for the pin-on-disk experiments of blended HPPs at temperatures of 25, 150, and 300 °C. For all polymers, the in-situ COF started with an initial running-in behavior and eventually reached a steady-state period. For RT experiments, both PEEK and ATSP composites showed the most stable friction after the running-in period. Unlike PEEK and ATSP, PI showed a transient period between two steady-state stages where instabilities in the COF occurred. These instabilities and variations in the COF caused the squeaking noise at the interface, which is undesirable in industrial applications. This behavior could be attributed to the inability of the material to form a transfer film on the counterpart, and therefore the pin continued to wear off due to the plowing of the asperities from the steel disk surface. When the temperature increased to 150 °C, ATSP and PI showed the most

stable friction with a decreasing trend, while the COF of PEEK composite followed an increasing trend and needed the longest time to reach steady-state behavior.

Figure 71(b) summarizes the variation of the average COF with temperature. The COF is calculated for the steady-state period, and the error bars in the figure designate the ± one standard deviation. When the temperature increased from RT to 150 °C, the COF of ATSP- and PI-based composites reduced by 36 and 58%, respectively, while it had an adverse effect on the COF of PEEK-based composite by increasing it by 71%. For ATSP and PI, the COF followed a decreasing trend with temperature and compared with RT, the COF reduced by 53 and 70% at 300 °C, respectively. Among all tested samples, the highest COF was obtained for PI (0.31) for experiments at RT followed by PEEK (0.29) at 150 °C, and the lowest COF occurred at 300 °C for both ATSP (0.099) and PI (0.092) polymer composites. The high friction of PI at RT could be attributed to its inability to form a uniform transfer film on the counterpart, as it will be discussed later.

The variations in COF with temperature could be attributed to several different reasons, such as the changes in real contact area due to changes in polymer elastic modulus, the changes in the interfacial shear strength, and the extent and uniformity of transferred polymer to the counterpart. Although the increase of temperature facilities easier sliding at the interface due to lower shear strength of the softened polymer and reduces friction, lower elastic modulus on the other hand could increase the real contact area and therefore increases the COF. Thus, different trends for friction could be obtained depending on which factor is more dominant. For example, as shown in **Figure 71(b)**, it can be postulated that the decrease of interfacial shear strength was the dominant factor

for PI and ATSP base composites, while the increase in real contact area could be the dominant factor for PEEK-based composite. This can be explained by the difference in Tg of the polymers. According to **Figure 70**, PEEK Tg was measured as 155 °C, similar to [167], while the Tg for the ATSP with oligomers CBAB was 307 °C, and the SP grades of Vespel had no Tg. Therefore, for the experiments at 150 °C, PEEK was exposed to temperatures in the vicinity of its Tg and softened more than the other two polymer composites. Similar behavior was observed in [167] where during temperature ramping from RT to 240 °C, a significant increase in COF was observed due to reduction in storage modulus at temperatures above Tg up to 180 °C.

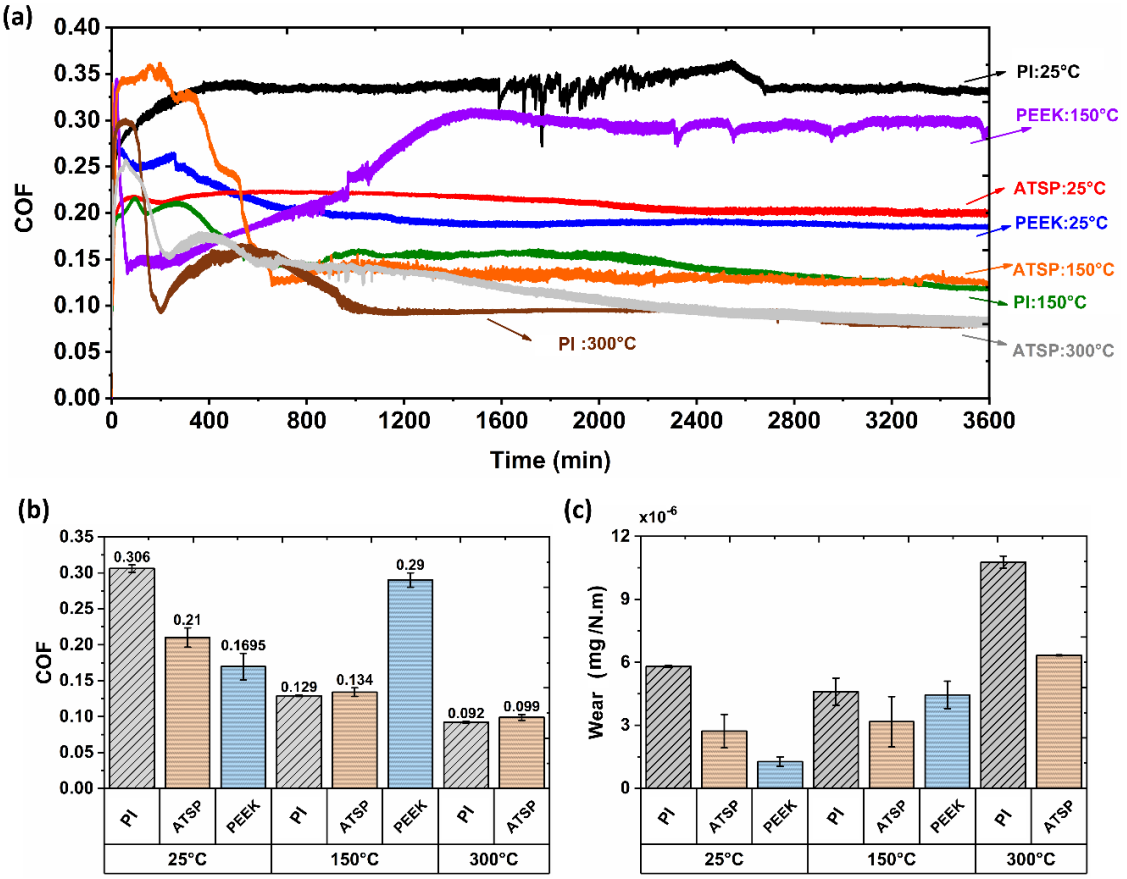

Figure 71. (a) In-situ COF vs. time for all polymer composites, (b) variation of average COF at steady-state, and (c) average calculated wear. Error bars designate ± 1 standard deviation. Reprinted with permissions from "Bashandeh K, et al. Tribology of self-lubricating high performance ATSP, PI, and PEEK-based polymer composites up to 300° C. Friction. 2022 Apr 28:1-3."

Figure 71(c) summarizes the variation of average wear rate of the tested polymers at different temperatures. The wear rates were calculated from the mass loss measurements shown in **Table 15** and using Eq. (1). A similar trend for all tested polymers is the increase of wear from room to elevated temperatures. However, the rate of increase in wear is lower for ATSP composite, compared with PEEK and PI composites. Compared with RT, the wear of ATSP and PI at 300 °C increased by 57 and 85%, respectively, and for PEEK the wear increased by 71% at 150 °C. In general, PEEK showed the lowest wear for RT

experiments, while ATSP showed minimal wear at elevated temperatures. Note that although the wear rate of PEEK and PI composites are relatively the same at 150 °C, the increased rate of wear compared to RT is significantly higher for PEEK compared with PI. The increase of PEEK wear at elevated temperature could be attributed to the significant softening of the polymer and the corresponding reduction in storage modulus at 150 °C (near Tg), which helped the easier removal of PEEK material by the hard asperities of the steel counterpart. Overall, ATSP composite could be considered as the best performing polymer considering the tribological performance (friction and wear) for this wide range of operating temperatures from 25 to 300 °C, making it an attractive solution for oil-less engineering applications.

Table 15. The average mass loss measurement for each polymer composite pin at different temperatures. Reprinted with permissions from "Bashandeh K, et al. Tribology of self-lubricating high performance ATSP, PI, and PEEK-based polymer composites up to 300° C. Friction. 2022 Apr 28:1-3."

Materials (pin)	**Temperature (°C)**		
	25	150	300
	Mass loss (mg)		
ATSP	1.20	1.45	2.88
Vespel SP-211 (PI)	2.82	2.24	5.23
PEEK bearing grade (HPV)	0.60	1.88	NA

7.3.3 Transfer film analysis

Introducing solid lubricants such as PTFE and graphite into polymer matrices is an effective way for friction and wear reduction through the formation of transfer films on the counterface [14,77,83]. During sliding, when the interfacial adhesion between the asperities of the tribo-pairs exceeds the cohesive strength of the softer material (typically

polymers), the material will begin to transfer to the counterpart in the form of a thin transfer film [36]. The formation of such transfer film is also observed in this study and is visually depicted in **Figure 72(a-c)** using optical microscopy images of the wear tracks on the steel disks.

The optical images of the RT experiments indicate the formation of a uniform and continuous transfer film on the disk surface after testing of ATSP and PEEK composite pins, which enabled the protection of the softer polymer against harder asperities of the steel disk. However, the transfer polymer from PI composite pin showed a patchy and non-continuous characteristic (i.e., transfer layer) and did not properly adhere to the counterface, which caused higher wear of PI compared to other polymer composites, as shown in **Figure 71(c)**. This behavior could be attributed to lower concentration of PTFE in the composition of PI, as will be shown in the EDS analysis of the pins' surfaces. The effectiveness of graphite in formation of transfer film is shown to be for temperatures greater than 100 °C, and its wear rate is shown to increase with temperature [168], and thus, it formed a non-uniform layer at RT. Increasing the temperature helped to develop a uniform and continuous transfer film after testing with ATSP and PI, which helped to reduce the friction. As shown in **Figure 71(a)**, the experiments at elevated temperatures took longer time to reach steady-state condition, compared with RT experiments, indicating a longer time to form the uniform transfer film on the counterface. Therefore, the increased wear rate at elevated temperatures could be attributed to continuous high material wear by the harder metallic counterpart asperities until a stable and uniform film was formed.

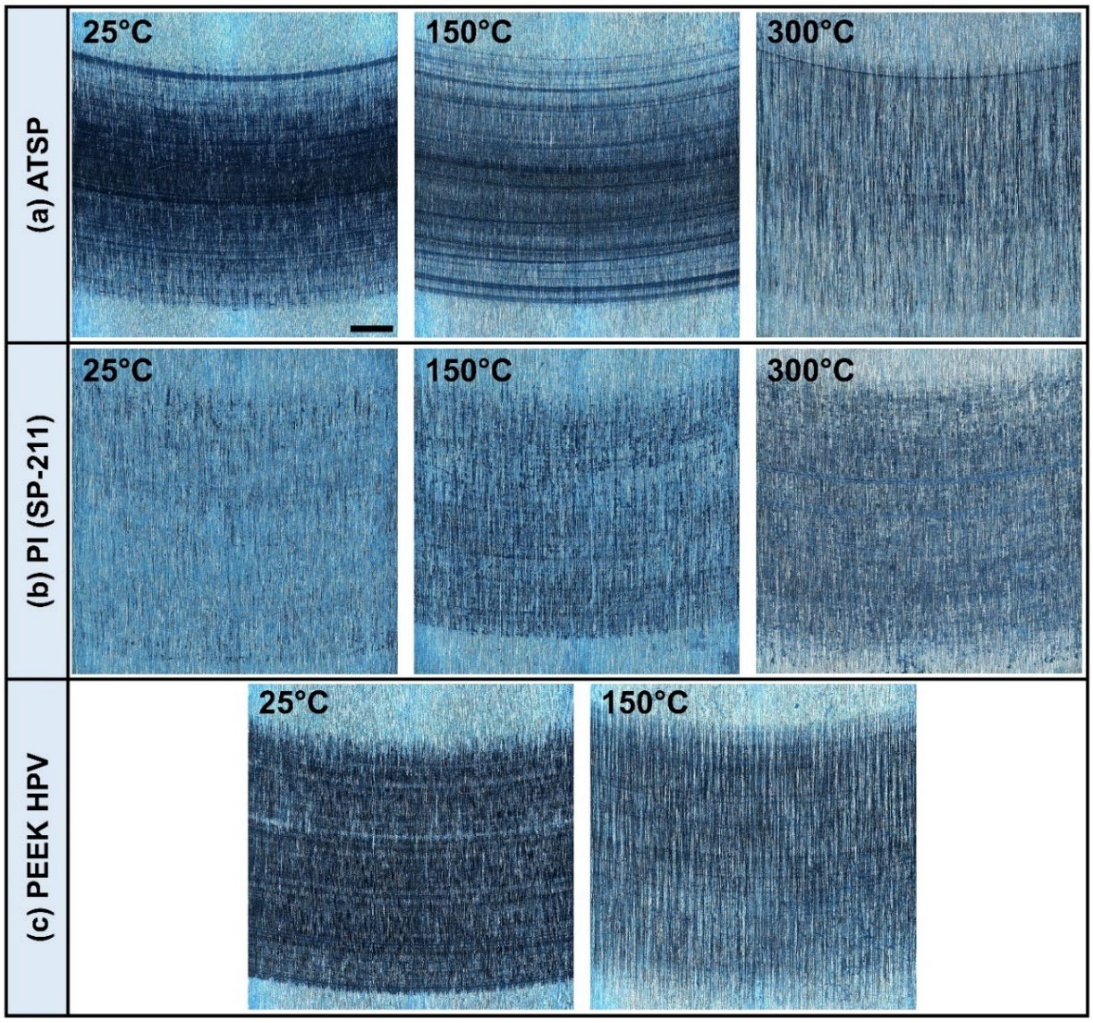

Figure 72. Optical microscopy images of the steel disks after experiments at different temperatures with (a) ATSP-based, (b) PI-based, and (c) PEEK-based polymer composites (scale bar is 1 mm for all images). Reprinted with permissions from "Bashandeh K, et al. Tribology of self-lubricating high performance ATSP, PI, and PEEK-based polymer composites up to 300° C. Friction. 2022 Apr 28:1-3."

Figure 73(a-c) show the SEM images and corresponding EDS mapping of the steel disk surfaces after testing with ATSP, PI, and PEEK composites at RT. The formation of transfer film from the polymer pins to the disk is clearly discernible from the SEM images, revealed by darker areas on the surface. However, the extent and uniformity

of the transferred films are not the same among the polymers. **Figure 73(a)** shows the transfer material from ATSP pin to the steel surface showing a continuous and uniform transfer film. PI on the other hand formed irregular transfer layer, and only small patches were developed on the asperity crevices at RT, as shown in **Figure 73(b)**. The obtained SEM image of the steel surface after testing with PEEK (shown in **Figure 73(c)**) indicates the evidence of continuous transfer film, but with lower area coverage compared with ATSP. The EDS analysis of the developed film on the steel surface shows that the dark areas on the wear track of the SEM images correspond to carbon elements, which are the dominant element in the structure of the polymer.

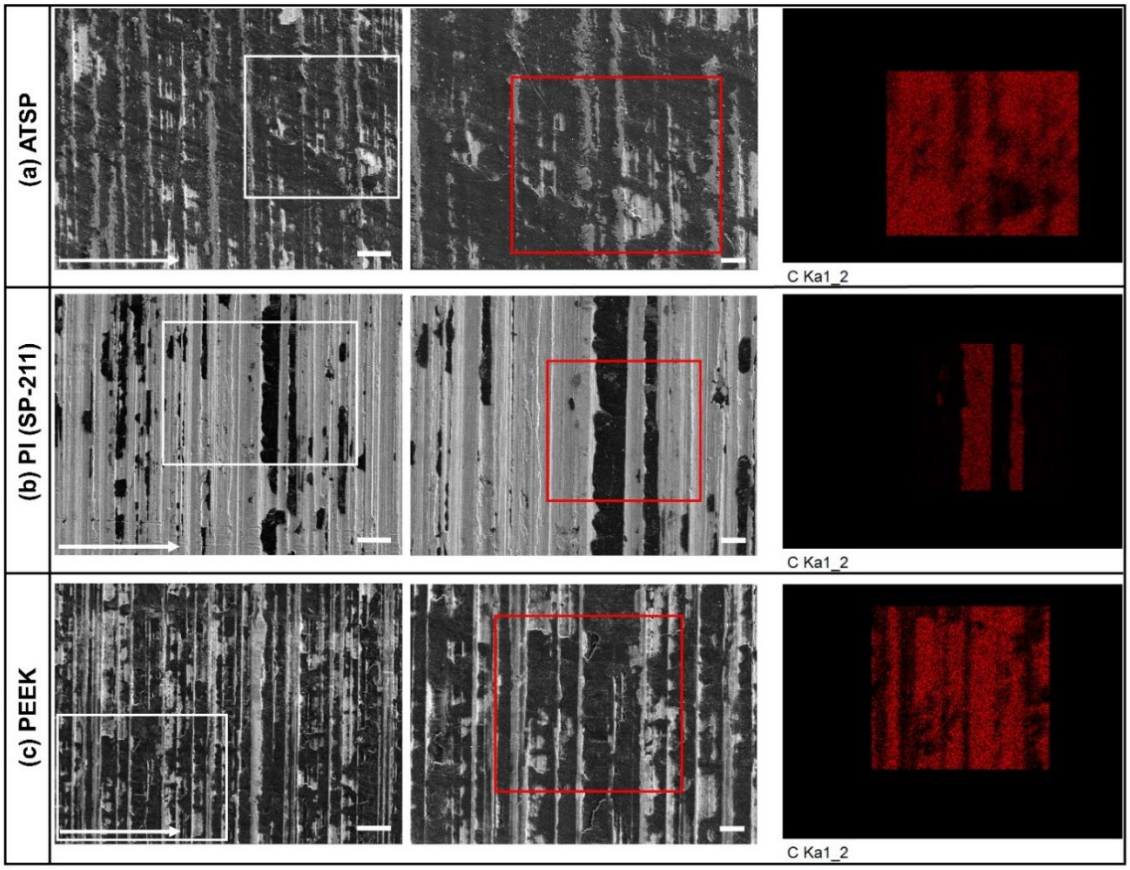

Figure 73. SEM images and corresponding EDS analysis of the steel surface showing the formation of transfer film by sliding of (a) ATSP, (b) PI, and (c) PEEK at RT (scale bar is 25 µm for low magnification (left) and 10 µm for high magnification (middle and right) images. The arrows show the sliding direction). Reprinted with permissions from "Bashandeh K, et al. Tribology of self-lubricating high performance ATSP, PI, and PEEK-based polymer composites up to 300° C. Friction. 2022 Apr 28:1-3."

To find the composition of the transferred films on the disks, X-ray photoelectron spectroscopy (XPS) was utilized, and the results are shown in **Figure 74**. The high-resolution C 1s spectra of the transferred films from PEEK-based, PI-based, and ATSP-based polymer composites after experiments at RT were investigated with an Omicron XPS system equipped with the Argus detector at X-ray voltage of 15,000 and X-ray power of 225 W. We used the CN10 charge neutralizer to avoid charging the sample and

increase the resolutions. Aperture 3 with a rectangular analysis area was selected to maximize the accuracy of the elemental analysis.

As shown in **Figure 74**, the high-resolution C 1s spectra of all the transferred films presented five common peaks at ~283.3 eV, 284.8 eV, 286 eV, 587.7 eV, and 289.3 eV, representing the C–F, C–C/C=C, C–O/C–N, C=O, and O–C=O groups, respectively. Unsimilar to the transferred films from PEEK-based and PI-based pins, the C 1s spectrum of the film generated by the ATSP-based pin showed an intense shoulder peak at 289.3 eV, which is originated by carbon atoms bonded to fluorine atoms by single bonds. This is while the same peaks formed by the PEEK-based and PI-based films that were fairly weak. This is why only the F 1s spectrum of the ATSP-based film was deconvoluted, which comprised of only C-F component. Therefore, it can be clearly concluded that (i) the concentration of PTFE was higher in the transferred film from ATSP-based polymer pin; (ii) fluorine only covalently bonded with carbon through a single bond, representing no bond formation between PTFE and ATSP during curing process and/or side reaction at the interface during sliding. Thus, the XPS spectra clearly show the presence of higher percentage of PTFE in the case of the ATSP-based film at the sliding regions that helped to reduce the friction and wear compared to PI-based pin.

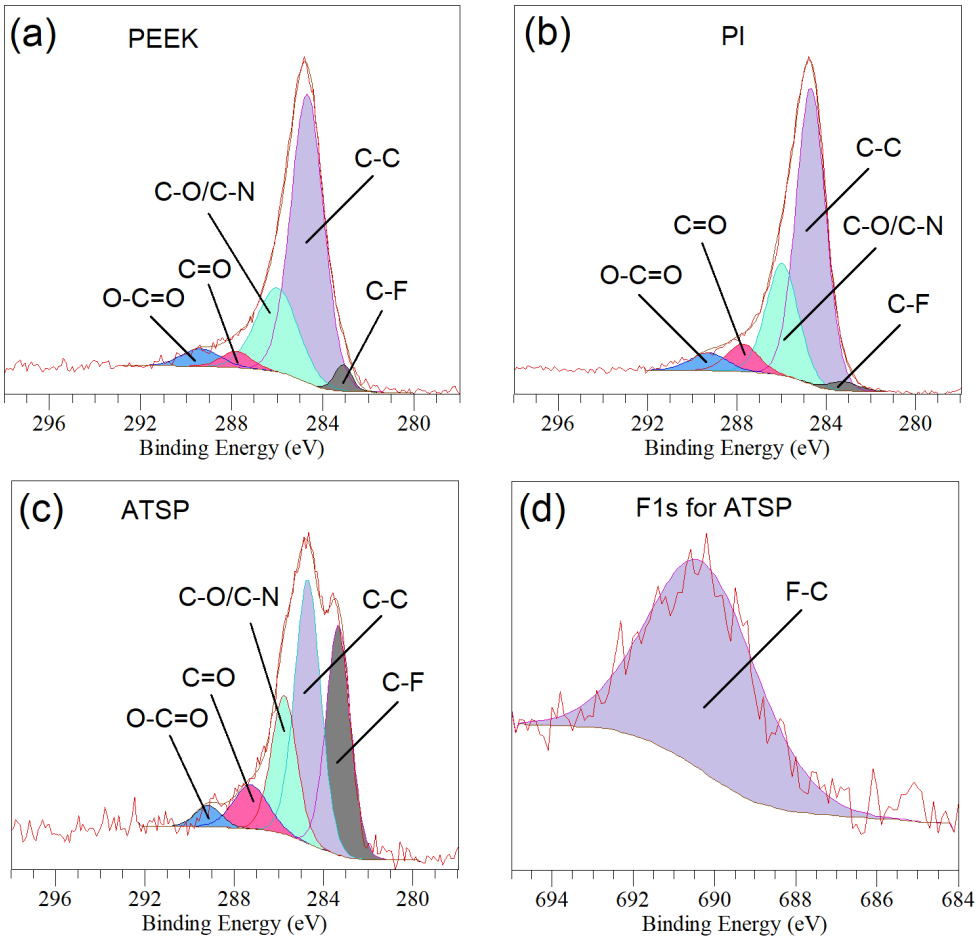

Figure 74. The high-resolution C 1s peak of transferred film on the steel disks from a) PEEK-based, b) PI-based, and (c) ATSP-based polymer composites after RT experiment. (d) The high-resolution F 1s peak for ATSP-based polymer. Reprinted with permissions from "Bashandeh K, et al. Tribology of self-lubricating high performance ATSP, PI, and PEEK-based polymer composites up to 300° C. Friction. 2022 Apr 28:1-3."

In addition, the elemental compositions for the samples are also provided in **Table 16**. In the same line with the results of the depicted spectrums, the transferred film from ATSP-based pin possessed higher F content compared to other polymers. Expectedly, the film from PEEK contained higher oxygen content (~20.7%).

Table 16. Elemental analysis obtained from high-resolution spectra in XPS for the transferred film from each polymer after RT experiment. Reprinted with permissions from "Bashandeh K, et al. Tribology of self-lubricating high performance ATSP, PI, and PEEK-based polymer composites up to 300° C. Friction. 2022 Apr 28:1-3."

Polymer composites	C (At%)	N (At%)	O (At%)	F (At%)
ATSP	68.5	4.4	19.2	7.9
PI	82.3	2.2	14.3	1.2
PEEK	74.6	3.2	20.7	1.5

Figure 75(a-c) show representative profilometric line scans across the wear track on the surface of the steel disks after testing with ATSP, PI, and PEEK composites, respectively. The scans were measured using a Dektak (Bruker) stylus profiler. From **Figure 75(a)**, a continuous transfer of material from ATSP is evident for experiments at RT and 150 °C, with transferred layer thickness of approximately 0.4 and 0.15 μm, respectively. For the experiment at 300°C, the thickness of the transferred film was less than the stylus resolution, and therefore it could not be measured. **Figure 75(b)** shows similar line scans for experiments with PI. All the scans show no change on the surface topography outside and inside the wear track due to the inability of the material to form a transfer film at RT, and inability of the stylus to measure the extremely thin transferred film at the temperatures of 150 and 300 °C. In the case of PEEK bearing grade, the profile at RT (**Figure 75(c)**) shows a uniform and continuous transferred layer with thickness of 0.5 μm. However, the scan at 150 °C shows the development of partial and non-continuous film. The formation of such discontinuous film and deterioration of the mechanical properties, namely elastic modulus at 150 °C, could be the reason for higher friction and wear for PEEK.

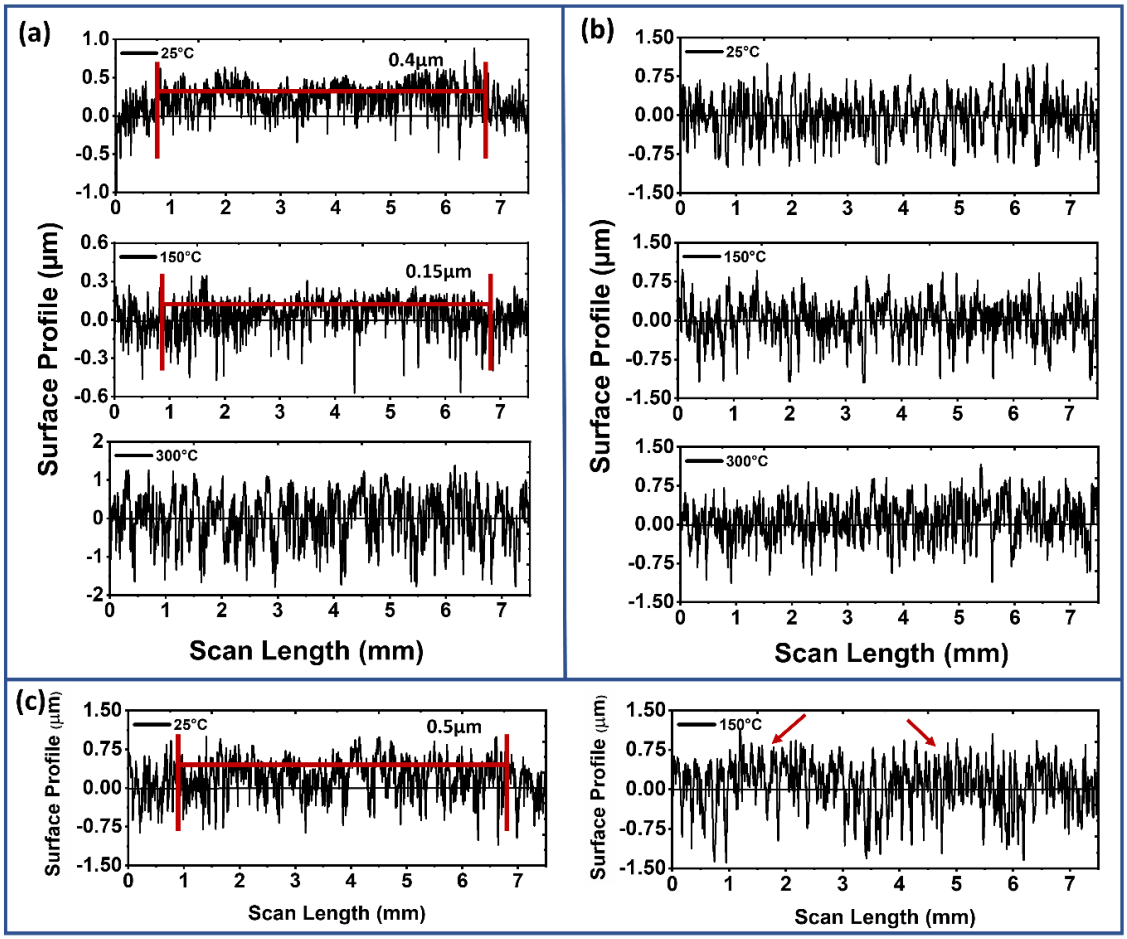

Figure 75. Profilometric measurements on the surface of steel disks after experiments at different temperatures with (a) ATSP, (b) PI, and (c) PEEK bearing grade polymers. Red lines represent the wear scar. Reprinted with permissions from "Bashandeh K, et al. Tribology of self-lubricating high performance ATSP, PI, and PEEK-based polymer composites up to 300° C. Friction. 2022 Apr 28:1-3."

7.3.4 SEM/EDS analysis of the worn surfaces

Figure 76(a-c) show the SEM-EDS analyses that were performed on the surface of each polymer composite pin surface. The analyses were performed in a JEOL JSM-7500F FE-SEM to provide a qualitative screening of PTFE additive distribution inside the polymer matrices. The EDS mapping on all polymers demonstrate the presence of fluorine

elements (indicated by cyan color) originating from the PTFE powders. The EDS maps show excellent distribution of the PTFE powders in the polymer matrix but with different intensities for each polymer. The ATSP contains the largest concentration of PTFE followed by PI and then PEEK.

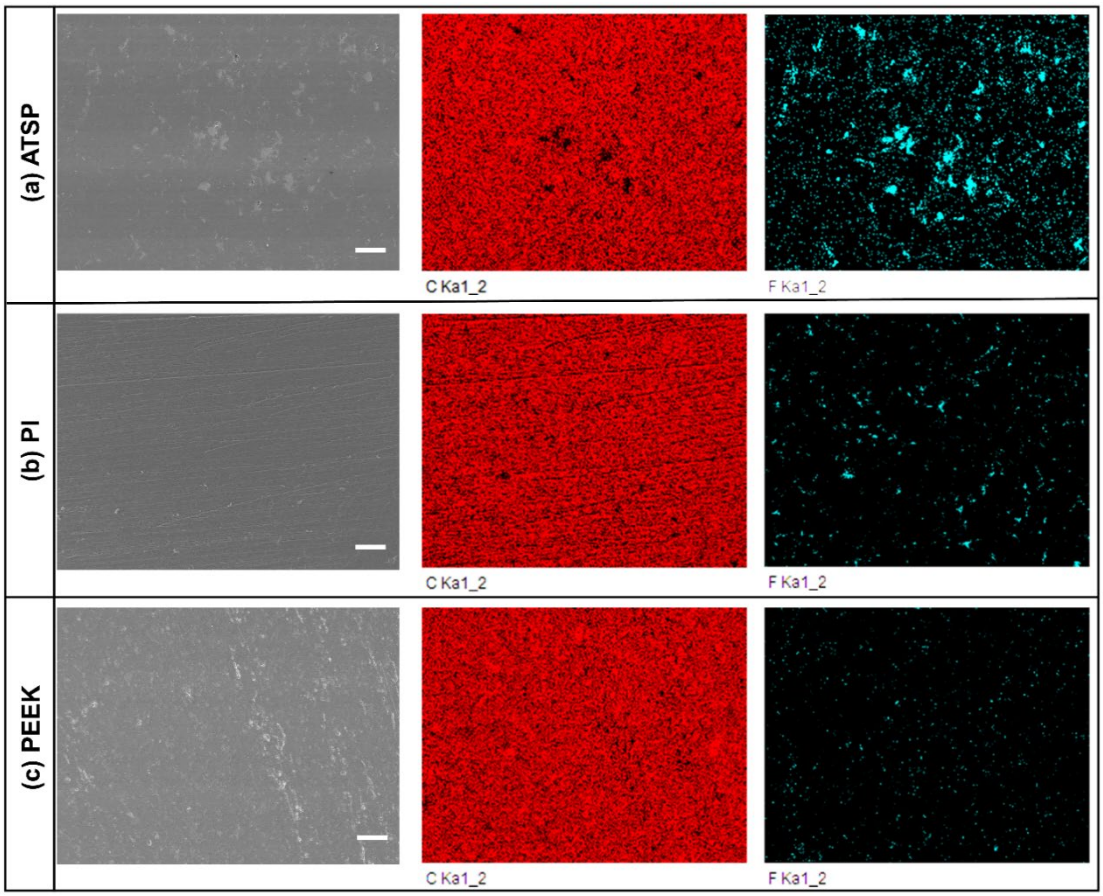

Figure 76. SEM and EDS mapping of (a) ATSP-base, (b) PI-base, and (c) PEEK-base polymer composite pins surfaces. Reprinted with permissions from "Bashandeh K, et al. Tribology of self-lubricating high performance ATSP, PI, and PEEK-based polymer composites up to 300° C. Friction. 2022 Apr 28:1-3."

The SEM images of the untested and worn surfaces of the polymeric samples were also used to study the wear mechanisms associated with the experiments at different

temperatures. A sputter coater machine was used to coat the samples with a 4 nm layer of Pt/Pd to obtain the SEM images. **Figure 77(a-d)** show the SEM images of the untested and tested surfaces of ATSP composite pins at different temperatures. The surface texture of the untested ATSP is depicted in **Figure 77(a)** showing a rough topography after machining. The SEM images of the worn surfaces after experiments in **Figure 77(b-d)** indicate that the dominant wear mechanism at all temperatures is polishing and removal of top asperities and initial irregularities in the topography of the surface.

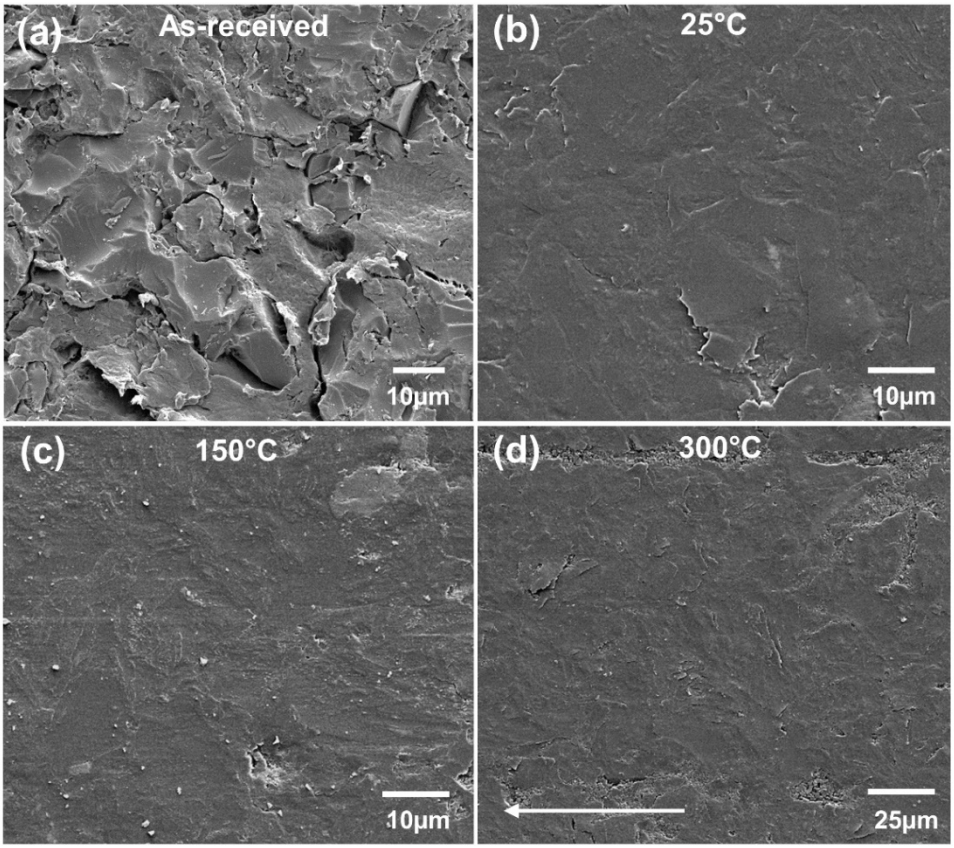

Figure 77. SEM images of ATSP composite pins (a) untested surface, and tested surfaces at temperatures of (b) 25 °C, (c) 150 °C, and (d) 300°C. The solid white arrow in (d) shows the sliding direction for all cases. Reprinted with permissions from "Bashandeh K, et al. Tribology of self-lubricating high performance ATSP, PI, and PEEK-based polymer composites up to 300° C. Friction. 2022 Apr 28:1-3."

Figure 78(a) shows the SEM image of the untested PI composite pin surface. In general, the surface features a smoother topography compared to ATSP and contains directional shallow grooves from machining. As shown in **Figure 78(b-d)**, the removal and polishing of the initial irregularities and grooves are characteristics of the worn surface of the PI composite pins after sliding at all temperatures causing the surface to become smoother than the as-received one. However, as shown in **Figure 78(a)**, sliding at RT caused severe micro-cuttings and scratches on the surface, implying harsh sliding conditions at the interface, which contributed to high friction and wear at RT.

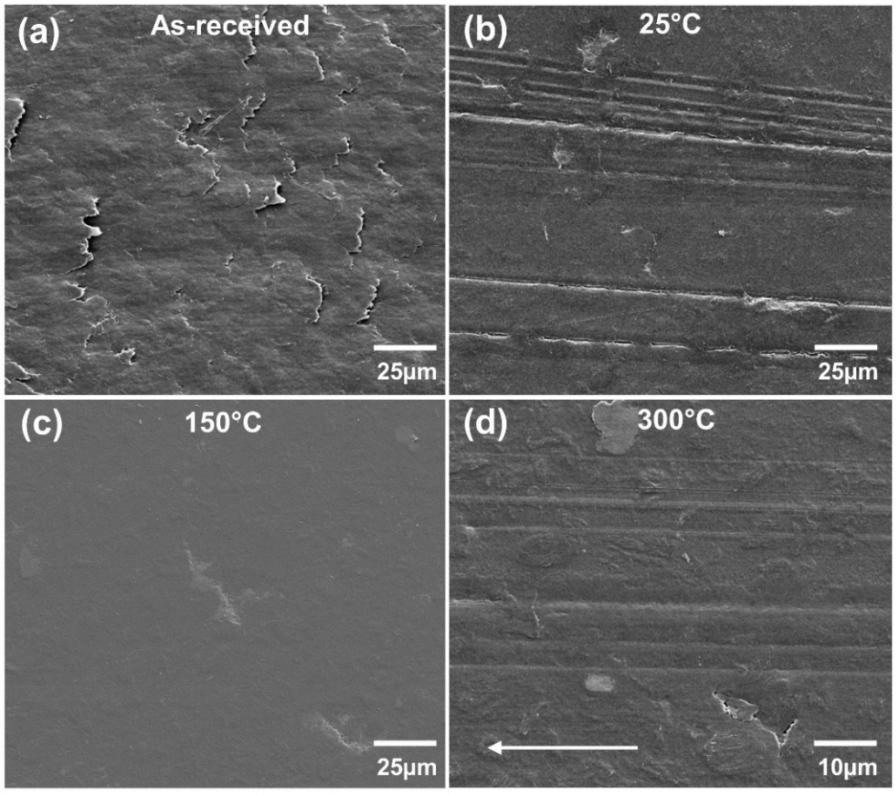

Figure 78. SEM images of PI composite pins (a) untested surface, and tested surfaces at temperatures of (b) 25 °C, (c) 150 °C, and (d) 300°C. The white solid arrow in (d) shows the sliding direction for all cases. Reprinted with permissions from "Bashandeh K, et al. Tribology of self-lubricating high performance ATSP, PI, and PEEK-based polymer composites up to 300° C. Friction. 2022 Apr 28:1-3."

The SEM image of the untested surface of PEEK composite pin is shown in **Figure 79(a)**. The surface features a rough topography and contains machining marks, tracks and scrapes from machining. However, similar to the other polymer composites, the surface became smoother upon sliding at both RT and 150 °C. The SEM image after the RT experiment in **Figure 79(b)** shows the exposed carbon fibers on the worn surface (shown with dashed arrows), which were embedded in the matrix in different orientations. Since PEEK is less wear resistant than carbon fibers, it can easily wear out, and therefore the majority of the load will be carried out by the fibers, which gives the composite high strength and wear resistance. Due to different modulus between carbon fiber and PEEK matrix, the stress concentration can be generated at the matrix/fiber interface, which contributes to debonding at the interface or detachment of fiber from the matrix [169]. From **Figure 79(c)**, some regions show pitting marks that could be from detachment of fibers and interfacial cracking (marked with the dashed circle). Note that the detached fibers serve as third-body abrasive particles and therefore generate abrasive marks on the surface, as shown with the white solid arrow in **Figure 79(b)**. Signs of plastic deformation and continuous grinding of carbon fibers are extra surface features once the polymer was slid at higher temperature (**Figure 79(d)**).

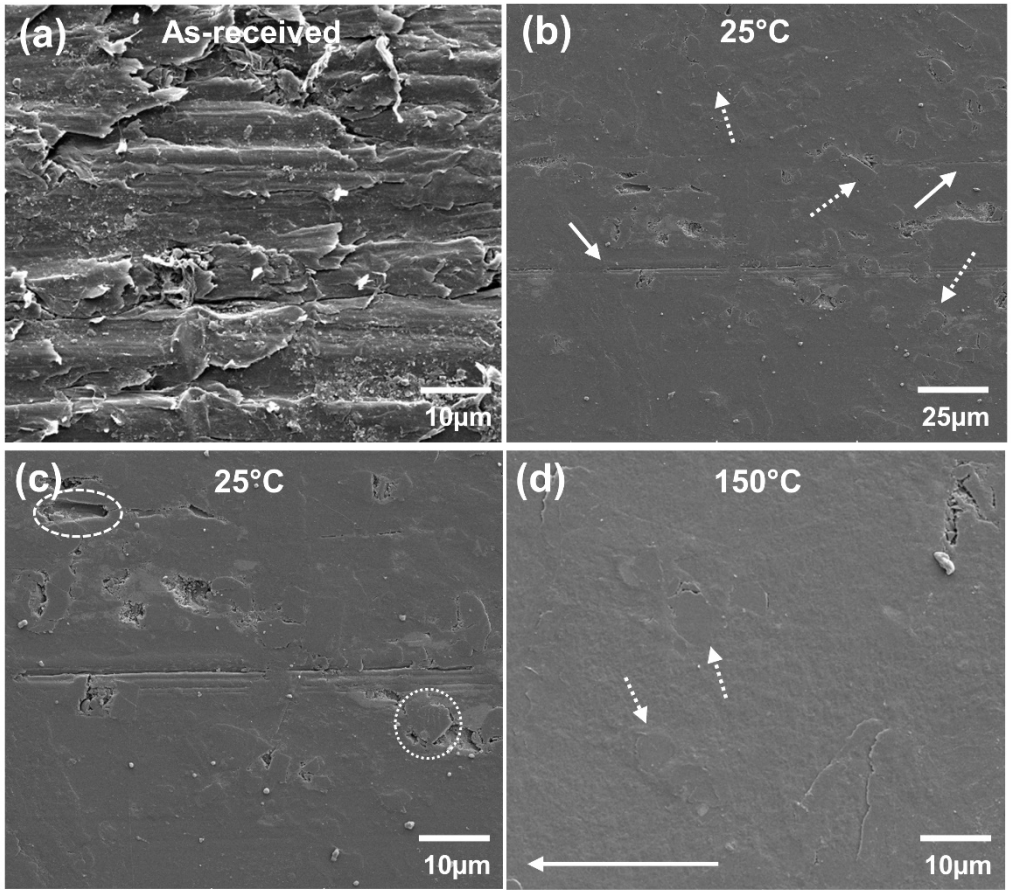

Figure 79. SEM images of PEEK composite pins (a) untested surface, and tested surfaces at temperatures of (b) 25 °C at low magnification, (c) 25 °C at high magnification, and (d) 150 °C. The solid arrows in (b) show the abrasive marks and dashed arrows show the embedded carbon fibers. The dashed circle in (c) show the interfacial cracking and pitting. The solid white arrow in (d) shows the sliding direction. Reprinted with permissions from "Bashandeh K, et al. Tribology of self-lubricating high performance ATSP, PI, and PEEK-based polymer composites up to 300° C. Friction. 2022 Apr 28:1-3."

The comparison of wear mechanisms among the polymers revealed that ATSP composite was the least affected polymer when the temperature changed from RT to 300 °C and the surface experienced only mild burnishing at all temperatures resulting in desirable friction and wear properties. The PI composite wear mechanism changed from severe micro-cutting and abrasive wear at RT, to burnishing effect at elevated temperatures resulting in lower friction at elevated temperatures. The PEEK composite

wear mechanism on the other hand showed plastic deformation of the surface at elevated temperatures, indicating the deterioration of mechanical properties at 150 °C that resulted in high COF, compared with RT. Therefore, based on the overall tribological performance (i.e., friction and wear), the ATSP composite could be recommended as the best performing polymer with excellent performance over a wide range of operating temperatures from RT up to 300°C.

7.4 Summary

The tribological behavior of three high-performance polymer composites, namely ATSP-based, PI-based, and PEEK-based polymer composites, were experimentally investigated under dry sliding conditions and different temperatures of 25, 150, and 300 °C. Variation of the COF and wear as well as evolution of transfer film on the counterface with temperature were investigated, and the following conclusions could be made:

- For ATSP and PI composites, the COF followed a decreasing trend with increase of temperature from 25 to 300 °C: It was reduced by 53 and 70% at 300°C, compared with RT. The COF of PEEK composite increased by 71% when the temperature raised to 150 °C due to formation of a discontinuous film and deterioration of mechanical properties.
- The transfer film was found to play significant role in the tribological performance at all temperatures. ATSP developed a uniform and continuous transfer film at all temperatures, whereas PI could not develop a transfer film and form patchy transfer layer at RT, resulting in high friction and wear. The increase in temperature helped to develop a uniform and continuous transfer film, leading to

a decrease in the COF. PEEK could not maintain its uniform developed transfer film at RT once the temperature was raised to 150 °C. In addition, due to proximity of tested temperature to Tg (155°C), the significant softening of PEEK as well as lower extent of transfer film resulted in higher COF and wear, compared with RT.

- For all polymer composites, the wear followed an increasing trend with temperature due to the inability of the polymers to develop the transfer film at the early stage of sliding period, and therefore the material was worn out faster until a stable film was formed on the counterface. The dominant wear mechanism for all polymers was polishing of the surface, as shown by SEM analysis. In addition, severe micro-cuttings and scratches formed on the PI surface at RT, which caused higher friction and wear.

Based on the overall tribological performance at all operating temperatures, the ATSP composite is recommended as the best performing polymer for use in oil-less engineering applications that demand reliable operation in a wide range of temperatures.

CHAPTER 8

CONCLUSIONS AND RECOMMENDATIONS FOR FUTURE WORK

8.1 Conclusions

A comprehensive experimental study was conducted in this research to systematically evaluate and compare the tribological performance of advanced high-performance polymer composites based on ATSP, PEEK, PI, and FP for use as bearing and/or sealing materials under extreme environmental conditions. The main objective was to assess the feasibility of employing polymers in coating formats for space-related applications such as the bearings of exploration devices for the Moon, Mars, Titan, etc. The research also investigated and proposed a surface treatment approach to mitigate the extent of wear and friction as well as dust at the interface under extreme temperature ranges from -196 to 300 °C. In addition, micro/nano indentations and various thermal, topographical, and chemical characterizations were performed to obtain a fundamental knowledge of the wear mechanism, transfer film formation, and failure analysis of the samples and correlations were made with tribological performance. The contributions and summary of main findings are summarized below:

(1) The ATSP coating was shown to significantly enhance the tribological performance of bare steel as a bearing material once applied as a thin coating with a thickness of ~30-40μm. The COF and wear were reduced by 80 and 95 %, respectively once the PA-steel interface was treated to PA-ATSP coated steel. The enhanced tribological performance was maintained at elevated temperatures up to

80 °C (beyond PA Tg), and the ATSP coating demonstrated unmeasurable zero wear under moderate (15 MPa) to high contact pressure (52 MPa) conditions and small to long duration test (1 to 5 hr). The high COF and wear of PA-steel were attributed to the detrimental effect of PA transferred layer on the steel counterpart. However, the lower surface energy of PTFE additive in the ATSP coating compared with steel impeded the PA transfer on the ATSP coating and reduced the friction and wear.

(2) In addition to the high bearing capability of ATSP coating, its elevated temperature tribological performance was demonstrated under unlubricated sliding from RT up to 300 °C. A decreasing trend in COF and wear was seen with temperature due to softening of the polymer and increased amount of transfer film on the steel counterparts. Nanoindentation experiments verified the softening of the polymer where the hardness and elastic modulus dropped by one order of magnitude at 260 °C, compared with RT. The steel on coating experiments showed formation of cracks on the ATSP/PTFE coating at 300 °C due to the fatigue wear mechanism, whereas at the lower temperatures, the wear was predominantly caused by burnishing of top asperities on the coating. The incorporation of 5 wt.% GNP additives was shown to enhance the crack resistance of ATSP coating at 300 °C, and no crack was identified from SEM analysis.

(3) Inspired by the beneficial effect of transfer layer, the ATSP/PTFE coating was deposited on both pins and disks to simulate polymer sliding on pre-deposited "transfer layer." The coating showed "zero wear" and controlled COF from -196

to 300 °C, spanning the capability of the coating to the range of approximately 500 °C. Similar to metal-on-polymer, the COF was reduced here as well from 25 °C to 150 °C, and 300 °C due to softening of the polymer with temperature. Compared with uncoated metal, the COF was reduced by 40% for ATSP-on-ATSP coating. The FP coating showed higher COF and wear than ATSP/PTFE, and PEEK/PTFE performed similarly to ATSP/PTFE up to 150 °C and could not survive at 300 °C. ATSP/PTFE and PEEK/PTFE coating showed burnishing wear mechanism, while adhesive wear was the dominant mechanism for FP. LN_2 increased the COF at -196 °C compared with cryogen N_2 gas at -100 °C, and abrasive wear was the dominant wear mechanism.

(4) The environmental temperatures of planets such as Titan, Moon, and Mars were simulated by conducting tribological experiments from -180 °C to 110 °C. The ATSP coating surface was under burnishing effect at all temperatures and showed zero wear and lower COF than PEEK coating. Adhesive wear was the major wear mechanism for PEEK coating and increased at cryogenic condition, particularly at -180 °C, where high COF and wear rate was obtained. The temperature was found to significantly affect the characteristics of transfer film from ATSP/PTFE and PEEK/PTFE coatings. The extent and thickness of transfer film from ATSP and PEEK coatings were increased by decreasing the temperature to cryogenic conditions. However, the film was shown to be uniform and homogeneous for ATSP coating at all temperatures, while PEEK coating formed a patchy and non-uniform film at -180 °C.

(5) The experiments under dust abrasive environment from -150 °C to 110 °C were designed to evaluate the abrasive wear resistance of ATSP/PTFE and PEEK/PTFE coatings under Moon and Mars simulated environment. The lowest COF and wear and degree of dust mitigation were achieved for polymer-on-polymer sliding, and ATSP coating demonstrated higher wear resistance and comparable friction to PEEK coating at all temperatures. Lower size particles were found to be more detrimental to tribological performance compared with larger size particles. Based on SEM analysis, the dominant wear mechanism for uncoated tribopairs, the metal-on-polymer, and polymer-on-polymer was micro-scuffing, two-body abrasion, and three-body abrasion, respectively. The environmental temperature significantly affected the dust accumulation, COF, and wear rate. The COF and the extent of dust deposition were increased at elevated temperatures, particularly for metal-on-polymer configurations.

(6) Last but not least, the ATSP-based polymer composite was fabricated in bulk format, and its tribological performance was compared with commercially available HPPs such as PEEK HPV and Vespel SP-211 (PI) from RT up to 300 °C. ATSP and Vespel showed a decreasing trend in COF with temperature, whereas PEEK COF increased at 150 °C due to formation of a discontinuous film and deterioration of mechanical properties. PI formed a patchy transfer layer at RT with severe micro-cutting and scratches, resulting in high friction and wear, while ATSP developed a uniform and continuous transfer film at all temperatures. For all polymer composites, the wear followed an increasing trend with temperature.

(7) The ATSP was shown to have superior tribological performance compared with other polymers in this research such as PEEK, PI, and FP, and could be identified as a candidate material for use in bearing components and tribological surfaces for applications such as space exploration devices that require long life bearings over a wide range of temperatures from -196 to 300 °C.

8.2 Recommendations for future work

The addition of 5 wt.% GNP was shown to significantly improve the tribological performance of ATSP coating at elevated temperatures, whereas the PTFE additive worked better at lower temperatures. Therefore, the synergistic effects of PTFE and GNP could be explored by mixing GNP and PTFE inside ATSP coating to form ATSP/PTFE/GNP and possibly obtain an improved tribological performance from RT up to 300 °C.

The experiments under cryogenic conditions were conducted under atmospheric pressure. However, the Moon environment is in a vacuum state. Further research is needed to evaluate the coatings performance under vacuum conditions by modifying the developed cryogenic setup equipped in the tribometer. The studies in this research could be expanded to rolling or slide to roll ratio experiments in addition to pure sliding to extend the application of the ATSP coating to rolling type bearings as well.

Based upon the tribological experimental results demonstrated in this research, ATSP polymer is an extremely wear resistant resin capable of withstanding extreme conditions such as cryogenic to HT, low to high contact pressure, and abrasive environment. Therefore, a possible application of ATSP could be to use the resin as an

additive to improve the wear resistance of polymers such as PTFE. Similar studies shown in this thesis could be conducted to explore this new capability of the developed polymer herein.

REFERENCES

[1] Cannaday ML, Polycarpou AA. Tribology of Unfilled and Filled Polymeric Surfaces in Refrigerant Environment for Compressor Applications. Tribol Lett 2005 194 2005;19:249–62. https://doi.org/10.1007/S11249-005-7441-9.

[2] Friedrich K. Polymer composites for tribological applications. Adv Ind Eng Polym Res 2018;1:3–39. https://doi.org/10.1016/J.AIEPR.2018.05.001.

[3] Li G, Qi H, Zhang G, Zhao F, Wang T, Wang Q. Significant friction and wear reduction by assembling two individual PEEK composites with specific functionalities. Mater Des 2017;116:152–9. https://doi.org/10.1016/J.MATDES.2016.11.100.

[4] Li J, Qu J, Zhang Y. Wear properties of brass and PTFE–matrix composite in traveling wave ultrasonic motors. Wear 2015;338–339:385–93. https://doi.org/10.1016/J.WEAR.2015.07.007.

[5] Lin L, Pei XQ, Bennewitz R, Schlarb AK. Friction and wear of PEEK in continuous sliding and unidirectional scratch tests. Tribol Int 2018;122:108–13. https://doi.org/10.1016/J.TRIBOINT.2018.02.035.

[6] Liu H, Wang T, Wang Q. Tribological Properties of Thermosetting Polyimide/TiO2 Nanocomposites Under Dry Sliding and Water-Lubricated Conditions. Http://DxDoiOrg/101080/002223482011624043 2012;51:2284–96. https://doi.org/10.1080/00222348.2011.624043.

[7] Rodriguez V, Sukumaran J, Schlarb AK, De Baets P. Reciprocating sliding wear behaviour of PEEK-based hybrid composites. Wear 2016;362–363:161–9. https://doi.org/10.1016/J.WEAR.2016.05.024.

[8] Schroeder R, Torres FW, Binder C, Klein AN, De Mello JDB. Failure mode in sliding wear of PEEK based composites. Wear 2013;301:717–26. https://doi.org/10.1016/J.WEAR.2012.11.055.

[9] Song F, Wang Q, Wang T. The effects of crystallinity on the mechanical properties and the limiting PV (pressure×velocity) value of PTFE. Tribol Int 2016;93:1–10. https://doi.org/10.1016/J.TRIBOINT.2015.09.017.

[10] Zhao G, Hussainova I, Antonov M, Wang Q, Wang T, Yung DL. Effect of temperature on sliding and erosive wear of fiber reinforced polyimide hybrids. Tribol Int 2015;82:525–33. https://doi.org/10.1016/J.TRIBOINT.2014.01.019.

[11] Zhang J, Polycarpou AA, Economy J. An improved tribological polymer-coating system for metal surfaces. Tribol Lett 2010;38:355–65. https://doi.org/10.1007/S11249-010-9615-3/FIGURES/13.

[12] Zhang J, Demas NG, Polycarpou AA, Economy J. A new family of low wear, low coefficient of friction polymer blend based on polytetrafluoroethylene and an aromatic thermosetting polyester. Polym Adv Technol 2008;19:1105–12. https://doi.org/10.1002/PAT.1086.

[13] Demas NG, Zhang J, Polycarpou AA, Economy J. Tribological characterization of aromatic thermosetting copolyester-PTFE blends in air conditioning compressor environment. Tribol Lett 2008;29:253–8. https://doi.org/10.1007/S11249-008-9303-8/FIGURES/9.

[14] Nunez EE, Gheisari R, Polycarpou AA. Tribology review of blended bulk polymers and their coatings for high-load bearing applications. Tribol Int 2019;129:92–111. https://doi.org/10.1016/J.TRIBOINT.2018.08.002.

[15] Nunez EE, Polycarpou AA. The effect of surface roughness on the transfer of polymer films under unlubricated testing conditions. Wear 2015;326–327:74–83. https://doi.org/10.1016/J.WEAR.2014.12.049.

[16] Dascalescu D, Polychronopoulou K, Polycarpou AA. The significance of tribochemistry on the performance of PTFE-based coatings in CO2 refrigerant environment. Surf Coatings Technol 2009;204:319–29. https://doi.org/10.1016/J.SURFCOAT.2009.07.042.

[17] Nunez EE, Demas NG, Polychronopoulou K, Polycarpou AA. Comparative scuffing performance and chemical analysis of metallic surfaces for air-conditioning compressors in the presence of environmentally friendly CO2 refrigerant. Wear 2010;268:668–76. https://doi.org/10.1016/J.WEAR.2009.11.002.

[18] Nunez EE, Yeo SM, Polychronopoulou K, Polycarpou AA. Tribological study of high bearing blended polymer-based coatings for air-conditioning and refrigeration compressors. Surf Coatings Technol 2011;205:2994–3005. https://doi.org/10.1016/J.SURFCOAT.2010.11.008.

[19] Bashandeh K, Lan P, Polycarpou AA. Tribological Performance Improvement of Polyamide against Steel Using Polymer Coating. 2019;62:1051–62. https://doi.org/10.1080/10402004.2019.1643517.

[20] Lan P, Polychronopoulou K, Zhang Y, Polycarpou AA. Three-body abrasive wear by (silica) sand of advanced polymeric coatings for tilting pad bearings. Wear 2017;382–383:40–50. https://doi.org/10.1016/J.WEAR.2017.04.002.

[21] Yeo SM, Polycarpou AA. Fretting experiments of advanced polymeric coatings and the effect of transfer films on their tribological behavior. Tribol Int 2014;79:16–25. https://doi.org/10.1016/J.TRIBOINT.2014.05.012.

[22] Lv M, Wang Q, Wang T, Liang Y. Effects of atomic oxygen exposure on the tribological performance of ZrO2-reinforced polyimide nanocomposites for low earth orbit space applications. Compos Part B Eng 2015;77:215–22. https://doi.org/10.1016/J.COMPOSITESB.2015.03.029.

[23] Park SY, Choi HS, Choi WJ, Kwon H. Effect of vacuum thermal cyclic exposures on unidirectional carbon fiber/epoxy composites for low earth orbit space applications. Compos Part B Eng 2012;43:726–38. https://doi.org/10.1016/J.COMPOSITESB.2011.03.007.

[24] Han JH, Kim CG. Low earth orbit space environment simulation and its effects on graphite/epoxy composites. Compos Struct 2006;72:218–26.

https://doi.org/10.1016/J.COMPSTRUCT.2004.11.007.

[25] Grossman E, Gouzman I. Space environment effects on polymers in low earth orbit. Nucl Instruments Methods Phys Res Sect B Beam Interact with Mater Atoms 2003;208:48–57. https://doi.org/10.1016/S0168-583X(03)00640-2.

[26] NASA. https://www.nasa.gov/ (accessed May 10, 2022).

[27] Harrison DA, Ambrose R, Bluethmann B, Junkin L. Next generation rover for lunar exploration. IEEE Aerosp Conf Proc 2008. https://doi.org/10.1109/AERO.2008.4526234.

[28] Matsumoto K, Suzuki M, Nishida S-I, Wakabayashi S. Wear of Materials in Lunar Dust Environment. In Proc. 11th Int. Symp. on" Materials in a Space Environment", Aix-en-Provence 2009.

[29] Turtle EP, Barnes JW, Trainer MG, Lorenz RD, Hibbard KE, Adams DS, et al. Dragonfly: In Situ Exploration of Titan's Prebiotic Organic Chemistry and Habitability. InEuropean Planetary Science Congress 2017. https://doi.org/10.1109/AERO.2013.6497165.

[30] Zacny K, Rehnmark F, Costa T, Bailey J, Traeden N, Mank Z, et al. Cryogenic Sample Acquisition and Delivery System (CryoSADS) for Titan and Europa. 42nd COSPAR Sci. Assem. 2018;B5-3.

[31] Chu P, Spring J, Zacny K. ROPEC-ROtary PErcussive coring drill for mars sample return. 42nd Aerosp. Mech. Symp. 2014.

[32] Paulsen G, Indyk S., Zacny K. Development of the RANCOR Rotary-Percussive Coring System for Mars Sample Return. 42nd Aerosp. Mech. Symp. 2014.

[33] Lan P, Gheisari R, Meyer JL, Polycarpou AA. Tribological performance of aromatic thermosetting polyester (ATSP) coatings under cryogenic conditions. Wear 2018;398–399:47–55. https://doi.org/10.1016/J.WEAR.2017.11.020.

[34] Holmberg K, Mathews A. Coatings tribology: a concept, critical aspects and future directions. Thin Solid Films 1994;253:173–8. https://doi.org/10.1016/0040-

6090(94)90315-8.

[35] Mangalgiri PD. Composite materials for aerospace applications. Bull Mater Sci 1999;22:657–64. https://doi.org/10.1007/BF02749982.

[36] Bahadur S. The development of transfer layers and their role in polymer tribology. Wear 2000;245:92–9. https://doi.org/10.1016/S0043-1648(00)00469-5.

[37] Myshkin NK, Petrokovets MI, Kovalev A V. Tribology of polymers: Adhesion, friction, wear, and mass-transfer. Tribol Int 2005;38:910–21. https://doi.org/10.1016/J.TRIBOINT.2005.07.016.

[38] Cannaday ML, Polycarpou AA. Tribology of Unfilled and Filled Polymeric Surfaces in Refrigerant Environment for Compressor Applications. Tribol Lett 2005;19:249–62. https://doi.org/10.1007/S11249-005-7441-9.

[39] Friedrich K. Friction and wear of polymer composites. Elsevier; 2012.

[40] Akram MW, Meyer JL, Polycarpou AA. Tribological interactions of advanced polymeric coatings with polyalkylene glycol lubricant and r1234yf refrigerant. Tribol Int 2016;97:200–11. https://doi.org/10.1016/J.TRIBOINT.2016.01.026.

[41] Fusaro RL, Sliney HE. Lubricating Characteristics of Polyimide Bonded Graphite Fluoride and Polyimide Thin Films 2008;16:189–96. https://doi.org/10.1080/05698197308982721.

[42] Unal H, Sen U, Mimaroglu A. Dry sliding wear characteristics of some industrial polymers against steel counterface. Tribol Int 2004;37:727–32. https://doi.org/10.1016/J.TRIBOINT.2004.03.002.

[43] Kurdi A, Kan WH, Chang L. Tribological behaviour of high performance polymers and polymer composites at elevated temperature. Tribol Int 2019;130:94–105. https://doi.org/10.1016/J.TRIBOINT.2018.09.010.

[44] Wang Y, Yin Z, Li H, Gao G, Zhang X. Friction and wear characteristics of ultrahigh molecular weight polyethylene (UHMWPE) composites containing glass fibers and carbon fibers under dry and water-lubricated conditions. Wear

2017;380–381:42–51. https://doi.org/10.1016/J.WEAR.2017.03.006.

[45] Jia B Bin, Li TS, Liu XJ, Cong PH. Tribological behaviors of several polymer–polymer sliding combinations under dry friction and oil-lubricated conditions. Wear 2007;262:1353–9. https://doi.org/10.1016/J.WEAR.2007.01.011.

[46] Guo Y, Ozaydin MF, Wang D, Liang H. Friction heating and effect on tribological properties of soft polyvinyl chloride sliding against steel. Eur Polym J 2018;106:85–91. https://doi.org/10.1016/J.EURPOLYMJ.2018.07.013.

[47] Kalin M, Zalaznik M, Novak S. Wear and friction behaviour of poly-ether-ether-ketone (PEEK) filled with graphene, WS2 and CNT nanoparticles. Wear 2015;332–333:855–62. https://doi.org/10.1016/J.WEAR.2014.12.036.

[48] Zhai W, Lu W, Zhang P, Wang J, Liu X, Zhou L. Wear-triggered self-healing behavior on the surface of nanocrystalline nickel aluminum bronze/Ti3SiC2 composites. Appl Surf Sci 2018;436:1038–49. https://doi.org/10.1016/J.APSUSC.2017.12.138.

[49] Sinha S, Briscoe B. Polymer tribology. World Sci; 2009.

[50] Lancaster JK. Estimation of the limiting PV relationships for thermoplastic bearing materials. Tribology 1971;4:82–6. https://doi.org/10.1016/0041-2678(71)90136-9.

[51] Zhou M, Lu W, Liu X, Zhai W, Zhang P, Zhang G. Fretting wear properties of plasma-sprayed Ti3SiC2 coatings with oxidative crack-healing feature. Tribol Int 2018;118:196–207. https://doi.org/10.1016/J.TRIBOINT.2017.10.009.

[52] Lan P, Meyer JL, Vaezian B, Polycarpou AA. Advanced polymeric coatings for tilting pad bearings with application in the oil and gas industry. Wear 2016;354–355:10–20. https://doi.org/10.1016/J.WEAR.2016.02.013.

[53] Lan P, Meyer JL, Economy J, Polycarpou AA. Unlubricated Tribological Performance of Aromatic Thermosetting Polyester (ATSP) Coatings under Different Temperature Conditions. Tribol Lett 2016;61:1–14.

https://doi.org/10.1007/S11249-015-0621-3/FIGURES/17.

[54] Bolvari A, Glenn S, Janssen R, Ellis C. Wear and friction of aramid fiber and polytetrafluoroethylene filled composites. Wear 1997;203–204:697–702. https://doi.org/10.1016/S0043-1648(96)07446-7.

[55] Zheng J, Palmer A, Brunning P, Gan CT. Indentation and external pressure on subsea single wall pipe and pipe-in-pipe. Ocean Eng 2014;83:125–32. https://doi.org/10.1016/J.OCEANENG.2014.03.028.

[56] Strong AB. Plastics: materials and processing. Prentice Hall; 2006.

[57] Wang J, Gu M. Wear properties and mechanisms of nylon and carbon-fiber-reinforced nylon in dry and wet conditions. J Appl Polym Sci 2004;93:789–95. https://doi.org/10.1002/APP.20483.

[58] Unal H, Mimaroglu A. Friction and wear performance of polyamide 6 and graphite and wax polyamide 6 composites under dry sliding conditions. Wear 2012;289:132–7. https://doi.org/10.1016/J.WEAR.2012.04.004.

[59] Meng H, Sui GX, Xie GY, Yang R. Friction and wear behavior of carbon nanotubes reinforced polyamide 6 composites under dry sliding and water lubricated condition. Compos Sci Technol 2009;69:606–11. https://doi.org/10.1016/J.COMPSCITECH.2008.12.004.

[60] Sirong Y, Zhongzhen Y, Yiu-Wing M. Effects of SEBS-g-MA on tribological behaviour of nylon 66/organoclay nanocomposites. Tribol Int 2007;40:855–62. https://doi.org/10.1016/J.TRIBOINT.2006.09.001.

[61] Chang L, Zhang Z, Zhang H, Schlarb AK. On the sliding wear of nanoparticle filled polyamide 66 composites. Compos Sci Technol 2006;66:3188–98. https://doi.org/10.1016/J.COMPSCITECH.2005.02.021.

[62] Pogačnik A, Kupec A, Kalin M. Tribological properties of polyamide (PA6) in self-mated contacts and against steel as a stationary and moving body. Wear 2017;378–379:17–26. https://doi.org/10.1016/J.WEAR.2017.01.118.

[63] Demas NG, Polycarpou AA. Tribological performance of PTFE-based coatings for air-conditioning compressors. Surf Coatings Technol 2008;203:307–16. https://doi.org/10.1016/J.SURFCOAT.2008.09.001.

[64] Yu ZZ, Yan C, Yang M, Mai YW. Mechanical and dynamic mechanical properties of nylon 66/montmorillonite nanocomposites fabricated by melt compounding. Polym Int 2004;53:1093–8. https://doi.org/10.1002/PI.1498.

[65] Pogačnik A, Kalin M. Parameters influencing the running-in and long-term tribological behaviour of polyamide (PA) against polyacetal (POM) and steel. Wear 2012;290–291:140–8. https://doi.org/10.1016/J.WEAR.2012.04.017.

[66] Lan P, Zhang Y, Dai W, Polycarpou AA. A phenomenological elevated temperature friction model for viscoelastic polymer coatings based on nanoindentation. Tribol Int 2018;119:299–307. https://doi.org/10.1016/J.TRIBOINT.2017.11.009.

[67] Greenwood JA, Williamson JP. Contact of nominally flat surfaces. Proc R Soc London Ser A Math Phys Sci 1966;295:300–19. https://doi.org/10.1098/RSPA.1966.0242.

[68] Zhang G, Liao H, Li H, Mateus C, Bordes JM, Coddet C. On dry sliding friction and wear behaviour of PEEK and PEEK/SiC-composite coatings. Wear 2006;260:594–600. https://doi.org/10.1016/J.WEAR.2005.03.017.

[69] Stuart BH. Surface plasticisation of poly(ether ether ketone) by chloroform. Polym Test 1997;16:49–57. https://doi.org/10.1016/S0142-9418(96)00026-8.

[70] Owens DK, Wendt RC. Estimation of the surface free energy of polymers. J Appl Polym Sci 1969;13:1741–7. https://doi.org/10.1002/APP.1969.070130815.

[71] Briscoe BJ, Sinha SK. Tribological applications of polymers and their composites: Past, present and future prospects. Tribol Interface Eng Ser 2008;55:1–14. https://doi.org/10.1016/S1572-3364(08)55001-4.

[72] Sinha S, Briscoe B. Polymer tribology. World Sci; 2009.

[73] Donnet C, Erdemir A. Solid Lubricant Coatings: Recent Developments and Future Trends. Tribol Lett 2004 173 2004;17:389–97. https://doi.org/10.1023/B:TRIL.0000044487.32514.1D.

[74] Liming Z, Yongyao L, Zhengwei W, Xin L, Yexiang X. A review on the large tilting pad thrust bearings in the hydropower units. Renew Sustain Energy Rev 2017;69:1182–98. https://doi.org/10.1016/J.RSER.2016.09.140.

[75] Holmberg K, Matthews A. Coatings tribology: properties, mechanisms, techniques and applications in surface engineering. Elsevier; 2009.

[76] Cui LJ, Geng HZ, Wang WY, Chen LT, Gao J. Functionalization of multi-wall carbon nanotubes to reduce the coefficient of the friction and improve the wear resistance of multi-wall carbon nanotube/epoxy composites. Carbon N Y 2013;54:277–82. https://doi.org/10.1016/J.CARBON.2012.11.039.

[77] Kasar AK, Menezes PL. Synthesis and recent advances in tribological applications of graphene. Int J Adv Manuf Technol 2018 979 2018;97:3999–4019. https://doi.org/10.1007/S00170-018-2019-5.

[78] Frich D, Goranov K, Schneggenburger L, Economy J. Novel High-Temperature Aromatic Copolyester Thermosets: Synthesis, Characterization, and Physical Properties. Macromolecules 1996;29:7734–9. https://doi.org/10.1021/MA960862D.

[79] Lan P, Polycarpou AA. High temperature and high pressure tribological experiments of advanced polymeric coatings in the presence of drilling mud for oil & gas applications. Tribol Int 2018;120:218–25. https://doi.org/10.1016/J.TRIBOINT.2017.12.035.

[80] Frich D, Hall A, and JE. Nature of adhesive bonding via interchain transesterification reactions (ITR). Macromol Chem Phys 1998;199:913–21.

[81] Rudnick LR, editor. Lubricant Additives : Chemistry and Applications, 2nd Edition 2009. https://doi.org/10.1201/9781420059656.

[82] Rodgers P. Nanoscience and technology: a collection of reviews from nature journals. World Sci; 2009.

[83] Berman D, Erdemir A, Sumant A V. Graphene: a new emerging lubricant. Mater Today 2014;17:31–42. https://doi.org/10.1016/J.MATTOD.2013.12.003.

[84] Zhai W, Srikanth N, Kong LB, Zhou K. Carbon nanomaterials in tribology. Carbon N Y 2017;119:150–71. https://doi.org/10.1016/J.CARBON.2017.04.027.

[85] Lee C, Wei X, Kysar JW, Hone J. Measurement of the elastic properties and intrinsic strength of monolayer graphene. Science 2008;321:385–8. https://doi.org/10.1126/SCIENCE.1157996/SUPPL_FILE/LEE-SOM.PDF.

[86] Ghosh S, Calizo I, Teweldebrhan D, Pokatilov EP, Nika DL, Balandin AA, et al. Extremely high thermal conductivity of graphene: Prospects for thermal management applications in nanoelectronic circuits. Appl Phys Lett 2008;92:151911. https://doi.org/10.1063/1.2907977.

[87] Masood MT, Papadopoulou EL, Heredia-Guerrero JA, Bayer IS, Athanassiou A, Ceseracciu L. Graphene and polytetrafluoroethylene synergistically improve the tribological properties and adhesion of nylon 66 coatings. Carbon 2017;123:26–33. https://doi.org/10.1016/J.CARBON.2017.07.026.

[88] Liu D, Zhao W, Liu S, Cen Q, Xue Q. Comparative tribological and corrosion resistance properties of epoxy composite coatings reinforced with functionalized fullerene C60 and graphene. Surf Coatings Technol 2016;286:354–64. https://doi.org/10.1016/J.SURFCOAT.2015.12.056.

[89] Puértolas JA, Castro M, Morris JA, Ríos R, Ansón-Casaos A. Tribological and mechanical properties of graphene nanoplatelet/PEEK composites. Carbon 2019;141:107–22. https://doi.org/10.1016/J.CARBON.2018.09.036.

[90] Kandanur SS, Rafiee MA, Yavari F, Schrameyer M, Yu ZZ, Blanchet TA, et al. Suppression of wear in graphene polymer composites. Carbon 2012;50:3178–83. https://doi.org/10.1016/J.CARBON.2011.10.038.

[91] Bakir M, Meyer JL, Sutrisno A, Economy J, Jasiuk I. Glass transition broadening via nanofiller-contiguous polymer network in aromatic thermosetting copolyester nanocomposites. J Polym Sci Part B Polym Phys 2018;56:1595–603. https://doi.org/10.1002/POLB.24747.

[92] Bakir M, Elhebeary M, Meyer JL, Sutrisno A, Economy J, Jasiuk I. Interfacial liquid crystalline mesophase domain on carbon nanofillers in aromatic thermosetting copolyester matrix. J Appl Polym Sci 2018;135:46584. https://doi.org/10.1002/APP.46584.

[93] Calleja G, Jourdan A, Ameduri B, Habas JP. Where is the glass transition temperature of poly(tetrafluoroethylene)? A new approach by dynamic rheometry and mechanical tests. Eur Polym J 2013;49:2214–22. https://doi.org/10.1016/J.EURPOLYMJ.2013.04.028.

[94] Ebnesajjad S, Morgan R. Fluoropolymer additives. William Andrew; 2019.

[95] Meyer JL, Bakir M, Lan P, Economy J, Jasiuk I, Bonhomme G, et al. Reversible Bonding of Aromatic Thermosetting Copolyesters for In-Space Assembly. Macromol Mater Eng 2019;304:1800647. https://doi.org/10.1002/MAME.201800647.

[96] Oliver WC, Pharr GM. An improved technique for determining hardness and elastic modulus using load and displacement sensing indentation experiments. J Mater Res 1992;7:1564–83. https://doi.org/10.1557/JMR.1992.1564.

[97] Wang H, Xie G, Zhu Z, Ying Z, Zeng Y. Enhanced tribological performance of the multi-layer graphene filled poly(vinyl chloride) composites. Compos Part A Appl Sci Manuf 2014;67:268–73. https://doi.org/10.1016/J.COMPOSITESA.2014.09.011.

[98] Chih A, Ansón-Casaos A, Puértolas JA. Frictional and mechanical behaviour of graphene/UHMWPE composite coatings. Tribol Int 2017;116:295–302. https://doi.org/10.1016/J.TRIBOINT.2017.07.027.

[99] Aliyu IK, Mohammed AS, Al-Qutub A. Tribological Performance of UHMWPE/GNPs Nanocomposite Coatings for Solid Lubrication in Bearing Applications. Tribol Lett 2018;66:1–11. https://doi.org/10.1007/S11249-018-1096-9/FIGURES/15.

[100] Kim KS, Lee HJ, Lee C, Lee SK, Jang H, Ahn JH, et al. Chemical vapor deposition-grown graphene: The thinnest solid lubricant. ACS Nano 2011;5:5107–14. https://doi.org/10.1021/NN2011865/SUPPL_FILE/NN2011865_SI_001.PDF.

[101] Schneider V, Liu HC, Bader N, Furtmann A, Poll G. Empirical formulae for the influence of real film thickness distribution on the capacitance of an EHL point contact and application to rolling bearings. Tribol Int 2021;154:106714. https://doi.org/10.1016/J.TRIBOINT.2020.106714.

[102] Bhushan B. Introduction to tribology. John Wiley & Sons; 2013.

[103] Liu H, Li Y, Wang T, Wang Q. In situ synthesis and thermal, tribological properties of thermosetting polyimide/graphene oxide nanocomposites. J Mater Sci 2012;47:1867–74. https://doi.org/10.1007/S10853-011-5975-9/FIGURES/10.

[104] Zhao B, Bai T. Improving the tribological performance of epoxy coatings by the synergistic effect between dehydrated ethylenediamine modified graphene and polytetrafluoroethylene. Carbon 2019;144:481–91. https://doi.org/10.1016/J.CARBON.2018.12.092.

[105] Barletta M. Dry sliding wear response of some industrial powder coatings. Tribol Int 2011;44:1236–50. https://doi.org/10.1016/J.TRIBOINT.2011.06.009.

[106] Fusaro RL, Fusako RL. Evaluation of Several Polymer Materials for Use as Solid Lubricants in Space. Tribol. Trans 2008;31:174–81. https://doi.org/10.1080/10402008808981813.

[107] Fusaro RL. Self-lubricating polymer composites and polymer transfer film lubrication for space applications. Tribol Int 1990;23:105–22.

https://doi.org/10.1016/0301-679X(90)90043-O.

[108] Burris DL. Investigation of the Tribological Behavior of Polytetrafluoroethylene at Cryogenic Temperatures. Tribol. Trans 2008;51:92–100. https://doi.org/10.1080/10402000701660618.

[109] Fusaro RL. Lubrication of Space Systems (c). No NAS 1995:111740.

[110] Holmberg K, Matthews A. Coatings tribology: properties, mechanisms, techniques and applications in surface engineering. Elsevier; 2009.

[111] Pratt, C. G. Bearing Materials: Plain Bearings. Emst 2011:488–96. https://doi.org/10.1016/B0-08-043152-6/00094-2.

[112] Donnet C, Erdemir A. Historical developments and new trends in tribological and solid lubricant coatings. Surf Coatings Technol 2004;180–181:76–84. https://doi.org/10.1016/J.SURFCOAT.2003.10.022.

[113] Miyoshi K. Solid lubricants and coatings for extreme environments: state-of-the-art survey. No. NASA/TM-2007-214668, 2007.

[114] Bashandeh K, Lan P, Meyer JL, Polycarpou AA. Tribological Performance of Graphene and PTFE Solid Lubricants for Polymer Coatings at Elevated Temperatures. Tribol Lett 2019;67:1–14. https://doi.org/10.1007/S11249-019-1212-5/FIGURES/11.

[115] Unal H, Mimaroglu A, Arda T. Friction and wear performance of some thermoplastic polymers and polymer composites against unsaturated polyester. Appl Surf Sci 2006;252:8139–46. https://doi.org/10.1016/J.APSUSC.2005.10.047.

[116] Lavielle L. Polymer-polymer friction: Relation to adhesion. Wear 1991;151:63–75. https://doi.org/10.1016/0043-1648(91)90346-V.

[117] Bakir M, Meyer JL, Economy J, Jasiuk I. Aromatic thermosetting copolyester nanocomposite foams: High thermal and mechanical performance lightweight structural materials. Polymer 2017;123:311–20.

https://doi.org/10.1016/J.POLYMER.2017.07.030.

[118] Economy J, Polycarpou A, Meyer J. Polymer coating system for improved tribological performance. U.S. Patent 9,534,138., 2017.

[119] Rahman MS, Ding J, Beheshti A, Zhang X, Polycarpou AA. Elevated temperature tribology of Ni alloys under helium environment for nuclear reactor applications. Tribol Int 2018;123:372–84. https://doi.org/10.1016/J.TRIBOINT.2018.03.021.

[120] Briscoe BJ, Fiori L, Pelillo E. Nano-indentation of polymeric surfaces. J Phys D Appl Phys 1998;31:2395. https://doi.org/10.1088/0022-3727/31/19/006.

[121] VanLandingham MR, Villarrubia JS, Guthrie WF, Meyers GF. Nanoindentation of polymers: an overview. Macromol Symp 2001;167:15–44.

[122] Yeo SM, Polycarpou AA. Micromechanical properties of polymeric coatings. Tribol Int 2013;60:198–208. https://doi.org/10.1016/J.TRIBOINT.2012.11.009.

[123] Humood M, Chowdhury S, Song Y, Tzeng P, Grunlan JC, Polycarpou AA. Nanomechanical Behavior of High Gas Barrier Multilayer Thin Films. ACS Appl Mater Interfaces 2016;8:11128–38. https://doi.org/10.1021/ACSAMI.5B11478/SUPPL_FILE/AM5B11478_SI_001.PDF.

[124] Davim JP, Cardoso R. Effect of the reinforcement (carbon or glass fibres) on friction and wear behaviour of the PEEK against steel surface at long dry sliding. Wear 2009;266:795–9. https://doi.org/10.1016/J.WEAR.2008.11.003.

[125] Kromer R, Costil S, Verdy C, Gojon S, Liao H. Laser surface texturing to enhance adhesion bond strength of spray coatings – Cold spraying, wire-arc spraying, and atmospheric plasma spraying. Surf Coatings Technol 2018;352:642–53. https://doi.org/10.1016/J.SURFCOAT.2017.05.007.

[126] Rask J, Vercoutere W, Navarro BJ, Krause I. Space faring: the radiation challenge introduction and module 1: radiation educator guide. Natl Aeronaut Sp Adm 2008.

[127] Crowther BG, Cannon BD, Brauer CS, Hansen SM, Myers TL. Proton and gamma irradiation of Fabry-Perot quantum cascade lasers for space qualification. Appl Opt 2015;54:527–34. https://doi.org/10.1364/AO.54.000527.

[128] Shulman H, Ginell WS. Nuclear and space radiation effects on materials. NASA SP-8053 1970.

[129] Lv M, Wang Y, Wang Q, Wang T, Liang Y. Effects of individual and sequential irradiation with atomic oxygen and protons on the surface structure and tribological performance of polyetheretherketone in a simulated space environment. RSC Adv 2015;5:83065–73. https://doi.org/10.1039/C5RA15441C.

[130] Pei X, Wang Q, Chen J. Tribological responses of Phenolphthalein Poly (ether sulfone) on proton irradiation. Wear 2005;258:719–24. https://doi.org/10.1016/J.WEAR.2004.10.002.

[131] Gates JD. Two-body and three-body abrasion: A critical discussion. Wear 1998;214:139–46. https://doi.org/10.1016/S0043-1648(97)00188-9.

[132] Eyre TS. Wear characteristics of metals. Tribol Int 1976;9:203–12. https://doi.org/10.1016/0301-679X(76)90077-3.

[133] Neale M, Gee M. A guide to wear problems and testing for industry. William Andrew; 2001.

[134] Afshar-Mohajer N, Wu CY, Curtis JS, Gaier JR. Review of dust transport and mitigation technologies in lunar and Martian atmospheres. Adv Sp Res 2015;56:1222–41. https://doi.org/10.1016/J.ASR.2015.06.007.

[135] Harsha AP, Tewari US. Two-body and three-body abrasive wear behaviour of polyaryletherketone composites. Polym Test 2003;22:403–18. https://doi.org/10.1016/S0142-9418(02)00121-6.

[136] Suresha B, Chandramohan G, Siddaramaiah, Samapthkumaran P, Seetharamu S. Three-body abrasive wear behaviour of carbon and glass fiber reinforced epoxy composites. Mater Sci Eng A 2007;443:285–91.

https://doi.org/10.1016/J.MSEA.2006.09.016.

[137] Ravi Kumar BN, Suresha B, Venkataramareddy M. Effect of particulate fillers on mechanical and abrasive wear behaviour of polyamide 66/polypropylene nanocomposites. Mater Des 2009;30:3852–8. https://doi.org/10.1016/J.MATDES.2009.01.034.

[138] Fernández-Álvarez M, Velasco F, Bautista A. Epoxy powder coatings hot mixed with nanoparticles to improve their abrasive wear. Wear 2020;448–449:203211. https://doi.org/10.1016/J.WEAR.2020.203211.

[139] Harsha AP, Tewari US, Venkatraman B. Three-body abrasive wear behaviour of polyaryletherketone composites. Wear 2003;254:680–92. https://doi.org/10.1016/S0043-1648(03)00142-X.

[140] Gheisari R, Polycarpou AA. Tribological performance of graphite-filled polyimide and PTFE composites in oil-lubricated three-body abrasive conditions. Wear 2019;436–437:203044. https://doi.org/10.1016/J.WEAR.2019.203044.

[141] Wang Q, Zhang X, Pei X. Study on the synergistic effect of carbon fiber and graphite and nanoparticle on the friction and wear behavior of polyimide composites. Mater Des 2010;31:3761–8. https://doi.org/10.1016/J.MATDES.2010.03.017.

[142] Rajesh JJ, Bijwe J, Tewari US. Influence of fillers on abrasive wear of short glass fibre reinforced polyamide composites. J Mater Sci 2001 362 2001;36:351–6. https://doi.org/10.1023/A:1004812109247.

[143] Bashandeh K, Tsigkis V, Lan P, Polycarpou AA. Extreme environment tribological study of advanced bearing polymers for space applications. Tribol Int 2021;153:106634. https://doi.org/10.1016/J.TRIBOINT.2020.106634.

[144] Bashandeh K, Marchert A, Takayuki U, Polycarpou AA, Meyer J, Lan P. The effect of surface texturing on thin film reversible adhesive bond strength. Int J Adhes Adhes 2021;107:102829.

https://doi.org/10.1016/J.IJADHADH.2021.102829.

[145] Matsumoto K, Suzuki M, Nishida S-I, Wakabayashi S. WEAR OF MATERIALS IN LUNAR DUST ENVIRONMENT. Proc. 11th Int. Symp. on" Mater. a Sp. Environ., 2009.

[146] Gaier JR. The effects of lunar dust on EVA systems during the Apollo missions. No. NASA/TM-2005-213610/REV1, 2007.

[147] Tsigkis V, Bashandeh K, Lan P, Polycarpou AA. Tribological behavior of PS400-related tribopairs for space exploration. Tribol Int 2021;153:106636. https://doi.org/10.1016/J.TRIBOINT.2020.106636.

[148] Totten GE. Glossary of Terms 2017. https://doi.org/10.31399/asm.hb.v18.a0006435.

[149] Reeves CJ, Menezes PL, Lovell MR, Jen TC. Tribology of Solid Lubricants. Tribol Sci Eng From Basics to Adv Concepts 2013;9781461419457:447–94. https://doi.org/10.1007/978-1-4614-1945-7_13.

[150] Roberts EW. Thin solid lubricant films in space. Tribol Int 1990;23:95–104. https://doi.org/10.1016/0301-679X(90)90042-N.

[151] Ren Y, Zhang L, Xie G, Li Z, Chen H, Gong H, et al. A review on tribology of polymer composite coatings. Frict 2020 93 2020;9:429–70. https://doi.org/10.1007/S40544-020-0446-4.

[152] Xue Y-H, Yan S-C, Chen | Yuan. Thermomechanical and tribological properties of polyimide and polyethersulfone blends reinforced with expanded graphite particles at various elevated temperatures. J Appl Polym Sci 2022:e52512. https://doi.org/10.1002/APP.52512.

[153] Li HL, Yin ZW, Jiang D, Jin LY, Cui YQ. A study of the tribological behavior of transfer films of PTFE composites formed under different loads, speeds and morphologies of the counterface. Wear 2015;328–329:17–27. https://doi.org/10.1016/J.WEAR.2015.01.028.

[154] Cui W, Raza K, Zhao Z, Yu C, Tao L, Zhao W, et al. Role of transfer film formation on the tribological properties of polymeric composite materials and spherical plain bearing at low temperatures. Tribol Int 2020;152:106569. https://doi.org/10.1016/J.TRIBOINT.2020.106569.

[155] Wang Q, Zheng F, Wang T. Tribological properties of polymers PI, PTFE and PEEK at cryogenic temperature in vacuum. Cryogenics (Guildf) 2016;75:19–25. https://doi.org/10.1016/J.CRYOGENICS.2016.01.001.

[156] Theiler G, Hübner W, Gradt T, Klein P, Friedrich K. Friction and wear of PTFE composites at cryogenic temperatures. Tribol Int 2002;35:449–58. https://doi.org/10.1016/S0301-679X(02)00035-X.

[157] Bashandeh K, Lan P, Polycarpou AA. Tribological Performance Improvement of Polyamide against Steel Using Polymer Coating. Tribol Trans 2019:1–11. https://doi.org/10.1080/10402004.2019.1643517.

[158] Nunez EE, Bashandeh K, Polycarpou AA. Thermal and Mechanical Properties of Polymer Coatings. Polym. Coatings. 1st ed., CRC Press; 2020, p. 157–75. https://doi.org/10.1201/9780429199226-9.

[159] Lan P, Nunez EE, Polycarpou A. Advanced polymeric coatings and their applications: Green tribology 2019. https://doi.org/10.1016/B978-0-12-803581-8.11466-3.

[160] Friedrich K, Zhang Z, Schlarb AK. Effects of various fillers on the sliding wear of polymer composites. Compos Sci Technol 2005;65:2329–43. https://doi.org/10.1016/J.COMPSCITECH.2005.05.028.

[161] Chang L, Zhang Z, Ye L, Friedrich K. Tribological properties of high temperature resistant polymer composites with fine particles. Tribol Int 2007;40:1170–8. https://doi.org/10.1016/J.TRIBOINT.2006.12.002.

[162] Tharajak J, Palathai T, Sombatsompop N. Recommendations for h-BN loading and service temperature to achieve low friction coefficient and wear rate for

thermal-sprayed PEEK coatings. Surf Coatings Technol 2017;321:477–83. https://doi.org/10.1016/J.SURFCOAT.2017.05.022.

[163] Roy A, Mu L, Shi Y. Tribological properties of polyimide-graphene composite coatings at elevated temperatures. Prog Org Coatings 2020;142:105602. https://doi.org/10.1016/J.PORGCOAT.2020.105602.

[164] Yanming W, Tingmei W, Qihua W. Effect of molecular weight on tribological properties of thermosetting polyimide under high temperature. Tribol Int 2014;78:47–59. https://doi.org/10.1016/J.TRIBOINT.2014.04.031.

[165] Zhang J, Demas NG, Polycarpou AA, Economy J. A new family of low wear, low coefficient of friction polymer blend based on polytetrafluoroethylene and an aromatic thermosetting polyester. Polym Adv Technol 2008;19:1105–12. https://doi.org/10.1002/PAT.1086.

[166] Demas NG, Zhang J, Polycarpou AA, Economy J. Tribological characterization of aromatic thermosetting copolyester-PTFE blends in air conditioning compressor environment. Tribol Lett 2008;29:253–8. https://doi.org/10.1007/S11249-008-9303-8/FIGURES/9.

[167] Ostberg GMK, Seferis JC. Annealing effects on the crystallinity of polyetheretherketone (PEEK) and its carbon fiber composite. J Appl Polym Sci 1987;33:29–39. https://doi.org/10.1002/APP.1987.070330103.

[168] Low MBJ. The effect of the transfer film on the friction and wear of dry bearing materials for a power plant application. Wear 1979;52:347–63. https://doi.org/10.1016/0043-1648(79)90072-3.

[169] Zhang G, Chang L, Schlarb AK. The roles of nano-SiO2 particles on the tribological behavior of short carbon fiber reinforced PEEK. Compos Sci Technol 2009;69:1029–35. https://doi.org/10.1016/J.COMPSCITECH.2009.01.023.

APPENDIX

TRIBOMETERS, OPERATION AND CALIBRATION

A1. Rtec Instruments

Rtec could be used to conduct pin-on-disk configuration experiments under unidirectional and reciprocating motions at RT and HTs up to 1000 °C, and under dry and lubricated conditions. The disk is the rotating part mounted on the disk holder located at the bottom, which is connected to the shaft rotated by the motor. The drive is mounted at the back side of the bottom stage and is connected to the shaft using a belt drive. The drive is capable of unidirectional experiments with rotational speeds up to 3000 rev/min in both clockwise and counterclockwise directions. The lower stage is capable of movement in both X and Y directions using two separate motors with a maximum speed of 50 mm/s. Both Z and X-Y stages can be manually or automatically controlled.

The disk could be enclosed in a furnace, shown in the photograph of **Figure A1(a)**, capable of reaching temperatures up to 1000 °C. The furnace is connected to an air-cooling system to reduce the surrounding temperature and prevent the transfer of heat to the motor. In addition, there are two insulating caps covering the top of the furnace to inhibit heat transfer to the top portion and transducers. The pin is mounted on the top using a holder, connected to a 16 mm diameter shaft, positioned perpendicular to the bottom rotating disk. The shaft is connected to a 2-axis force transducer at the bottom side of the top stage (Z-stage) capable of measuring the in-situ friction and normal forces.

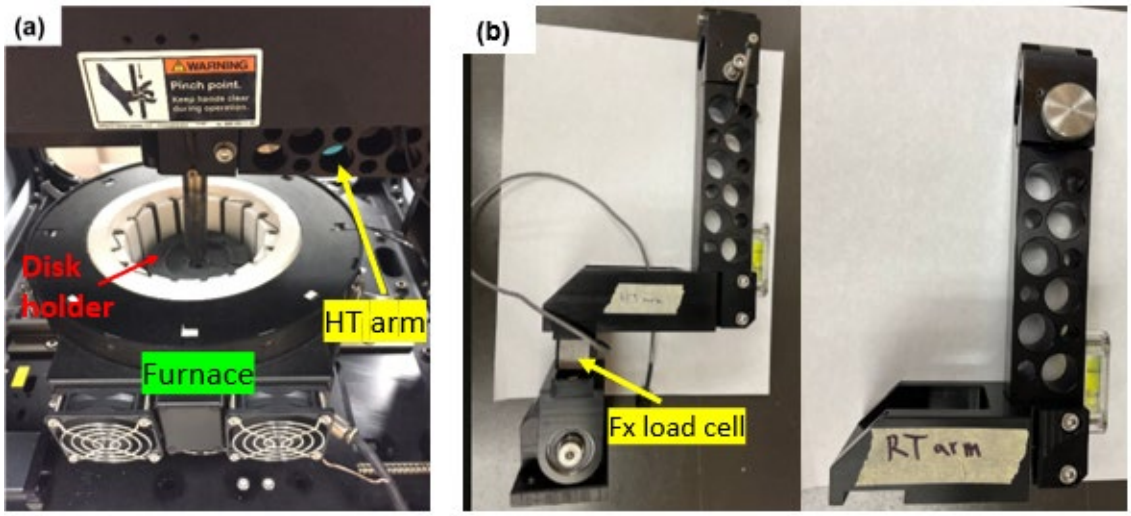

Figure A1. (a) Equipped HT furnace showing the pin holder inside the one-axis load cell, and (b) the two arms used for HT and RT tests.

Normal forces up to 200 N can be achieved using the 2-axis force transducer (**Figure A2(b)**). To conduct the experiments at higher loads, there exists two more one-axis high load transducer capable of reaching normal forces up to 500 and 5000N. The two one-axis load cells are shown in **Figure A2(a)**. The installation of this load cell requires an arm to hold the friction measurement load cells, as shown in **Figure A1(b)**. One arm could be employed for both HT and RT tests and the other only at RT. The advantage of the arms is more pronounced in obtaining higher accuracy of the results in reciprocating type experiments. Note that it is suggested to replace the Fx load cell installed in the arms with the Piezo load cell shown in **Figure A2(c)** for conducting the reciprocating test.

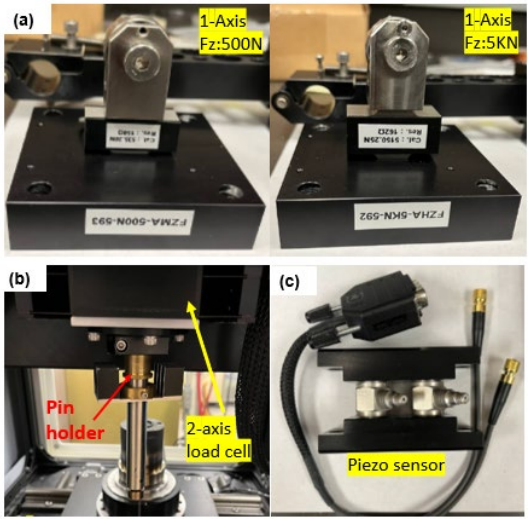

Figure A2. (a) the picture of 500N and 5KN one-axis load cells, (b) 200N 2-axis load cell, and (c) Piezo sensor.

The pin holders for 2-axis and one-axis transducers are shown in **Figure A2(a)**. In addition to the disk holder shown in **Figure A2(b)**, which can hold disks with 2inches diameter, an extra holder was fabricated from Inconel material to hold a 1inch×1inch square disk, as shown in **Figure A2(b)**. Note that disk holder 2 must be placed on disk holder 1 for use in the setup. The link "here" provides access to the videos which describe how to use the software, how to conduct RT and HT tests, and how to run the microscope.

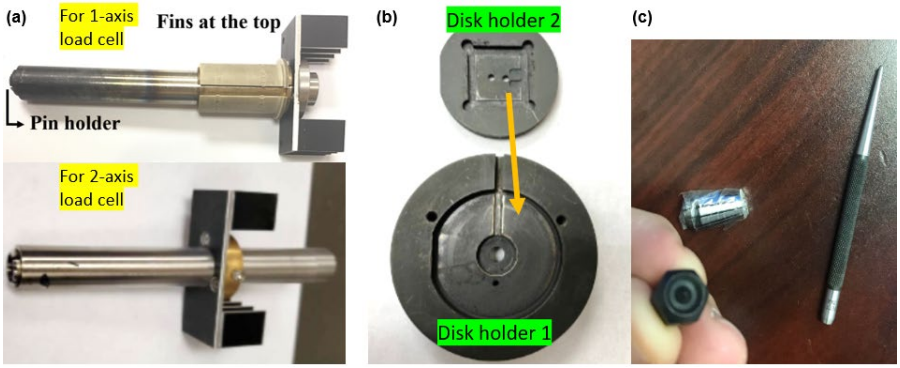

Figure A2. (a) The pin holders for use with 1-axis and 2-axis load cells, (b) the picture of disk holders for use in HT and RT tests, and (c) the toolkits for homing of the tribometer.

A1.1 Calibration

To conduct the experiments at the exact input wear track radius in the software, the user needs to ensure that the homing is precisely conducted and the (0,0) of (X,Y) location in the software is the actual center of the XY stage. If there is a mismatch between the values in the software and the actual center position in the XY stage after homing, the homing should be manually performed using the toolkit shown in **Figure A2(c)**. The user can use any other toolkit (or pin) that is good enough to touch the disk surface at the center position. The procedure below could be followed for readjustment of the zero position:

First home the system and then use the jog box and align the upper sample (e.g., pin holder) to lower sample (e.g., disk holder) so it is at the center (eyeball it). Go to setting config and click XYZ config button. Click "set as home position" and click save. Home again and check the (0,0) to ensure the setpoint is correct.

A2. HPT: high pressure tribometer

The HPT is equipped with a 6-axis force transducer that can measure normal forces from 10 to 1000 lb and friction forces up to 500 lb. The rotary drive is capable of unidirectional and oscillatory experiments up to 2000 rpm and 5 Hz, respectively. The high-pressure chamber can be pressurized up to 250 psi and the environmental temperature can be raised up to 120 °C. General instructions on how to operate the HPT can be found through the videos listed in provided “link” herein.

A2.1 High pressure testing procedure at RT

To conduct the high-pressure environment experiments with HPT, the operator needs to bring up the disk at the bottom part first until the pin and disk are 1-2 mm apart.

This ensures that the chamber is in its closed and sealed state before supplying the gas inside. To supply the desired gas (e.g., refrigerants, CO_2, etc.), any of the gas inlet ports shown in **Figure A3(a)** could be used. In the current Figure, the right port is used for supplying refrigerant into the chamber, and therefore, the left port must be closed to avoid leakage. **Figure A3(b)** shows the valve which is used for releasing the gas after the test is finished. Note that this valve must be closed before supplying the gas to pressurize the chamber. The pressure gauge shown in **Figure A3(c)** can be used to measure the pressure inside the chamber.

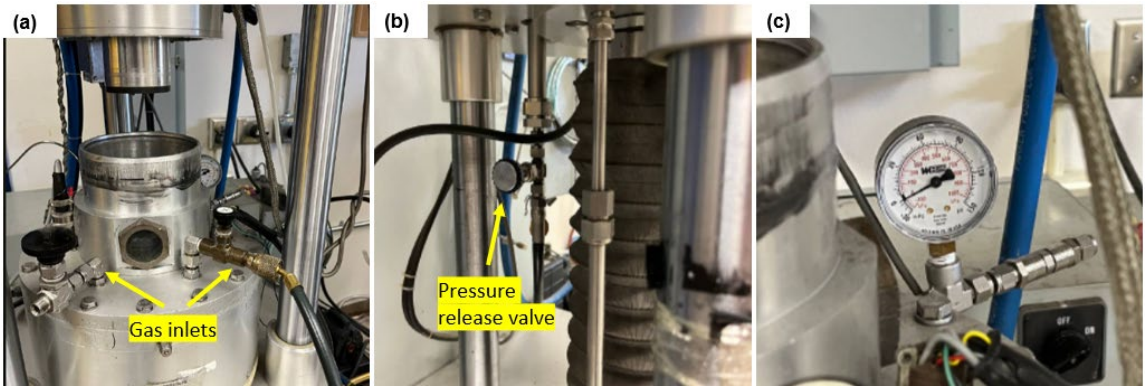

Figure A3. (a) The gas inlets to supply desired gas into the chamber, (b) the pressure release valve, and (c) the pressure gauge.

A2.2 Force transducer calibration

Figure A4 shows the setup that can be used to calibrate the force transducer (when necessary) on the X and Y directions (i.e., friction forces of Fx and Fy).

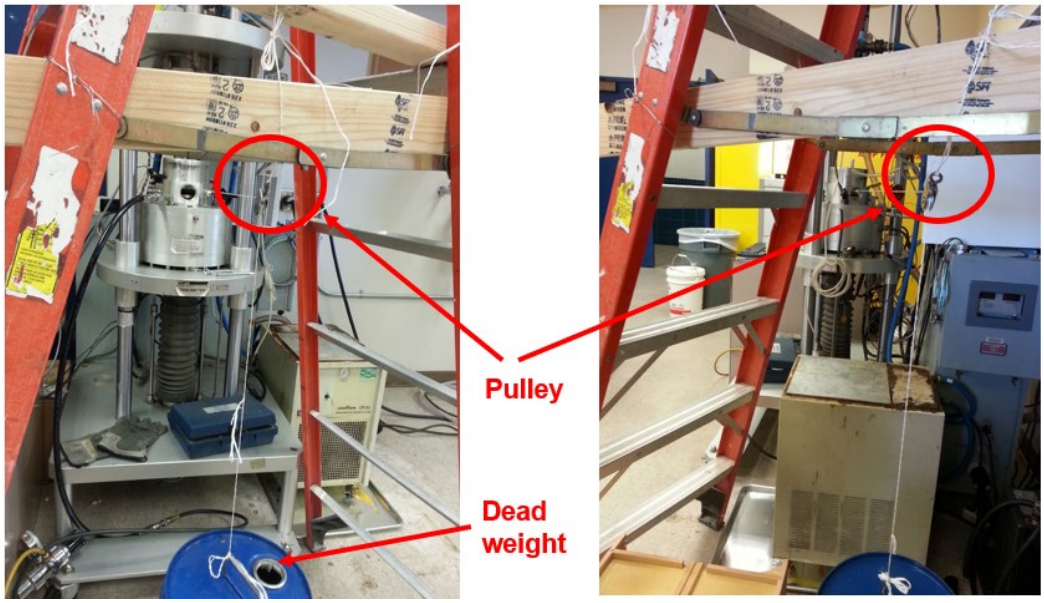

Figure A4. The setup for calibration of friction forces on the X and Y directions.

During the calibration and setting up the pulleys direction, it is necessary to find the right direction that yield "zero force" for the other direction which is not used for calibration. For example, if the user is trying to calibrate the Fx, the pulley should be on the direction which yields zero voltage (or force) on the Fy. **Table A1** illustrates an example of a calibration procedure that was conducted with several values of dead weights. According to the given calibration data, the conversion factor for Fx and Fy were obtained as 1.1 and 1.97, respectively. The users are encouraged to recalibrate the machine if the reading values are far from the current calibration constants. For the Fz calibration, simply put dead weights of known masses directly on the force transducer and record the output voltage for different weights to obtain the average calibration constant. More details of the calibration can be found in "link".

Table A1. The example of calibration of friction forces on the X and Y directions.

Dead weight(lb)	Voltage (0.01V, gain =1000)			Resolution(lb/0.01V)
	X direction	**Y direction**	Z direction	
2.95	0	3	0	0.983333333
6.045	0	5	1	1.209
11.02	0	10	1	1.102
17.13	0	16	2	1.070625
24.15	0	22	4	1.097727273
31.28	0	29	5	1.07862069
38.91	0	33	8	1.179090909
				Average: 1.10

Dead weight(lb)	Voltage (0.01V, gain =1000)			Resolution(lb/0.01V)
	X direction	Y direction	Z direction	
6.045	3	0	3	2.015
15.715	8	0	9	1.964375
23.855	12	0	14	1.987916667
31.28	16	0	18	1.955
38.91	20	0	23	1.9455
				Average: 1.97